Functional and structural studies of the human ABC Transporter ABCB8

Belinda Raffaella Faust

New College

A thesis submitted to the Medical Sciences Division for the degree of Doctor of Philosophy in the University of Oxford

Trinity Term, 2017



Structural Genomics Consortium

Nuffield Department of Medicine

University of Oxford

Structural and functional studies of the human ABC Transporter ABCB8

Belinda Raffaella Faust, New College

Trinity Term 2017

Abstract

ATP-binding cassette (ABC) transporters are one of the largest families of membrane proteins and are ATP-driven transport systems, which are found universally in all pro- and eukaryotes. Human ABC transporters have key roles in many physiological processes in the plasma membrane and within membranes of cell organelles, such as peptide transport, lipid flipping and multi-drug resistance. ABCB8, a subfamily B ABC transporter of the inner mitochondrial membrane, was found to be crucial for normal cardiac function, regulation of mitochondrial iron levels and cytosolic iron-sulphur cluster enzyme function and oxidative stress. Impaired function of ABCB8 resulted in mitochondrial iron accumulation, oxidative stress and cell death.

In this thesis I developed a protocol for the purification of human ABCB8 providing yields and stable protein sufficient for structural studies using X-ray crystallography. Strategic optimisation of the purification protocol and crystallisation methods, resulted in crystals that diffracted to a resolution of 3.8 Å and allowed me to solve the first structure of human ABCB8. The ABCB8 structure adopted an outward-facing conformation that resembles a post-ATP-hydrolysis state in the alternating access mechanism, that was not yet observed in type I ABC exporters. In addition to the structural studies on ABCB8, I set out to explore the effects of ATP analogues, ATP transition state analogues and ADP on purified ABCB8 with biochemical and biophysical methods. Furthermore, I find that ATPase activity of ABCB8 in proteoliposomes is dependent on cardiolipin (CDL).

The first structure of ABCB8 in an outward-facing conformation gives new insights into the alternating-access mechanism of subfamily B ABC transporters. Moreover, the purification and reconstitution protocol provided in this thesis is the foundation for further studies aiming to understand ABCB8's function in more detail.

Authorship Declaration

This thesis and the work presented in it were completed at the University of Oxford (Nuffield Department of Medicine) between October 2013 and October 2017, under the supervision of Prof. Liz Carpenter and Dr Chitra Shintre. All contributions made by others have been stated clearly in the text. This work has not been submitted in full or partial fulfilment of any other degree.

Belinda Faust

October 2017

Acknowledgements

First and foremost, I would like to express my gratitude to my supervisor, Prof. Liz Carpenter, for supporting me throughout this thesis, and for sharing her enthusiasm for the field, as well as her immense expertise, with me. Her guidance has been essential in allowing me to develop my own ideas as a scientist, whilst also providing an invaluable source of fruitful scientific discussion. I also would like to thank Dr Chitra Shintre for her careful guidance and patience throughout my time in the laboratory, as well as for her mentoring outside of it.

The work in this thesis was only possible due to the constant help and support offered by all members of the SGC "IMPS1" group. In particular, I would like to thank Dr Ashley Pike for his patience and for sharing his vast knowledge about X-crystallography and structure solving with me. My sincere thanks also go to Dr Andrew Quigley, Dr Yin Dong, Dr Karin Rodstrom and Dr Simon Bushell, who have been a great support in the laboratory, but also through the writing of this thesis. I must also acknowledge all of the SGC Biotech team here in Oxford for their help in cloning and the maintainence of cells. The work of this thesis would not have been possible without their efforts.

I would like to thank my examiners Prof. Mark Sansom and Prof. Thomas Meier for a stimulating discussion of the work in this thesis during the viva.

I like to acknowledge the Clarendon Scholarship and the Medical Research Council for their financial support over the last four year.

I would like to thank the many friends I have made in the SGC, across the university, but particularly through New College MCR. I would like to thank Kira, Marjolein, Charlotte and Liselotte for making life in Oxford so enjoyable. A special thank goes to Richard, who has been an invaluable support with his cheerful and kind character and helped me through the good and bad times of finishing this thesis.

Mein größter Dank geht an meine Eltern, Sabine und Detlef, ohne deren nicht endende Unterstüzung diese Doktorarbeit nie hätte geschrieben werden können. Worte können nicht widergeben, wie dankbar ich dafür bin, dass ihr mich in meinen akademischen Zielstrebungen so unterstüzt habt.

List of Abbreviations

ABC	ATP-binding cassette
ADP	adenosine diphosphate
AMPPCP	β,γ-methyleneadenosine 5-triphosphate
AMPPNP	β,γ-Imidoadenosine 5-triphosphate
ATP	adenosine triphosphate
ATPγS	adenosine 5'-O-(3-thio)triphosphate
bicine	N,N-bis(2-hydroxyethyl)glycine
C10E9	polyoxyethylene(9)decyl ether
C12E10	polyoxyethylene(10)dodecyl ether
C12E8	octaethylene glycol monododecyl ether
C12E9	polyoxyethylene(9)dodecyl ether
C13E8	polyoxyethylene(8)tridecyl ether
C8E5	octyl pentaethylene glycol ether
cAMP	cyclic adenosine monophosphate
CDL	cardiolipin
CFTR	cystic fibrosis transmembrane conductance regulator
CHAPS	3-[(3-Cholamidopropyl)-dimethylammonio]-1-propane sulfonate
CHS	cholesteryl hemisuccinate
CYMAL-3	3-cyclohexyl-1-propyl-β-D-maltoside
CYMAL-4	4-cyclohexyl-1-butyl-β-D-maltoside
CYMAL-5	5-cyclohexyl-1-Pentyl-β-D-maltoside
CYMAL-6	6-cyclohexyl-1-hexyl-β-D-maltoside
d-ALA	δ-amino levulinic acid
DDAO	N,N-dimethyldecylamine-N-oxide
DDM	n-dodecyl β-D-maltoside
DM	n-decyl-β-D-maltopyranoside
DMNG	decyl maltose neopentyl glycol
DMPC	1,2-dimyristoyl-sn-glycero-3-phosphorylcholine
DOPC	1,2-dioleoyl-sn-glycero-3-phosphocholine
DSF	differential scanning fluorimetry
DSS	disuccinimidyl suberate
ECL	extracellular loop
EGS	ethylene glycol bis(succinimidyl succinate)
ELB	elbow helix
EMTS	ethyl-mercury-p-toluenesulfanilide
FC12	n-dodecylphosphocholine
Fe-S	iron sulphur
GSH	glutathione
GSSG	glutathione disulfide
HEGA-11	cyclohexylpentanoyl-N-hydroxyethylglucamide
HEPES	4-(2-hydroxyethyl)-1-piperazineethanesulfonic acid
ICL	intracellular loop (coupling helix)
IMAC	ion mobility affinity chromatography
Kir	inwardly rectifying potassium channel
LDAO	lauryldimethylamine-N-oxide
LMNG	lauryl maltose neopentyl glycol
MEGA-10	decyl-N-methylglucamide

MEGA-8	octanoyl-N-methylglucamide
MEGA-9	nonanoyl-N-methylglucamide
MPP	mitochondiral processing peptidase
MR	molecular replacement
MST	microscale thermophoresis
NBD	nucleotide binding domain
NCS	non-crystallographic symmetry
NG	n-nonyl-β-D-glucopyranoside
OG	n-octyl-β-D-glucopyranoside
OGNG	octyl glucose neopentyl glycol
PBS	phosphate buffered saline
PEG	polyethylene glycol
PI	L-α-phosphatidylinositol
POPC	1-palmitoyl-2-oleoyl-sn-glycero-3-phosphocholine
POPE	1-palmitoyl-2-oleoyl-sn-glycero-3-phosphoethanolamine
POPG	1-palmitoyl-2-oleoyl-sn-glycero-3-phospho-(1'-rac-glycerol)
POPS	1-palmitoyl-2-oleoyl-sn-glycero-3-phospho-L-serine
RMSD	root mean square deviation
SDS	sodium dodecyl sulfate
SDS-PAGE	SDS polyacrylamide gel electrophoresis
SEC	size exclusion chromatography
SUR	sulfonylurea receptor
TCEP	tris-2-carboxyethyl phosphine
TDM	N-Tridecyl-β-maltoside
TIM	translocase of the inner mitochondrial membrane
T_M	melting temperature
TMD	transmembrane domain
TMH	transmembrane helix
TOM	translocase of the outer mitochondrial membrane
UDAO	n-Undecyl-N,N-Dimethlamine-oxide
UDM	n-Undecyl-β-D-maltoside
vdW	van der Waals

Contents

1 Introduction **1**
- 1.1 Membrane transport . . . 1
- 1.2 ABC transporters . . . 4
  - 1.2.1 History of the discovery of ABC transporters . . . 4
  - 1.2.2 Structural fundamentals of ABC transporters . . . 5
  - 1.2.3 The nucleotide binding domains . . . 7
  - 1.2.4 Non-hydrolysable ATP analogues and ATP transition states 12
  - 1.2.5 ABC importers and exporters . . . 15
  - 1.2.6 Type 1 ABC exporters in different conformations . . . 17
  - 1.2.7 Coupling between the NBDs and TMDs . . . 21
  - 1.2.8 Alternating access mechanism in type 1 ABC exporters . . . 22
  - 1.2.9 Eukaryotic ABC transporters . . . 25
- 1.3 Mitochondrial ABC transporters . . . 29
  - 1.3.1 Mitochondrial metabolism . . . 29
  - 1.3.2 ABC transporters in mitochondria . . . 33
- 1.4 Introduction to purification and crystallisation . . . 42
  - 1.4.1 Expression and purification of eukaryotic membrane proteins 42
  - 1.4.2 Expression and purification of eukaryotic ABC transporters . 43
  - 1.4.3 Crystallisation of eukaryotic ABC transporters . . . 44
  - 1.4.4 Overview of the membrane protein pipeline at the Structural Genomics Consortium (SGC) . . . 49
  - 1.4.5 Reconstitution of ABC transporters into proteoliposomes . . 50
- 1.5 Aims of the thesis . . . 52

2 Materials and Methods **54**
- 2.1 Contributions . . . 54
- 2.2 Cloning of ABCB8 . . . 55
- 2.3 Expression of ABCB8 in Sf9 cells . . . 55
- 2.4 Detergent solubilisation test . . . 57
- 2.5 Monodispersity screen . . . 58

2.5.1 Cell lysis and extraction of ABCB8 for monodispersity screens . . . 58
2.5.2 IMAC and SEC of ABCB8 in monodispersity screens 59
2.6 Large-scale purification 60
2.6.1 Chemical modification of lysines and cysteines during purification 62
2.7 Preparation of nucleotides 63
2.8 Crystallisation 65
2.8.1 Crystallisation set-up and crystal optimisation 65
2.8.2 Crystal mounting and cryo-cooling 67
2.8.3 Crystal screening and data collection 68
2.8.4 Crystal data processing 68
2.8.5 Structure building and refinement 69
2.8.6 Structure presentation and analysis 71
2.9 ATPase assays 72
2.9.1 "Chifflet's assay" 72
2.9.2 ADP-Glo kinase assay 73
2.9.3 ATPase assay data analysis 74
2.10 Nano differential scanning fluorimetry (nanoDSF) measurements . 75
2.10.1 Theory of nanoDSF 75
2.10.2 Experimental procedure of nanoDSF 77
2.11 Nucleotide binding measured with Microscale thermophoresis (MST) 78
2.11.1 Theory of MST 78
2.11.2 Labelling of ABCB8 for MST 81
2.11.3 Experimental procedure for MST measurements 81
2.12 Cross-linking with DSS and EGS 83
2.13 Reconstitution of ABCB into proteoliposomes 84
2.14 Mass spectrometry 86
2.14.1 Intact mass spectrometry on ABCB8 86
2.14.2 ESI-QTOF measurements of nucleotides 87
2.15 Bioinformatics methods 88

3 Establishing a purification and crystallisation protocol for ABCB8 89

3.1 Introduction 89
3.2 Results 90
3.2.1 Construct design for ABCB8 90
3.2.2 Small scale detergent solubilisation test 93
3.2.3 Monodispersity screens 95
3.2.4 Optimisation of large-scale purification 99
3.2.5 Lipid screens 106
3.2.6 Chemical modifications 109
3.2.7 Crystallisation 118
3.3 Conclusion 128

4 Functional studies on ABCB8 129

4.1 Introduction 129
4.2 Results Part I 130

4.2.1 Optimisation of reconstitution of ABCB8 into proteoliposomes . . . 130
4.2.2 The ATPase activity of ABCB8 in proteoliposomes is dependent on CDL . . . 133
4.3 Conclusion Part I . . . 136
4.4 Results Part II . . . 138
4.4.1 Effects of ATP, ADP and ATP-analogue binding to ABCB8 138
4.5 Conclusion Part II . . . 156

5 Outward-facing conformations of ABCB8 and the alternating-access mechanism 157
5.1 Introduction . . . 157
5.2 Results . . . 158
5.2.1 Solving the structure of human ABCB8 . . . 158
5.2.2 Overall structural features of ABCB8 . . . 166
5.2.3 Conservation of residues in the dimer interface . . . 171
5.2.4 The nucleotide binding domains . . . 172
5.2.5 The coupling helices . . . 176
5.2.6 The transmembrane domains . . . 181
5.2.7 The cholesteryl hemisuccinate binding site . . . 187
5.2.8 Additional structures of ABCB8 in outward-facing states obtained without nucleotide and with ADP . . . 190
5.3 Conclusion . . . 197

6 Discussion 198
6.1 Purification and crystallisation of ABCB8 . . . 198
6.2 Cardiolipin stimulates the basal ATPase activity of ABCB8 in proteoliposomes . . . 199
6.3 Effects of ATP analogue binding on ABCB8 . . . 201
6.4 Interaction of ADP with ABCB8 . . . 203
6.5 Potential conformational changes induced by nucleotide analogue binding . . . 205
6.6 Structures of ABCB8 in outward-facing states . . . 205

7 Conclusion and Outlook 213
7.1 Conclusion . . . 213
7.2 Outlook . . . 216

8 Appendix 218
8.1 Appendix: Introduction . . . 219
8.2 Appendix: Material and Methods . . . 222
8.3 Appendix: Optimisation of purification and crystallisation of ABCB8 . . . 226
8.4 Appendix: Exploring effects of nucleotide and putative substrate binding on ABCB8 . . . 231
8.5 Appendix: Outward-facing conformations of ABCB8 give and the alternating-access mechanism . . . 235

So that I may perceive whatever holds
The world together in its inmost folds.

Johann W. v. Goethe

CHAPTER 1

Introduction

1.1 Membrane transport

Biological membranes surround an enclosed space, an essential prerequisite for life, due to their selective permeability. A so-called fluid mosaic model was proposed by Singer & Nicolson [1972] with lipid molecules forming a bilayer, in which the hydrophobic lipid tails face towards the core of the bilayer and the hydrophilic and partly charged head groups interact with the hydrophilic cytoplasm or extracellular medium. Membrane proteins that are either associated with the lipid membrane (peripheral) or embedded in it (integral) form part of the mosaic arrangement. Their interactions with the membrane are mediated by the amphipathic character of proteins and lipids. This model remains consistent with the most recent evidence; however, adjustments were made to account for e.g. curvature and asymmetry of the lipid bilayer, as well as restricted lateral motion of the integral membrane proteins and lipids as reviewed in Nicolson [2014].

Due to the hydrophobic barrier, only small gaseous molecules, such as CO_2, N_2 or O_2, small polar but uncharged molecules, such as water, and hydrophobic molecules can cross lipid bilayers, whereas unaided passive diffusion is restricted for charged molecules and larger polar metabolites, as they cannot be dissolved in the hydrophobic interior of a biological membrane. However, metabolism in cells or in cellular compartments within eukaryotic cells requires the exchange of substrates and reaction products across membranes. Integral membrane proteins facilitate diffusion of these metabolites through the hydrophobic barrier of the membrane by providing a hydrophilic or charged pore, so that ions and polar compounds can pass. The driving force for passive diffusion of solutes (X) from one side of the membrane (A) to the other (B) is the negative free energy value ΔG reflecting a net flow with the concentration gradient towards a side of the membrane with the lower concentration. This so-called chemical potential is a concentration gradient across a membrane and can be described by Eq.1.1.1 with R being the ideal gas constant and T the temperature in Kelvin.

$$G_B - G_A = \Delta G = RT \ln [\frac{X_B}{X_A}] \tag{1.1.1}$$

The term for the difference in free energy in Eq.1.1.1 is extended by an electrical energy term with $\Delta\Psi = \Psi_B - \Psi_A$ accounting for the distribution of charged molecules across the membrane. This gives the so-called electrochemical potential (membrane potential) (Eq.1.1.2), which combines the gradient of charged and uncharged molecules across the membrane.

$$G_B - G_A = \Delta G = RT \ln [\frac{X_B}{X_A}] + Z_X \mathscr{F} \Delta\Psi \tag{1.1.2}$$

Transport against a concentration gradient can be required for enriching metabolites within cells and cellular compartments in order to provide substrate excess, which drives the equilibrium of enzymatic reactions towards product generation or for removing waste products out cells. Furthermore, neuronal signalling requires

a resting potential, a membrane potential created by an opposing concentration gradient of potassium and sodium ions. Sudden depolarisation of the membrane potential creates an action potential running along an axon as an electric signal. In contrast to the previously described passive transport, this so-called "active transport across biological membranes requires energy. The energy for this can be provided by co- or anti- transport of a second molecule along its concentration gradient (in sym or antiporter), by light (photosynthesis) or by exergonic chemical reactions (e.g. ATP hydrolysis). Active transport can be further divided into primary and secondary active transport depending on whether the energy is directly provided by a chemical reaction (primary active transport; e.g. ATPases) or comes from the chemical gradient of a second molecule (secondary active transport, e.g. solute carriers). The Transporter Classification Database (TCDB) [Saier *et al.,* 2006; Saier *et al.,* 2016] creates a unique identifier for all membrane transporters including ion channels from over 800 protein families according to their mode of transport and sequence similarity.

Adenosine triphosphate (ATP) serves as an "energy currency" of the cell. The chemical energy released in the hydrolysis of the first and second P-O-P bond in ATP, resulting in adenosine diphosphate (ADP) and adenosine monophosphate (AMP), can be used as a source of free energy. However, enzymatic activity is required for hydrolysis, as the molecule is kinetically stabilised due to de-localised electrons in the phosphate groups. The Gibb's energy for hydrolysis of ATP to ADP varies depending on the physiological environment and values between -50 kJ/mol and -72 kJ/mol were measured in *Escherichia coli* [Bennett *et al.,* 2009] and in human skeletal muscle [Wackerhage *et al.,* 1998], respectively.

1.2 ABC transporters

1.2.1 History of the discovery of ABC transporters

ATP binding cassette (ABC) transporters, found universally in prokaryotic and eukaryotic cells, are a family of primary active transporters, that use ATP-hydrolysis as an energy source for transport. The first ABC transporters discovered were amino acid up-take systems, found when *E. coli* were placed under starvation conditions [Berger & Heppel, 1974]. These systems interact with substrate binding proteins (SBPs), which bind the substrate and deliver it to the transporter. Transport was shown to be dependent on ATP hydrolysis, but not on the membrane potential. Cloning the operon sequences that assembles a histidine permease from *Samonella typhimurium* and a maltose permease from *E. coli* revealed the high sequence similarity of these transporters in their cytoplasmic domains [Higgins *et al.,* 1982; Gilson *et al.,* 1982]. Similar transport systems, with highly conserved cytoplasmic domains, have been found in a huge variety of bacteria, facilitating import and export of metabolites, in a process driven by ATP hydrolysis [Higgins *et al.,* 1986]. At the same time, mammalian P-glycoprotein (ABCB1), a protein involved in multi-drug resistance in mammalian cells [Juliano & Ling, 1976; Kartner *et al.,* 1983], was found to have the same conserved ATP binding domain, hinting at a universal transporter superfamily among all life forms [Chen *et al.,* 1986; Gros *et al.,* 1986; Gerlach *et al.,* 1986]. Further studies uncovered the function of these transporters as importers, SBP independent exporters or even ion channels (e.g. the cystic fibrosis conductance regulator; CFTR [Tsui & Dorfman, 2013]) and regulators of ion channels (sulfonyl urea receptor, ABCC8/9 [Aittoniemi *et al.,* 2009]).

1.2.2 Structural fundamentals of ABC transporters

The functional transport unit usually consists of two transmembrane domains (TMDs), embedded in the lipid bilayer, that are linked to two cytoplasmic nucleotide binding domains (NBDs). The TMDs bind the transport substrate, whereas ATP binding and hydrolysis takes place in the NBDs (Fig. 1.1). In contrast to the highly conserved NBDs, TMDs show much lower sequence conservation among related transporters with a broad range of functions. The substrates transported by ABC transporters are highly diverse, including ions, hormones, solutes, large hydrophobic molecules, peptides and even lipids. For bacterial importers, the TMDs and NBDs are almost always encoded on four separate polypeptide chains. For bacterial exporters one TMD and NBD are encoded on one polypeptide chain, whereas the NBD and the TMD can be fused together in either order. Bacterial importers additionally rely on periplasmic SPBs, encoded on the same operon as the TMDs and NBDs (Fig. 1.1). Prokaryotic exporters assemble as full functional transporters by dimerisation as homo- or heterodimers of two polypeptide chains, encoding one TMD and NBD ("half transporter) each and they do not require SBPs. In contrast, some eukaryotic ABC transporters encode all four domains on one polypeptide chain, allowing more synchronised regulation of gene expression of all four domains in the absence of operons (Fig. 1.1). ABC transporters can have large additional C-terminal and N-terminal domains, as well as inserted domains between TMDs and NBDs, that are found to be involved in regulation (e.g. ABCC7 [Chappe *et al.,* 2005], interactions with binding partners (e.g. SUR1/2 [Li *et al.,* 2017; Martin *et al.,* 2017]) and substrate recruitment (e.g PCAT [Lecher *et al.,* 2012]).

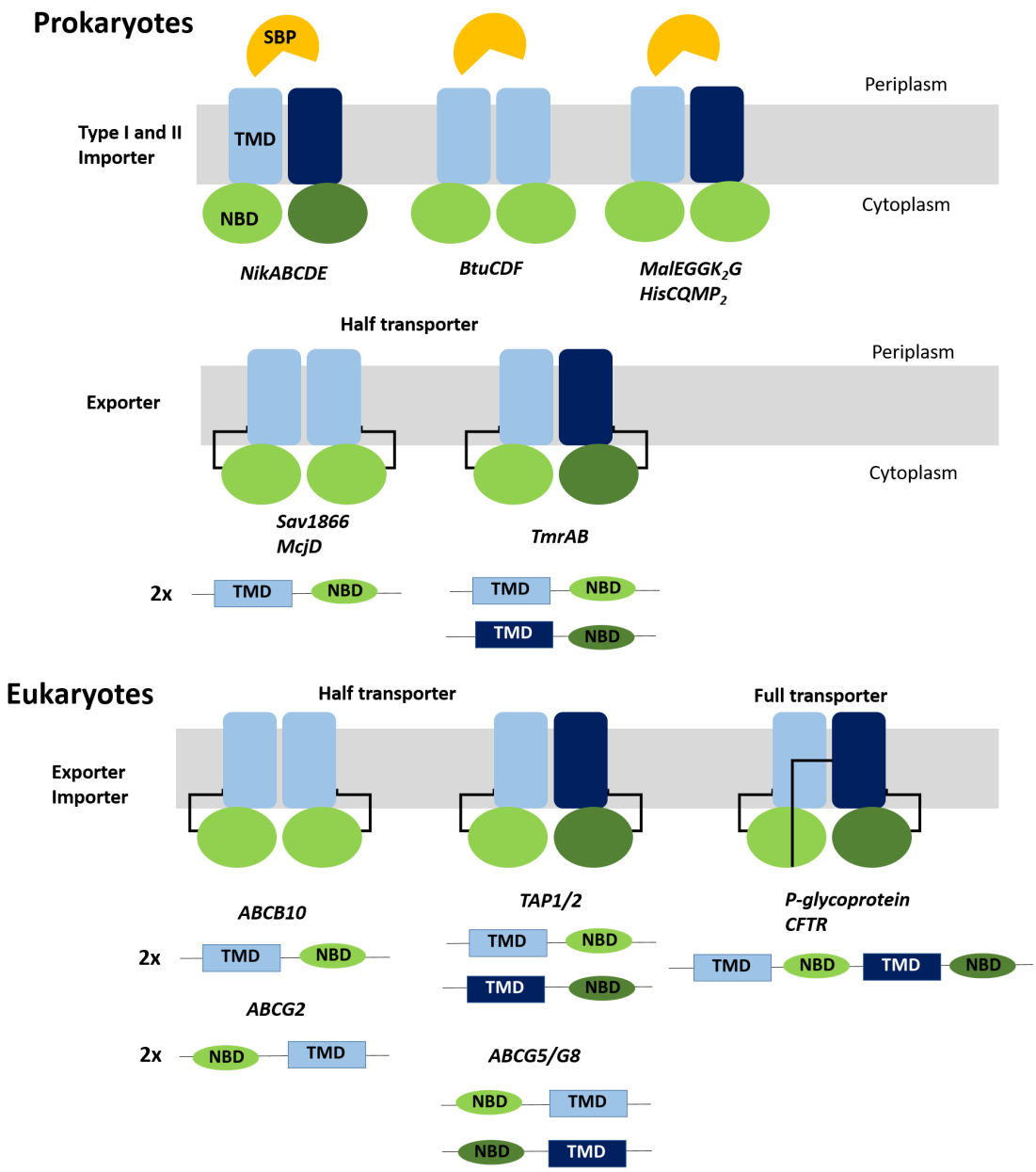


Figure 1.1 – Scheme for ABC transporter assembly from different chains in prokaryotes and eukaryotes with SBPs in yellow, TMDs (transmembrane domains) in blue and NBDs (nucleotide binding domains) in green. (Figure adapted from Theodoulou & Kerr [2015]).

1.2.3 The nucleotide binding domains

The overall structure of NBDs

ABC transporters show a high degree of conservation in the NBDs, independent of species and substrate specificity or direction of transport (importer and exporter). On the basis of sequence alignments with other nucleotide binding proteins, such as the adenylate kinase, it was found that NBDs share a so-called RecA-like subdomain [Hyde *et al.,* 1990]. This was later confirmed by the crystal structure of isolated NBDs such as HisP of the histidine permease $HisQMP_2$ from *Salmonella typhimurium* [Hung *et al.,* 1998], Rad50cd of Rad50 from *Pyrococcus furiosus* [Hopfner *et al.,* 2000] and the NBD from the archaeal ABC transporter MJ0796 [Smith *et al.,* 2002].

The RecA-like subdomain has a conserved Walker A motif (GXXGXGK(T/S)T, where X is any amino acid residue) and a Walker B motif (hhhhDE, where h indicates a hydrophobic residue) (Fig. 1.2A). Both motifs were first identified by Walker and colleagues in 1982 in the α and β proteins of the *E. coli* ATPase by comparing their protein sequence with other nucleotide binding proteins of known three dimensional structure such as the adenylate kinase and phosphofructokinase [Walker *et al.,* 1982]. The conserved A-loop, H-loop and D-loop are also part of the conserved RecA-like subdomain (Fig. 1.2A and B). An α-helical subdomain, that is attached to the RecA-like subdomain, contains the conserved ABC transporter specific C-loop or so-called ABC signature motif ((L/Y)SGGQ(K/R)) (Fig. 1.2A and B) [Zaitseva *et al.,* 2005].

The NBDs in ABC transporter can dimerise in a head-to-tail arrangement facilitated by ATP binding in the dimer interface. This interface is formed by residues of opposite chains as observed for crystal structures of isolated NBDs of Rad50 and MJ0796 [Hopfner *et al.,* 2000; Smith *et al.,* 2002], as well as in the full BtuCD importer crystal structure [Hollenstein *et al.,* 2007] and full ABC exporter crystal

structures such as Sav1866, MsbA and McjD [Dawson & Locher, 2006; Choudhury *et al.*, 2014; Ward *et al.*, 2007b].

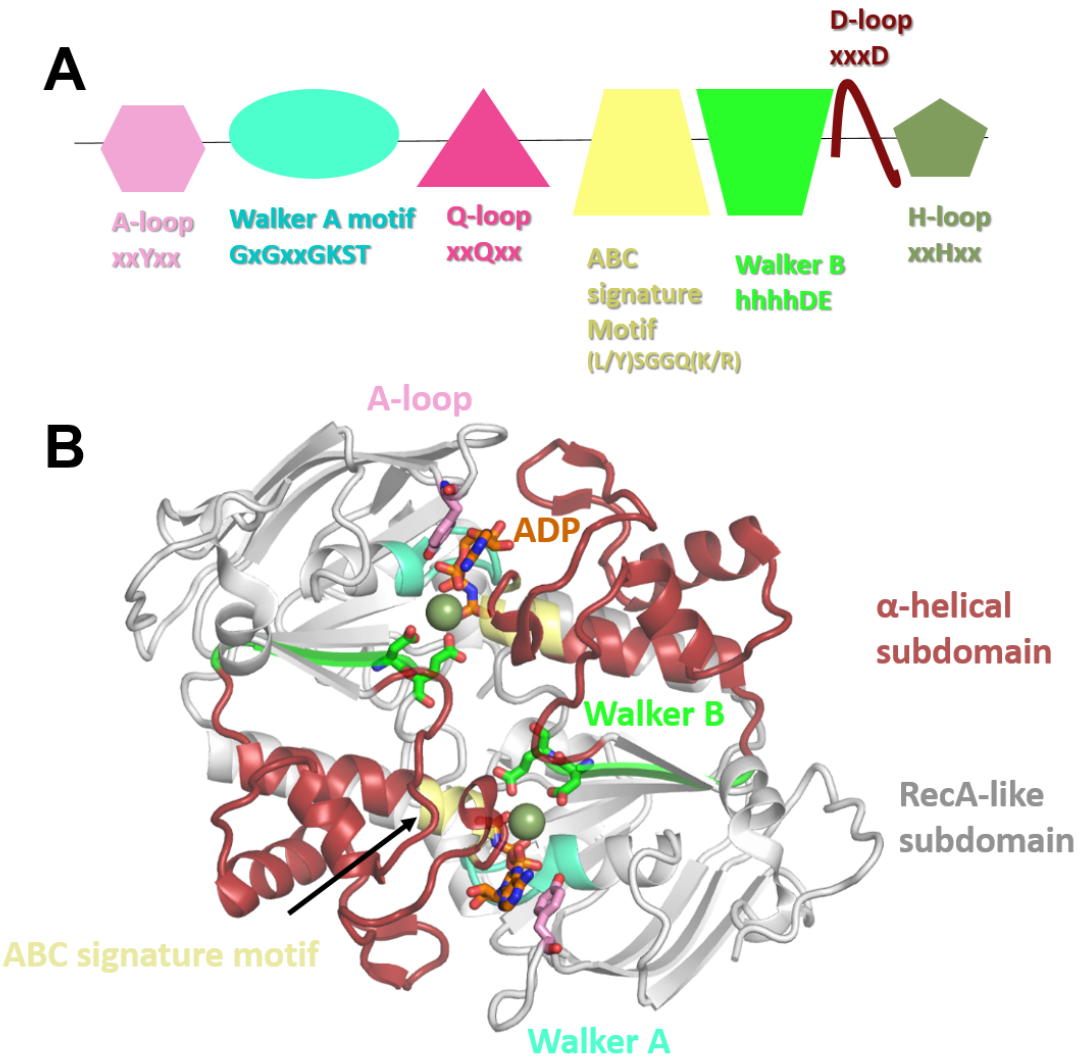


Figure 1.2 – Representation of dimerised ABC transporter NBDs from the outward-occluded McjD structure (4PL0; [Choudhury *et al.*, 2014]) A) Top-view of NBD dimer from membrane plane. RecA-like domain is presented in greyor coloured according to motif, including the conserved Walker A (cyan) and B motifs(green), the A-loop (pink). The α-helical subdomain is coloured in red and yellow for the ABC signature motif as part of this domain. ADP is shown as orange sticks and Mg^{2+} as dark green sphere. B) Schematic representation of conserved motifs in ABC transporter NBDs in order of primary sequence.

ATP binding

ATP's adenine ring is bound via π-π stacking with a tyrosine in the A-loop downstream from the Walker A motif. The Walker A motif forms a nest like structure coordinating the nucleotide's phosphate groups with the conserved lysine and threonine/serine side chains, as well the backbone amide hydrogens coordinating oxygens of the nucleotide's phosphate groups [Ramakrishnan *et al.,* 2002]. For AMMPNP bound to Sav1866 (2ONJ), MsbA (3B60) and McjD (4PL0) the α, β and γ phosphate groups and for ADP bound to Sav1866 only the α and β phosphate groups interact with the Walker A motif [Dawson & Locher, 2007a; Ward *et al.,* 2007a; Choudhury *et al.,* 2014; Dawson & Locher, 2006]. In a dimer the γ phosphate group moiety of the ATP forms an additional interactions with the ABC signature motif of the α-helical subdomain on the adjacent chain [Rees *et al.,* 2009]. Therefore, dimerisation coordinates the phosphate moieties of the ATP between both the Walker A motif and the ABC signature motif of the α-helical subdomain on the adjacent chain [Rees *et al.,* 2009], which is a prerequisite for ATP hydrolysis.

Moreover, a Mg^{2+} ion interacts with the oxygens of the β and γ phosphate group and orients the γ phosphate group for the hydrolysis reaction. Glutamine in the Q-loop, that hydrogen bonds with the γ phosphate group and binds the Mg^{2+} ion in the dimerised conformation, is responsible for communication between the NBDs and TMDs [Zolnerciks *et al.,* 2014]. The aspartates in the D-loops are involved in the allosteric control between the two ATP binding sites by interacting with the Walker A motifs of the adjacent chains [Jones & George, 2012]. ATP hydrolysis itself is mainly assisted by two residues; the histidine residue in the H-loop polarises a water molecule to support its nucleophilic attack on the γ-phosphate and the glutamate in the Walker B motif helps to electrostatically stabilise the oxygen of the γ phosphate allowing for it to be nucleophilicly attacked (Fig. 1.3A/B) [Story & Steitz, 1992; Guenther *et al.,* 1997]. However the glutamate has been shown to

not be crucial for nucleotide binding [Guenther *et al.,* 1997; Putnam *et al.,* 2001].

Inward-facing states with the ATP-analogues AMPPCP and AMPPNP bound but with the NBDs separated were observed in crystal structures of ABCB10 and TM287/288 [Shintre *et al.,* 2013; Hohl *et al.,* 2012]. The nucleotide binding site of ABCB10 with AMPPNP bound (4AYW) is presented here as an ATP-analogue bound open inward-facing conformation (Fig. 1.3C). It is evident that the ABC signature motif, shown in yellow, is too far from the AMPPNP to allow interactions with the nucleotide. Instead the AMPPNP and AMPPCP for the other inward-facing structures of ABCB10 (4AYT,4AYX) are bound to only one chain. Their phosphates are coordinated by residues of the Walker A motif and their adenine rings interact with the tyrosine of the A-loop. The occupancies for the ATP-analogues in both NBDs in these ABCB10 crystal structures were close to 100%, whereas for the TM287/288 crystal structure, AMPPNP was only bound to the canonical high-affinity nucleotide binding site. In contrast to the outward-facing structures, the glutamate in the Walker B motif faces away from the γ phosphate in the binding site and the histidine in the H-loop is disordered. ABCB10's nucleotide-free inward-facing state indicates that the sequence of the Walker A motif forms a helix in the absence of nucleotide, that unwinds upon nucleotide binding to accommodate phosphate groups (Fig. 1.3D).

Most structures suggest dimerisation of the NBDs in a symmetrical way (e.g. Sav1866, McjD, P-glycoprotein, ABCB10, Atm1 and ABCC1) allowing formation of two nucleotide binding sites that could hydrolyse ATP simultaneously [Dawson & Locher, 2006; Choudhury *et al.,* 2014; Shintre *et al.,* 2013; Srinivasan *et al.,* 2014; Johnson & Chen, 2017]. However, some asymmetric full or heterodimeric half ABC transporters have one degenerate nucleotide binding site, that lacks the ability to hydrolyse ATP. These degenerate nucleotide binding sites are found in heterodimeric half transporters TmrAB, TM287/288 and TAP1/2, potentially causing catalytic asymmetry, or in non-canonical full transporters like the ion-channel CFTR and the sulfonylurea receptor SUR1/2 (ABCC8/9) [Zutz *et al.,* 2011; Hohl

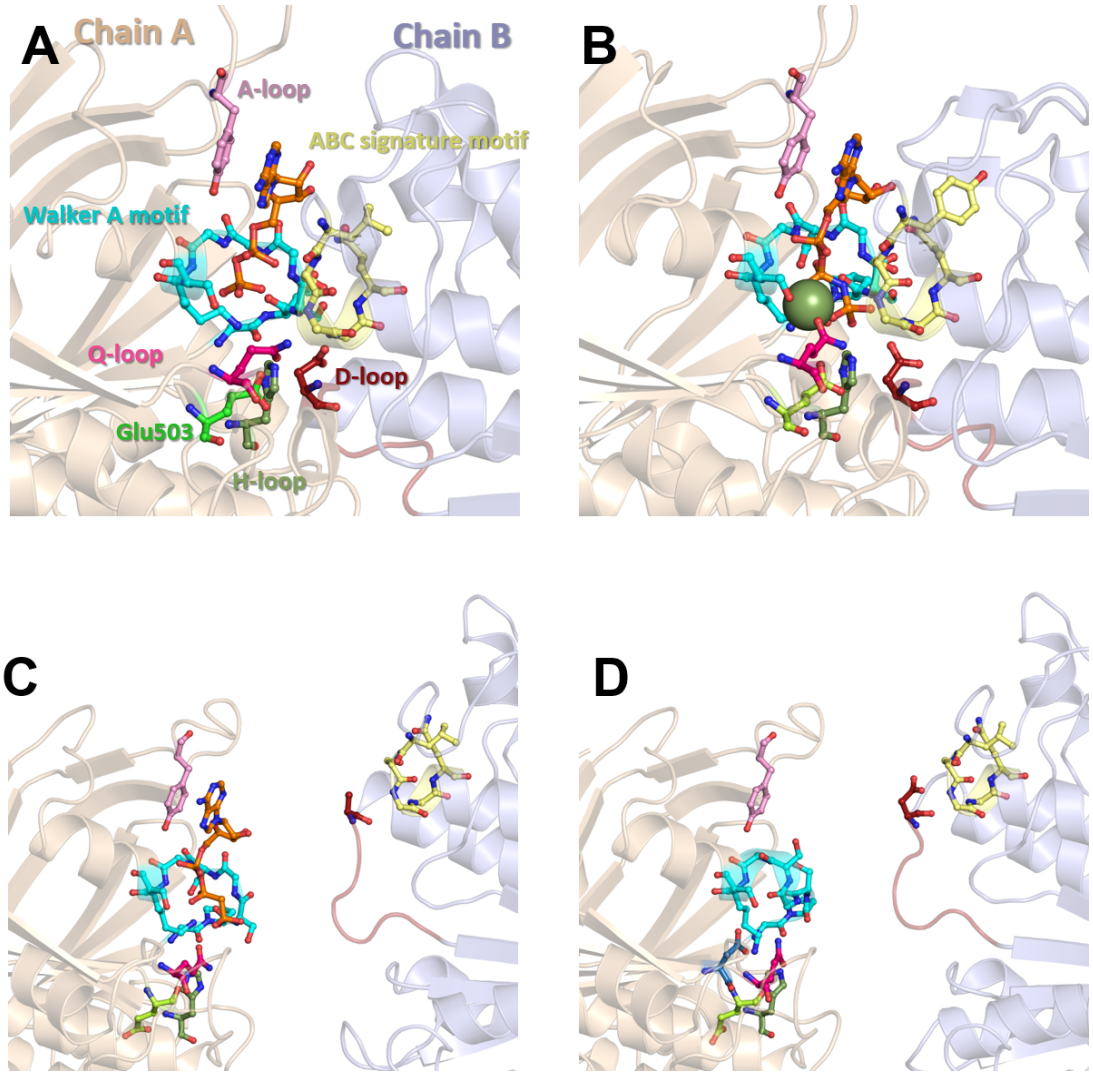


Figure 1.3 – Comparison of nucleotide binding to NBDs of A) the outward-facing ADP-bound state of Sav1866 (2HYD), B) the outward-facing occluded AMPPNP-bound state of McjD (4PL0), C) the AMPPCP-bound inward-facing state of ABCB10 (4AYX) and D) the nucleotide-free inward-facing state of ABCB10 (3ZDQ). Conserved residues that are part of the nucleotide coordination are presented as sticks with colouring according to element (N=blue and O=red) and with carbons and phosphates colour coded according to motif (A-loop=light pink, Walker A motif=cyan, Q-loop=pink, glutamate in Walker B=light green, H-loop=dark green, D-loop=dark red, ABC signature motif=yellow). The carbons and phosphorous in the nucleotide are coloured in orange, nitrogen in blue and oxygen in red.

et al., 2012; Hohl *et al.,* 2014; Abele & Tampé, 2004; Aleksandrov *et al.,* 2002; Vedovato *et al.,* 2015].

1.2.4 Non-hydrolysable ATP analogues and ATP transition states

Non-hydrolysable ATP analogues and analogues of the hydrolysis transition state have been extremely useful tools to study the mechanism of ABC transporters structurally [Ward *et al.,* 2007b; Oldham & Chen, 2011; Choudhury *et al.,* 2014; Shintre *et al.,* 2013] and functionally [Hohl *et al.,* 2014; Timachi *et al.,* 2017; Collauto *et al.,* 2017; Verhalen *et al.,* 2017]. Studies on human CFTR showed extended opening of the channel in the presence of AMPPNP and ATPγS and thus identified ATP binding as the trigger for activating CFTR [Gunderson & Kopito, 1994; Hwang *et al.,* 1994]. Increasing concentrations of AMPPNP and ATPγS impaired binding of the transport substrate vinblastine to P-glycoprotein, suggesting that these nucleotide analogues trigger occlusion of the substrate binding site in the TMDs [Martin *et al.,* 2000; Martin *et al.,* 2001]. In AMPPCP and AMPPNP the bridging oxygen between β and γ phosphate group is replaced by an -NH group or a -CH2 group, respectively. The electro-negativity is reduced in the following order from oxygen to -NH and -CH2, causing an attenuated partial charge distribution between the γ phosphate group and the bridging atom compared to ATP. Subsequently, the strong electrophilic properties of the adjacent phosphorus atom in the γ phosphate group, required for hydrolysis, are decreased. AMPPCP and AMPPNP both coordinate magnesium with similar affinity to ATP between the P_β and γ phosphate oxygens [Yount *et al.,* 1971]. Whereas the angles between P-N-P and P-O-P are similar, P-C-P forms a more acute angle. This difference might explain the observed lack of ATP analogue properties for AMPPCP in the actinomyosin and nitrogenase systems [Moos *et al.,* 1960; Duval *et al.,* 2013]. Similar charge distribution and P-X-P angle with ATP make AMPPNP a better ATP

analogue than AMPPCP, but also allow for easier hydrolysis compared to AMP-PCP. In contrast, ATPγS, in which one of the non-bridging oxygens on the γ phosphate group is replaced by a sulphur, is more negatively charged than ATP, which explains why in some systems it has the strong inhibitory properties, for example with the ATPase activity of the ATP-dependent potassium channel KATPase [Ashcroft & Kakei, 1989]. However, the difference in the steric and electronic properties of the sulphur over the oxygen impacts ATP hydrolysis in most enzymes due to a change in magnesium coordination [Eckstein, 1983; Cohn, 1982; Frey & Sammons, 1985]. Although AMPPNP and ATPγS are useful ATP mimics when studying ATP binding, they have both been shown to be hydrolysed by various enzymes. For example, AMPPNP hydrolysis was observed by the motor domain of the ncd kinesin-related protein and a cAMP-dependent protein kinase A (PKA) [Suzuki *et al.,* 1997; Bastidas *et al.,* 2013]. ATPγS hydrolysis was detected with the actomyosin subfragment-1 and the eukaryotic translation initiation factor eIF4A [Resetar & Chalovich, 1995; Peck & Herschlag, 2003]. ATPγS and AMPPNP will also hydrolyse spontaneously at $<$ pH 7.

Orthovanadate (VO_3^{-3}), a mimic of the γ phosphate group, substitutes for the released inorganic phosphate following ATP hydrolysis. Consequently, incubation of ATPases with ATP and orthovanadate yield an ADP-V_i-bound state [Shimizu & Johnson, 1983]. Thus, samples incubated with ATP+V_i can be assumed to contain an ADP+V_i following ATP hydrolysis. Structures of the maltose ABC importer $MalFGK_2$ from *E.coli* co-crystallised with nucleotide analogues and transitions states highlight the difference between the AMPPNP bound state and the ADP+V_i transitions state. Whereas the γ phosphate group adopts a tetrahedral geometry in the AMPPNP bound state, the vanadate binds in a trigonal bipyramidal geometry mimicking the ATP-hydrolysis transition state [Oldham & Chen, 2011].

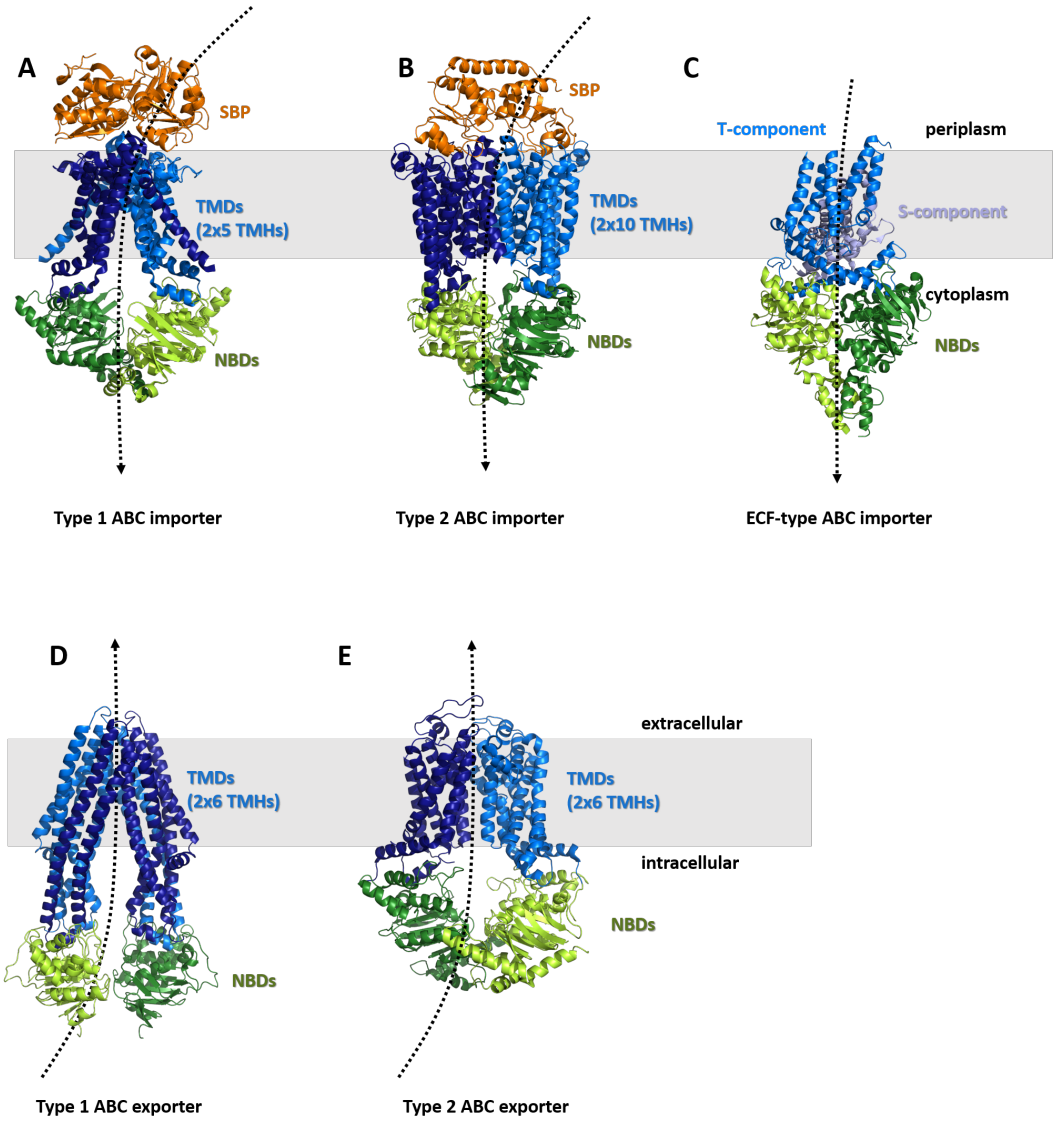


Figure 1.4 – Structures of different ABC transporter folds. From A to E: Type 1 importer ModBC-A from *Archaeoglobus fulgidus* [Locher *et al.*, 2002], type 2 importer BtuCD-F from *E. coli* [Hollenstein *et al.*, 2007], ECF-type importer EcfAST from *Lactobacillus brevis* [Xu *et al.*, 2013a], type 1 ABC exporter ABCB10 from *H. sapiens* [Shintre *et al.*, 2013] and type 2 ABC exporter ABCG5/G8 *Homo sapiens* [Lee *et al.*, 2016]. TMDs are presented in blue and NBDs in green with different shades indicting different polypeptide chains. Periplasmic SBPs are presented in orange. The dashed arrows indicated potential substrate pathways. Labels indicate the minimal number of TMHs required for the transporter fold.

1.2.5 ABC importers and exporters

In contrast to the highly conserved NBDs, the transmembrane region of ABC transporter can vary significantly in their fold and number of transmembrane helices (TMH; 10-20 TMHs). Thus, ABC transporters are categorised into five different types according to their TMD fold; type 1 ABC importers, type 2 ABC importers and energy-coupling factor (ECF) type ABC importers, as well as type 1 and type 2 ABC exporters (Fig. 1.4). Transporters of the type 1, 2 and ECF-type ABC importers are only found in prokaryotes, whereas type 1 exporters exists in both prokaryotes and eukaryotes. Type 2 exporters have only been identified in eukaryotes so far. The classification of the different TMD folds into importers and exporters was based on prokaryotic ABC transporter function. However, it is worth noting that although the vast majority of ABC transporters with the eukaryotic exporter fold are actually exporters, there are a number of ABC transporters with this fold that in fact have an importer function. Examples of these include the N-retinylidene-phosphatidylethanolamine importer ABCA4 found in retinal photoreceptor cells [Quazi *et al.,* 2012] and malate importer ABCB14 in Arabidopsis [Lee *et al.,* 2008]. However, nowadays the term "exporters" is used in reference to the fold rather than the transport direction.

Type 1 and 2 ABC importers

Type 1 ABC importers have at least ten TMHs, with each transporter half contributing five TMHs forming the minimal functional unit of type 1 importers, as observed for the methionine importer MetI [Kadaba *et al.,* 2008]. Molybdate importer ModB [Hollenstein *et al.,* 2007] and maltose importer MalGF [Oldham *et al.,* 2007] have additional two or four TMHs, respectively. In the type 1 importer fold, TMH2-TMH5 of one transporter half form the transport gate, whereas TMH1 wraps around the four other helices (Fig. 1.4A).

In contrast, type 2 importers form larger TMDs with a minimal number of 20

TMHs and ten TMHs in each transporter half. The BtuCD structure, which was the first type 2 importer solved [Locher *et al.,* 2002], revealed that TMH2-5 and TMH7-10 within one transporter half are structurally related by a pseudo two-fold symmetry. The dimer interface is formed from TMH5 and TMH10 of opposing subunits (Fig. 1.4B).

ECF transporters

ECF transporters, required for uptake of micro-nutrients, such as vitamins and trace metals, can be regarded as a third family of ABC importers. Although, their transport is coupled to ATP hydrolysis facilitated by NBDs that are structurally similar to the other ABC importers and exporters. their transmembrane domain is not formed by dimerisation of two TMDs. Instead it consists of a conserved transmembrane protein (T-component) and a substrate specific transmembrane protein (S-component). S-components share little sequence identity (∼15 %), but share a common fold of 6 TMHs (Fig. 1.4C). ECF transporters do not require a soluble SBP [Rodionov *et al.,* 2009].

Type 1 ABC exporters

The first ABC exporter structure solved was the lipid flippase MsbA from *E. coli* [Chang & Roth, 2001]. It was initially incorrectly interpreted, but was subsequently corrected after another exporter structure, namely the bacterial multi-drug transporter Sav1866 from *S. aureus* was published [Chang *et al.,* 2006; Dawson & Locher, 2006; Ward *et al.,* 2007b] (Fig. 1.4D). The TMDs of type 1 ABC exporters consist of a minimum of twelve TMHs, formed by dimerisation of two half transporters, that contributes six TMHs each. These six helices interact with each other in a domain swap arrangement, in which two helices of one chain interact with the other four helices of the adjacent chain. Particular striking in comparison to the importer fold is the elongation of the transmembrane helices into the cytoplasmic

space, leading to the NBDs being separated from the membrane by $\sim$ 25 Å, compared to only $\sim$ 10-15 Å for the bacterial importers. In particular, TMH2 to TMH6 in both transporter halves, are up to 55 residues long (Fig. 1.4D). Two short helices, inserted between TMH2 and TMH3 and between TMH4 and TMH5, connect the TMHs on the cytoplasmic side. These small helices, referred to as coupling helices, run parallel to the membrane plane and form the main interaction surface with the NBDs. The N-terminus has a short so-called elbow helix (ELB) that runs parallel along the intracellular face of the membrane and kinks into the first TMH.

Type 2 ABC exporters

The ABCG5/G8 structure revealed a novel mammalian ABC transporter fold, that was named "type 2 ABC exporter" in accordance with the classification in prokaryotes (Fig. 1.4E). This fold distinguishes itself from the "type 1 exporter" fold by its lack of a domain swap arrangement and the shorter TMDs that are comparable to prokaryotic ABC importers. Nonetheless, the TMDs differ structurally from type I or type II ABC importers. Although ABCG5/G8 was found in a nucleotide-free inward-facing state, the NBDs interact with each other at their far cytoplasmic ends via a subfamily G specific NPXDF motif [Lee *et al.,* 2016].

Structures of prokaryotic and eukaryotic ABC exporters are summarised in Table 8.1.

1.2.6 Type 1 ABC exporters in different conformations

The outward-facing state of Sav1866 is characterised by the upper half of the TMDs opening up into two wings to allow access to the centre of the transporter, whereas the lower half of the TMDs are tightly packed against each other, restricting access of the core towards the cytoplasmic side. The helices of two TMDs are swapped, so that TMH1-2 of one chain and TMH3-6 of the other chain form one wing [Dawson & Locher, 2006]. The same conformation of Sav1866 was obtained

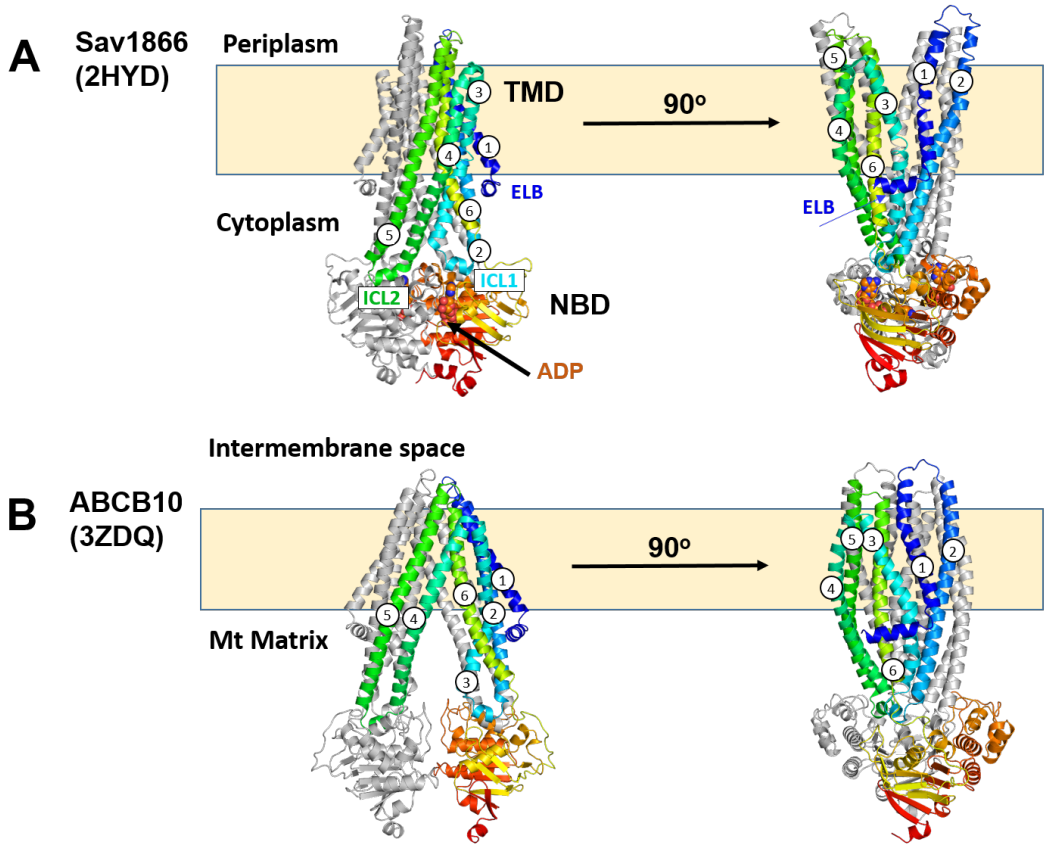


Figure 1.5 – Representation of two distinct conformational states of the alternating-access cycle. A) Sav1866 (2HYD) in the ADP (coloured according by element: C/P=orange, N=blue, O=red) bound outward-facing state and B) ABCB10 (3ZDQ) in a nucleotide-free inward-facing state. Both are shown as cartoon representations perpendicular to the two-fold symmetry axis embedded in the membrane as front view and rotated 90º around their symmetry axis. Chain A is shown in grey and chain B in rainbow colours with transmembrane helices labelled from 1-6. In addition, the elbow helix (ELB), as well the intracellular coupling helices (ICL1 and ICL2) are labelled. Membrane boundaries were obtained from the OPM database [Lomize *et al.*, 2012].

with AMPPNP bound in the nucleotide binding site when Sav1866 crystals were soaked with AMPPNP after co-crystallisation in the presence of ADP [Dawson & Locher, 2007b] (Fig. 1.5A).

ABCB10 shows how the domain-swap composition changes in the alternating-access cycle [Shintre *et al.,* 2013]. In this state access to a substrate binding cavity in the transmembrane part is possible from the intracellular/matrix side by separation of the NBDs and TMDs forming an upside-down V-shape (Fig. 1.5B). One arm of the "V" is formed by TMH1, TMH2, TMH3 and TMH6 of one chain with TMH4 and TMH5 of the adjacent chain. The hinge at the top of the upside-down "V" is provided by the short extracellular/intermembrane loops (ECL) between TMH3-TMH4 and TMH5-TMH6. The structural monomers have to undergo dimerisation in addition to a 90^o rotation against each other in order to convert into the outward-facing state. The alternating-access cycle involves the conversion from an inward to an outward-facing state. However, the structure of the antimicrobial peptide transporter McjD from *E.coli* exhibits an intermediate transition state, which occludes access to a large substrate binding cavity from both sides [Choudhury *et al.,* 2014].

For the inward-facing states of ABCB10 observed with either AMPPNP or AMP-PCP bound, as well as in the nucleotide-free form, the NBDs are separated to different extents (Fig. 1.6). The distance between the ABC signature motif (C_α of first conserved glycine) and the Walker A motif (C_α of the last conserved glycine) can range from 20 Å for the fully open AMPPCP-bound state to 16 Å in the more occluded AMPPCP-bound form. In solution a broad distribution of the NBD separation in the inward-facing state is observed [Mishra *et al.,* 2014; Verhalen *et al.,* 2017]. Crystal packing might have influenced the extent of opening for the ABCB10 and other crystal structures in inward-facing states. In contrast, the NBDs come as close as 11-12 Å for the outward-facing open state of Sav1866 and the outward-facing occluded state of McjD.

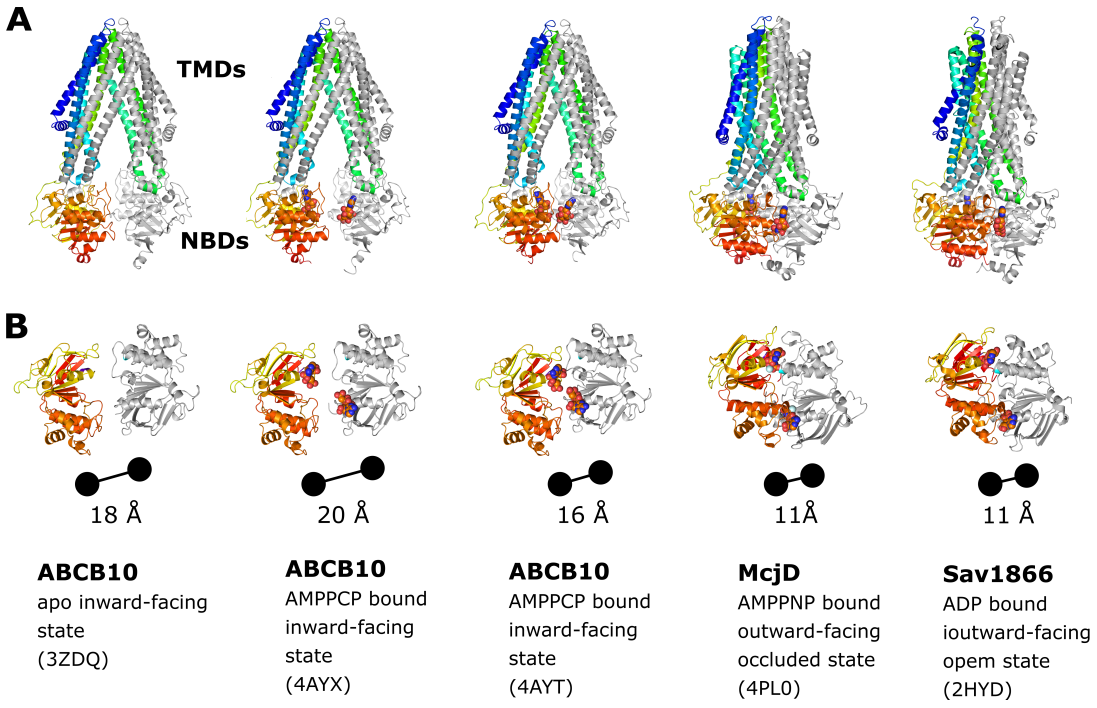


Figure 1.6 – Comparison of inward-facing states of ABCB10 (3ZDQ,4AYX, 4AYT) as a representative of an eukaryotic ABC B-family transporter with outward-facing occluded and outward-facing open states of McjD (4PL0) and Sav1866 (2HYD), respectively. A) Transporters are presented perpendicular to their twofold symmetry axes with chain A presented in grey and chain B presented in rainbow colouring according to residue number (from dark blue (N-terminus) to red (C-terminus)). Nucleotides are presented in spheres coloured according to elements (C/P=orange, N=blue, O=red). B) NBDs presented with view from the membrane to indicate different extent of opening. Lines and labelled length describe measured C_α-C_α distance between first glycine of ABC signature motif in chain A (cyan) and last conserved glycine in Walker A motif of chain B (purple).

1.2.7 Coupling between the NBDs and TMDs

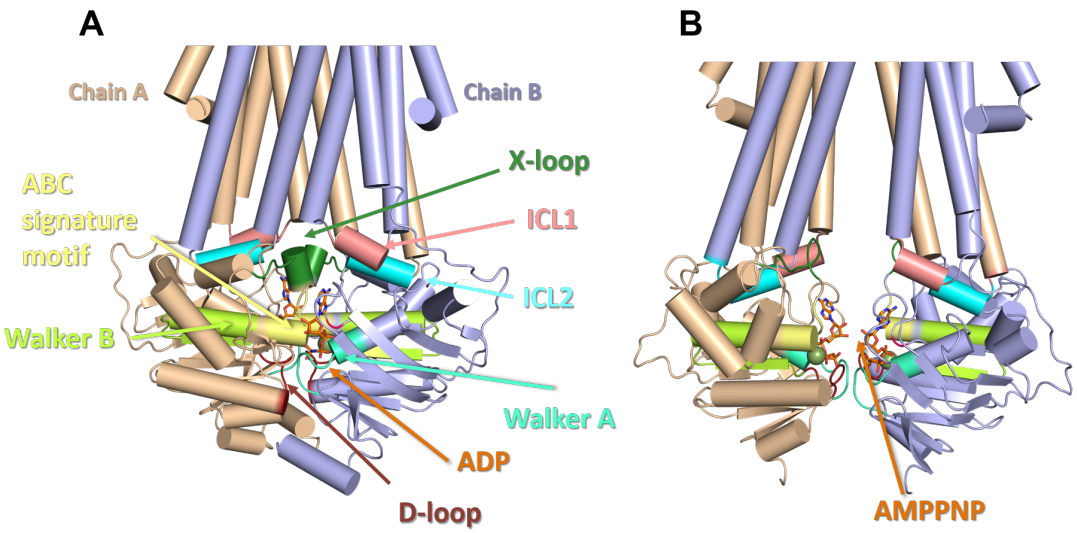


Figure 1.7 – Coupling helices ICL1 (TMH2-3) and ICL2 (TMH4-5) link ATP binding and hydrolysis in the NBDs to conformational changes in the TMDs. Position of ICL1 (salmon) and ICL2 (cyan) in interaction with X-loop (green) and glutamine in Q-loop (pink) in Sav1866 (A, 2HYD) and AMPPCP-bound ABCB10 (B, 4AYX). Colouring of cylindrical representation of helices is according to motif as labelled. ADP and AMPPNP are shown as sticks with colouring according to element (C/P= orange, N=blue and O=red).

Energy released by ATP binding and hydrolysis has to be transferred from the NBDs to the TMDs in order to trigger conformational changes that allow substrate translocation accross the membrane. In ABC exporters, the intracellular loops form so-called "coupling-helices" [Dawson & Locher, 2006] between TMH2 and TMH3 (ICL1) and TMH4 and TMH5 (ICL2), respectively. The coupling-helices, which lie parallel to the membrane plane, have a shared interface between the TMDs and the NBDs in a typical exporter domain-swap arrangement, in which ICL1 interacts with both NBDs, and ICL2 only with the NBD of the adjacent transporter half. In the outward-facing Sav1866 (2HYD) and MsbA (3B60) structures and the occluded McjD (4PL0) structures, ICL1 interacts with residues downstream of the Walker A motif of the same chain and the residues of the so-called X-loop in the adjacent chain (Fig. 1.7A). The X-loop with the sequence ϕ-x-ϕ-x-(E/N)-(K/R)-G (ϕ=hydrophobic; x=any residues) is only conserved in ABC exporters and precedes

the ABC signature motif in the α-helical subdomain.

In the outward-facing and occluded states of Sav1866 (2HYD), MsbA (3B60) and McjD (4PL0) X-loops of two transporter chains interact with each other and the ICLs. Communication between the X-loop and the nucleotide binding domain is mediated by the ABC signature motif, that follows the X-loop sequence in the primary sequence. In the inward-facing states of ABCB10, the X-loop is disordered due to the lack of interactions with ICL1 or the Q-loop (Fig. 1.7B).

1.2.8 Alternating access mechanism in type 1 ABC exporters

In 1966 Jardetzky proposed the alternating-access mechanism for facilitated transport of substrates across membranes, in which a transporter undergoes conformational changes rocking between two states that grant access to only one side of the membrane at a time (Fig. 1.8A) [Jardetzky, 1966]. The mechanism was suggested before any structural data were available and has been shown to hold true in a broader sense for most membrane transporters in various solute carrier families, as well as for the ABC transporter family.

An asymmetrical alternating-access mechanism for P-glycoprotein was proposed by Senior *et al.* [1995], which suggested ATP hydrolysis in the two catalytic sites would take place in an alternating fashion with only ATP binding and hydrolysis in one site at a time driving transport (Fig. 1.8B). This proposal was dismissed by Higgins & Linton [2004] in their ATP switch model (Fig. 1.8C). In accordance with Jardetzky, they suggested a symmetrical switch between an inward- and outward-facing state in the transport cycle. According to their model ATP binding and hydrolysis takes place simuntanuously in both catalytical sides. ATP binding but not hydrolysis is suggested as the "power stroke" required for converting the transporter from a high affinity state that binds the substrate on one side (inward-facing state for exporters) to a low affinity state for substrate release on the opposite side

(outward-facing state for exporters). It was proposed that ATP and substrate binding was required to cause dimerisation of the NBDs and the subsequent conformational changes in the TMDs. Following hydrolysis of ATP, ADP and P_i are released and the transporter can be restored to the initial state.

However, the ATP switch model does not explain AMPPCP and AMPPNP bound inward-facing states, as observed recently in crystal structures of TM287/288 and ABCB10, in which the NBDs remained separated (Fig. 1.8D). This challenges the proposal that the conformational change from inward-facing to outward-facing state is triggered by ATP binding as the power stroke.

It might also be suggested that both ATP binding and transport substrate binding is required for the dimerisation of the NBDs. The scheme in Fig. 1.8D also addresses the questions of whether the order of transport substrate and ATP binding is crucial for the alternating-access mechanism. Moreover, occluded states, in which the substrate binding cavity is not accessible from either side of the membrane, were observed in crystal structures of McjD from *E.coli* and PCAT from *Clostridium thermocellum*, co-crystallised in the presence of AMPPNP and ATPγS, respectively [Choudhury *et al.,* 2014; Lin *et al.,* 2015]. Consequently, the alternating access mechanism of ABC exporters is extended to include these states as depicted in panel D of Fig. 1.8.

On the basis of the PglK structure, which was solved in an inward-facing state without nucleotide at high resolution (2.9 Å) and in an outward-facing state in the presence of ADP at low resolution (5.9 Å), an "outward-only mechanism" for lipid transport in ABC exporters was proposed (Fig. 1.8E) [Perez *et al.,* 2015; Locher, 2016]. The crucial aspect of this mechanism is that the inward-facing state is suggested not to be populated under physiological relevant conditions. Instead, the transporter cycles between a fully outward-open and a partially occluded outward-facing state. First the lipid linked oligosaccharide (LLO) substrate binds on the transporter surface adjacent to the lipid bilayer, followed by ATP binding and flip-

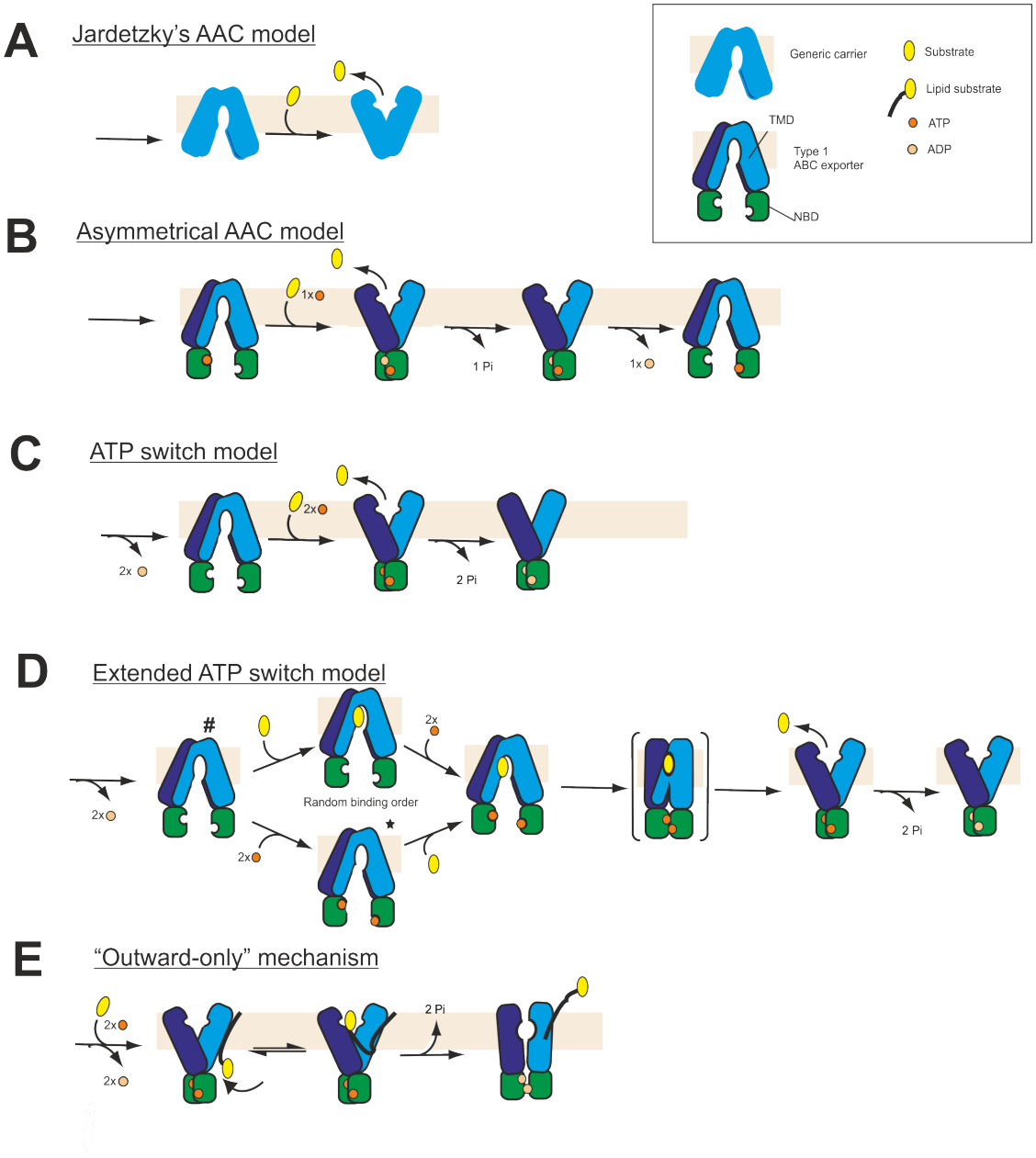


Figure 1.8 – Alternating access mechanisms proposed for ABC exporter. TMDs are represented in blue and NBDs in green. Different shades indicate transporter halves. Transport substrate is shown in yellow, ATP in orange and ADP in beige. A) Alternating access mechanism as first proposed by Jardetzky [1966] for carriers B) Asymmetric mechanism proposed for P-glycoprotein by Senior *et al.* [1995]. C) ATP switch model for ABC transporters proposed by Higgins & Linton [2004]. D) Extended ATP switch model including order of substrate and nucleotide binding, as well as an occluded state as discussed in Shintre *et al.* [2013]. E) "Outward-only" mechanism for lipid transport of ABC exporters as proposed in Perez *et al.* [2015].

ping of the lipid. Finally, ATP-hydrolysis causes separation of the NBDs allowing exchange of ADP and ATP in the outward-facing state and conversion of the TMD to a state of low LLO binding affinity.

It remains unclear how ATP binding and hydrolysis changes the conformation of the TMDs, and what role substrate binding and release plays in the alternating-access cycle. As Kaspar Locher pointed out in his review [Locher, 2016], one mechanism might not fit all ABC exporters and could be influenced by substrate type (hydrophobicity and size) or fold (diversity within ABC exporters; ABCB family versus ABCG family). For structures solved by X-ray crystallography and recently cryo-EM, we predominantly observe the inward-facing state. Moreover, all eukaryotic ABC transporters have been solved in inward-facing states to date. Structures in different conformations of the same or similar transporters are necessary to follow conformational changes from one state to the other (section 5.1). Thus, structural information in particular on eukaryotic ABC exporters are desired to fill these gaps in the alternating access cycle and understand whether there are deviations from the conformational states observed in bacterial ABC exporters.

1.2.9 Eukaryotic ABC transporters

Classification of eukaryotic ABC transporters

Eukaryotic ABC transporters can be divided into seven subfamilies (A-G), although only subfamilies A-D and subfamily G have transmembrane domains and act as transporters. Transporters of the subfamilies A and B can either dimerise from two TMD-NBD half transporters or come as full transporters from one TMD-NBD-TMD-NBD polypeptide chain. The subfamily C is only encoded as full transporters with all four domains on one polypeptide chain. In contrast, the subfamily D consists of dimerised half transporters TMD-NBD (with exception of some full transporters of the D family found in certain land plants). For the subfamily G the arrangement of TMDs and NBDs is swapped and can exist as either half or

full transporters (only half transporters in humans). ABCE and ABCF proteins only consist of the nucleotide binding domain in the so-called ABC2 structure with two NBD domains conjugated. These soluble proteins are involved in ribosome recycling [Shoemaker & Green, 2011; Pisarev *et al.,* 2010] and translation initiation [Paytubi *et al.,* 2009], respectively. They are classified into the ABC transporter family due to their clear evolutionary link to the other ABC transporter NBDs. ABCB, ABCC. ABCE and ABCF transporters are found in all eukaryotic organisms studied to date [Xiong *et al.,* 2015]. Humans, like most other eukaryotic organisms, have ABC transporters of all seven subfamilies, and 49 ABC transporters in total.

Phylogeny of eukaryotic ABC transporters

Phylogenetic analysis of the NBDs suggests dividing the seven subfamilies into three groups. ABCA and ABCG form one group having the same NBD ancestor. This NBD ancestor fused with different TMDs to half transporters to form the subfamily A and G. Evidence for that is given by the different order of fusion found in the subfamily A and G, but also the significantly different length of the TMDs in A and G. The second major group is formed by ABCB, ABCC and ABCD transporters. The similarity between the NBDs in this group is particularly high (30% between the ABCB and ABCC tranporter NBDs, 25% between the ABCB and ABCD transporter NBDs and 24% between the ABCC and ABCD transporter NBDs). A common progenitor for the ABCB, ABCC and ABCD transporters is likely to be a half transporter that already developed in the prokaryotic life form. In contrast to the subfamily A and G, this half transporter only diverged into transporters of the B,C or D family, after fusion of TMDs and NBDs. Full transporters with all four domains on one chain could have arisen from heterofusion (fusion of two divergent half transporters) and homofusion (fusion of two half transporters that were recently duplicated). Some transporters of the subfamily B, that were subject to homofusion, show high similarity between the two transporter halves. The third

group is formed by ABCE and ABCF NBDs [Xiong *et al.*, 2015].

Structures of eukaryotic ABC transporters

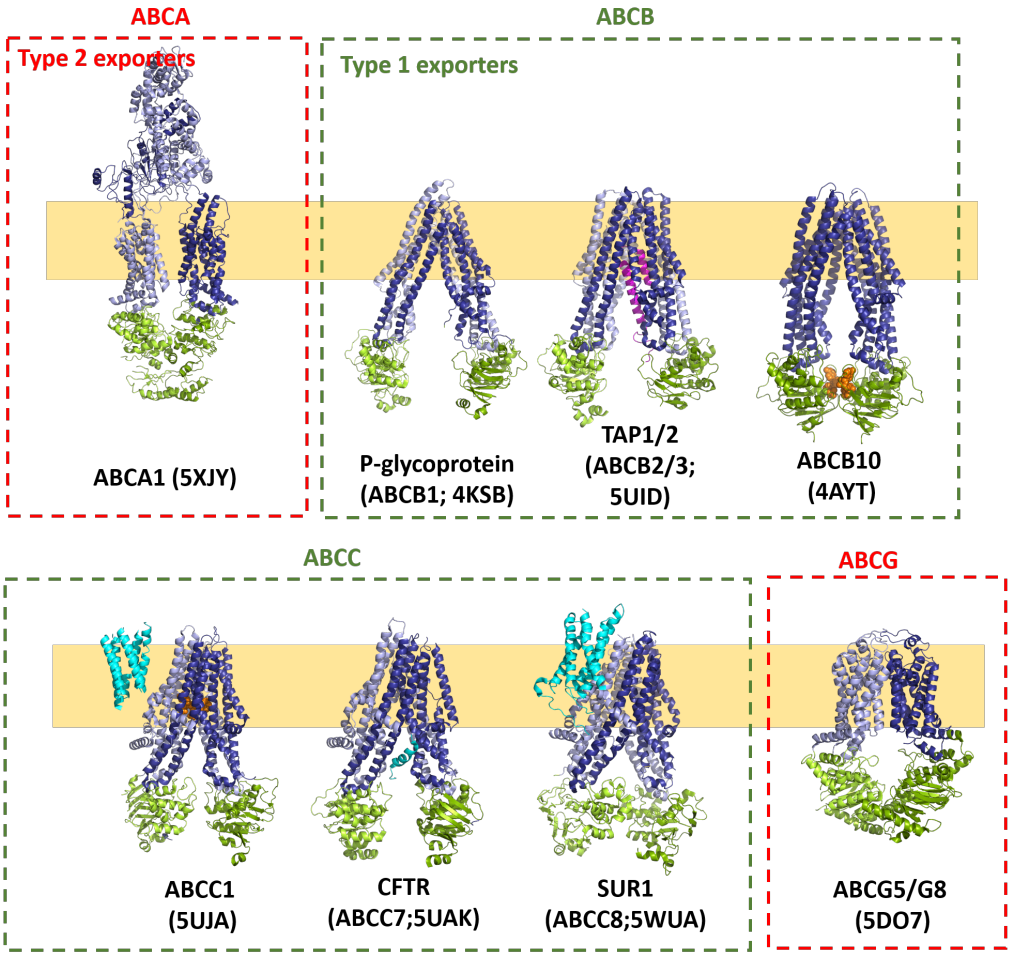


Figure 1.9 – Collection of representative mammalian ABC transporter structures of the ABCA, ABCB, ABCC and ABCG subfamilies. Structures are presented in cartoon representation with TMDs (blue) and NBDs (green) coloured in same shades for homo-dimeric half transporters and different shades for hetero-dimeric half transporters or full transporters according to Fig. 1.1. Nucleotide and substrates are presented as orange spheres and pink cartoons, respectively. Membrane boundaries are indicated as a yellow boxes.

Structural biology made a big leap over the last two years with cryo-electron microscopy enabling structure determination of proteins of the size of ABC transporters and smaller without the requirement for crystallisation. This recent development brought a wealth of novel mammalian ABC transporter structures. With the exception of the subfamily D, we now have information on the TMD folds of

the ABCA, ABCB, ABCC and ABCG families. ABC transporters of the ABCB and ABCC families are found to have the type 1 exporter fold in the core TMD domains and are structurally similar to the bacterial ABC exporters like Sav1866 or MsbA (Fig. 1.9).

In particular, the subfamily B structures of the full transporter P-glycoprotein (ABCB1) [Ward *et al.,* 2013], heterodimer forming half transporter TAP1/2 (ABCB2/3) [Oldham *et al.,* 2016] and homodimer forming half transporter ABCB10 [Shintre *et al.,* 2013] only show conformational variations unlikely to be a special feature of the transporters themselves. These differences are more likely to be the result of different conformational states, as explained in section 1.2.8 of this chapter. Some transporters of the subfamily B carry extra N-terminal domains, as observed for TAP-like transporter (ABCB9), required for correct sub-cellular localisation, but not for transport activity [Abele & Tampé, 2004]. However, no structural information is available to date of its structure.

ABC transporters of the subfamily C carry N-terminal TMD0 domains that are at least partly embedded in the lipid bilayer, but whose functions are poorly understood. The SUR1 (ABCC8) cryo-EM structure was solved as a large complex consisting of the Kir 6.2 potassium channel tetramer bound to four ABC transporters. The C-terminal domain of ABCC8 interacts with the potassium channel and subsequently acts as regulator between the ABC transporter and potassium channel function [Li *et al.,* 2017; Martin *et al.,* 2017]. In contrast, the N-terminal domain (turquoise domain in Fig. 1.9) in the cryo-EM structure of ABCC1, the multidrug resistance protein 1 (MRP1), is poorly resolved reflecting its high degree of flexibility [Johnson & Chen, 2017], perhaps due to the absence of an interaction partner (Fig. 1.9). Cystic fibrosis transmembrane conductance regulator (CFTR) (ABCC7), which was solved for a zebra fish and a human homologue [Zhang & Chen, 2016; Liu *et al.,* 2017] by cryo-EM is structurally similar to other representative of the C subfamily. However, CFTR has an ion channel function instead of being a substrate transporter. Its function is regulated by ATP binding in the

NBDs and phosphorylation of the R domain, that connects the two transporter halves.

The aforementioned type 2 ABC exporter fold, that was first observed for the subfamily G transporter ABCG5/G8, was also found in the cryo-EM structures of the homodimer ABCG2 (a multi drug resistance protein over-expressed in various cancer types) and ABCA1 (a lipid transporter responsible for high density liposomes (HDL) maturation) [Taylor *et al.,* 2017; Qian *et al.,* 2017], reflecting the phylogenetic similarity of the ABCA and ABCG subfamilies, as predicted in Xiong *et al.* [2015]. Furthermore, the fold seems to be independent of the order of TMDs and NBDs in the primary sequence, as only ABCG but not ABCA subfamily transporters exhibit a reversed TMD-NBD order. ABCA genes encode proteins of ∼250 kDa size, including large extracellular domains, as observed in the cryo-EM structure of ABCA1 [Qian *et al.,* 2017]. In ABCA1 these domains are inserted between TMH1 and TMH2 (ECD1) and TMH7 and TMH8 (ECD2) and interact with apoA-I, the protein component forming HDLs (Fig. 1.9).

1.3 Mitochondrial ABC transporters

1.3.1 Mitochondrial metabolism

Structure and origin of mitochondria

Mitochondria have two membranes (an inner and outer mitochondrial membrane), which is a relict of the endosymbiosis. Both membranes have to be crossed by small molecules and proteins, so that they can enter the mitochondrial matrix. The inner membrane encloses the matrix and is highly invaginated, providing a large surface area for the processes involved in respiration [Cogliati *et al.,* 2013]. The outer mitochondrial membrane has 2-3 nm pores, that are freely permeable by ions and small molecules [Colombini, 1979]. The inner mitochondrial membrane

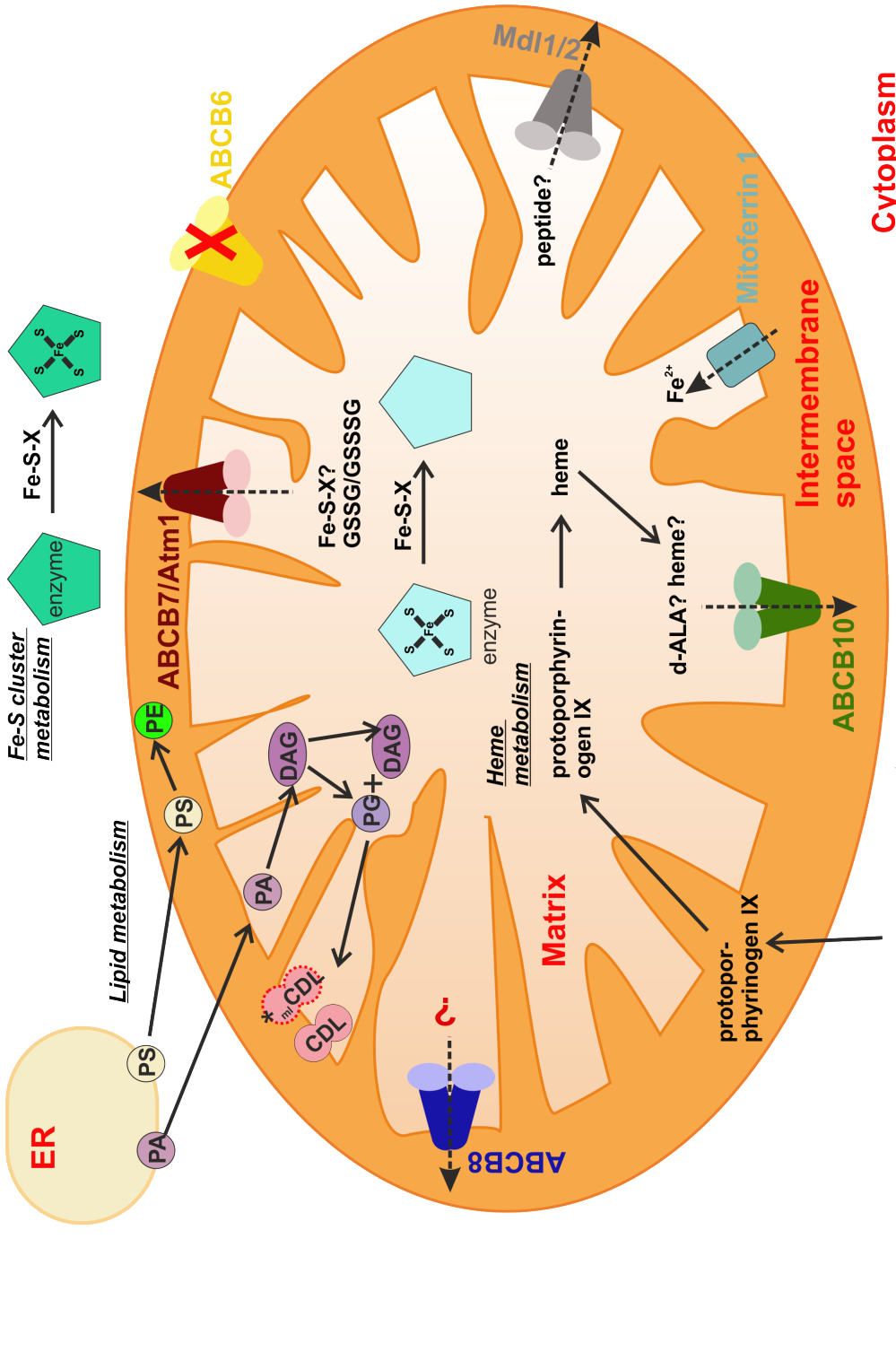


Figure 1.10 – Scheme representing mitochondrium with selection of metabolism relevant for understanding mitochondrial ABC transporter function.

is impermeable to ions and small molecules, therefore transporters are required to move solutes across the membrane.

Mitochondria originated from the insertion of an α-proteo-bacterium into another prokaryote, the process that lead to the development of all eukaryotic cells [Andersson *et al.,* 1998; Gray & Doolittle, 1982; Gray *et al.,* 1989]. It was hypothesised that the increase in energy supply provided by the endosymbiont enabled complexity of eukaryotic cells by providing the energy to maintain and express proteins from a 200,000-fold bigger genome compared to a simple prokaryotic cell [Lane & Martin, 2010]. During the change from living as an independent prokaryote to an organelle inside eukaryotic cells, mitochondria lost genetic material or transferred it to the cell nucleus. Only 13 genes, mainly encoding proteins for the respiratory complexes, remained in the mitochondria to allow for responsive gene regulation. Approximately, 1000 (e.g. *Saccharomyces cerevisiae*) proteins found in mitochondria are encoded in the cell nucleus and expressed in the cytoplasm [Gabaldón & Huynen, 2004; Sickmann *et al.,* 2003]. Therefore, transport of proteins into the mitochondrial matrix requires protein translocation systems in both membranes-the so-called translocases for the outer (TOM) and inner membrane (TIM) [Neupert & Herrmann, 2007; Schmidt *et al.,* 2010].

Mitochondria perform many different roles in metabolism including the tricarboxylic acid cycle and the oxidative phosphorylation. They are also required for vital functions in the cell, such as β-oxidation, iron and copper metabolism and phospholipid synthesis [Smith & Robinson, 2011].

Iron related metabolism in mitochondria

Mitochondria are key players in heme and iron-sulphur (Fe-S) cluster synthesis and both these processes have been associated with ABCB transporters in the inner mitochondrial membrane. Iron, required in heme and Fe-S cluster biogenesis, is imported via the solute carriers mitoferrin 1 and 2 [Paradkar *et al.,* 2009; Shaw

et al., 2006].

Heme (iron-protoporphyrin) is required as a prosthetic group in haemoglobin, myoglobin and cytochromes (e.g. electron transport chain) and sulphite oxidase (amino acid synthesis). The heme biosynthesis pathway requires enzymes in the mitochondrial matrix and intermembrane space, as well as in the cytosol. The first step of the pathway is the production of δ-aminolevulinic acid (d-ALA) in the mitochondria, followed by synthesis of coproporphyrinogen III via several cytosolic enzymes and subsequent transformation into protoporphyrinogen IX in the intermembrane space. In the final step the iron is incorporated into protoporphyrinogen IX by the ferrochelatase in the mitochondrial matrix. Subsequently, heme used outside of the mitochondria, has to be exported. Little is known about the transport processes that shuttle precursors (e.g. d-ALA, protoporphyrinogen) or heme itself across the inner mitochondrial membrane.

Fe-S clusters are another important cofactor of many enzymes both in the cytosol and mitochondria. They are involved in the electron transport chain, redox reactions, ribosome assembly, DNA damage repair and DNA replication. Fe-S clusters are assembled in the mitochondrial matrix with the proteins ISCU or NFU1 acting as a scaffold [Adam *et al.,* 2006; Wiedemann *et al.,* 2006]. Iron-glutathione complexes have been proposed as iron donors binding to glutaredoxin for transferring the iron [Wingert *et al.,* 2005] onto the scaffold. In the mitochondrial matrix the Fe-S clusters can be transferred from the scaffold into the target proteins by chaperones. Cytosolic Fe-S cluster proteins require the synthesis machinery of the mitochondria to be functional in order for their Fe-S clusters to be formed, but it remains unclear, how the Fe-S clusters pass the inner mitochondrial membrane (reviewed in Xu *et al.* [2013b]).

Lipid metabolism in mitochondria

Phospholipids phosphatidyl ethanolamine (PE) and cardiolipin (CDL) are synthesized solely in the mitochondrial membrane and need phosphatidic acid (PA) and phosphatidyl serine (PS) as precursors, respectively. However, both these precursors are generated in the membranes of the endoplasmic reticulum (ER). The enzymes necessary for converting PS into PE are located in the mitochondrial intermembrane space, so that PA has to be transported into the inner leaflet of the outer membrane or the outer leaflet of the inner mitochondrial membrane, both of which face the intermembrane space. The enzymes that convert PA into CDL are mainly found in the mitochondrial matrix, where they catalyse the conversion of PA into CDP-diacylglycerol (CDP-DAG) and then PG. Subsequently, cardiolipin synthase combines one CDP-DAG and PG molecule to form a CDL molecule. Further maturation of CDL involves deacylation aided by the cardiolipin-specific phospholipase A Cdl1. Following this, monolyso-CDL is flipped to the outer leaflet of the inner mitochondrial membrane, where subsequent reacylation with unsaturated acyl chains takes place (reviewed Tamura *et al.* [2014]).

1.3.2 ABC transporters in mitochondria

Mitochondria have a distinct function compared to their predecessor, the α-proteobacterium, so their transport systems have evolved to fulfil the requirements of an organelle in a cell. Most of the transporter function required in mitochondria for shuttling a variety of compounds like amino acids, nucleotides, di- and tricarboxylates and vitamins is fulfilled by $\sim$30 "carrier" proteins. These carrier proteins are thought to substitute for the versatile function of the many ABC transporters once used in the ancestor of the mitochondrium [Lill & Kispal, 2001]. Thus, in mitochondria, the number of ABC transporters is comparatively small, varying from only two in yeast and three in plants and metazoan. All mitochondrial ABC transporters are members of the subfamily B (apart from the mitochondrial subfamily

C cytochrome c maturation complex CcmAB, which is only found in plants [Schulz *et al.,* 1999]). Phylogenetic analysis revealed that these subfamily B mitochondrial transporters show early separation from the ABCB clade during evolution and they are closer to α-proteobacterial ABC half transporters than other subfamily B members [Xiong *et al.,* 2015]. ABCB7, ABCB8 and ABCB10, as well as the fungal homologues Atm1, Mdl1 and 2, have an N-terminal mitochondrial targeting sequence and are translocated into the inner mitochondrial membrane via TIM and TOM complex. This targeting sequences are not conserved and were found to be over 100 amino acids long (e.g. mouse ABCB10 [Graf *et al.,* 2004]) They are removed by a mitochondrial matrix peptidase (MPP) in order to provide full function of the transporter. In Atm1 ATPase activity was only detectable after removal of the 58 amino acids on the N-terminus [Srinivasan *et al.,* 2014]. ABCB8 and ABCB10 are phylogenetically more distantly related to bacterial ABC transporters and in contrast to ABCB7, they are only found in metazoa. ABCB8 and ABCB10 show a high homology with the primary sequence of yeast Mdl1 and Mdl2 (Fig. 1.11, Fig. 8.1) (32% and 42% sequence identity for ABCB8 or ABCB10 with Mdl1 and 2 [Lill & Kispal, 2001]). ABCB6, another B-family transporter was proposed to be located in the outer mitochondrial membrane with its NBDs facing the cytosol [Mitsuhashi *et al.,* 2000; Paterson *et al.,* 2007; Krishnamurthy *et al.,* 2006]. However, the subcellular localisation of ABCB6 is ambiguous, with experimental evidence that ABCB6 is also found in the plasma membrane and in the Golgi-apparatus [Paterson *et al.,* 2007; Krishnamurthy *et al.,* 2006; Tsuchida *et al.,* 2008].

ABCB7

ABCB7 and its fungal homologue Atm1 are phylogenetically the closest to the bacterial homologues (e.g *Na*Atm1 [Lee *et al.,* 2014]) (Fig. 1.11) [Schaedler *et al.,* 2015]. Knock-outs or mutations of yeast Atm1 and mouse ABCB7 show a similar phenotype, in which iron homoeostasis is impaired and iron accumulates in

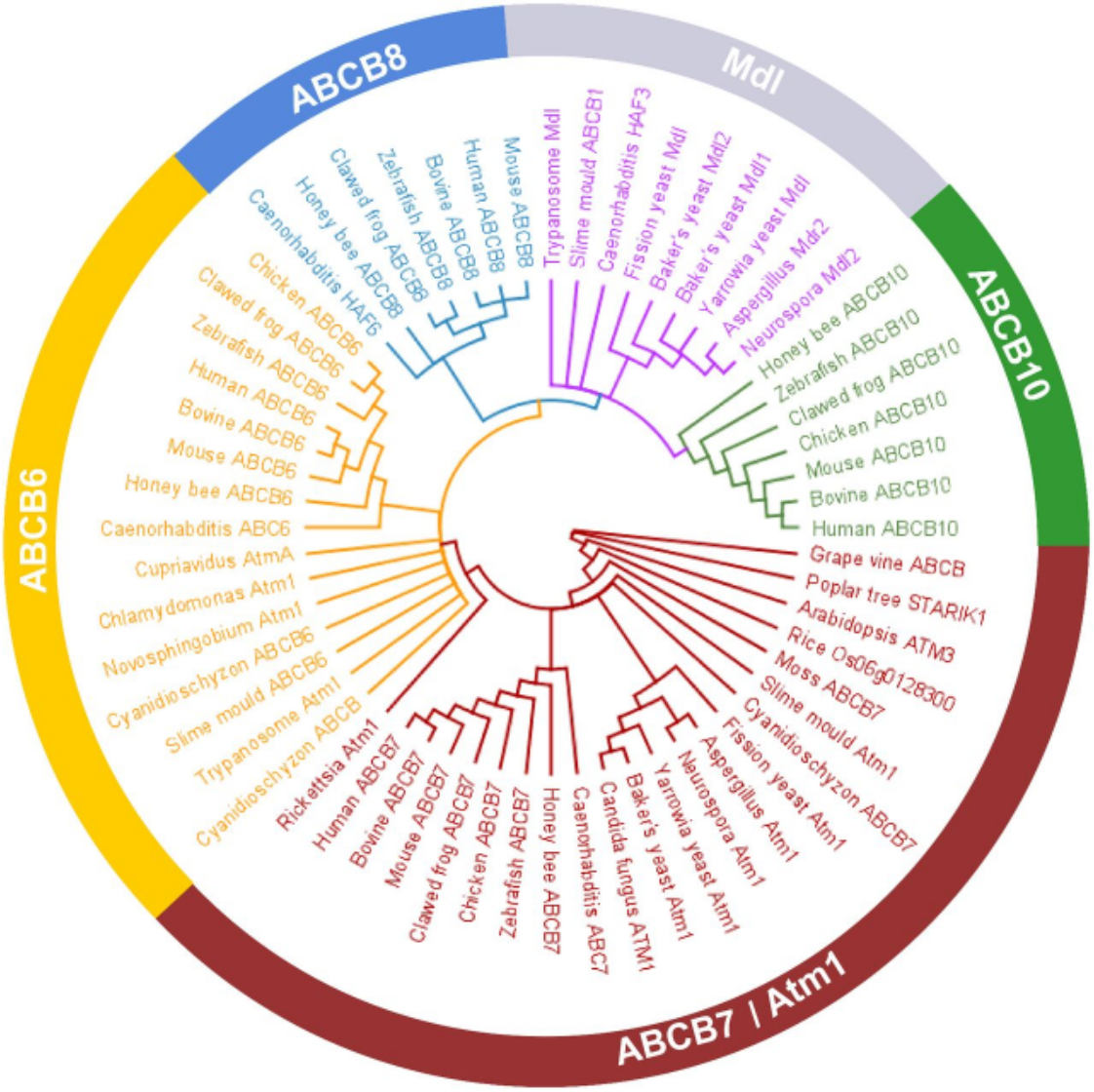


Figure 1.11 – Phylogenetic analysis of mitochondrial ABC transporters of the B-family with model organisms covering the evolutionary spectrum generated with the Geneious 6.1.6 server (Figure taken from Schaedler *et al.* [2015])

the mitochondria, causing oxidative stress and DNA damage [Kispal *et al.,* 1997; Pondarré *et al.,* 2006; Pondarré *et al.,* 2007]. In addition, defects of the cytosolic but not mitochondrial Fe-S cluster proteins for Atm1, ABCB7 and ATM3 (plant homologue of ABCB7 in *Arabidopsis*) knock outs are observed. It remains unclear, whether these phenotypes observed are primarily caused by lack of Atm1/ABCB7 function, or are secondary effects caused by impaired mitochondrial function due to triggered oxidative stress. Pathogenic mutations in human ABCB7 can cause X-linked sideroblastic anaemia, a disease linked to impaired iron homoeostasis [Kispal *et al.,* 1999; Lill, 2009; Bernard *et al.,* 2013; Pondarré *et al.,* 2006]. On the basis of these phenotypes a Fe-S cluster precursor was proposed as transport substrate. Transport into inverted vesicles formed of Atm1 containing lactococcus was shown for an iron-glutathion complex and GSSSG, both mimicking potential Fe-S cluster precursors, as well as oxidised glutathion itself [Qi *et al.,* 2014; Li & Cowan, 2015; Schaedler *et al.,* 2014; Lee *et al.,* 2014; Kessler, 2006]. Inward-facing structures of GSH bound yeast Atm1 and GSSG bound *Na*Atm1, a bacterial Atm1 homologue from *Novosphingobium aromaticivorans*, give insights into how a glutathione-based transport substrate could bind in the central cavity of the transporter. However, GSH and GSSG coordination in the inward-facing state seems incomplete and reveals little interaction between the substrate and the transporter.

Mdl1 and Mdl2

The conservation of potential binding site residues observed in the ABCB10 structure with Mdl1 or Mdl2 is particularly striking [Shintre *et al.,* 2013]. It was demonstrated in inverted vesicles that Mdl1 can transport peptides [Young *et al.,* 2001]. However, both peptide transport into proteoliposomes, as well as stimulation of ATPase activity in presence of the peptide, could not be recorded in a second study. However, the second study was performed with protein purified in the harsh detergent foscholine-14, that is known to unfold membrane proteins [Hofacker *et al.,* 2007]. Unexpectedly, it was shown that over-expression of Mdl1 could replace

the function of Atm1 in yeast [Chloupková *et al.,* 2003].

ABCB10

ABCB10 was linked to heme biosythesis, as suggested on the basis of ABCB10 knock-out studies in mice. Homozygous knock-outs died *in utero* after 12 days with the embryos showing a reduced heme content [Hyde *et al.,* 2012]. In contrast heterozygous knock-outs were apparently healthy, although hearts from these animals showed increased damage under induced oxidative stress after ischemia and reperfusion [Liesa *et al.,* 2011]. The question remains as to whether ABCB10 is directly involved in heme biosynthesis, transporting a precursor into mitochondria or the final heme product out of the mitochondria. Erythrocytes with hindered ABCB10 function lack heme, and this effect could be overcome by external addition of the heme precursor d-ALA [Bayeva *et al.,* 2013]. However, ABCB10 knockouts in hematopoietic cells also showed an accumulation of protoporphyrin IX and iron accumulation in mitochondria [Yamamoto *et al.,* 2014]. The accumulation of protoporphyrin IX contradicts the idea that d-ALA export is facilitated by ABCB10, as protoporphyrin IX accumulation indicates intact d-ALA synthesis and subsequent cytosolic steps in the heme biosythesis. It has also been proposed that ABCB10 may interact with the mitochondrial iron importer mitoferrin-1, stabilising this transporter and thus iron import [Chen *et al.,* 2010b]. Given the number and diversity of the roles proposed for ABCB10, it is clear that the role of ABCB10 in mitochondria, and the nature of its transport substrate, is still unknown.

ABCB8

ABCB8 was first mentioned in the literature as ABC transporter 1 (M-ABC1), an ABC transporter associated with the mitochondrial membrane on the basis of a polyclonal antibody tagged with fluorescein that co-localised with MitoTracker Red in HEK cells [Hogue *et al.,* 1999]. Five slicing variants of the canonical sequence

(735 amino acids long;$\sim$ 80 kDa have been reported, whereas all of the isoforms contain the transporter core consisting of one TMD and one NBD region forming a half transporter (Fig. 1.12). Homodimer formation has been demonstrated by detection of a 120-130 kDa and a larger 160-170 kDa complex in crosslinking experiments in ABCB8 over-expressing HEK293 cells and subsequent SDS-PAGE analysis [Ardehali *et al.,* 2005a]. ABCB8 over-expressing HEK293 cells showed that the first 55 amino acids of ABCB8 act as a mitochondrial targeting sequence, as studies in Hogue *et al.* [1999] by generating a $^{1-55}$ABCB8-EGFP construct that was targeted to the mitochondria, whereas EGFP alone remained in the cytosol [Hogue *et al.,* 1999]. Although ABCB8 is located in the inner mitochondrial membrane, it is encoded in the cell nucleus. Thus, ABCB8 tagged with an N-terminal targeting sequence has to be translocated into the inner mitochondrial membrane using the TOM and TIM protein translocation machinery and subsequently the targeting sequence is removed by a matrix peptidase [Neupert & Herrmann, 2007]. MitoFates predicted the TOM20 recognition motif as Leu-Val-His-Leu-Phe and the mitochondrial peptidase (MPP) cleavage site as Phe25 in human ABCB8(Fig. 1.12) [Fukasawa *et al.,* 2015]. The wheel presentation of the N-terminal sequence in ABCB8 shows the helix has significant amphipathic character, with positively charged residues facing one side of the helix (Fig. 1.13). This has been shown to be a secondary structure feature of mitochondrial targeting sequences [von Heijne, 1986].

ABCB8 was shown to protect mitochondria against oxidative stress and ischemia, as siRNA down-regulation of ABCB8 in HEK293 cells increased levels of reactive oxygen species [Ardehali *et al.,* 2005b]. Ichikawa *et al.* [2012] analysed the effects of ABCB8 knock-outs on mice heart and in neonatal rat cardiomyocytes (NRCM) in more detail. Cardiac specific knock-outs of ABCB8 in mice, induced by tamoxifen treatment when ABCB8 expression was under the control of the cardiac-specific α-myosin heavy chain promoter, produced a phenotype that exhibited impaired pumping action and contractility of the heart muscle after four weeks. There were

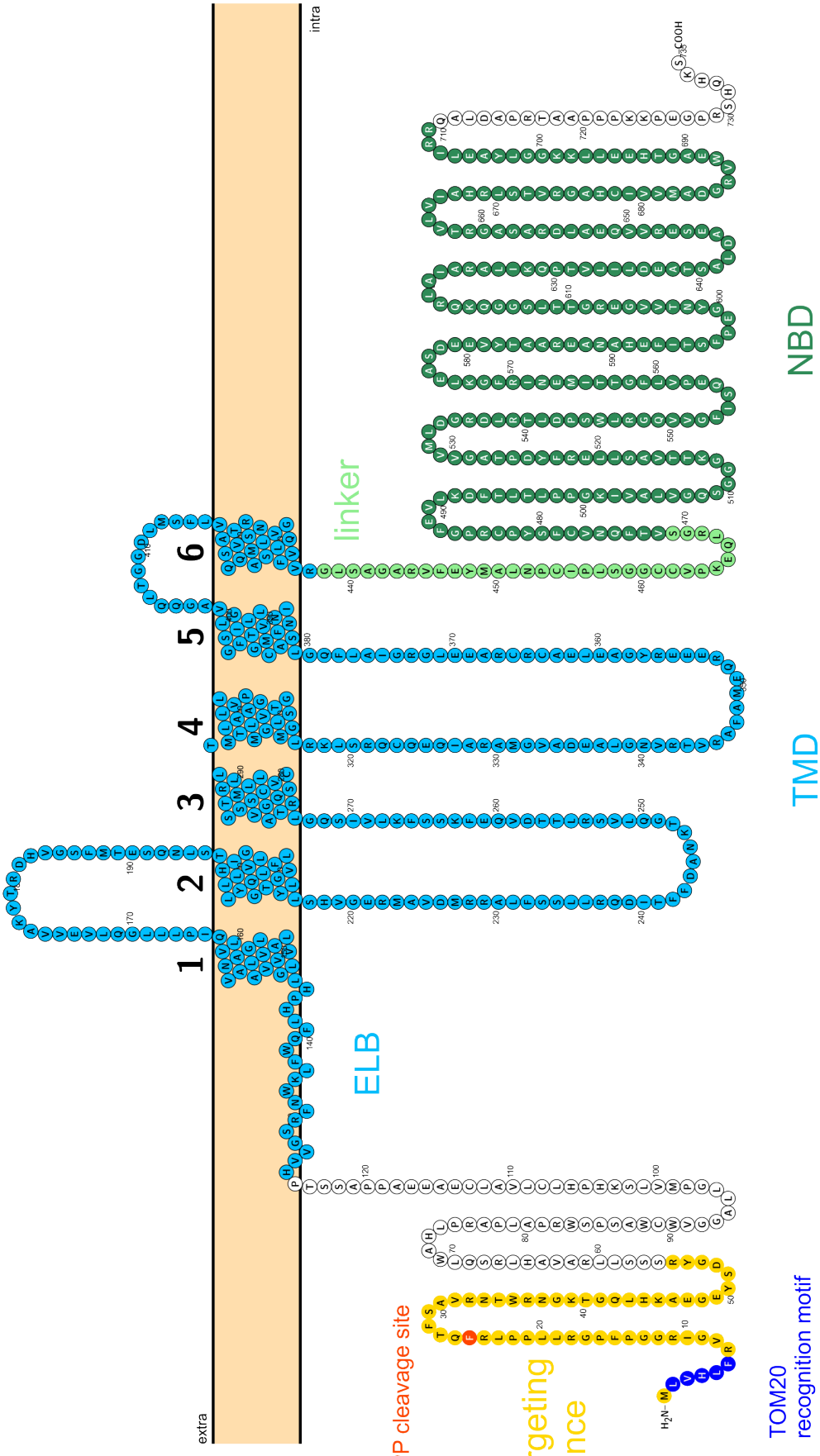


Figure 1.12 – Topology model of human ABCB8 isoform 1 as analysed with OCTOPUS [Viklund & Elofsson, 2008] and visualised with PROTTER [Omasits *et al.*, 2014]. The TMD and NBD region is coloured in blue and green, respectively. The signalling sequence is depicted in yellow with the TOM20 recognition sequence in dark blue and the MPP cleavage site in red, both predicted with MitoFates [Fukasawa *et al.*, 2015].

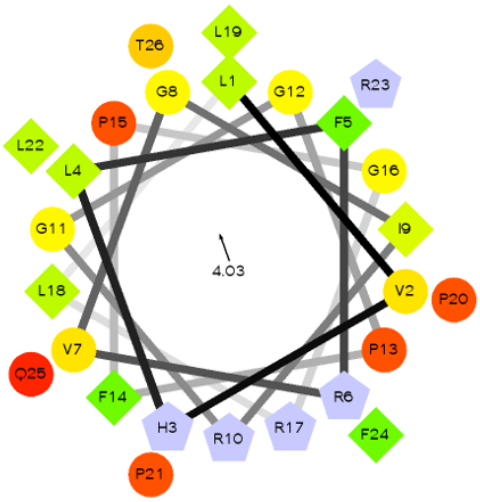


Figure 1.13 – Wheel presentation of the predicted signalling sequence showing amphipathic character created with wheel.pl,v 1.4 (Dr Raphael Zidovetzki)

also changes in the appearance of the heart after 8 weeks (increase of heart weight and elevated left venticular diastolic diameter) with severe fractional shortening and reduction of the cardiac output (volume of blood pumped per min). These changes in heart power, leading to cardiomyopathy but not complete heart failure, were also reflected in the histological analysis of the hearts, revealing severe cardiac fibrosis eight weeks after tamoxifen treatment. The ABCB8$^{\Delta/\Delta}$ cardiomyocytes contained large vacuoles and mitochondria with reduced size and deformed cristae. Additionally, cryo-EM of these cells revealed an increase of electron-dense material in mitochondria that was proven to be non-heme iron. The accumulation of iron was further confirmed by down-regulation of ABCB8 levels with siRNA in NRCM, in which radioactive iron was held back in mitochondria, whereas ABCB8 over-expression reversed the effect. Furthermore, iron export from HEK cell mitochondria was elevated upon ABCB8 over-expression. Lipid peroxidation in the ABCB8$^{\Delta/\Delta}$ mice heart supports the hypothesis that ABCB8 is protective against reactive oxygen species. However, reactive oxygen species were only found in NRCM after additional exposure to hydrogen peroxide. Increased iron levels in mitochondria under down-regulated ABCB8 conditions correlated with decreased enzymatic activity of cytosolic Fe-S cluster proteins, such as xanthine oxidase and

cytosolic aconitase. In contrast, mitochondrial iron sulphur cluster proteins, such as the complex II of the electron transfer chain remained unaffected [Ichikawa *et al.,* 2012].

The fact that ABCB8 was over expressed in doxorubicin resistant leukemic cells and several melanoma cell lines lead to the assumption that ABCB8 mediates doxorubicin resistance and that doxorubicin could be a transport substrate for ABCB8 [Gillet *et al.,* 2004; Heimerl *et al.,* 2007]. Elliott & Al-Hajj [2009] showed that 80% knock down of ABCB8 with shRNA leads to increased mitochondrial DNA damage, thought to be induced by doxorubicin itself. However, this hypothesis of DNA damage caused by doxorubicin was later discounted and attributed to the raised iron levels and the reactive oxygen species associated with doxorubicin. The mode of action for doxorubicin induced toxicity was proposed to be one of an iron chelator shuttling iron into the mitochondria and preventing its export, as well as reducing iron export by inhibiting ABCB8 expression in the cell nucleus. Treatment with doxorubicin increased iron levels in NRCM mitochondria drastically. ABCB8 over-expression reduced cardiomyopathy, induced by doxorubicin in NRCM, and decreased lipid peroxidation by decreasing iron levels due to additional iron export. Additionally, ABCB8 deletion mutants increased the cardiotoxic effect of doxorubicin [Ichikawa *et al.,* 2014]. It was suggested that ABCB8 would function as an exporter for non-heme iron in mitochondria [Ichikawa *et al.,* 2012; Ichikawa *et al.,* 2014].

Although ABCB8 deletion had similar effects on cytosolic iron sulphur cluster maturation as ABCB7 had, it is unproven whether ABCB8 transports an Fe-S cluster precursor that binds iron, another iron chelator or iron itself. It cannot be excluded the the observed phenotypes of ABCB8 knock-outs are secondary effect caused by impairing other crucial mitochondrial pathways. In order to study ABCB8 in an isolated system *in vitro*, a purification protocol has to be established. Additionally, developing a protocol for reconstitution of ABCB8 into proteoliposomes is essential for identifying and studying a putative transport substrate.

1.4 Introduction to purification and crystallisation

Obtaining structural information with X-ray crystallography and cryo-EM requires a monodisperse and pure protein sample. For X-ray crystallography sufficient amounts of material (0.1-0.3 mg of protein for testing 96-well crystal conditions) are required as well. Unfortunately, expression and purification strategies are almost impossible to be predicted on the basis of protein fold and can vary significantly even for homologues. Being the major bottle neck for structure determination, optimisation of expression and purification strategies have to be considered carefully and can be subject to extensive optimisation including choice of expression systems and conditions, protein construct, extraction and purification detergents and buffer conditions.

1.4.1 Expression and purification of eukaryotic membrane proteins

Heterologous expression in baculoviral insect cell systems [Ciccarone *et al.,* 1998] using *Spodoptera frugiperda* or *Trichoplusia ni* have been successfully applied for structure determination of a broad range of different IMPs including mammalian ABC transporters ABCA1 and ABCB10 [Qian *et al.,* 2017; Shintre *et al.,* 2013]. Although more expensive and time-extensive, over-expression in HEK293 cells had been particular successful for eukaryotic ABC transporter structures such as TAP1/2, ABCC1, SUR1 and ABCG2 determined using cryo-EM [Johnson & Chen, 2017; Zhang *et al.,* 2017; Liu *et al.,* 2017; Martin *et al.,* 2017; Li *et al.,* 2017; Taylor *et al.,* 2017].

Due to their partially hydrophobic nature, integral membrane proteins (IMPs) have to be extracted from cell membranes using detergents, that cover their hydrophobic surface and therefore are used to solubilise and stabilize IMPs in aqueous solutions.

This procedure often results in denaturation and aggregation of the proteins. This solubilisation step has an important impact on protein stability throughout the whole purification process. Consequently, finding the right detergent that keeps the protein stable is crucial for the success of the structure determination [Carpenter *et al.,* 2008]. The length of the hydrophobic chain including variations, such as cyclic additions (Cymals) or saturation of the chain, as well as the head group type (zwitterionic, ionic and non-ionic), affect the extent of extraction and the preservation of the fold of the protein. Although ionic and zwitterionic detergents have a greater ability to disrupt the membrane bilayer and therefore allow for better extraction, they often have a negative effect on non-covalent interactions in the secondary and tertiary structure of the protein [Thomas & Tate, 2014]. Non-ionic detergents interfere less with the protein structure and consequently can stabilize the membrane protein.[He *et al.,* 2014; Carpenter *et al.,* 2008]. However, the chain length and detergent head group required for preserving the protein fold cannot be predicted and has to be discovered empirically.

1.4.2 Expression and purification of eukaryotic ABC transporters

Obtaining a high yield is particularly challenging for IMPs, since their production can be limited as over-expression of a membrane protein can cause toxicity to the host (e.g. increase in membrane permeability), require specific membrane translocation and insertion machineries or a certain lipid environment [Mancia & Love, 2010]. Although over-expression in *E. coli* or yeast is inexpensive, time-saving and allows for easy genetic manipulation, both expression systems often do not provide the right expression environment in particular for mammalian IMPs with complicated post-translational modifications and specific protein-lipid interactions [Gulati *et al.,* 2014]. However, *Pichia pastoris* or the related *Komagataella pastoris* were successfully applied for expression of mouse and *C. elegans* P-glycoprotein,

as well as human ABCG5/G8 (Table 1.1) [Jin *et al.,* 2012; Aller *et al.,* 2009; Lee *et al.,* 2016].

N-dodecyl-β-D-maltoside (DDM) has been shown to be efficient in stably extracting membrane proteins of various kinds [He *et al.,* 2014] including most of the eukaryotic ABC transporters for which a structure could be solved (Table 1.1). However, this observation might be biased, as DDM is often used as an default option for purifying membrane proteins in most laboratories favouring homologues and constructs that are stable in DDM. The addition of lipids, as well as chemical modifications of the surface, can be used to overcome stabilisation and crystallisation problems.

1.4.3 Crystallisation of eukaryotic ABC transporters

With the immense improvements in resolution in cryo-EM, six novel eukaryotic ABC transporter structures were deposited into the pdb within the last two years. However, the vast majority of ABC transporter structures were previously solved by X-ray crystallography using vapour diffusion crystallisation of detergent solubilised protein. In this process, a small volume of protein in buffer containing precipitant (150 nL-2 μL) is equilibrated against a reservoir solution containing buffer with higher concentrations of precipitant. The protein containing solution can be placed as a "sitting drop" or "hanging drop". As both protein solution and reservoir solution are placed in a closed system, vapour diffusion will equilibrate the system, so that the precipitant concentration in the protein drop is increased slowly over time. This leads to over-saturation of the protein solution and subsequently to potential nucleation and crystal formation (red horizontal arrow in Fig. 1.14). Crystallisation is aborted with removal of protein and return to an under-saturated protein solution (red vertical arrow) or if equilibration proceeds towards precipitation (dotted red arrow) [Patrick, 2007].

Establishing conditions in which the protein crystallises requires screening crystalli-

Table 1.1 – Expression and purification of eukaryotic ABC transporters for structure determination using X-ray crystallography and cryo-EM

ABC Transporter	**Organism**	**Expression system**	**Purification detergent**	**Detergent/lipid in structure**	**Method**	**Ref.**
ABCA1	*H.sapiens*	*Sf9*	DDM/CHS	digitonin	cryo-EM	[Qian *et al.*, 2017]
P-glycoprotein (ABCB1)	*C.elegans*	*P. pastoris*	DDM	n-undecyl-β-d-thiomaltopyranoside	crystallography	[Jin *et al.*, 2012]
P-glycoprotein (ABCB1)	*Mus musculus*	*P. pastoris*	DDM	DDM	crystallography	[Aller *et al.*, 2009]
TAP1/2	*H. sapiens*	*Komagataella pastoris*	DDM	C12E8	cryo-EM	[Oldham *et al.*, 2016]
Atm1	*S. cerevisiae*	*E.coli*	DDM	DDM	crystallography	[Srinivasan *et al.*, 2014]
ABCB10	*H.sapiens*	*Sf9*	DDM/CHS, DDM/CDL	DDM/(CHS or CDL)	crystallography	[Shintre *et al.*, 2013]
MRP1(ABCC1)	*Bos taurus*	HEK293	LMNG/CHS	digitonin	cryo-EM	[Johnson & Chen, 2017]
CFTR(ABCC7)	*Danio rerio*	HEK293	LMNG/CHS	digitonin	cryo-EM	[Zhang *et al.*, 2017]
CFTR(ABCC7)	*H.sapiens*	HEK293	LMNG/CHS	digitonin	cryo-EM	[Liu *et al.*, 2017]
SUR1 (ABCC8)	*Cricetus cricetus*	HEK293	digitonin	digitonin	cryo-EM	[Martin *et al.*, 2017]
SUR1 (ABCC8)	*Mesocricetus auratus*	HEK293	digitonin	digitonin	cryo-EM	[Li *et al.*, 2017]
ABCG2	*H.sapiens*	HEK293	DDM/CHS	nanodiscs	cryo-EM	[Taylor *et al.*, 2017]
ABCG5/G8	*H.sapiens*	*Komagataella pastoris*	DMNG/cholate/CHS	bicelles	crystallography	[Lee *et al.*, 2016]

sation conditions in a 96-well format (150 nL drops). Initial crystallisation trials normally use so-called sparse-matrix screens containing a set of selected conditions that were shown to facilitate membrane protein crystallisation [Newstead *et al.*, 2008; Iwata, 2003] (section 3.2.7). Subsequently, follow-up screens are used with variation around the conditions that gave initial protein crystals.

Nucleation is essential for crystallisation and can be slow. The "seeding" method, in which small crystals of the same (homogenous seeding) or a different crystal form (heterogenous seeding) are added to the crystallisation drop, can facilitate crystal growth out of the nucleation phase.

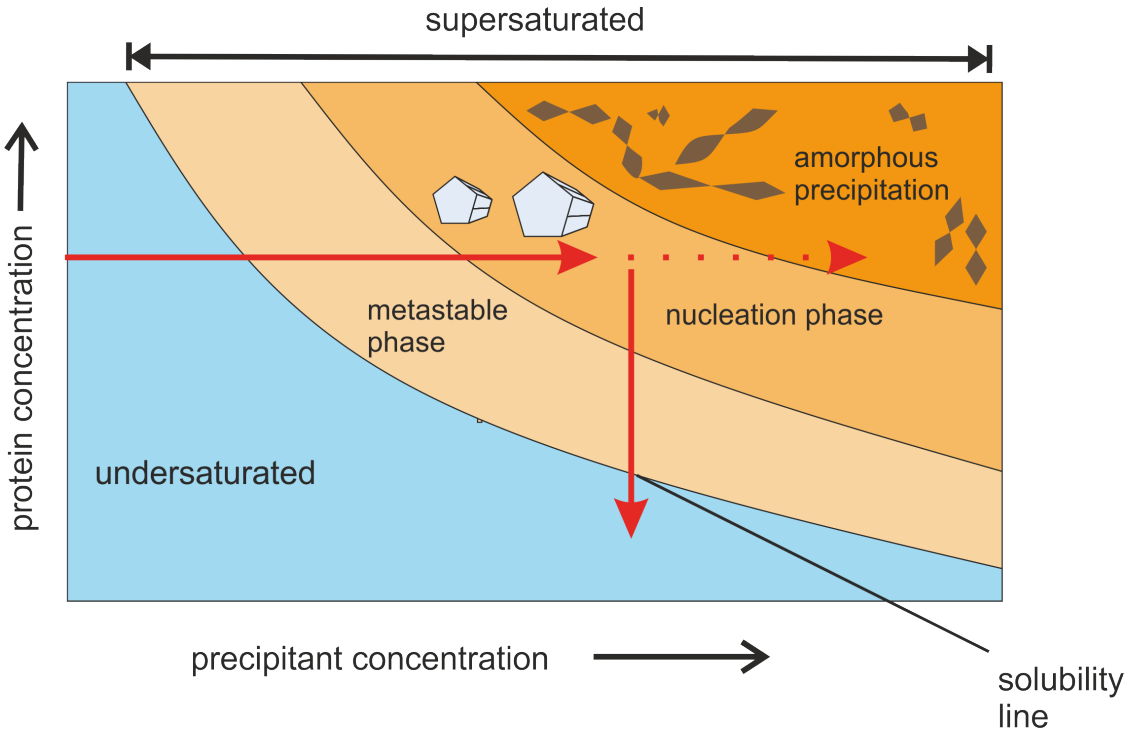


Figure 1.14 – Schematic crystallisation phase diagram for vapour diffusion crystallisation presented as function of initial protein concentration used in the crystallisation experiment over the precipitant concentration changing over time. Red arrows indicate an example trajectory for crystal formation (horizontal line) and abortion of crystallisation (vertical line and horizontal dotted line).

In addition to challenges in the protein production pipeline, finding the right hydrophobic environment for tight crystal packing presents another hurdle, for example, detergents are required that simultaneously provide stability for the membrane protein (with their longer hydrophobic chain) but at the same time do not hinder

formation of crystal contacts [Privé, 2007]. DDM was also suitable for crystallisation of *C. elegans* P-glycoprotein and human ABCB10 [Aller *et al.,* 2009; Shintre *et al.,* 2013]. Mouse P-gp was crystallised in n-undecyl-β-d-thiomaltopyranoside, a detergent that is structurally related to maltosides. Crystallisation in detergents results in Type II crystals, in which only the hydrophilic surface unoccupied by detergent molecules can form the crystal contacts. Crystallisation techniques that embed the protein in a membrane-like environment, such as lipidic cubic phase (LCP) [Cherezov, 2011], high-lipid-detergent (HiLiDe) crystallisation [Gourdon *et al.,* 2011] or crystallisation in bicelles [Faham & Bowie, 2002] can offer an alternative, as Type I crystals can be formed. Type I crystals have continuous membrane bilayers, that allow membrane proteins to additionally pack in the hydrophobic regions, potentially causing higher order diffraction of the crystals. HiLiDe crystallisation can be performed under standard vapour diffusion conditions after enriching the protein sample with high concentrations of lipid (up to 3 mg/ml) and detergent (up to 15 mg/ml) [Gourdon *et al.,* 2011]. Both the LCP and bicelle approach are methodically more challenging, as they require reconstitution of the protein into the lipid environment. For LCP, developed by Landau & Rosenbusch [1996], the protein is inseretd into a lipidic mesophase formed by lipids such as monoolein or 7.7 and 7.9 MAGs. However, this method remains unsuccessful so far for ABC exporters. ABCG5/G8, that was solved after producing crystals of protein reconstituted into DMPC/cholesterol/CHAPSO bicelles, is the only example of an ABC exporter solved with crystallisation using lipid environments [Lee *et al.,* 2016]. For ABCB10 diffraction was improved after addition of cardiolipin to the detergent during purification and crystallisation [Shintre *et al.,* 2013].

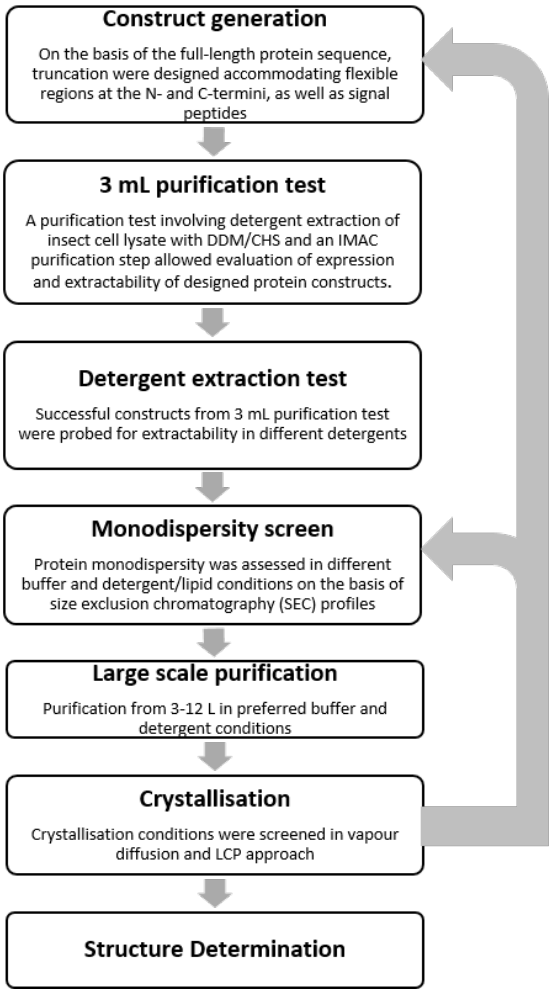


Figure 1.15 – Flow-chart describing the SGC pipeline for membrane proteins from initial screening of constructs to the final structure.

1.4.4 Overview of the membrane protein pipeline at the Structural Genomics Consortium (SGC)

Fig. 1.15 outlines the different steps of optimisation, from construct design to structure determination, performed for human membrane proteins in Prof. Liz Carpenter's group in the SGC. This pipeline approach is based on the optimisation protocol for human soluble proteins previously established at the SGC [Savitsky *et al.,* 2010].

The membrane protein pipeline involves several steps. After construct design, cloning and transfer into the baculo virus expression system, a 3 mL purification test is performed, which gives a first readout of whether the construct can be expressed, as well as extracted and purified in the detergent mix DDM/CHS. DDM/CHS was chosen, as it was shown to extract mainly folded membrane protein [Vanaken *et al.,* 1986; Seddon *et al.,* 2004]. Selected constructs from the 3 mL test are subsequently analysed for extraction in 12 different detergent/CHS combinations using the same scale and purification protocol as for the 3 mL test, but replacing DDM with other detergents successfully used in crystallisation attempts of membrane proteins (section 3.2.2). CHS was added to all detergents tested with this protocol, as it has been shown to stabilise membrane proteins of the SGC pipeline (unpublished data Prof. Liz Carpenter's group) by either directly interacting with the protein or changing the size of the detergent micelles. Since extraction yields do not necessarily reflect the quality of a protein sample and its stability in a certain detergent, a monodispersity screen on a 0.25 -1 L scale, involving a small-scale SEC on the Dionex HPLC system, is used to identify detergents in which the membrane protein remains in a monodisperse stable form. This system also helps to narrow down purification buffer conditions, as well as types of lipids, added during the first purification step (IMAC), facilitating protein stability and crystallisation (section 3.2.3). On the basis of the screened purification conditions, a large-scale purification is performed on a 3-24 L culture volume scale with the

aim of producing a monodisperse protein sample for crystallisation trials (section 3.2.4). Purification conditions are further optimised by testing variations of constructs, addition of lipids and chemical modifications in order to obtain crystals that diffract well enough for data collection and structure solution. In the process of achieving stable protein with diffracting crystals sufficient for three-dimensional structure determination, it is often helpful to return to earlier steps in the pipeline e.g. construct design or monodispersity screening with additional detergents or lipids.

1.4.5 Reconstitution of ABC transporters into proteoliposomes

Most eukaryote ABC transporters with notable exceptions (CFTR or SUR1/2), have been found to function as active transporters that use ATP hydrolysis to transfer substrates of different chemical nature (e.g. lipids, hormones, small hydrophilic molecules and hydrophobic drugs) across the membranes. In order to analyse the transport activity, a two-compartment system is required that traps the transported component for further analysis. For that, purified protein can be inserted into liposomes of any lipid mixture in a process called reconstitution. Although the transport function can be studied in inverted vesicles without the requirement of isolating the protein, more thorough analysis often has to be done on a purified and reconstituted protein sample to avoid misinterpretation of results due to presence of other membrane proteins. Furthermore, the reconstitution allows us to study the lipid composition that is required to obtain full function and identify specific lipids that alter the protein function.

Reconstitution of membrane proteins into lipid bilayers requires mixing of detergent purified protein with detergent solubilised liposomes, followed by the gentle removal of detergent during the incorporation process using polystyrene beads (Bio-Beads), dialysis, SEC or dilution (reviewed in Rigaud & Lévy [2003] and Seddon *et al.*

[2004]). For that, parameters, such as solubilisation detergent, method of detergent removal and lipid composition have to be optimised. Detergents used to solubilise the liposomes prior to reconstitution have to be carefully considered. Detergents such as non-ionic octylglucoside (OG), zwitterionic 3-[(cholamidopropyl)-dimethyl-ammonio]-1-propane- sulfonate (CHAPS) and ionic bile acid salts (sodium cholate and sodium deoxycholate) can be easily removed by dialysis, SEC or dilution due to their high CMCs, but are also harsher and can lead to impairing the membrane protein stability. These removal methods are not suited for milder detergents with low CMCs such as DDM or Triton X-100. However, they can be removed using polystyrene beads, that bind detergents in their hydrophobic pores. The method of detergent removal also has an impact on the rate of insertion of protein into the proteoliposomes. If removal is too quick, the membrane proteins will not have time to insert into the proteoliposomes, which results in precipitation. However, if the detergent removal is too slow, it might impair protein stability due to too long exposure of the membrane protein to the solubilisation detergent [Lévy *et al.,* 1990]. Geertsma *et al.* [2008] describe a reconstitution method for ATP-binding cassette (ABC) transport proteins with polystyrene beads, that has been proven to be an efficient protocol for several ABC transporters.

Table 1.2 – Overview of the lipid composition of the outer (OMM) and inner mitochondrial membranes (IMM) from rat liver as reviewed in [Horvath & Daum, 2013]

	OMM	IMM
Phospholipids (mg/mg protein)	0.45	0.2
Sterols (mg/mg protein)	0.04	< 0.01
	% of phospholipids	
Phosphatidylcholine (PC)	54	40
Phosphatidylethanolamine (PE)	29	34
Phosphatidylinositol (PI)	13	5
Phosphatidylserine (PS)	2	3
Cardiolipin (CDL)	<1	18
Phosphatic acid (PA)	1	-

Besides optimisation of the reconstitution protocol itself, mimicking the lipid com-

position of the native environment of the membrane protein might be important for the reconstitution yield and the its function. In fact, the lipid composition of different organelles in the eukaryotic cell is diverse. Lipids of the mitochondrial membrane have to be considered for reconstitution of ABCB8, since it is embedded in the inner mitochondrial membrane. PC and PE are the most abundant phospholipids with up to 80% in the outer and 74% in the inner mitochondrial membrane. The inner mitochondrial membrane is particularly enriched with CDL (10-15 % of phospholipids). In particular, sterols and sphingolipids are reduced in the inner mitochondrial membrane compared to other cellular compartments (Table 1.2) [Horvath & Daum, 2013].

1.5 Aims of the thesis

The ABC transporter ABCB8, the subject of this thesis, was discovered to be essential for mitochondrial iron homoeostasis and function of cytosolic Fe-S cluster enzymes. Cardiac specific knock-outs of ABCB8 in mice resulted in cardiomyopathy. ABCB8 has a crucial role in normal cardiac function, yet, the direct involvement of ABCB8 in these functions is still unknown. Production of ABCB8 by over-expression and purification is the first step towards the identification of the transport substrate and de-orphanising its role in the mitochondria. Moreover, structural information on orphan ABC transporters can be crucial as conserved residues in potential binding sites can be analysed. The work described in this thesis comprises the establishment of a purification and crystallisation protocol for the human ABC transporter ABCB8 (chapter 3), that sets the foundation for structural and functional studies carried out in the scope of this thesis.

The introduction of this thesis described the structural information on ABC transporters available to date and emphasises the lack of knowledge regarding the coupling of ATP binding and ATP hydrolysis with the conformational changes in the TMDs for ABC exporters. Consequently, the work described in the thesis aimed

at understanding the alternating-access cycle of ABCB8 and the role ATP-binding and hydrolysis plays in conformational changes of the overall transporter. To learn more about different conformations of ABCB8, the function was studied in presence of different non-hydrolysable ATP analogues, ATP-transition state mimics and the hydrolysis product ADP using nano differential scanning fluorimetry (nanoDSF), microscale thermophoresis (MST), an ATPase inhibition assay and lysine cross-linking studies (chapter 4). Despite the wealth in ABC exporters structures, other conformations than the inward-facing state are rare in particular for eukaryotic ABC transporter. However, in order to understand alternating access mechanisms in eukaryotic ABC exporters, structural information of an occluded or outward-facing state is required. Chapter 5 describes the first crystal structure of human ABCB8 at 3.8 Å, that was obtained in an outward-facing state with two ADPs bound in the NBDs. This structure represents a post-ATP hydrolysis state giving a new insight into the alternating access cycle of type 1 ABC exporters in eukaryotes.

CHAPTER 2

Materials and Methods

2.1 Contributions

Construct indicated with * in Table 2.1 were designed by Chitra Shintre, whereas all other constructs and mutants were designed by myself. Cloning of constructs, transfer into the baculo/insect cell expression system, and initial 3 mL purification tests were carried out by the Biotechnology group at the SGC, which is lead by Dr Nicola Burgess-Brown. I performed all subsequent purification optimisation steps from detergent extraction, monodispersity screening to large-scale purification and steps leading to structure determination. All functional studies, as well as the reconstitution protocol were established and carried out by myself.

2.2 Cloning of ABCB8

The ABCB8 gene (UniProt KB identifier Q9NUT2-2) was purchased from the Mammalian Gene Collection (IMAGE-ID:40147981). However, residue numbers used in this thesis refer to the isoform 1 sequence of ABCB8 (Q9NUT2-1). Constructs with different N-terminal and C-terminal truncations of the full length sequence (Table 2.1) and mutants on the basis of ABCB8$^{Ala111-A711}$ (c016) (Table 2.2) were cloned into the pFB-LIC-Bse and pFB-CT10HF-LIC vectors (8.2). Cloning was performed using ligation-independent cloning (LIC) [Haun *et al.*, 1992].

The vectors include an N-terminal tag with a 6x His purification sequence or a C-terminal 10x His and FLAG purification sequence (Fig. 2.1). Both vectors also include a tobacco etch virus (TEV) protease cleavage site between insertion site and purification tags. *S. frugiperda* (Sf9) insect cells in Sf900IITM serum free, protein free insect cell medium with L-glutamine (Thermofisher Scientific) were infected with recombinant baculovirus for virus amplification for 65 h at 27 °C (250 ml in 1 L shaker flasks) and the supernatant containing the virus was harvested for further infections. Baculoviruses were produced by transformation of these vectors into DH10Bac cells.



Figure 2.1 – Plasmids used for cloning ABCB8 in the bacmid expression system with tag-type added to construct.

2.3 Expression of ABCB8 in Sf9 cells

1L Spodoptera frugiperda (Sf9) insect cells in SF900 medium (Invitrogen) were infected at a cell density of 1.0-1.2 10^6/L cells with previously generated recombinant

Table 2.1 – Constructs of ABCB8 isoform 1 (UniProt KB identifier Q9NUT2-1) with N- and C-terminal truncations, vectors and molecular weight in Da. Constructs indicated with * were designed by Dr Chitra Shintre

Construct	N-terminal end	C-terminal end	Vector	Molecular weight (Da)
c001*	M1	S735	pFB-LIC-Bse	78168.1
c002*	G53	S735	pFB-LIC-Bse	74315.5
c003*	P85	S735	pFB-LIC-Bse	70679.3
c004*	G129	S735	pFB-LIC-Bse	66134.9
c005*	M1	D713	pFB-LIC-Bse	75811.4
c006*	G53	D713	pFB-LIC-Bse	71958.9
c007*	P85	D713	pFB-LIC-Bse	68322.6
c008*	G129	D713	pFB-LIC-Bse	63778.3
c009*	P81	S735	pFB-LIC-Bse	71984.8
c010*	G92	S735	pFB-LIC-Bse	70628.2
c011*	P98	S735	pFB-LIC-Bse	70159.6
c012*	A111	S735	pFB-LIC-Bse	68703.8
c013*	P81	A714	pFB-CT10HF-LIC	69699.2
c014*	G92	A714	pFB-CT10HF-LIC	68342.6
c015*	P98	A714	pFB-CT10HF-LIC	67874
c016*	A111	A714	pFB-CT10HF-LIC	66418.2
c017*	P81	H668	pFB-CT10HF-LIC	64626.3
c018*	G92	H668	pFB-CT10HF-LIC	63269.7
c019*	P98	H668	pFB-CT10HF-LIC	62801.1
c020*	A111	H668	pFB-CT10HF-LIC	61345.3
c021*	P81	G685	pFB-CT10HF-LIC	66393.4
c022*	G92	G685	pFB-CT10HF-LIC	65036.8
c023*	P98	G685	pFB-CT10HF-LIC	64568.3
c024*	A111	G685	pFB-CT10HF-LIC	63112.4
c025	G129	A714	pFB-CT10HF-LIC	64628.2
c026	G129	H668	pFB-CT10HF-LIC	59555.3
c027	G129	G685	pFB-CT10HF-LIC	61322.4
c028	G129	A719	pFB-CT10HF-LIC	65053.7
c029	A118	S735	pFB-CT10HF-LIC	67958
c030	A118	A714	pFB-CT10HF-LIC	65672.4
c031	A118	H668	pFB-CT10HF-LIC	60599.5
c032	A118	G685	pFB-CT10HF-LIC	62366.6
c033	A118	A719	pFB-CT10HF-LIC	66097.9
c034	A151	S735	pFB-CT10HF-LIC	64236.6
c035	A151	A714	pFB-CT10HF-LIC	61951
c036	A151	H668	pFB-CT10HF-LIC	56878.1
c037	A151	G685	pFB-CT10HF-LIC	58645.2
c038	A151	A719	pFB-CT10HF-LIC	62376.5
c039	P81	A719	pFB-CT10HF-LIC	70124.7
c040	G92	A719	pFB-CT10HF-LIC	68768.1
c041	P98	A719	pFB-CT10HF-LIC	68299.5
c042	A111	A719	pFB-CT10HF-LIC	66843.7
c043	P81	S735	pFB-LIC-Bse	66448.4
c044	G92	S735	pFB-LIC-Bse	66420.3
c045	P98	S735	pFB-LIC-Bse	66420.3
c046	A111	S735	pFB-LIC-Bse	66445.3
c047	G92	A714	pFB-LIC-Bse	66431.3
c048	P98	A714	pFB-LIC-Bse	66432.3
c049	A111	A714	pFB-LIC-Bse	66446.3
c050	P81	H668	pFB-LIC-Bse	66420.3
c051	G92	H668	pFB-LIC-Bse	66466.4
c052	P98	H668	pFB-LIC-Bse	66450.4
c053	A111	H668	pFB-LIC-Bse	66389.2
c054	P81	G685	pFB-LIC-Bse	66275.1
c055	G92	G685	pFB-LIC-Bse	66363.1
c056	P98	G685	pFB-LIC-Bse	71205.9
c057	A111	G685	pFB-LIC-Bse	69849.3
c058	G92	A718	pFB-LIC-Bse	69380.8
c059	P98	A718	pFB-LIC-Bse	67924.9
c060	A111	A718	pFB-LIC-Bse	67563.7
c061	G129	A714	pFB-LIC-Bse	67095.2
c062	G129	H668	pFB-LIC-Bse	65639.3
c063	G129	G685	pFB-LIC-Bse	63847.4
c064	G129	A718	pFB-LIC-Bse	62490.8
c101*	M1	S718	pFB-CT10HF-LIC	78946.9
c102*	G36	S718	pFB-CT10HF-LIC	75094.4
c103*	P68	S718	pFB-CT10HF-LIC	71458.2
c104*	G112	S718	pFB-CT10HF-LIC	66913.8
c105*	M1	A697	pFB-CT10HF-LIC	76590.3
c106*	G36	A697	pFB-CT10HF-LIC	72737.7
c107*	P68	A697	pFB-CT10HF-LIC	69101.5
c108*	G112	A697	pFB-CT10HF-LIC	64557.1

Table 2.2 – Mutations in ABCB8$^{Ala111-Ala711}$, construct number, forward and reverse primers.

Construct	**Mutation**	**Forward Primer**	**Reverse Primer**
c082	E353A/E354A/E355A	ATGGAGCAACGGGCCGC CGCCCGCTATGGGGCA	TGCCCCATAGCGGGCG GCGGCCCGTTGCTCCAT
c084	K698A/K699A	GAAGAGCTCCTGGC CGCCGGCGGGCTATAC	GTATAGCCCGCCGGC GGCCAGGAGCTCTTC
c085	E114A/E116A/E117A	ATGGCCCTGTGTGCCGC AGCCGCCGCCCCTCCTGCC	GGCAGGAGGGGCGGCGGC "TGCGGCACACAGGGCCAT
c125	E638Q	CTGATACTGGATCAGGC TACCAGCGCG	CGCGCTGGTAGCCTGAT CCAGTATCAG

"

baculovirus and incubated for 65 h at 27C in a 3 L flask. After incubation for 72h at 27 °C in shaker flasks, cells were harvested at 1,500 x g at 4 °C for 15 minutes at a cell density of about 2 10^6 cell/L. The cell pellet was washed with 20 ml(per L cells) phosphate buffered saline (PBS) and pelleted at 1,500 x g for 20 minutes. After removing the supernatant cells were snap frozen in liquid nitrogen and stored at -80 °C.

2.4 Detergent solubilisation test

Solubilisation of ABCB8 was tested using a set of 12 or 24 different detergents (complete list of detergents used in Table 2.3). Cells from a 50 ml (12 detergent test) or 100 ml (24 detergent test) expression scale were defrosted in 24 ml or 48 ml for a 50 ml or 100 ml cell culture volume. Lysis buffer (50 mM HEPES, pH 7.5; 5 % glycerol; 300 mM NaCl, 0.5 mM $MgCl_2$, 1 tablet protease inhibitor cocktail (Roche cOmplete EDTA-free) per 50 ml buffer). Following lysis, cells were transferred into a 24-well block (2 ml per well) and lysed with a 24-well probe sonicator (3 seconds on/15 seconds off) for 2 minutes on a water/ice mixture. 950 μL of lysate were transferred into 96-well block and 95 μL of 10% w/v detergent stock were added for solubilisation of ABCB8. After 1 hour incubation at 4 °C with slow rotation of block, cell debris were removed from sample by centrifugation at 3500 x g for 30 minutes. After supernatant was transferred to new block, 100 μL of 50 % v/v Co^{2+}-TALON resin (Clontech) pre-equilibrated in wash buffer (50 mM HEPES, pH 7.5; 5 % glycerol; 20 mM imidazole (Fluka); 300 mM NaCl, 0.5 mM $MgCl_2$) was added to each well for immobilized metal affinity chromatography (IMAC) in batch binding mode. Samples were incubated for 1 hour at 4 °C at 6 rpm rotation before transfer into filter plate (Chromacol Cat No: CLS-370011- 800ul polypropylene plate, 10-20 um UHMW PE filter or Thomson Instruments Cat no: 921673B). Two washing steps by adding 1.25 ml wash buffer containing 3x CMC (critical micelle concentration) of detergent were performed. Supernatant and wash buffer

were removed by brief centrifugation at 200 x g for 1 minute. Finally, 35 μL of elution buffer (50 mM HEPES, pH 7.5; 5% glycerol; 500 mM imidazole; 300 mM NaCl, 0.5 mM $MgCl_2$) with 3x CMC were placed on top of resin and incubated for 5 minutes at 4 °C. Finally, elutions fractions were collected in 96-well plate after centrifugation at 500 x g for 3 min. 4 μL 4x SDS PAGE sample buffer (NuPAGE) with 250 mM DTT was added to 12 μL elution fractions. 10 μL of these samples were analysed by Coomassie SDS-PAGE, using precast gels (Criterion XT gels) in XT-MES running buffer.

Table 2.3 – Detergents used for ABCB8 purification and crystallisation. CMC is the critical micelle concentration

Detergent	Abbreviation	CMC % (w/v)	conc. In buffer % (w/v)
n-Decyl-β-D-maltopyranoside	DM	0.087	0.26
n-Undecyl-β-D-maltoside	UDM	0.029	0.09
n-Dodecyl β-D-maltoside	DDM	0.009	0.03
N-Tridecyl-β-maltoside	TDM	0.001	0.00
n-Octyl-β-D-glucopyranoside	OG	0.585	0.88
n-Nonyl-β-D-glucopyranoside	NG	0.200	0.60
Octyl glucose neopentyl glycol	OGNG	0.058	0.17
Decyl maltose neopentyl glycol	DMNG	0.003	0.01
Lauryl maltose neopentyl glycol	LMNG	0.001	0.00
Octyl pentaethylene glycol ether	C8E5	0.051	0.15
Polyoxyethylene(9)decyl ether	C10E9	0.072	0.22
Polyoxyethylene(10)dodecyl ether	C12E10	0.013	0.04
Octaethylene glycol monododecyl ether	C12E8	0.005	0.01
Polyoxyethylene(9)dodecyl ether	C12E9	0.003	0.01
Polyoxyethylene(8)tridecyl ether	C13E8	0.006	0.02
3-Cyclohexyl-1-propyl-β-D-maltoside	CYMAL-3	1.610	1.93
4-Cyclohexyl-1-butyl-β-D-maltoside	CYMAL-4	0.365	1.10
5-Cyclohexyl-1-Pentyl-β-D-Maltoside	CYMAL-5	0.120	0.36
6-Cyclohexyl-1-hexyl-β-D-maltoside	CYMAL-6	0.028	0.09
Octanoyl-N-methylglucamide	MEGA-8	1.668	1.83
Nonanoyl-N-methylglucamide	MEGA-9	0.839	1.68
Decyl-N-methylglucamide	MEGA-10	0.168	0.50
Cyclohexylpentanoyl-N-hydroxyethylglucamide	HEGA-11	0.055	0.17
n-Undecyl-N,N-Dimethlamine-oxide	UDAO	0.069	0.21
N,N-Dimethyldecylamine-N-oxide	DDAO	0.209	0.63
Lauryldimethylamine-N-oxide	LDAO	0.046	0.14
3-[(3-Cholamidopropyl)-dimethylammonio]-1-propane sulfonate	CHAPS	0.369	1.11
n-Dodecylphosphocholine	FC12	0.047	0.14

2.5 Monodispersity screen

2.5.1 Cell lysis and extraction of ABCB8 for monodispersity screens

Cells were defrosted in 25 ml (per L cell culture) wash buffer (50 mM HEPES, pH 7.5; 10 % glycerol; 20 mM imidazole; 200 mM NaCl, 0.5 mM $MgCl_2$ and 2 mM TCEP; containing 1 tablet protease inhibitor cocktail (Roche cOmplete EDTA-free)

per 50 ml buffer). Cell were lysed with a probe sonicator on a water/ice mixture for 1 min (per L cells) in a 5 seconds on/15 seconds off cycle at 35 % amplitude. Alternatively, cells were lysed by homogenising twice using an EmulsiFlex-C5 homogeniser (Avestin) at 11-13mPa. Membranes were pelleted at 30,000 x g for 1 hour at 4 °C. For the high salt wash, membranes were re-suspended in buffer containing 50 mM HEPES (pH 7.5) and 1 mM NaCl, followed by a centrifugation step at 30,000 x g for 40 minuted at 4 °C. This step was repeated twice. Subsequently membranes without and with high salt wash treatment were re-suspended in 50 ml wash buffer containing 1 tablet protease inhibitor cocktail per 50 ml buffer. For extraction of ABCB8, membranes were incubated with 1% w/v detergent (and 0.1% w/v CHS, if indicated in result section) from stock solution (10% w/v stock solution made up with deionised water) or by adding detergent powder directly to membrane suspension. Samples were incubated for 1-2 hours at 4 °C under gentle stirring. Insoluble fractions were removed by centrifugation at 30,000 g for 40 minutes at 4 °C.

2.5.2 IMAC and SEC of ABCB8 in monodispersity screens

IMAC was used to purify protein from supernatant by incubating 1 mL 50% (v/v) Co^{2+} loaded TALON resin (Clontech) with supernatant for 1 hour at 4 °C at 6rpm rotation. Prior to purification, TALON resin was washed with deionised water and equilibrated with wash buffer. After incubation, samples were transferred into a filter plate and excess liquid was removed by centrifugation at 200 x g for 1 min. Resin was subsequently washed with 1.25 ml wash buffer containing 3 x CMC of detergent of choice. and wash fractions were removed by centrifugation at 200 x g for 1 min. The washing step was repeated 4 times. Following the washing step, protein was eluted with 500 μL elution buffer (50 mM HEPES, pH 7.5; 5% glycerol; 300 mM imidazole; 200 mM NaCl, 0.5 mM $MgCl_2$ and 2 mM TCEP,

3x CMC detergent) at 500 x g for 2 minutes. Elution was repeated once more. For detergent plus lipid screens, washing and elution buffer contained detergent and lipid (1:50 (w/w) lipid:detergent ratio). ABCB8 concentrations in elution fractions were determined with UV absorbance at 280 nm. Elution fractions were exchanged into size exclusion chromatography (SEC) buffer (20 mM HEPES, pH 7; 200 mM NaCl, 0.5 mM $MgCl_2$ and 2 mM TCEP, 3x CMC detergent) with G25-desalting columns (GE healthcare). 200 μg TEV protease (*Tobacco Etch Virus* nuclear-inclusion-a endopeptidase; (purified in-house)) were added to protein and incubated over-night at 4 °C. His-tagged TEV was removed the next day with reverse IMAC by incubating the samples with 80 μL 50 % (v/v) Co^{2+}-TALON resin. The flow-through from the reverse IMAC step was collected and concentrated to 50 μL using 2ml Vivaspin 100 kDa concentrator (Sartorius). SEC was performed on a Dionex HPLC system (Thermo Fisher Scientific) in combination with a SRT SEC-300 column (Sepax technologies) using SEC buffer as mobile phase. The polyoxyethylene detergent screen was run on a Superdex200 Increase 5/150 GL (GE Healthcare) with SEC buffer instead. For the buffer monodispersity screen, wash, elution and SEC buffer were prepared as indicated with different pH or salt concentrations, whereas all buffers contained 0.5 mM $MgCl_2$, 0.5 or 2 mM TCEP and glycerol concentrations as mentioned in chapter 3.

2.6 Large-scale purification

The crystal structure, as well as all functional assays reported in this thesis were obtained from ABCB8$^{Ala111-Ala714}$. ABCB8$^{Ala111-Ala714}$ is referred to as "wild type" to distinguish it from the mutants generated on the basis of this construct.

After cell lysis and extraction of protein from membranes as described for the monodispersity screening protocol section 2.5.1, ABCB8 was purified by IMAC using Co^{2+}-loaded TALON resin (Clontech). Prior to purification, TALON resin was washed with water and equilibrated with wash buffer. 2 ml (per L cell culture)

of 50% (v/v) TALON resin was added to supernatant and mixture was rotated at 6 rpm for 1 hour at 4 °C. Resin was washed with 50 column volumes (CV; resin volume) of wash buffer containing 3x CMC of detergent added from 10 % w/v stock. Washing of the resin was performed in batch mode by repeated pelleting of resin at 400 x g for 5 min at 4 °C and re-suspension in wash buffer. Resin was transferred into glass chromatography column and protein was eluted in 1 CV steps with ELB300 (50 mM HEPES, pH 7.5; 5% glycerol; 300 mM imidazole; 200 mM NaCl, 0.5 mM $MgCl_2$ and 2 mM TCEP, 3x CMC detergent). ABCB8 concentrations in elution fractions were determined via UV absorbance at 280 nm. Fractions were pooled and buffer exchanged into desalting buffer (20 mM HEPES, pH 7; 10 % glycerol; 200 mM NaCl, 0.5 mM $MgCl_2$ and 2 mM TCEP, 3x CMC detergent) with PD10-desalting columns (GE healthcare). TEV protease (purified in-house) (1:5 w/w ratio of TEV and ABCB8) was added to protein and incubated over-night at 4 °C, if removal of His/FLAG-tag was desired (e.g. the fusion tag was not cleaved off for microscale thermophoresis experiments).

His-tagged TEV was removed from protein sample using reverse IMAC with Co^{2+}-TALON, that was incubated with sample for 1 hour at 6rpm at 4 °C (5:1 ratio of TEV:volume of resin in μL). The flow-through was collected and concentrated with a 6 ml Amicon 100kDa concentrator (GE Healthcare) for SEC to $\sim$7 mg/ml of protein concentration. SEC was performed by injection of 500 μL using a Supradex-200 10/300 GL column (GE Healthcare) with SEC buffer (20 mM HEPES, pH 7; 200 mM NaCl, 0.5 mM $MgCl_2$ and 2 mM TCEP, 2x CMC detergent). Peak fractions identified in the gel filtration chromatogram and from measuring UV absorbance at 280 nm were pooled and concentrated to 8-10 mg/ml using a 2 ml vivaspin 100 kDa concentrator (Sartorius) for crystallisation. Prior to crystallisation and functional assays, protein was centrifuged at 20,000 x g for 10 minutes to remove aggregates.

2.6.1 Chemical modification of lysines and cysteines during purification

Chemical modification of lysines or cysteines was performed after the first IMAC and desalting step for tagged protein used in microscale thermophoresis (MST) experiments and after the reverse IMAC step for untagged protein used in functional assays and crystallisation.

Lysine methylation using dimethylamine borane and formaldehyde

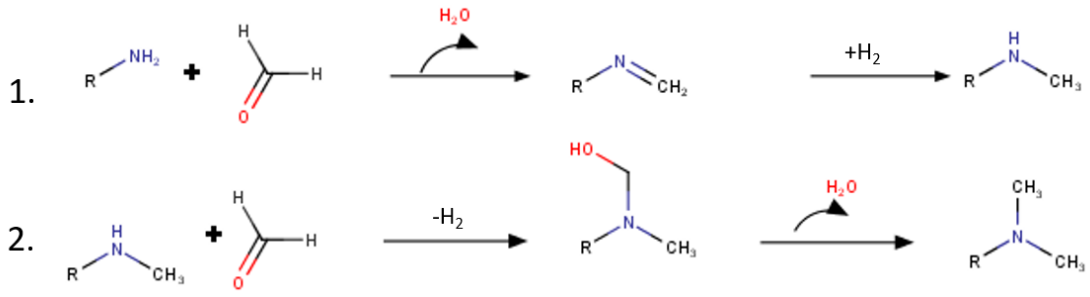


Figure 2.2 – Chemical reaction for lysine methylation with formaldehyde and dimethylamine borane (ABC) as a catalyst in two steps.

Lysine methylation was produced in a two step reaction with formaldehyde (Sigma Aldrich) using dimethylamine borane (ABC) (Sigma Aldrich) as a catalyst. In the first step a Schiff base between the ϵ-amino group of the lysine and the formaldehyde is formed, which is reduced to a secondary amine (step 1; Fig. 2.2). This step is followed by another rapid reaction with a second formaldehyde molecule to the dimethylated product (step 2).

For that, 10 ml protein (at $\sim$ 0.7 mg/ml) were incubated with 20 mM of ABC and 20 mM formaldehyde for 90 minutes at 4 °C. This step was repeated once more and finally another 10 mM ABC were added and incubated at room temperature for 90 minutes. Reagents were removed with PD-10 columns equilibrated in quenching buffer (20 mM HEPES, pH 7; 20 mM Tris, pH 7 (quenches methylation reaction); 10 % glycerol; 200 mM NaCl, 0.5 mM $MgCl_2$ and 2 mM TCEP, 3x CMC detergent).

Cysteine modification with iodoacetamide, iodoacetic acid and DTNB

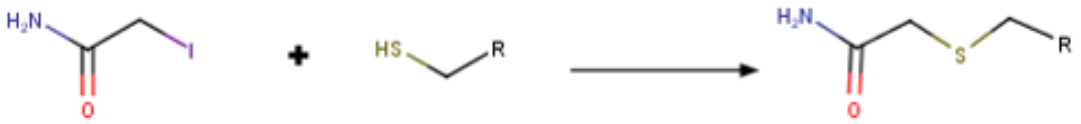


Figure 2.3 – Chemical reaction of iodoacetamide with sulfhydryl groups of cysteine sidechains

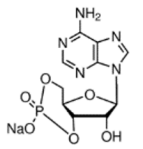
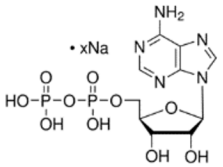
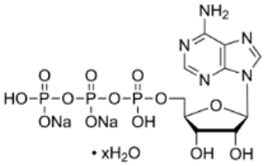
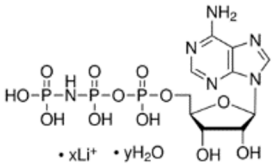
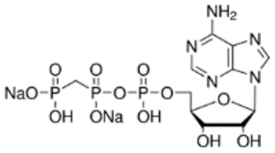
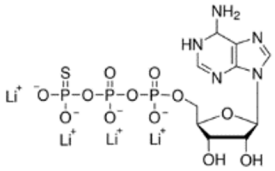
Cysteines are modified with iodoacetamide in a substitution reaction with the thiol group (Fig. 2.3). The modification with iodoacetamide (Sigma Aldrich) was performed by adding 25 mM iodoacetamide (made up freshly in deionised prior to reaction) to 10 ml ABCB8 (0.7-1 mg/ml) and incubating it for 30 minutes at room temperature (provides a $\sim$ 125-fold excess of iodoacetamide over 13 cysteines per ABCB8 monomer). Samples were kept shielded from light during incubation due to light labile iodoacetamide. Excess of iodoacetamide was removed with PD-10 columns equilibrated in desalting buffer. A similar protocol was performed for labelling with iodoacetic acid (Sigma Aldrich) and 5,5-dithio-bis-2-nitrobenzoic acid (DTNB; Thermo Fisher Scientific). Iodoacetic acid was added in the same ratio as iodoacetamide. For DTNB treatment, 1.7 mM were added to 8 mg ABCB8 (providing a 10-fold excess of DTNB over 13 cysteins per monomer in ABCB8).

2.7 Preparation of nucleotides

Nucleotides (Table 2.4, all purchased by Sigma Aldrich) were prepared by re-suspending powder in 100 mM HEPES (pH 7.5) followed by immediate adjusted to neutral pH of solution. Aliquots of nucleotides were stored at - 20 °C for up to 6 months. For transitions state analogues, 5 mM ATP (purchased from Sigma Aldrich; prepared as previous nucleotides) was mixed with 5 mM orthovanadate (V_i; Sigma Aldrich). V_i was prepared by re-suspending sodium orthovanadate powder in deionised water and adjusting the pH to pH 10. Upon boiling of the or-

thovanadate solution to 90 °C the yellow colour indicating an oligomeric structure of the molecule becomes clear as monovanadate is formed.

Table 2.4 – Chemical structures of nucleotides used for ABCB8 crystallisation and in functional studies.

Nucleotide	Abbreviation	Structure	Sigma product number
Adenosine 3′,5′-cyclic monophosphate	cAMP		A6885
Adenosine 5′-diphosphate	ADP		A2754
Adenosine 5′-triphosphate	ATP		A2383
Adenosine 5′-(β,γ-imido)triphosphate	AMPPNP		A2647
β,γ-Methyleneadenosine 5′-triphosphate	AMPPCP		M7510
Adenosine 5′-[γ-thio]triphosphate	ATPγS		A1388

2.8 Crystallisation

2.8.1 Crystallisation set-up and crystal optimisation

Preparation of ABCB8 with nucleotides

Prior to crystallisation, protein was incubated with 5 mM ATPγS, AMPPNP, AMPPCP or ADP with additional 5 mM $MgCl_2$ or 5 mM ATP plus V_i and 5 mM $MgCl_2$. Co-crystallisation with ATP plus aluminium fluoride or beryllium fluoride transition analogues were prepared by adding 1 mM ATP, 8 mM NaF and 1 mM $MgCl_2$ to protein solution in the presence of either 2 mM $AlCl_3$ or 2 mM BeF_2, respectively. All mixtures were incubated for 1 hour at 4 °C before crystallisation plates were set up.

Vapour diffusion crystallisation

150 nL or 300 nL sitting drops were set up with a Mosquito crystallisation robot (TTP Labtech) into a 3-position 96-well plates (SwissCI). Ratio between reservoir solution (20 μL) and the protein solution were set to 2:1, 1:1 and 1:2. Screens used for crystallisation were MemGold2 (Molecular Dimensions) and in-house optimisations of the MemGold and MemSysStart screen, as well as custom-designed follow-up screens. Plates were incubated at 4 °C or 20 °C for three months in a Minstrel imaging incubator. Follow-up crystallisation screens were designed to explore conditions that gave initial crystallisation hits and were made using an MPII liquid handling robot. Chemicals used for follow-up screens were purchased from Hampton Research. Most crystals appeared within 2-7 days of incubation.

Additive screening

Additive screens using salts, volatiles and detergents were performed using a follow-up screen that allowed screening 24 different additives per 96x3 well plate (screening

4 different PEG concentrations at constant pH and salt concentrations per additive). 2 μL of additive stock were added to 20 μL reservoir solution.

Seeding

Seeding was performed with the monoclinic crystal form harvested from drops set-up with bicine pH 8.5 and varying PEG2000MME concentrations (22-24 %). 1 μL of stabilising solution (bicine pH 8.5, 26% PEG2000MME, 100 mM NaCl, 0.12% OGNG, 0.012% CHS) was added to crystal drop and crystals were pestled and transferred to a Seed Bead Ceramic tube (Seed Bead Kit Hampton Research) into 50 μL stabilising solution. Tube was vortexted for 10 seconds and placed on ice (repeated two times). Finally, volume was topped up to 300 μL with the stabilising solution and 1/10 and 1/100 dilutions were prepared. 20 nL seed solution was added to 175 nL drops (2:1 and 1:2 ratio of protein and reservoir solution) using the Mosquito crystallisation robot. Crystals were mainly obtained with the undiluted seeding stock.

HiLiDe, bicelle and LCP crystallisation

For HiLiDe crystallisation, 30 μL ABCB8 at 8 mg/ml with 5 mM nucleotide and 5 mM $MgCl_2$ was prepared as described in section 2.8.1 and incubated on 45 μg or 90 μg DMPC:Cardiolipin (3:1 wt/wt) lipid film (dried down prior to experiment with argon gas). 225 μg and 450 μg OGNG/CHS were added to protein samples with both lipid amounts and incubated for 14-18 hours at 4 °C under gentle shaking. Sample was spun at 150,000 g for 30 minutes prior to set-up in vapour crystallisation attempts (section 2.8.1).

Bicelles were prepared by resuspending 140 mg DMPC with 45 mg CHAPSO in 500 μL deionised water and vortexted for 4 hours at 4 °C to give 35% (wt/wt) bicelle stock. Alternatively, 18 mg CDL and 112 mg DMPC were mixed in chloroform and tried under argon. Then lipid film was resuspended with 600 uL containing 50 mg

CHAPSO giving 30 % (wt/wt) bicelle solution. Several cycles (50-200 cycles) of freezing with liquid nitrogen and incubation at ice, followed by vortexing until solution became clear and fluid at 4 °C. Protein pre-incubated with 5 mM nucleotide and 5 mM $MgCl_2$ was mixed to give a final 7 % (wt/wt) bicelle solution on ice for 1 hour before crystal plates were set-up in standard vapour diffusion protocol (section 2.8.1)

For LCP attempts ABCB8 at 14 mg/ml was mixed with monoolein, 7.7 MAG or 7.9 MAG (Avanti Polar Lipids) in a 10:15, 11:15 or 10:12 ratio (protein/lipid vol./vol), respectively. The produced lipidic cubic mesophase should be clear and viscous, as well as non bi-refringent. 40 nl of mixed LCP solution were aliquoted onto glass sandwich plates (Molecular Dimensions) using a mosquito robot. Following, 800 nL of crystallisation screen (0.7 dilutions of the MemGold, MemSysStart, MemGold2 and SGC-LCP1 and SGC-LCP1, an in house designed screen) were pipetted onto the LCP drop. The sealed crystallisation plates were incubated at 20 °C for three months.

2.8.2 Crystal mounting and cryo-cooling

Since crystals for ABCB8 only grew in higher molecular weight PEGs and low salt concentration additional cryo-protection had to be provided, before crystals were cryo-cooled. Prior to cryo-cooling, crystals were stabilised with 1 μL reservoir solution containing 0.12 % OGNG and 0.012 %CHS. Then, PEG400 concentrations were increased stepwise by exchange of drop solution with reservoir solution containing 5 %- 20 % PEG400 by addition and removal of 1 μL volumes. Crystals cryo-cooled with 10 %- 15 % PEG400 yielded the best diffraction. With the same procedure, 5 % to 20 % glycerol and ethylene glycol were tested as cryo-protectant, but impaired resolution of the diffraction of the monoclinic crystal form. For dehydration experiments, crystals were incubated for 1 hour to 24 hours in solution containing 5 % to 20 % PEG400. Crystals were mounted from drop with nylon cryo

loops (Hampton Research) varying from 0.05 - 1.0 mm, plunged into liquid nitrogen and stored in liquid nitrogen until screening of diffraction at the synchrotron beam line.

2.8.3 Crystal screening and data collection

Crystal screening and data collection were performed at 100 K at the Diamond Light Source Beamline I03, I04 and I24 using Pilatus6M detector. Crystals were screened by X-ray (operating wavelength of beamline at $\sim$ 1 Å) exposure at three different angles 45 ° apart with exposure time and oscillation angle, set to 0.5 seconds and 0.5 °, respectively. Transmission energy varied from 10 % to 100 % transmission depending on the diffraction quality and whether further data collection was performed on crystal. Data collection strategies were developed with help of iMOSFLM [Battye *et al.,* 2011] on the basis of the 3 screening images. Diffraction patterns were indexed and a strategy that increased the chance for maximal data completeness was applied. The transmission energy and exposure time were estimated on the basis of the test images to minimise radiation damage.

2.8.4 Crystal data processing

Data processing was performed using the XDS program package [Kabsch, 2010] that identifies spots and indexes, intergates and scales the data. POINTLESS and AIMLESS were run to merge the data and obtain a reflection file in the mtz format [Winn *et al.,* 2011; Evans, 2006; Evans & Murshudov, 2013]. Scales were kept constant for the AIMLESS run. CTRUNCATE was used before AIMLESS to boost small positive intensities of weak reflections [French & Wilson, 1978; Dauter, 2006; Winn *et al.,* 2011]. Using the CCP4 program MATTHEWS COEF, the number of molecules in the asymmetric unit was estimated on the basis of solvent content, calculated from the unit cell and molecular weight of the protein molecule [Matthews, 1968; Kantardjieff & Rupp, 2003; Winn *et al.,* 2011].

Data set d003 (Table 8.2) was obtained from ATPγS co-crystals formed by iodacetamide treated ABCB8 in a $P12_11$ space group. These data were successfully phased by molecular replacement (MR). For that, PHASER-MR was run with a structural monomer (Fig. 8.3) of the nucleotide-free ABCB10 structure in an inward-facing state (3ZDQ; nucleotide-free 2.85 Åcrystal structure of ABCB10) used as an input model [Winn *et al.,* 2011; McCoy *et al.,* 2007; McCoy *et al.,* 2007]. Only the structural monomer, but not the dimer in an inward-facing state provided a correct MR solution. In addition, a model of Sav1866 (2HYD), that was modified with the CCP4 program CHAINSAW [Stein, 2008] pruning side chains with no conservation in ABCB8, also resulted in a correctly placed solution. An initial model of ABCB8 was built based on the MR solution of the structural monomer as a starting model. An occluded model of ABCB10 (unpublished data Dr Ashley Pike and Dr Chitra Shintre) aided building of TM helices into electron densities derived from MR with a model of ABCB8, that only contained the NBDs and lower halves of the TMDs. Due to improvement of the purification protocol and cryo-protection procedure a slightly better data set (d014) for the same monoclinic crystal form with resolution to 3.8 Å was collected, which improved map quality and allowed completion of the model (Table 5.1). Since data were highly anisotropic, the STARANISO webserver was used to define an anisotropic resolution cut-off, that changes with direction in reciprocal space instead of creating a spherical average [Tickle *et al.,* 2017]. The loss of completeness plotted against resolution is shown in Fig. 8.4.

2.8.5 Structure building and refinement

Model building was performed in Coot [Emsley *et al.,* 2010] using σ-weighted 2Fo-Fc and Fo-Fc (B-factor sharpened) maps from PHASER-MR, as well as maps improved with PHENIX RESOLVE [Adams *et al.,* 2010] (including prime and switch) and PARROT [Winn *et al.,* 2011]. In addition, maps were created with

PHASER-MR for polyalanine models and a model containing only the NBDs and the lower TMDs halves. This aided model building into maps, that were less biased by the staring model. MR ROSETTA was used for automatic model optimisation [Terwilliger *et al.,* 2012]. Model building was aided by Dr Ashley Pike.

Refinement was performed with BUSTER using automated NCS refinement [Bricogne *et al.,* 2015]. In order to find the best restraints for the refinement process, input parameters like individual B-factors and TLS refinement were varied throughout the structure solving process and are listed in Table 8.3 in detail for all refinement rounds. Flow-chart in Fig. 2.5 gives an overview over the individual steps performed in the structure solving process for ABCB8 with datasets d003 and d014.

In order to obtain a final model, building and refinement cycles were pursued until Rwork/Rfree factors stabilised, all electron densities occupied and geometrical constraint requirements were fulfilled according to data quality as evaluated with MolProbity [Chen *et al.,* 2010a] (Fig. 2.4).

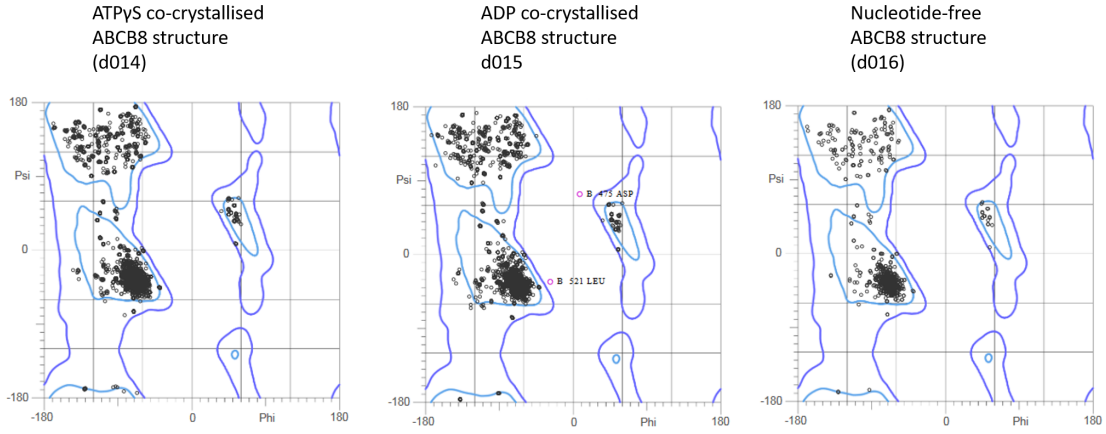


Figure 2.4 – Ramachandran plots for a all three structures solved in context of this thesis. Ramachandran plots were obtained form Molprobity [Chen *et al.,* 2010a].

Additional datasets d015 and d016 were obtained for ABCB8 co-crystallised with ADP and from a nucleotide-free crystal, respectively. Dataset d015 was phased using the final model of the previously described ABCB8 structure. Initial refinement steps were performed with BUSTER. Dataset d016 was phased with a structural monomer of the previous ABCB8 model. Due to low resolution, only

rigid body refinement was performed on d016 using REFMAC [Murshudov *et al.*, 2011; Nicholls *et al.*, 2012; Willis & Schleich, 1996].

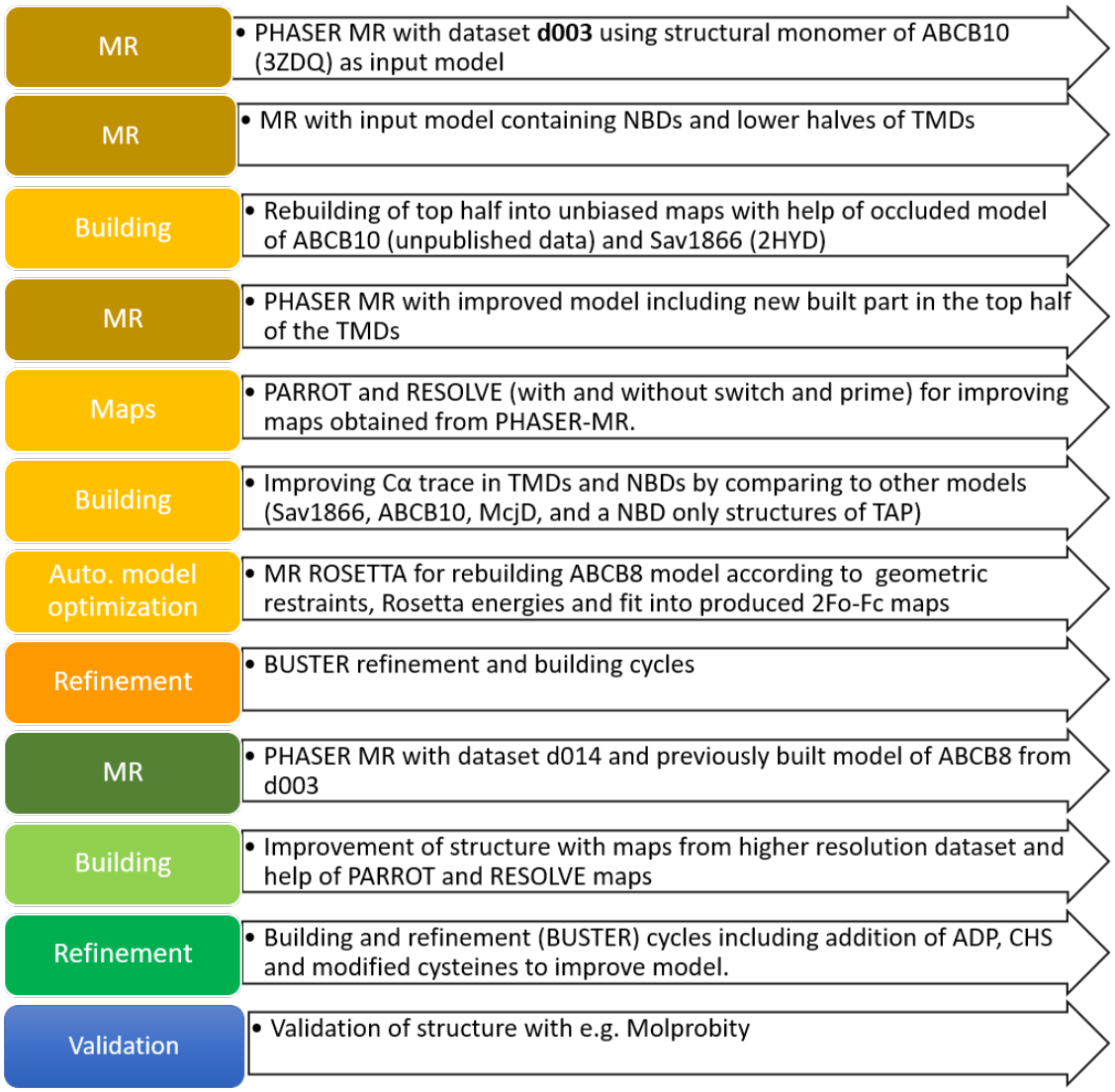


Figure 2.5 – Flow-chart presenting steps in process for structure solution using datasets d003 (yellow/orange) and d014 (green). Table 8.3 lists the refinement steps performed in BUSTER in detail.

2.8.6 Structure presentation and analysis

PYMOL and Chimera were used for visualisation of structural features in ABCB8 [DeLano, 2014; Pettersen *et al.*, 2004]. Electron density maps visualised in PYMOL were generated using FFT [Read & Schierbeek, 1988; Winn *et al.*, 2011]. PDBePISA was used to assess molecule interfaces within the dimer and different

dimers in the asymmetric unit, as well as interactions between CHS and ADP with protein [Krissinel & Henrick, 2007]. The Adaptive Poisson-Boltzmann Solver (APBS) Software was used to evaluate the electrostatic properties of the ABCB8 surface [Baker *et al.,* 2001].

2.9 ATPase assays

2.9.1 "Chifflet's assay"

ATPase activity of ABCB8 was measured by a modified "Chifflet's assay" that determines amounts of released phosphate after ATP hydrolysis Chifflet *et al.* [1988] and Taylor *et al.* [2001]. In this colorimetric assay molybdenum forms a complex with phosphate under reducing conditions provided by ascorbic acid. The absorbance of this so-called molybdenum blue can be measured at 850 nm. 30 μL of 0.45 μM ABCB8 (in SEC buffer containing 0.2% OGNG and 0.02% CHS) were incubated with 20 μL ATP (0-1 mM or 0-5 mM final concentration) in ATPase buffer (50 mM HEPES, pH 7; 150 mM NaCl; 10 mM $MgSO_2$, 2 mM TCEP) at 37 °C for 20 minutes. No detergent was added to the SEC buffer used in ATPase assays with reconstituted ABCB8. The reaction was quenched by addition of 40 μL of 12% SDS solution. Phosphate concentrations were quantified by addition of ammonium molybdate, that forms a coloured complex with inorganic phosphate. Ascorbic acid is added to stop the complex from oxidising. An excess of molybdate ions was removed with metarsenite. The absorbance of the formed molybdate complex was measured at 850 nm using a SpectraMax M Series Multi-Mode Microplate Reader (Molecular Devices). Measured absorbance was normalised by subtraction of the absorbance in the absence of ATP. Absorbance was translated into phosphate amounts with an inorganic phosphate standard that was run with each measurement in triplicate For measurements of orthovanadate inhibition, 5 mM V_i was added to ABCB8 prior to incubation with ATP.

For reconstituted protein, the protein amounts were estimated with densitometry from bands on a Coomassie-stained SDS-PAGE gel and compared to an ABCB8 concentration standard (5-0.31 μg) using the "Qualitative Tool" in the Image Lab Software 6.0 (Bio-Rad).

2.9.2 ADP-Glo kinase assay

ADP-Glo kinase assay kit (Promega) [Zegzouti *et al.,* 2009] was used as alternative to the "Chifflet's assay" for measuring ATPase activity for ABCB8, in particular for reconstituted ABCB8 samples due to it higher sensitivity. The ADP-Glo assay quantifies ADP in a two-step process following the ATPase reaction. In the first step the ADP-glo reagent is added, which terminates the reaction and removes residual ATP. The second step involves the conversion of ADP to ATP and luciferase reaction that produces luminescence driven by newly produced ATP. The measured luminescence is proportional to ADP generated in the ATPase reaction [Zegzouti *et al.,* 2009]. For that, 6 μL of $\sim$ 1 mM reconstituted ABCB8 or 0.45 μM ABCB8 in detergent both in SEC buffer was mixed with 4 μL ATP dilutions of increasing concentrations (0-1 mM) in ATPase buffer (50 mM HEPES, pH 7; 150 mM NaCl; 10 mM $MgSO_2$, 2 mM TCEP). The mixture was incubated for 20 minutes at 37 °C and subsequently quenched using an equal volume (10 μL) of ADP-Glo Reagent, provided in the kit. The mixture was incubated for 45 minutes at room temperature, followed by addition of 10 μL of the Kinase Detection Reagent. 8 μL of this sample was mixed in equal amounts with ATPase buffer (to dilute the signal) and transferred into a 384-well plate. Luminescence was measured at 590 nm using a PHERAstar (BMG Labtech) plate reader. An ADP dilution series in SEC buffer was run in parallel to obtain a standard curve.

The luminescence emission was normalised with an ATP-free sample and translated into ADP concentrations using the ADP standard curve. Subsequently, The ATPase activity was normalised by the amount of reconstituted ABCB8, estimated

from UV absorbance readings for protein in detergent and with densitometry from bands on a Coomassie-stained SDS-PAGE gel as decribed above for reconstiuted protein samples.

2.9.3 ATPase assay data analysis

The Michaelis constant for ATP (K_M) and the maximal enzyme activity (V_{max}) were obtained from detection of inorganic phosphate (Chifflet assay) or ADP (ADP-glo assay) amounts during ATP hydrolysis providing a measurement of the reaction velocity. For that, inorganic phosphate or ADP amounts normalised by protein concentration and incubation time were plotted over an ATP ([S]) concentrations gradient. Kinetic parameters were obtained by nonlinear least-squares regression of the Michaelis-Menten equation (Eq.2.9.1)

$$V = \frac{V_{max}[S]}{K_M + [S]} \tag{2.9.1}$$

IC50 values for nucleotide analogues or ADP were obtained from ATPase activity in the presence of 1mM ATP and increasing concentrations of nucleotide analogue or ADP. ATPase activity was normalised to maximal ATPase activity and zero inhibition in the absence of nucleotide analogue (I_0) and maximal inhibition (I_{max}) at maximal nucleotide analogue concentrations. The resulting response curve was fitted with a one site inhibition model shown in Eq.2.9.2.

$$I = I_{max} + \frac{I_0 - I_{max}}{1 + 10^{([S] - LogIC50)}} \tag{2.9.2}$$

Graphpad Prism software was used for data analyses. All measurements were performed in triplicate for one protein sample, and the experiment was repeated for N=2 or N=3 purifications unless otherwise stated. Error bars of data points represent standard deviations. Kinetic parameters are presented with standard

errors derived from fit.

2.10 Nano differential scanning fluorimetry (nanoDSF) measurements

2.10.1 Theory of nanoDSF

Differential scanning fluorimetry (DFS) involves following the unfolding of a protein induced by changing the temperature or other conditions. This method has been widely used to study not only protein unfolding, but also stabilizing conditions for proteins and the binding of small molecules to proteins. A protein unfolds by losing its ordered secondary and tertiary structure, which occurs if the difference in the Gibbs free energy ΔG_{unfold} for unfolding becomes negative. Unfolding can be favoured by a change of buffer conditions (salt concentrations, pH), addition of chaotropic agents (urea or guanidinium hydrochloride) or temperature. Thermal shift assays allow testing the effects of ligand binding on the stability of the protein, by monitoring the unfolding process of the protein upon increase in temperature. The inflection point of the melting curve from folded (X_{folded}) to unfolded ($X_{unfolded}$) state is defined by a 1:1 ratio of unfolded and folded protein that results in a ΔG_{unfold} of zero (Eq.2.10.1 and 2.10.1).

$$G_{unfold} - G_{fold} = \Delta G_{unfold} = -RT \ln[\frac{X_{unfolded}}{X_{folded}}] \tag{2.10.1}$$

$$\Delta G_{unfold} = -RT \ln[1] = 0 \tag{2.10.2}$$

The temperature associated with the inflexion point is called melting temperature (T_M) and is characteristic for the stability of the protein under those conditions. However, thermal shift assays are not suited for determining K_D values, as the T_M

values have no linear correlation with ligand binding, although a dose-response can be observed. Nevertheless, it detects stabilising or destabilising effects on the protein fold. There are a number of methods available to detect changes in the folded state of a protein. One common technique for high throughput stability screening of membrane proteins involves the use of the coumarin derivative dye, fluorochrome N-[4-(7-diethylamino-4-methyl-3-coumarinyl)phenyl]maleimide (CPM). Due to its thiol-specific reactivity CPM binds to cysteines that become exposed upon unfolding of the protein, which makes the compound fluorescent [Alexandrov *et al.,* 2008; Niesen *et al.,* 2007]. However, ABCB8 is unsuited for this method, as it has a large number of cysteines exposed on the surface (section 3.2.6), which react with the CPM dye before the protein has unfolded, leading to an excessively high background. In contrast, label free nano differential scanning calorimetry (nanoDSF) provides a valuable alternative for measuring thermal stability of membrane proteins, including ABCB8. This technique has been successfully used for testing stability of a membrane-bound esterase PA2949 from *Pseudomonas aeruginosa* in a range of detergents [Bleffert *et al.,* 2016] and for ligand binding to human adenosine A2A receptor [Haffke *et al.,* 2016]. NanoDSF exploits the fact that intrinsic fluorescence of aromatic residues, particularly tryptophans, can be excited at 295 nm and is strongly dependent on the polarity of their environment. Changes in the protein structure upon unfolding often leads to movement of these residues from the hydrophobic environment of the protein core or detergent micelle into a more hydrophilic environment. Consequently, the fluorescence emission is altered in intensity (quantum yield decreases) and peak intensity shifts to longer wavelengths, a phenomenon that is referred to as a "red" shift. If the polarity decreases, by exposure of the aromatic residues into the hydrophobic environment, e.g. detergent covering the unfolded protein, the quantum yield and so fluorescence increases, but is "blue" shifted to shorter wavelengths. In addition, fluorescence of aromatic residues buried in the protein structures can be quenched and fluorescence may increase upon unfolding due to the release of the fluorescent residue. Experiments

in this thesis were performed with the Nanotemper Prometheus NT.48 instrument, allowing simultaneous measurements of up to 48 samples, placed in quartz capillaries. A melting curve can be obtained by plotting the temperature versus the fluorescence emission at 330 nm, 350 nm or a ratio of the two wavelengths, accounting for both change in fluorescence intensity and shift of emission wavelength upon unfolding of the protein.

2.10.2 Experimental procedure of nanoDSF

20 μL of SEC buffer (+0.12% OGNG, 0.012% CHS) with nucleotide analogue and/or substrate candidate at 2-fold the final concentration were set up. Following this, 20 μL of ABCB8 (0.8-1 mg/ml) in SEC buffer (+0.12% OGNG, 0.012% CHS) was added to 2-fold mix of nucleotide to give a final protein concentration of 0.4-0.5 mg/ml of protein. After incubation at 4 °C for 30 minutes, samples were loaded into UV capillaries (Nanotemper Technologies) and measured using the NT.48 Prometheus (Nanotemper Technologies) with a temperature gradient set to increase from 20 °C to 95 °C at 1 °C/min. Melting curves were generated using PR.ThermControl v2.0.3 (Nanotemper Technologies), that estimates a 8^{th} order polynomial fit to the transition region and subsequently melting temperatures (T_M) were determined as the maximum of the first derivative of these melting curves. Thermal shifts (ΔT_M) were obtained from subtraction of the T_M value measured from ABCB8 in the absence of nucleotide from the T_M value obtained in the presence of it. Data were obtained for N=2 and N=3 biological repeats (with exception of ABCB8 E637Q measured as N=1) measured in triplicate. Error bars in the bar chart represent the standard deviations.

2.11 Nucleotide binding measured with Microscale thermophoresis (MST)

2.11.1 Theory of MST

Microscale thermophoresis is a biophysical method that detects the rate of movement of protein molecules such as ABCB8 in a temperature gradient. Differences in the speed of movement of molecules can be indicative of binding of small molecules and changes in protein conformation. Biomolecules like proteins and DNA move in a temperature gradient depending on their size, charge and solvation shell and the rate of movement can be altered by binding of ligands or by interactions with other macromolecules like DNA or proteins, which can induce a change in conformation. This movement can be followed by fluorescently labelling the biomolecule. In addition to the thermophoresis effect, another phenomenon which can be recorded in an MST instrument is the change in fluorescence due to the change in temperature, called temperature jump (T-jump).

Microscale thermophoresis (MST) measures the movement of biomolecules in this temperature gradient, as well as the change of fluorescence due to the T-jump, both induced by an infrared (IR) laser. Results from MST measurements described in this thesis were run with a Monolith NT.115 Blue/Red instrument (Nanotemper Technologies). In this instrument, thermophoresis is induced in small capillaries of 4 μL volume, that contains a fluorescently labelled biomolecule incubated with a series of ligand concentrations. An infra red (IR) laser (λ = 1480 nm), focused on the capillary with an objective, causes a microscopic temperature gradient of 2-6 °C in a volume of 50 μL (Fig. 2.6A). Movement of the molecules is detected by following changes in the fluorescence measured at 515-530 nm after excitation at 460-490 nm. Before the application of a temperature gradient, the fluorescently labelled biomolecules are evenly distributed. The fluorescence emission is detected through the same objective as the IR laser.

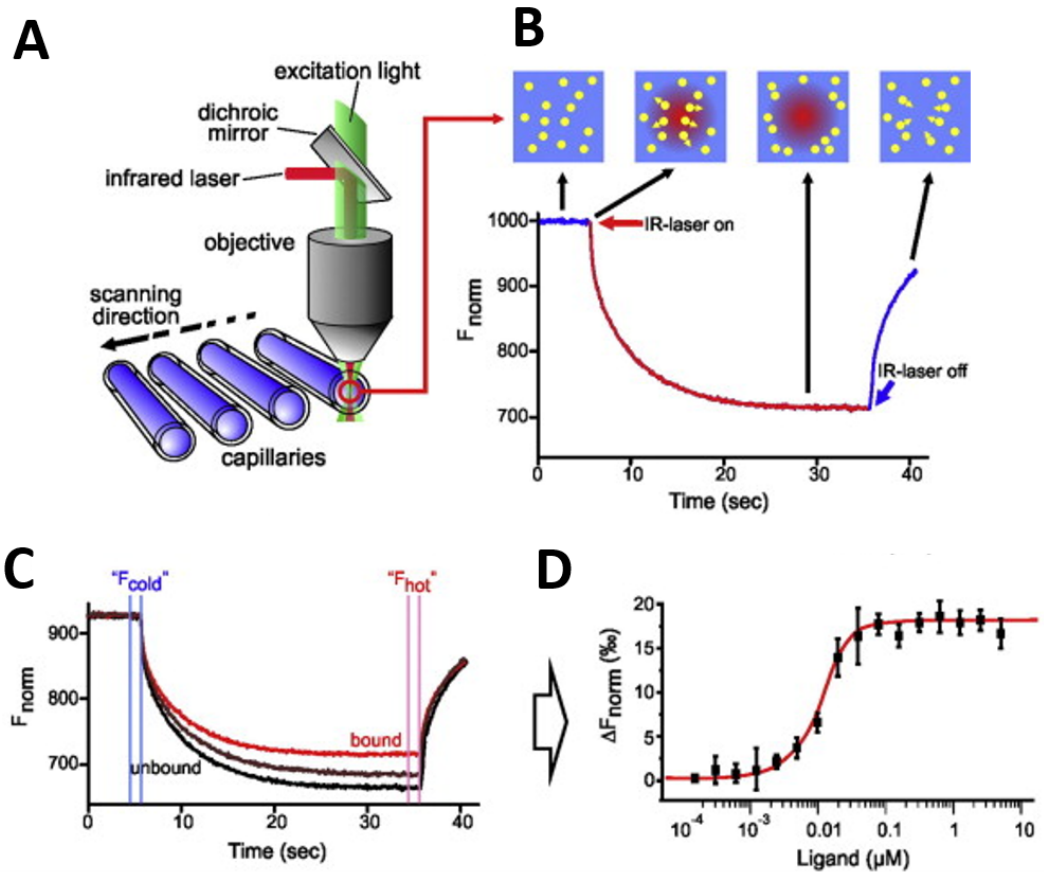


Figure 2.6 – A) The optics for the MST system with IR laser and fluorescence excitation and emission detection through the same objective, focused on the capillary B) Raw signal as normalised fluorescence over time as detected during an MST experiment with "T-jump" and "thermophoresis" phases depicted in schematic pictures. C) Binding experiment with raw trace of unbound (black) and ligand bound (red) fluorescently labelled protein D) The difference between fluorescence before (F_{cold}) and after 30 seconds of IR laser application (F_{hot}) plotted against the titrated ligand concentrations. The data points for the gradual change of fluorescence difference (Δ F) against increasing non-fluorescent ligand concentrations can be used to fit a binding curve for obtaining binding constants. (Figure adopted from Jerabek-Willemsen *et al.* [2014]).

The application of the IR laser induces a T-jump, that is caused by rapid change of photophysical properties of the fluorophore with the change in temperature (Fig. 2.6B). This effect occurs in less than a second and is dependent on the environment of the fluorophore, which can change upon ligand binding, due to interaction of the fluorophore with the ligand or conformational changes that expose the fluorophore to an environment of different polarity. Since the polarity of the environment influences the quantum yield of the dye, the T-jump can probe the rigidity of the surrounding protein scaffold.

The T-jump is followed by the thermophoresis step, which happens on a second to minute time scale and can be described by the depletion (or accumulation) of fluorescent molecules due to their movement in the temperature gradient. The rate at which the molecules migrate is said to be dependent on their hydration shell. The hydration shell of a protein can be altered by release of water molecules from the ligand-binding site, as they are displaced by the ligand. Moreover, conformational changes induced by ligand binding will also change the hydration shell significantly and consequently its movement in the temperature gradient. Both T-jump and thermophoresis can be used to derive binding curves for ligand binding to a protein. By consecutive scanning of multiple capillaries with increasing ligand concentrations, followed by plotting the change in fluorescence in the T-jump or thermophoresis phase, a binding curve can be fitted to obtain the dissociation constant for ligand binding [Jerabek-Willemsen *et al.,* 2011; Jerabek-Willemsen *et al.,* 2014].

Binding of a ligand [L] to a macromolecule [M] to form a complex [LM] is described by the following equation:

$$L + M \rightleftharpoons LM$$

the equilibrium constant (K_D) can be defined as:

$$K_D = [L] \cdot \frac{[M]}{[LM]}$$

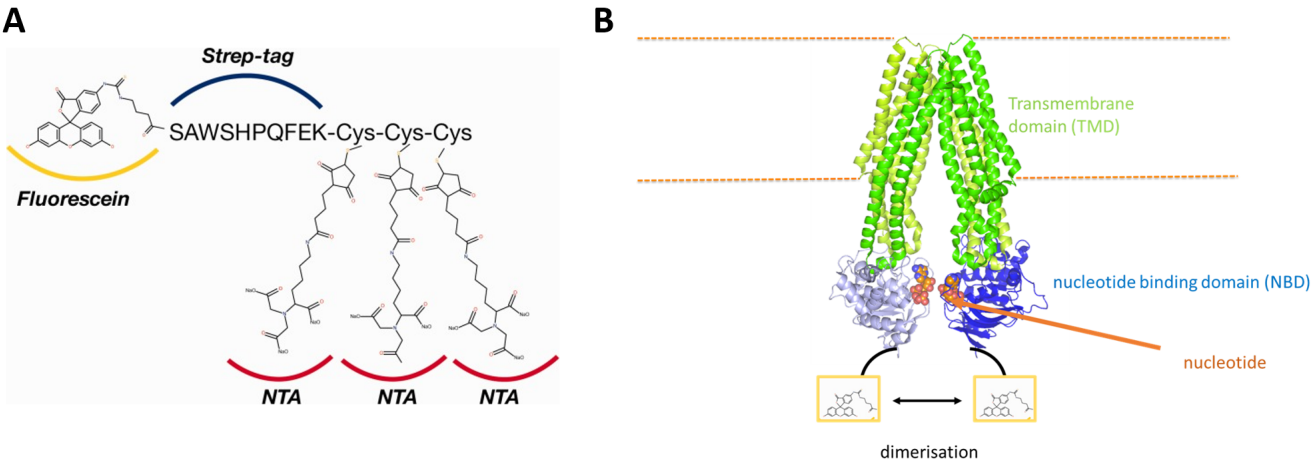


Figure 2.7 – A) Chemical structure of the peptide based fluorescent probe P3NTA (produced in house by Dr Andrew Quigley) that can link a fluorescein molecule to a histidine tag via three NTA residues as adopted from Backmark *et al.* [2013] B) Labelling position of P3NTA probe and attached fluorescein molecule on a ABCB8 homodimer.

2.11.2 Labelling of ABCB8 for MST

To enable analysis of nucleotide binding to ABCB8, the protein was labelled with a fluorophore using the P3NTA probe that links a fluorescein molecule with the decahistidine fusion tag on the C-terminus of the ABCB8 monomer (Fig. 2.7) [Backmark *et al.*, 2013].

The labelling was performed by adding a final concentration of $\sim$ 5 μM P3NTA to 15 μM of protein, followed by incubation at room temperature for 20 to 30 minutes. Excess of fluorophore was removed by desalting into SEC buffer (+0.12% OGNG, 0.012% CHS) using a G-25 column (GE Healthcare).

2.11.3 Experimental procedure for MST measurements

Nucleotide binding was determined from the T-jump signal in MST measurements using the Monolith NT.115 system (Nanotemper Technologies). Dilution series for nucleotides were prepared in SEC buffer (+0.12% OGNG, 0.012% CHS) reaching from 20 mM to 10 μM or 2 mM to 1 μM (2-fold of final concentration), as op-

timised according to binding affinities. The nucleotide dilutions were mixed 1:1 with ABCB8 (∼10 μM) in SEC buffer (+0.12% OGNG, 0.012% CHS) with a final protein concentration of 5 μM, followed by incubation for 10 minutes at room temperature. Samples were loaded into standard treated capillaries (NanoTemper Technologies).

Measurements were performed using 100% LED and 20% IR-laser power with laser on and off times set to 30 seconds and 5 seconds (before and after IR laser exposure), respectively. Fluorescence was detected with the blue LED-filter setting with excitation and emission wavelengths of 460 to 480 nm and 515 to 530 nm, respectively.

From the MST raw trace differences of fluorescence for different time points were extracted using the MO.Affinity Analysis v2.1.5 software (Nanotemper technologies). For that, changes in fluorescence were determined between different time points (T_1 and T_2) in the MST trace in order to measure the T-jump signal, thermophoresis signal or a signal accounting for both effects as summarised in Table 2.5. For all measurements on ABCB8 wild type, binding curves were obtained from the the T-jump signal plotted against increasing nucleotide concentrations ([S]). Binding curves for ABCB8 E637Q were obtained from the combination of the T-jump and thermophoresis signals plotted against the nucleotide concentrations. Binding curves with resulting equilibrium constants (K_D) and Hill coefficients (h) for all measurements were fitted with a "specific binding with Hill slope" model (Eq.2.11.1) analysed in the Graphpad Prism software. B represents the fraction of ligand occupied binding sites in ABCB8 and B_{max} the maximal binding site occupation. Data were obtained from N=2 and N=3 ABCB8 purifications (with exception of N=1 protein purifications for ABCB8 E637Q) measured in triplicate. Error bars in graph represent the standard deviations. K_D values and Hill coeffi-

cients are given with ±S.E..

$$B = B_{max}[\frac{[S]^h}{K_D^h + [S]^h}] \tag{2.11.1}$$

Table 2.5 – Summary of signals determined from MST raw data trace by calculating difference of averaged fluorescence over time points T_1 and T_2.

Signal	**Time points T_1 and T_2 relative to length of IR-laser exposure**		
	T_1 (s)	**T_2 (s)**	
T-jump	-1-0	0.5-1.5	Fluorescence change promptly after heating of sample
thermophoresis	1-2	28.88-29.88	Fluorescence change due to diffusion of fluorescently labelled biomolecule along temperature gradient
T-jump+ thermophoresis	-1-0	28.88-29.88	Combination of both effects

2.12 Cross-linking with DSS and EGS

Disuccinimidyl suberate (DSS) and ethylene glycol bis(succinimidyl succinate) (EGS) (Fig. 2.8) are irreversible membrane permeable crosslinkers that react with primary amines of lysines and the N-terminus at pH 7-9. Their reactive group is a N-hydroxysuccinimide (NHS) ester that can form an amide group with the amine (Fig. 2.9). If the spacer arms of DSS (11.4 Å) or EGS (16.4 Å) are long enough, two lysines can be crosslinked by two consecutive reactions of lysines with the two NHS groups on either end of the crosslinker.

ABCB8 (2 μM) was incubated with 1 mM nucleotide for 30 minutes at room temperature prior to the crosslinking experiment. Subsequently, 1 mM DSS or EGS (both Thermo Fisher Scientific) were added to the samples and incubated at 37 °C for 30 minutes. DSS and EGS were made up in DMSO at 25 mM stock concentrations.

Following incubation with the crosslinker, the reaction was quenched by addition of 50 mM ammonium bicarbonate. SDS-PAGE was performed by mixing 4 μL

of 4x sample buffer (NuPAGE; containing 250 mM DTT) with 12 μL of the DSS incubated ABCB8 samples. Bands on the Coomassie-stained gel were quantified using the "Quantitative Tool" in the Image Lab Software 6.0 (Bio-Rad).

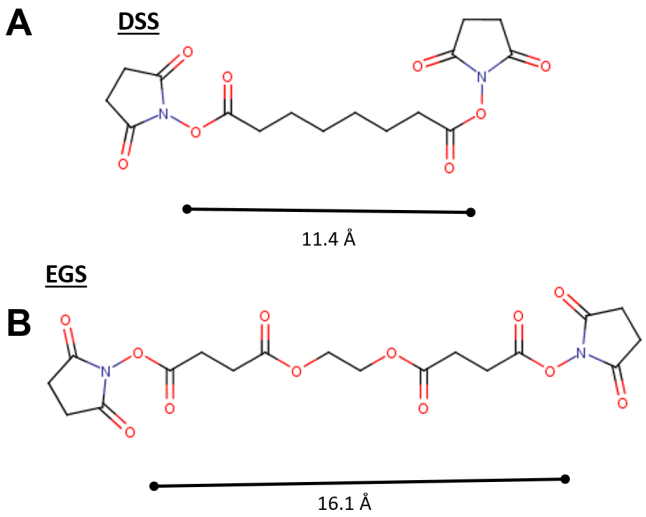


Figure 2.8 – Structural formulas of disuccinimidyl suberate (DSS;A) and ethylene glycol bis(succinimidyl succinate) (EGS;B) with length of spacer arm.

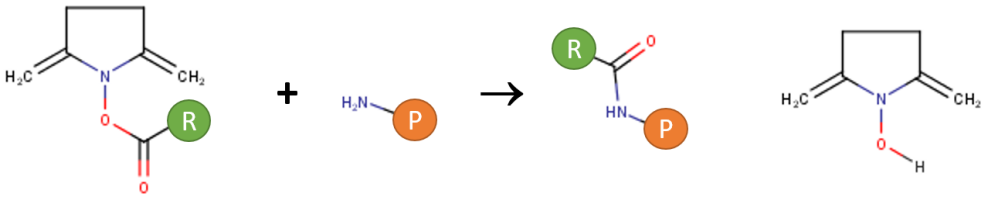


Figure 2.9 – Crosslinking reaction of DSS or EGS (spacer "R") with primary amino group in protein (P) (lysine or N-terminus).

2.13 Reconstitution of ABCB into proteoliposomes

ABCB8 was reconstituted into proteoliposomes of different lipid combinations described in chapter 4.2.1. Reconstitution was performed as summarised in Fig. 2.10. Lipids (Avanti Lipids; Table 2.6), solubilised in chloroform were dried in a round-bottom flask with argon gas to form a thin film. Following residual chloroform removal by further incubation under vacuum for 1 hour, lipids were solubilised with 20 mM cholate in SEC buffer to give a lipid stock solution of 25 mg/ml. Prior

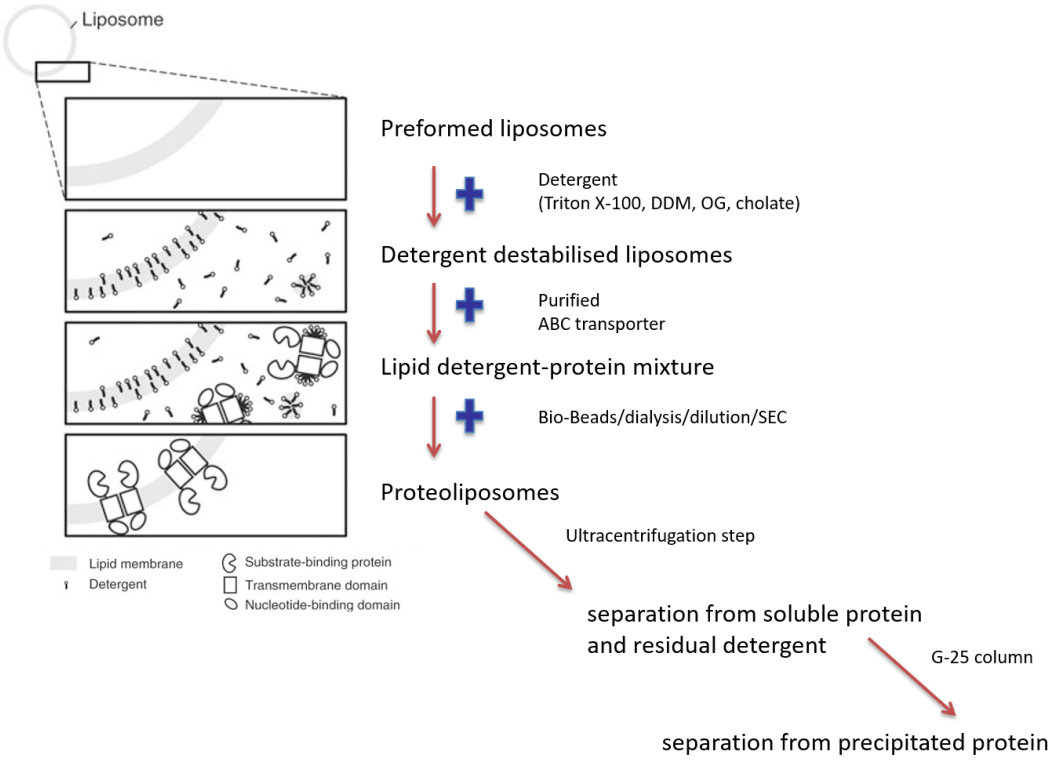


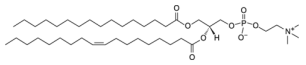
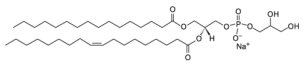
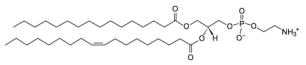
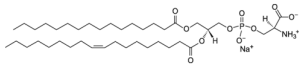
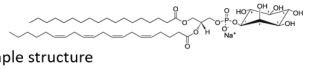
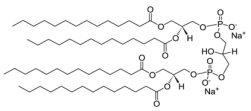
Figure 2.10 – Flow-chart for reconstitution process of ABCB8 adapted from Geertsma *et al.* [2008].

to reconstitution, lipids were mixed in ratios indicated in the result section in chapter 4.2.1 and diluted to 8 mg/ml final concentration (including volume required for protein addition). Furthermore, cholate was added to adjust to a concentration of 20 mM. Then, the mixture underwent five freeze and thaw cycles, as well as incubation in an ultrasonic bath for 10 minutes at room temperature. Subsequently, protein in a 30:1 lipid:protein (w/w) ratio was added and incubated on ice for 30 minutes. Reconstitution samples were diluted to cholate concentrations below CMC (about 2.2-fold) and SM2-Bio-Beads (Bio-Rad) washed with SEC buffer were added. After 1 hour rotation at 4 °C, more SM2-Bio-Beads were added for incubation at 4 °C over-night. The sample was further incubated with a new addition of SM2-Bio-Beads for another hour at 4 °C, before proteoliposomes were pelleted in an ultra centrifuge at 100,000 g for 1 hour at 4 °C. Samples were re-suspended in 500 μL SEC buffer (without detergent) and precipitated protein was removed with a G-25 column. Proteoliposomes were concentrated by another ultracentrifugation

step at 100,000 g for 1 hour at 4 °C. Samples were re-suspended in SEC buffer for further functional studies. Protein amount was estimated with densitometry from bands on a Coomassie-stained SDS-PAGE gel and compared to an ABCB8 concentration standard (1-0.06 μg) using the the "Qualitative Tool" in the Image Lab Software 6.0 (Bio-Rad).

For TEV cleavage of protein reconstituted into proteoliposomes, 0.05 mg/ml ABCB8 was incubated with 1 mg/ml TEV protease for 1 hour at room temperature.

Table 2.6 – Structure and nomenclature of lipids used for reconstitution

Lipid	Abbreviation	Fatty acids	Structure
1-palmitoyl-2-oleoyl-*sn*-glycero-3-phosphocholine	POPC	16:0-18:1	
1-palmitoyl-2-oleoyl-*sn*-glycero-3-phospho-(1'-*rac*-glycerol)	POPG	16:0-18:1	
1-palmitoyl-2-oleoyl-*sn*-glycero-3-phosphoethanolamine	POPE	16:0-18:1	
1-palmitoyl-2-oleoyl-*sn*-glycero-3-phospho-L-serine	POPS	16:0-18:1	
L-α-phosphatidylinositol mix from liver extract	PI*	mixture of different fatty acid adducts	 example structure
1',3'-bis[1,2-dimyristoyl-*sn*-glycero-3-phospho]-*sn*-glycerol	CDL	4x 14:0	

2.14 Mass spectrometry

2.14.1 Intact mass spectrometry on ABCB8

Intact mass spectrometry using electron mass spectrometry (ESI-QTOF) was used to identify whether ABCB8 constructs were truncated or whether mixed disulphides in the presence of glutathione were formed. Glutathione (oxidised and reduced) was dissolved at 100 mM in 100 mM HEPES pH 7.5. 5 mM of glutathion were added to protein sample in SEC buffer and incubated for 1 hour at room temperature.

Reversed-phase chromatography was performed in-line prior to mass spectrometry using an Agilent 1290 uHPLC system (Agilent Technologies, Palo Alto, CA, USA). Concentrated protein samples were diluted to 1 mg/ml in 1% formic acid and 50 μL was injected on to a 2.1 mm x 12.5 mm Zorbax 5 μm 300SB-C3 guard column housed in a column oven set at 40 °C. The solvent system used consisted of 0.1% formic acid in ultra-high purity water (Millipore) (solvent A) and 0.1 % formic acid in methanol (LC-MS grade, Chromasolve) (solvent B). Chromatography was performed as follows: Initial conditions were 90 % A and 10 % B and a flow rate of 1.0 ml/min. A linear gradient from 10 % B to 80 % B was applied over 35 seconds. Elution then proceeded isocratically at 95 % B for 40 seconds followed by equilibration at initial conditions for a further 15 seconds. Protein intact mass was determined using a 6530 electrospray ionisation quadrupole time-of-flight mass spectrometer (Agilent Technologies, Palo Alto, CA, USA). The instrument was configured with the standard ESI source and operated in positive ion mode. The ion source was operated with the capillary voltage at 4000 V, nebulizer pressure at 60 psi, drying gas at 350 °C and drying gas flow rate at 12 L/min. The instrument ion optic voltages were as follows: fragmentor 250 V, skimmer 60 V and octopole RF 250 V.

Quantitative Analysis software (Mass Hunter) was used for data evaluation. Peaks on HPLC chromatogram were de-convoluted between 1500-3000 m/z and mass of 10-100 kDa with signal to noise cut off of 3 for better detection sensitivity.

2.14.2 ESI-QTOF measurements of nucleotides

Direct infusion of 5 mM nucleotides in 100 mM HEPES buffer (pH 7.5) for mass spectrometry was performed using an 6530 electrospray ionisation quadrupole time-of-flight mass spectrometer (Agilent Technologies, Palo Alto, CA, USA). The instrument was configured with the standard ESI source and operated in negative ion mode. The ion source was operated with the capillary voltage at 4000 V, nebulizer

pressure at 17 psi, drying gas at 350 °C and drying gas flow rate at 5 L/min. The instrument ion optic voltages were as follows: fragmentor 250 V, skimmer 65 V and octopole RF 750 V.

2.15 Bioinformatics methods

Sequence were aligned using Clustal Omega with MBED-like clustering iteration set on, and "number of combined iterations", "max guide tree iteration" and "max HMM iteration" set to default. [McWilliam *et al.,* 2013; Sievers *et al.,* 2011]. Alignments were visualised with ESPript [Robert & Gouet, 2014].

CONSURF was used to analyse conservation of residues in structures. For that multiple sequence alignments (generated with Clustal Omega) for 50 ABCB8 homologues, as well as for sequences of all human ABC transporters of the B family, were produced and provided for the CONSURF web server. [Celniker *et al.,* 2013].

MODELLER was used to create a homology model of ABCB8 on the basis of ABCB10 (3ZDQ) using the ModWeb web server [Eswar *et al.,* 2007; Webb & Sali, 2014]. The ABCB10 structure used for this model was solved with X-ray crystallography to 2.85 Å.

CHAPTER 3

Establishing a purification and crystallisation protocol for ABCB8

3.1 Introduction

The following chapter describes how a purification protocol for human ABCB8 was established using the SGC pipeline approach (section 1.4.4) for initial optimisation of protein yields, purity and monodispersity sufficient for crystallisation attempts. Furthermore, it is shown how crystallisation of ABCB8 was established and optimised to give diffraction beyond 4 Å suitable for structure determination.

3.2 Results

3.2.1 Construct design for ABCB8

Optimising expression, purification and crystallisation of human membrane proteins involves testing different variations of the original gene by truncating full-length constructs at C- and N-termini. For example, less ordered regions on the constructs ends can negatively influence the protein stability or its ability to form tight crystal contacts. However, truncations into fully folded domains can prevent proper folding of secondary and tertiary structure elements. Therefore, homology models based on the inward-facing state of ABCB10 (3ZDQ) using MODELLER [Eswar *et al.,* 2007], and a secondary structure and domain predictions using PSIPRED [McGuffin *et al.,* 2000], were generated for the construct design of ABCB8 (section 2.15).

As ABCB8 has an N-terminal mitochondrial targeting sequence (section 1.3.2), over-expression of the full-length construct of ABCB8 might overload the translocation machinery of the mitochondria and therefore could reduce expression yields. However, expression of the membrane protein into its natural lipid environment can be necessary for its stability. On this basis, ABCB8 constructs were designed to have full-length N- and C-termini, as well as truncated versions that would lack an N-terminal signalling peptide or more flexible C-terminal regions. Ideally boundaries were chosen so that they preserve the functional core of an ABC transporter (TMH1-6 and NBD region).

Constructs designed had an N-terminal hexahistidine tag (pFB-LIC-Bse) or a C-terminal FLAG and decahistidine purification tags (section 2.2) Initial constructs were designed by Dr Chitra Shintre and subsequently by myself in order to optimize crystallisation. Fig. 3.1 gives an overview of truncation constructs designed (construct marked with * were designed by Dr Chitra Shintre) and qualitative evaluation of purification yields from a 3 mL purification test (conducted by the

Construct	N-terminus	C-terminus	tags	expression yield
c001*	M1	S735	6x His	none
c002*	G53	S735	6x His	medium
c003*	P85	S735	6x His	none
c004*	G129	S735	6x His	none
c005*	M1	D713	6x His	none
c006*	G53	D713	6x His	none
c007*	P85	D713	6x His	none
c008*	G129	D713	6x His	none
c009*	P81	S735	10x His-FLAG	none
c010*	G92	S735	10x His-FLAG	low
c011*	P98	S735	10x His-FLAG	low
c012*	A111	S735	10x His-FLAG	low
c013*	P81	A714	10x His-FLAG	low
c014*	G92	A714	10x His-FLAG	high
c015*	P98	A714	10x His-FLAG	high
c016*	A111	A714	10x His-FLAG	high
c017*	P81	H668	10x His-FLAG	medium
c018*	G92	H668	10x His-FLAG	low
c019*	P98	H668	10x His-FLAG	low
c020*	A111	H668	10x His-FLAG	low
c021*	P81	G685	10x His-FLAG	low
c022*	G92	G685	10x His-FLAG	medium
c023*	P98	G685	10x His-FLAG	medium
c024*	A111	G685	10x His-FLAG	low
c025	G129	A714	10x His-FLAG	medium
c026	G129	H668	10x His-FLAG	low
c027	G129	G685	10x His-FLAG	none
c028	G129	A719	10x His-FLAG	high
c029	A118	S735	10x His-FLAG	high
c030	A118	A714	10x His-FLAG	high
c031	A118	H668	10x His-FLAG	none
c032	A118	G685	10x His-FLAG	low
c033	A118	A719	10x His-FLAG	high
c034	A151	S735	10x His-FLAG	low
c035	A151	A714	10x His-FLAG	none
c036	A151	H668	10x His-FLAG	none
c037	A151	G685	10x His-FLAG	none
c038	A151	A719	10x His-FLAG	none
c039	P81	A719	10x His-FLAG	high
c040	G92	A719	10x His-FLAG	high
c041	P98	A719	10x His-FLAG	high
c042	A111	A719	10x His-FLAG	high
c043	P81	S735	6x His	high
c044	G92	S735	6x His	medium
c045	P98	S735	6x His	high
c046	A111	S735	6x His	high
c047	G92	A714	6x His	high
c048	P98	A714	6x His	high
c049	A111	A714	6x His	high
c050	P81	H668	6x His	low
c051	G92	H668	6x His	low
c052	P98	H668	6x His	low
c053	A111	H668	6x His	low
c054	P81	G685	6x His	low
c055	G92	G685	6x His	low
c056	P98	G685	6x His	low
c057	A111	G685	6x His	low
c058	G92	A718	6x His	medium
c059	P98	A718	6x His	high
c060	A111	A718	6x His	high
c061	G129	A714	6x His	high
c062	G129	H668	6x His	low
c063	G129	G685	6x His	low
c064	G129	A718	6x His	none
c101*	M1	S718	10x His-FLAG	none
c102*	G36	S718	10x His-FLAG	medium
c103*	P68	S718	10x His-FLAG	none
c104*	G112	S718	10x His-FLAG	low
c105*	M1	A697	10x His-FLAG	low
c106*	G36	A697	10x His-FLAG	medium
c107*	P68	A697	10x His-FLAG	medium
c108*	G112	A697	10x His-FLAG	none

Figure 3.1 – Constructs designed on the basis of the ABCB8-isoform 2 (numbering isoform 1) with sequence construct number, N- (red) and C-terminal (blue) truncation. N-terminal and C-terminal purification tags were added by cloning into plasmid pFB-LIC-Bse and pFB-CT10HT-LIC, respectively. Constructs marked with * were designed by Dr Chitra Shintre.

Biotech group at the SGC). The 3 mL purification test not only tests for expression, but also whether the protein can be extracted with DDM followed by a crude IMAC purification. Extractability by DDM can be a good indicator that folded protein can be expressed and purified in a particular detergent.

Prior to starting this project, constructs c001-c008 and c101-c108 had been tested in small-scale expression tests and large-scale expression, but expression yields were low and the protein could not be isolated in a stable form (unpublished data from Prof. Liz Carpenter's group). In order to identify whether the mitochondrial targeting sequence was cleaved off in the mitochondria, a full-length construct (c101) with C-terminal FLAG and His_{10}-tag was retested, but gave no expression. To allow for greater compatibility with a species specific mitochondrial recognition sequence, c101 and c105 were tested in a mammalian expression system. Unfortunately no expression was detected for these constructs. Over-expression of the full-length protein was potentially inhibited by the requirement for the protein to be transported into the mitochondria using the TIM and TOM translocation machinery that may be overloaded in the cells. Constructs with N-terminal truncations excluding a mitochondrial targeting signal are likely to be over-expressed in the ER, as it has been observed for ABCB10 [Liesa *et al.,* 2012].

Apart from the N-terminal full-length constructs, all other truncations were chosen on the basis of mitochondrial targeting sequence predictions. In order to assess the minimal length of construct that would work, a series of constructs were tested. Constructs ABCB8$^{Gly92-Ala714}$, ABCB8$^{Pro98-Ala714}$ or ABCB8$^{Ala111-Ala714}$ (c014, c015 or c016) with C-terminal purification tags gave the highest expression yields in the 3 mL purification test among the ones tested at that time (*). Consequently, constructs ABCB8$^{Pro98-Ala714}$ and ABCB8$^{Ala111-Ala714}$ were selected for further tests. Further truncations on the C-terminus to His668 and Gly685 only give negligible expression. This is in accordance with a homology model created with MODELLER [Sali, 2008; Webb & Sali, 2014] on the the basis of the inward-facing state of ABCB10 (pdb code: 4AYT). The model shows that the

constructs ABCB8$^{Ala111-Ala714}$ (c016) only contains the transporter core, which consists mainly of the TMDs and NBDs.

3.2.2 Small scale detergent solubilisation test

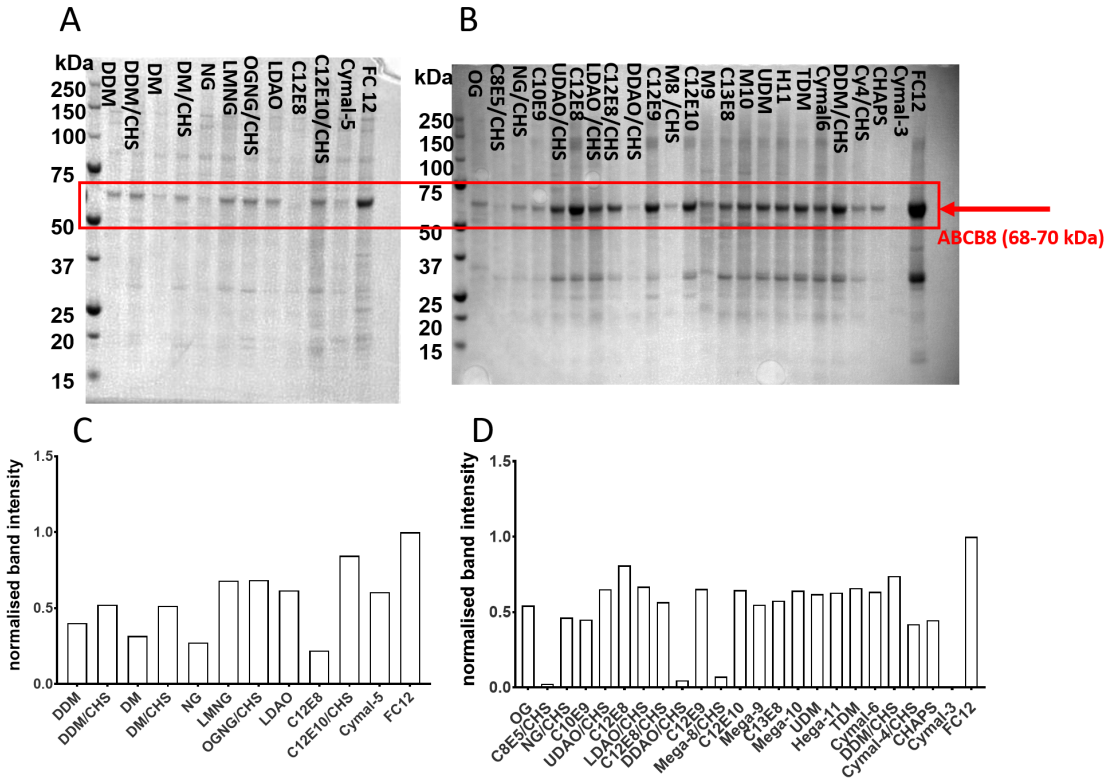


Figure 3.2 – Coomassie-stained SDS-PAGE gels of "12 detergent solubilisation test" of ABCB8A-c015 (expected mass of ABCB8^{+tag}: 70 kDa)(A) and an extended "24 detergent solubilisation test" on ABCB8A-c016 (expected mass of ABCB8^{+tag}: 68 kDa) (B). Proteins in the markers on the right with labels for the molecular weight of the standard. C) and D) represent yields of detergent extraction quantified by densitometry and normalized against FC12.

Although DDM could extract constructs of ABCB8 in the previous 3 mL test, it might not be the best detergent for also providing stability and monodispersity of the protein, as evaluated in a subsequent monodispersity test. Prior to this monodispersity screen, 12 detergents are pre-tested simultaneously to test how well they extract ABCB8 in order to narrow down the detergent options. For that, a range of mainly non-ionic detergents are used for solubilisation (1 % detergent concentration) of ABCB8 on a 4 mL cell culture scale.

The "12 detergent solubilisation test" was first applied to construct c015 (Fig. 3.2A). Zwitterionic Foscholine- 12 (FC12) was used as a control for maximal level of expressed protein. FC12 is a relatively harsh ionic detergent which is thought to extract all available membrane protein regardless of whether the protein is folded or not [Thomas & Tate, 2014]. For ABCB8A-c015 the maltoside detergents DDM, DDM/CHS, DM/CHS and the neopentyl glycol detergents LMNG and OGNG/CHS, as well as the polyoxyethylene C12E10/CHS showed high levels of extraction. In addition, a 24 detergent test was designed and used with construct c016 in order to probe an extended set of detergents that can be used for solubilisation and purification (DDM/CHS and Foscholine 12 were used as positive controls) (Fig. 3.2B). A strong band indicating sufficient extraction of ABCB8 was found for the longer chain polyoxy ethylene detergents C12E8, C12E8/CHS, C12E9 and C12E10 , as well as for C13E8 to a lesser extent. C8E5/CHS and C10E9 however did not solubilise ABCB8 well, potentially due to their shorter carbon chains. Cymal-6 extracted ABCB8 at comparable levels to DDM/CHS, whereas shorter chain Cymal-4 and Cymal-3, as well as Cymal-5 in the 12 detergent test were less effective. The same trend is evident for methylglucamides Mega-8 (M8)/CHS, Mega-9 (M9) and Mega-10 (M10), and hydroxyethylglucamide HEGA-11, which showed higher extraction yields with increasing chain lengths. Although Mega-10 produced decent extraction, it was not considered for a follow-up screen due to its relatively high CMC of 0.21 % (w/v) and precipitation at 4 ^{o}C. Despite being zwitterionic, CHAPS showed significantly little extraction, which can be caused by the extraction concentration being only twice its CMC value of 0.5 % (w/v).

In-gel tryptic digest followed by tandem mass spectrometry (MS/MS) was performed by the Biotech group in the SGC to confirm that the bands contained ABCB8 on the 12 and 24 detergent solubilisation tests.

3.2.3 Monodispersity screens

Monodispersity screens: detergents

Although the 12 or 24 detergent test is a useful tool to judge what detergents the protein can be extracted in, it does not evaluate the stability and monodispersity of this protein. To address this question, ABCB8 was purified on a 250 ml scale in selected detergents (in parallel) following protocols that included extraction of protein from membranes, an IMAC purification and a reverse IMAC purification step, followed by size exclusion chromatography (SEC) on the Dionex HPLC system using a Sepax SRT SEC-300 column. The SEC profiles obtained from this experiment provide information on the type of detergent that is likely to give stable and monodisperse protein required for successful crystallisation experiments. The flow-chart in Fig. 3.3 gives an overview of the purification protocol used in the monodispersity screen and large-scale purification protocol. Co^{2+}-TALON resin was shown to yield more and purer mammalian membrane proteins in the IMAC purification step compared to Ni^{2+}-NTA resin (unpublished data Prof. Liz Carpenter's group).

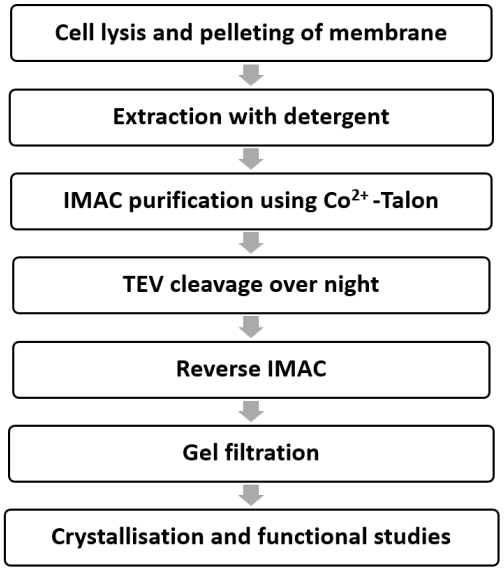


Figure 3.3 – Flow-chart with overview of purification protocol for ABCB8 used for small-scale monodispersity screening and large-scale purifications. Chemical modification was later added to the purification protocol as mentioned in section 3.2.6.

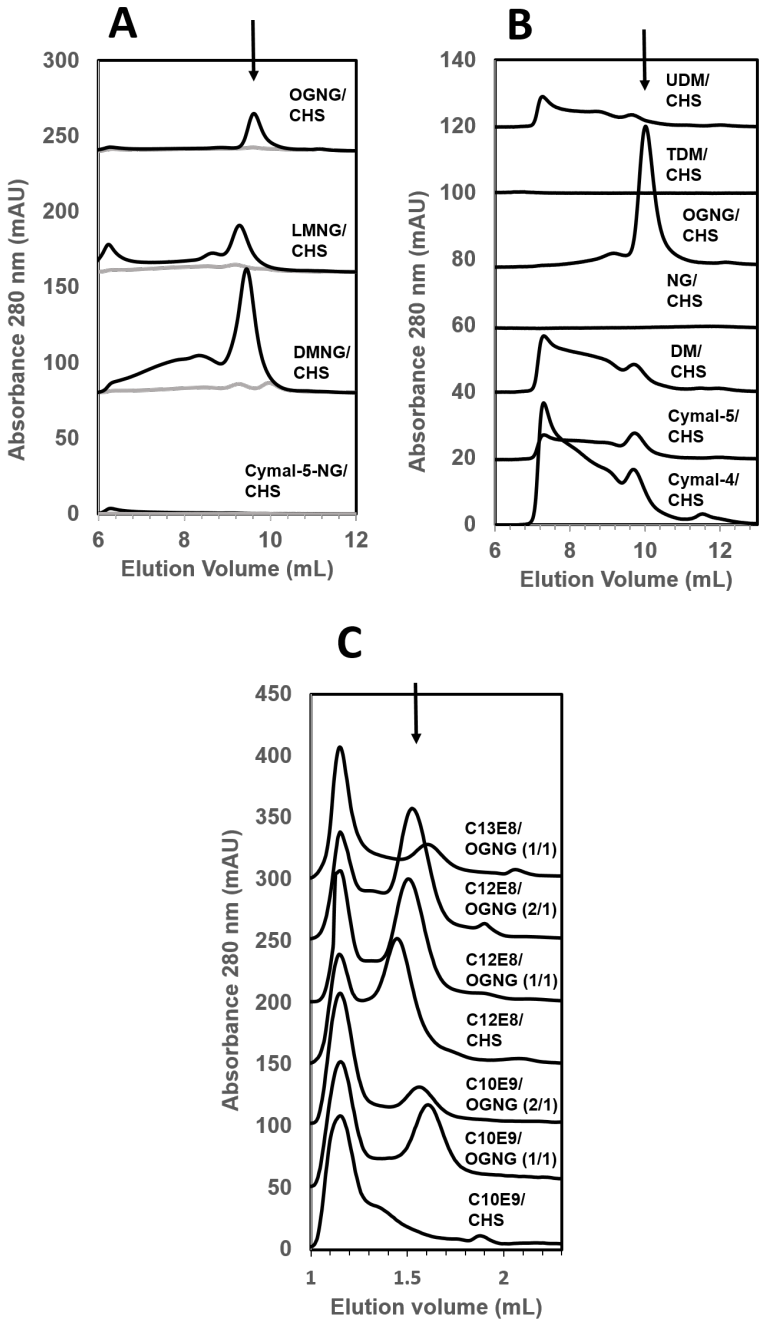


Figure 3.4 – A and B: SEC chromatograms (monitored by UV absorption at 280 nm) obtained using the Dionex HPLC system in combination with a Sepax SRT SEC-300 column: A) ABCB8-c015 (grey) and ABCB8-c016 (black) purified in HEPES pH 7.5, 200 mM NaCl, 0.5 mM TCEP and 0.5 mM $MgCl_2$. B) ABCB8-c016 purified in MES pH 6.5, 200 mM NaCl, 2 mM TCEP and 0.5 mM $MgCl_2$ and 5 % glycerol. C) ABCB8-c016 purified in MES pH 6.5, 200 mM NaCl, 2 mM TCEP and 0.5 mM $MgCl_2$ and 5 % glycerol using an ÄKTA purification system in combination with a Superdex 10/300 column (GE Healthcare). The elution volume for dimeric ABCB8 is indicated with a black arrow.

Constructs ABCB8$^{Pro98-Ala714}$ and ABCB8$^{Ala111-Ala714}$ (c015 and c016) were both tested in neopentyl glycol detergents OGNG/CHS, LMNG/CHS, DMNG/CHS and Cymal-5-NG/CHS in HEPES pH 7.5, 200 mM NaCl, 0.5 mM $MgCl_2$ and 0.5 mM TCEP (Fig. 3.4A). Although construct c015 showed a high level of extraction in various detergents, purification in the selected detergents including OGNG/CHS used in the 12 detergent test did not yield single non-void protein peaks in SEC runs. In contrast, construct c016 gave a single sharp peak in OGNG/CHS and single but broad peaks in DMNG/CHS and LMNG/CHS. Cymal-5-NG failed to give peaks for either construct. Only OGNG/CHS and DMNG/CHS were taken further for scale-ups, as LMNG forms larger micelles compared to DMNG and OGNG and is not considered optimal for crystallisation in vapour diffusion.

Furthermore, maltoside detergents DM/CHS, UDM/CHS and TDM/CHS were tested, as well as NG and cymal detergents (Cymal-4 and Cymal-5) in optimised buffer conditions using MES pH 6.5, 200 mM NaCl, 0.5 mM $MgCl_2$, 2 mM TCEP and 5 % glycerol (Fig. 3.4B). Only the control OGNG/CHS gave a sharp peak, indicating monodisperse protein. Cymal-5/CHS and DM/CHS generated a small integrated peak, but also contained an extensive shoulder.

Additional detergents, which were identified from the 24 detergent test (see section 3.2.2) were evaluated in a Dionex monodispersity screen. The purification protocol was carried out without SEC, which could not be performed due to a breakdown of the Dionex SEC system. Nevertheless, it could be concluded that all polyoxyethylenes, TDM/CHS, Cymal-6/CHS and Mega-10/CHS showed a significant loss of yield after TEV cleavage over-night, as apparent from the measured concentrations (Fig. 8.5A) and SDS-PAGE analysis (Fig. 8.5B). In particular, Cymal-6 had a comparable yield to OGNG/CHS after the IMAC step, but 90% of protein was lost after incubation with TEV over-night.

Longer chain (C10-C13) polyoxyethylenes showed comparable extraction of ABCB8 to DDM/CHS in the solubility screen, but failed to give good yields after removal of

the C-terminal tag in the previous experiment. Thus, an additional detergent screen with polyoxyethylenes C10E9/CHS and C12E8/CHS, as well as polyoxyethylen OGNG mixtures (2:1 and 1:1 ratios) without the TEV cleavage and reverse IMAC step (Fig. 3.4C) was performed. The SEC step was run on a Superdex 200 10/300 GL column on the AKTA purification system (GE Healthcare). All tested combinations gave high void peaks relative to the integrated protein peaks, but C12E8/CHS and C12E8/OGNG (2:1) gave the best void to integrated protein signal and were later used in a large-scale purification.

Monodispersity screens: buffer conditions

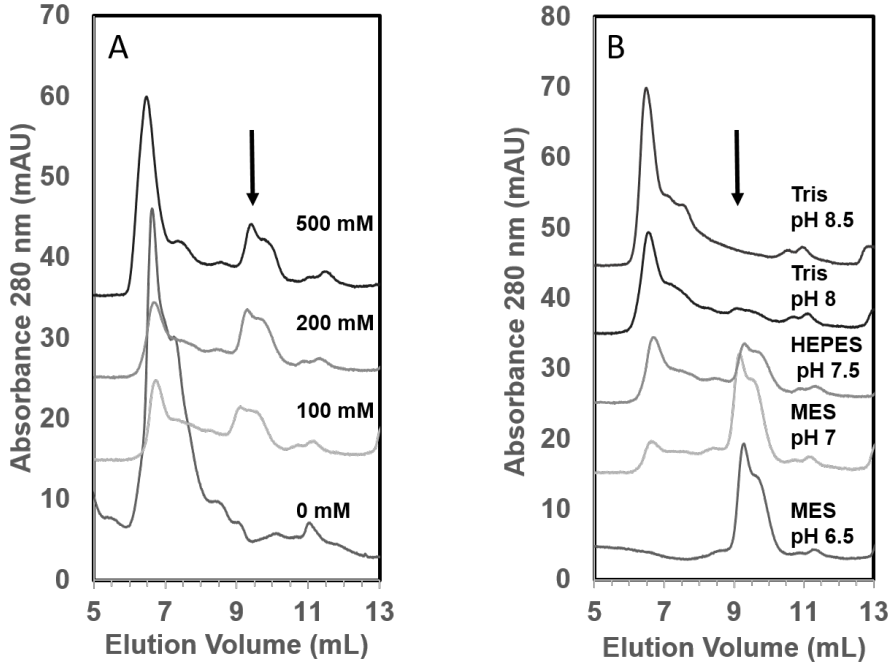


Figure 3.5 – A and B: SEC chromatograms obtained for ABCB8-c016 in OGNG/CHS using the Dionex HPLC system in combination with a Sepax SRT SEC-300 column: A) Different NaCl concentrations in HEPES pH 7.5, 0.5 mM $MgCl_2$, 0.5 mM TCEP. B) pH screen at 200 mM NaCl, 0.5 mM $MgCl_2$, 0.5 mM TCEP. The elution volume for dimeric ABCB8 is indicated with a black arrow.

Furthermore, a monodispersity screen was used to optimise buffer conditions (pH and NaCl concentrations) of ABCB8 using OGNG/CHS as extraction and purification detergent. Fig. 3.5A shows the SEC profiles obtained from purification of ABCB8 with different sodium chloride concentrations ranging from 0 mM to 500

mM in HEPES pH 7.5, 0.5 mM $MgCl_2$ and 0.5 mM TCEP. No sodium chloride or high amounts (0 mM and 500 mM) of sodium chloride gave large void peaks, whereas 100 and 200 mM NaCl increased the yield in the integrated peak. Furthermore, purification buffers of different pH with 200 mM NaCl, 0.5 mM $MgCl_2$ and 0.5 mM TCEP were tested. As evident from the SEC profiles in Fig. 3.5B, low pH buffers (MES pH 6.5 and MES pH 7) reduce the void peak significantly. A homology model of ABCB8 shows that 11 out of 13 cysteines in the primary structure are likely to be located on the protein surface (see subsection 3.2.6). The lower pH may decrease the probability of cysteines forming non-specific intermolecular disulphide bonds that can lead to aggregation.

Conclusion

The monodispersity screen proved to be a useful tool for evaluating quality of the ABCB8 sample purified in different detergents and buffers on a small scale (250 ml cell culture) to narrow down purifications conditions used on a larger scale for crystallisation attempts. Here, it was established, that purification in OGNG/CHS or DMNG/CHS in MES pH 6.5-7, 200 mM NaCl, 0.5 mM TCEP and 0.5 mM $MgCl_2$ gave the best results regarding protein yield and monodispersity.

3.2.4 Optimisation of large-scale purification

In order to obtain enough protein for crystallisation trials, large-scale purifications (3-8 L of insect cell culture) of ABCB8$^{Ala111-Ala714}$ were performed. On the basis of previously screened constructs, buffer conditions, detergent and detergent-lipid combinations, a scale-up protocol was developed. Briefly, cells from 3-10 L of insect cell culture were harvested by centrifugation and lysed. Subsequently, membranes were collected and ABCB8 extracted by incubation with 1 % OGNG supplemented with 0.1 % CHS. ABCB8 was purified by IMAC using Co^{2+}-TALON resin, followed by TEV protease cleavage over-night, TEV protease removal by reverse IMAC and

SEC on a Superdex 200 5/150 GL column (Fig. 3.3). Details are given in Material and Methods section 2.6.

Improving buffer conditions in large-scale purification

Membrane proteins can be extracted directly from the cell lysate or from purified membranes. The latter, which was used in all monodispersity screenings and large-scale ABCB8 purifications, can yield purer and less degraded protein, as soluble proteases and other impurities are removed prior to purification of the membrane protein. In addition, proteases and impurities that are associated with the membrane but not entirely embedded in it can be removed using a high salt wash (1 M NaCl) of the membranes prior to membrane protein extraction. Comparing membrane preparation protocols with and without a high salt wash of the membranes, it was observed that the stability of ABCB8 was highly impaired when membranes were treated with 1 mM NaCl (Fig. 3.6) resulting in a broad SEC peak. This does not come as a surprise, since high salt concentrations already affected ABCB8 in the monodispersity screen described in the last section. From the same buffer screen it is also clear that reducing the buffer pH to 6.5 or 7 decreased the void peak on SEC. Indeed, reducing the pH in the large-scale protocol increased yields of ABCB8 after SEC. Furthermore, the addition of 2 mM TCEP had a significant impact on yield and monodispersity of ABCB8 after SEC (Fig. 3.6A/B). In particular, during the protein concentration steps precipitation was observed prior to SEC in the absence of TCEP. The reducing reagent TCEP prevents formation of intermolecular disulphide bonds between the cysteines on the surface of the ABCB8 dimer, thus preventing aggregation. While SEC yields significantly improved in the presence of the reducing reagent, IMAC yields were independent of reducing agent concentrations (Fig. 3.6A).

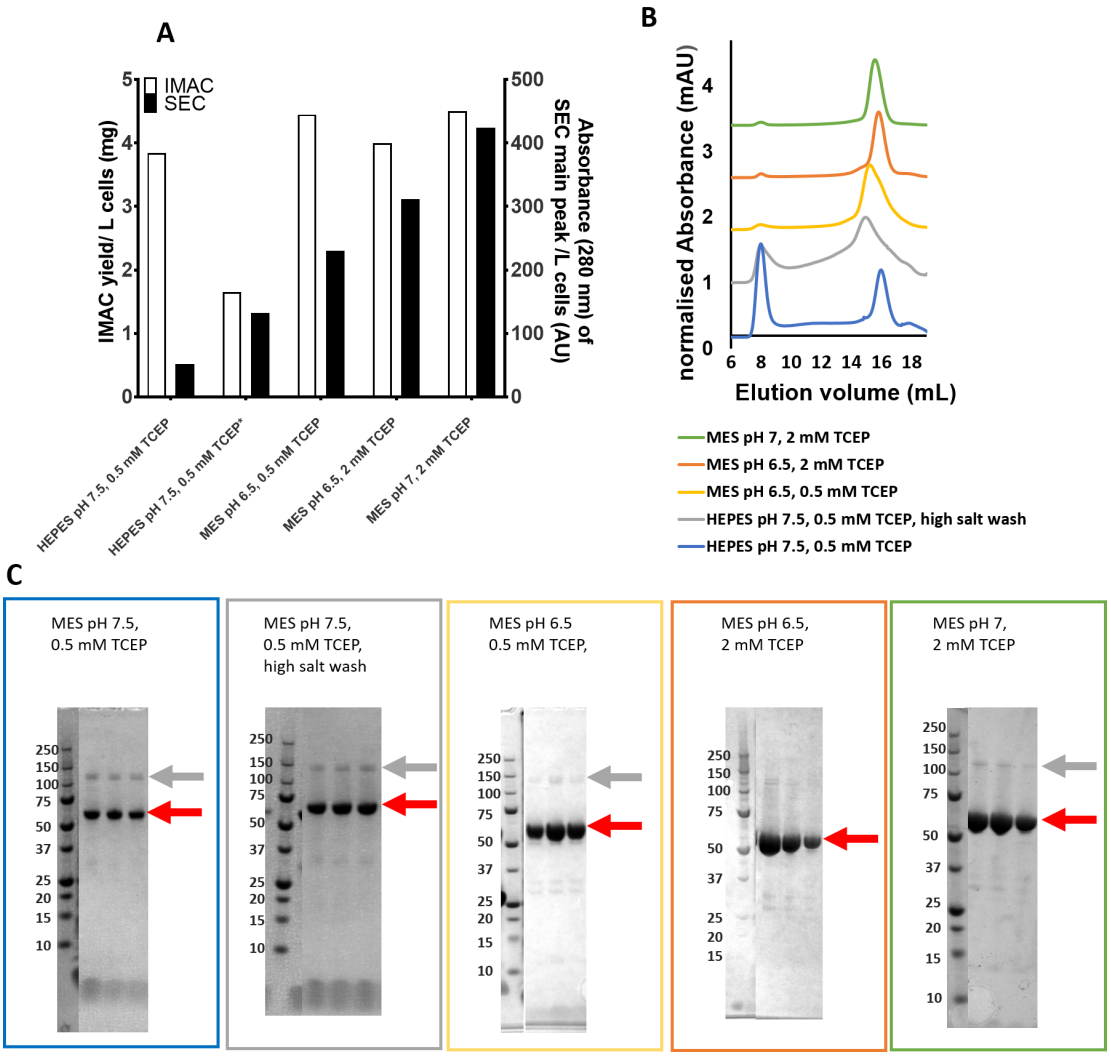


Figure 3.6 – Purification of ABCB8$^{Ala111-Ala714}$ in OGNG/CHS with different buffer conditions, increasing TCEP concentrations, and a high salt wash. A) Bar chart representing yields after IMAC and SEC peak heights both normalised for L of cells used for the purifications B) SEC profiles in different buffers and TCEP concentrations. The following components of the buffer were kept constant: 200 mM NaCl, 0.5 mM $MgCl_2$, 0.12 % OGNG and 0.012 % CHS. C) Peak fractions from SEC on Coomassie-stained SDS-PAGE gels with arrows indicating ABCB8 (red:monomer, grey: dimer).

Detergents tested in large-scale expression

Detergent/CHS combinations that gave a high degree of monodisperse protein in the SEC screens (subsection 3.2.3) were subsequently used for large-scale purifications of ABCB8$^{Ala111-Ala714}$, in order to test their effect in crystallisation trials with ABCB8. OGNG/CHS and DMNG/CHS gave single narrow peaks. OGNG/CHS was used extensively for scale-ups and subsequent crystallisation trials, as it has been proven effective for structure determination of several membrane proteins in the SGC.

The C12E8/CHS combination looked promising in the previous monodispersity screen, but failed to give stable protein in a scale-up protocol that included removal of the purification tag. The previously screened C12E8/OGNG (2:1) could stabilise ABCB8 after TEV protease cleavage (Fig. 3.7).

Although several detergents were tested for ABCB8, OGNG was the only detergent that produced crystals. Being a relatively mild detergent with a low CMC value, but having a relatively short hydrophobic tail (C8), OGNG combines the ideal properties for ABCB8 in order to achieve successful crystallisation. Although DMNG has a low CMC, its hydrophobic carbon chain (C10) potentially hinders formation of crystal contacts with ABCB8.

Intact mass spectrometry of purified ABCB8$^{Ala111-Ala714}$

Intact mass spectrometry was performed on ABCB8$^{Ala111-Ala714}$ to obtain information on potential post-translational modifications and whether the ABCB8 construct was degraded during expression and purification. Only one species at 66288 Da was detected (including sodium adducts of the protein), which is consistent with the molecular weight for the untagged ABCB8$^{Ala111-Ala714}$ (66418 Da) after methionine loss (- 131 Da) (Fig. 3.8). Although mitochondrial proteins have been shown to be glycosylated and/or phosphorylated [Burnham-Marusich & Berninsone, 2012;

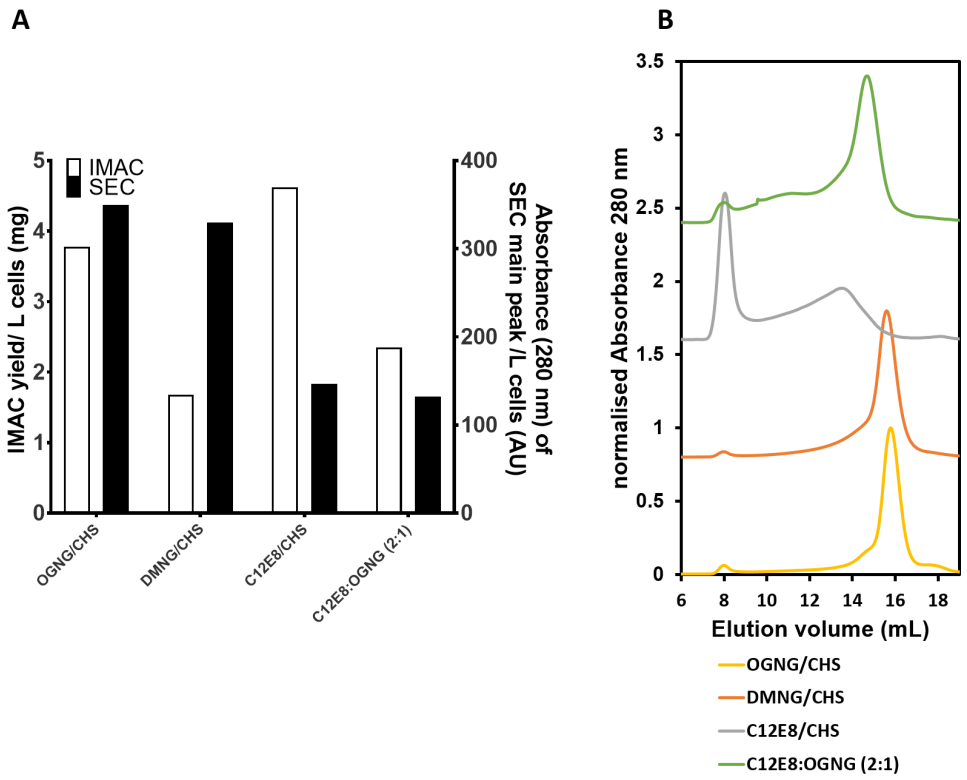


Figure 3.7 – Scale-up purification of ABCB8$^{Ala111-Ala714}$ in different detergents A) Bar chart representing yield after IMAC and absorbance of main SEC peak, both normalised against L of cells culture used for purification B) SEC profiles of ABCB8$^{Ala111-Ala714}$ in different detergents (with CHS, as labelled in the chart) and SEC buffer (containing 3xCMC detergent).

Lim *et al.*, 2016], any further post-translational modifications of ABCB8 were not detected. This is consistent with predictions on the basis of the primary structure.

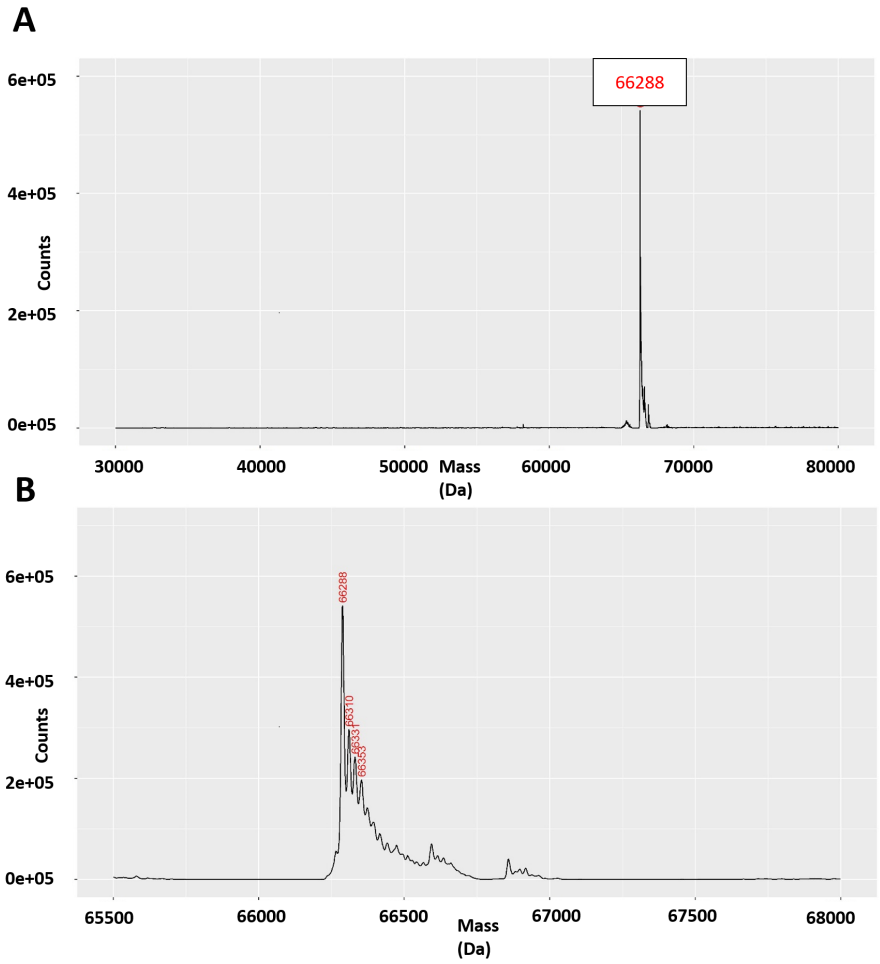


Figure 3.8 – A) Deconvoluted spectrum from intact mass spectrometry of ABCB8-c016 after TEV protease cleavage and SEC. B) Zoomed-in spectrum for 65000-68000 Da.

Conclusion

After optimisation of the purification conditions (buffer and detergent) in a large-scale protocol, the purity and stability of ABCB8 were improved. IMAC purification using Co^{2+}-TALON yielded $\sim$ 3 mg protein/L cells. Following TEV protease cleavage and reverse IMAC with Co^{2+}-TALON to remove the TEV protease and contaminating proteins, the protein yield was reduced by up to 60 %, but the purity of the protein was improved (Fig. 3.9A). SEC on a Superdex 200 5/150 GL column

Table 3.1 – Purification yields for ABCB8 large-scale purification. Values were obtained for n=11 individual purifications

purification step	yield (mg/L cell culture)
IMAC	3.01±0.75
reverse IMAC	1.95±0.65
SEC	0.39±0.14

was required to separate aggregated from monodisperse ABCB8 (Fig. 3.9B, Table 3.1).

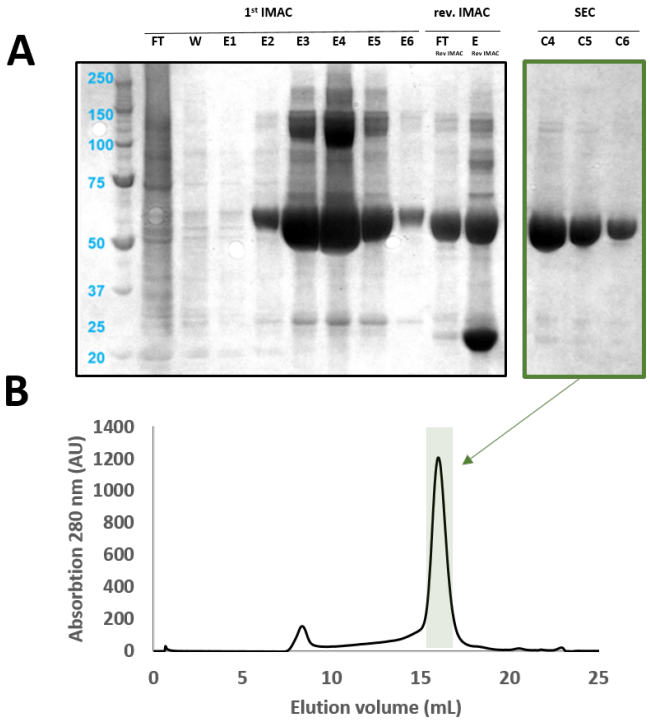


Figure 3.9 – A))Coomassie-stained SDS-PAGE gel with samples from different purification steps described in the flow chart (Fig. 3.3) (FT= flow through fraction, W=wash fraction, E1-E5= elution fractions and C1-C10=SEC fractions) B) Example SEC profile of ABCB8-c016 in MES pH 7, 200 mM NaCl, 0.5 mM $MgCl_2$, 2 mM TCEP and 0.12 % OGNG/CHS

The optimised purification protocol with low pH buffer (MES pH 6.5 or 7) and increased amounts of TCEP in OGNG/CHS gave initial crystals in an orthorhombic crystal form (crystal form 1) that diffracted to 7 Å (Fig. 3.18). Further attempts were undertaken to optimise these crystals by using constructs with a C-terminal purification tag of a different length (longer and shorter than ABCB8$^{Ala111-Ala711}$; c028, c029, c030, c033, c040, c041 and c042; see Table 2.1) and with an N-terminal

purification tag (c059, c060, c061 and c062; see Table 2.1). Additionally, surface mutations of ABCB8 were purified and put into crystallisations trials (c082,c084 and c085; see Table 2.2). Unfortunately, none of these constructs could improve the resolution of crystals form 1.

3.2.5 Lipid screens

Extraction of membrane proteins into a detergent environment can disturb the native structure. Depending on the extent of extraction (time and detergent concentration) and the chemical nature of detergents, bound lipids can be removed from the protein surface. Providing a specific lipid during the purification can preserve the protein structure. Alternatively, adding lipid to the detergent micelles can stabilise the protein in an unspecific manner due to its ability to change the micelle e.g. by size and shape [Laganowsky *et al.,* 2014]. In addition, binding of lipids to membrane proteins can change the conformation, allowing different packing in a new crystal form.

Monodispersity screening for lipid additives

Lipids were added to both OGNG only and OGNG/CHS in order to investigate their effect on the ABCB8 yield and monodispersity (Fig. 3.10A). Bovine heart lipid extract was chosen as a supplement for OGNG, as it contains a relatively high proportion of lipids found in mitochondria. In this experiment bovine heart lipids were only added to OGNG, but not to OGNG/CHS, since the lipid extract already contained cholesterol.

The addition of any type of lipid to OGNG/CHS led to an increase of purification yield after SEC while maintaining the monodispersity of the sample. Particularly CDL gave a higher integrated peak (5 x more than OGNG/CHS only sample). POPG, which is structurally related to CDL, as well as POPC, could increase the yield of the integrated peak to a similar extent.

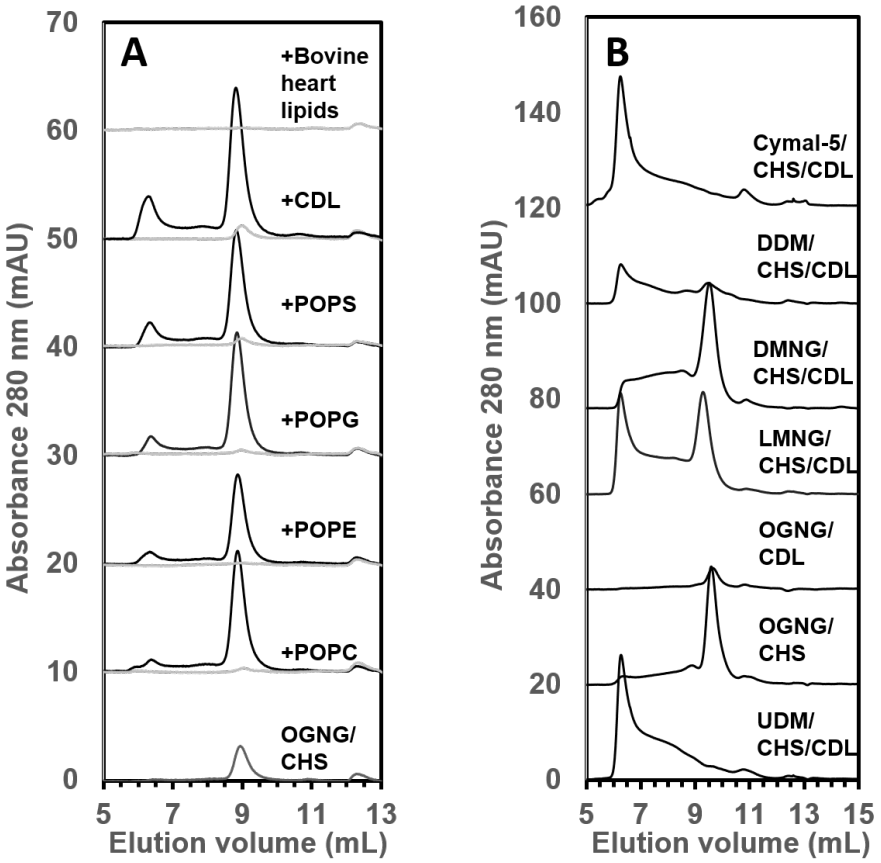


Figure 3.10 – A and B: SEC chromatograms obtained for ABCB8-c016 in MES pH 7, 200 mM NaCl, 0.5 mM $MgCl_2$, 2 mM TCEP using the Dionex HPLC system in combination with a Sepax SRT SEC-300 column: A) Extraction in OGNG/CHS and purification in OGNG only plus lipid (grey) and OGNG/CHS plus lipid (black). B) Extraction in detergent/CHS only and purification in detergent/CHS/CDL with an OGNG/CHS and OGNG/CDL control. Both experiments were performed with a 1:50 lipid to detergent ratio.

As observed previously in an attempt to purify ABCB8 in OGNG only, CHS is an essential component for the protein stability and could not be replaced with lipid or even the lipid mixture from bovine heart extract. Only OGNG/CDL allowed recovery of a small amount, 25 % of the main peak in OGNG/CHS. Due to the increase in yield with POPG and particularly CDL and the fact that CDL is most abundant in mitochondria (up to 18 % of the total phospholipid weight of the inner mitochondrial membrane in mammalian cells) [Horvath & Daum, 2013], OGNG/CHS/CDL and OGNG/CHS/POPG were chosen for large-scale purifications and crystallisation attempts, as later described in section 3.2.7.

Furthermore, since CDL increased the yield of OGNG/CHS purified protein, monodispersity screens with other detergents in the presence of CHS and CDL were attempted, including a repeat of the OGNG/CDL sample from the previous screening experiment (Fig. 3.10B). Addition of CDL to these detergents could not produce monodisperse protein in maltoside detergents (UDM and DDM) or Cymal-5. Previously obtained monodispersity for neopentyl glucosides DMNG and LMNG could be repeated in the presence of CDL, but did not improve compared to the detergent/CHS samples (see Fig. 3.4 for comparison).

Large-scale purification with POPG and CDL

From the outcome of the lipid monodispersity screen, as described in section 3.2.3, CDL and POPG were selected for a large-scale purification. Addition of POPG or CDL to OGNG/CHS increased the yield of the ABCB8$^{Ala111-Ala714}$ purification (Fig. 3.11). However, no crystals of ABCB8 grew when lipid was added during the purification. Basal ATPase activity tested for these samples were comparable to protein purified in OGNG/CHS (data not shown).

Addition of CDL or POPG during the IMAC step for purification of ABCB8 in detergent could not increase the yield in a monodispersity screen in comparison to an OGNG/CHS sample. Unfortunately, addition of these lipids during the

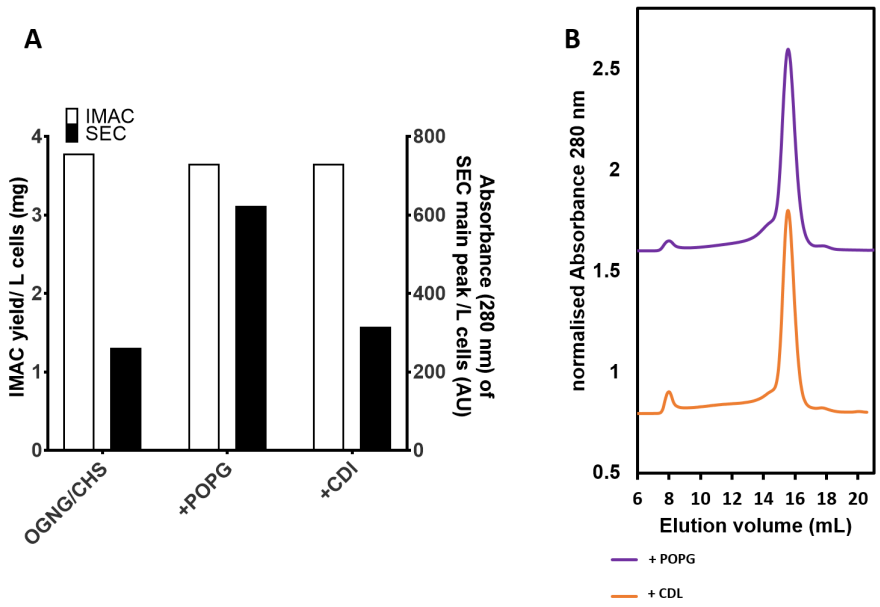


Figure 3.11 – Scale-up purification of ABCB8$^{Ala111-Ala714}$ with OGNG/lipid combinations A) Bar chart representing yields after IMAC purification and absorbance of SEC main peaks, both normalised for L culture volume used for purification B) SEC profiles of ABCB8$^{Ala111-Ala714}$ in SEC buffer containing 0.12% OGNG and 0.012% CHS and either POPG or CDL in a 1:50 lipid:detergent ratio.

purification obstructed ABCB8's crystallisation.

3.2.6 Chemical modifications

In addition to alterations of the construct, chemical modification of certain amino acids has been used as a method to improve crystals [Sainsbury *et al.*, 2010; Milić & Veprintsev, 2015; McPherson *et al.*, 2011]. This method changes the physicochemical properties of the protein surface and has been used successfully to enhance crystal lattice contacts. In order to change the crystallisation properties of ABCB8 and improve the resolution, chemical modifications of lysine and cysteine residues were introduced in the purification protocol prior to SEC.

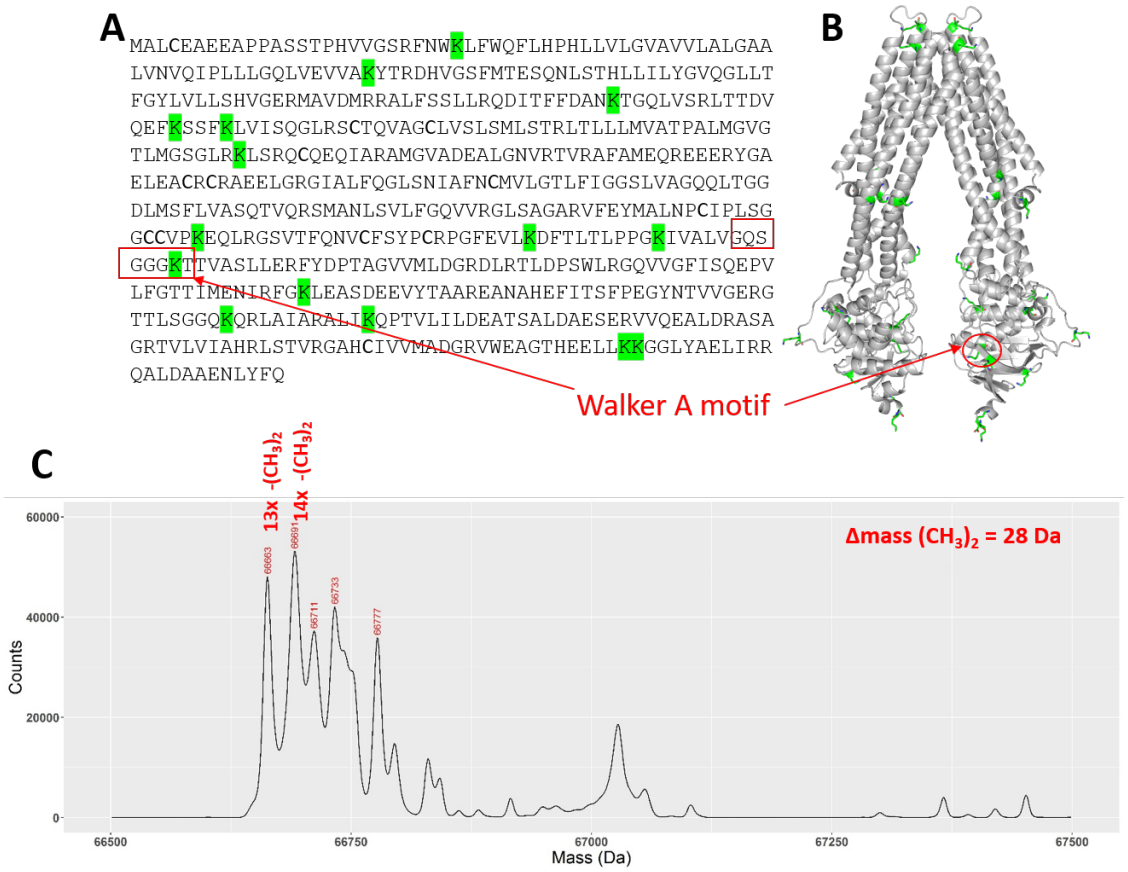
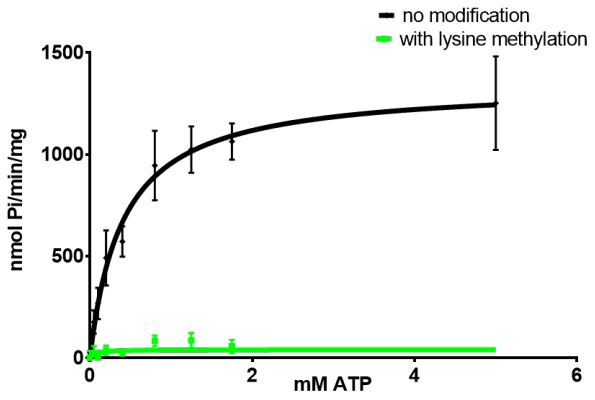


Figure 3.12 – A) Sequence of ABCB8 construct c016 with lysines highlighted in green. B) Homology model of ABCB8 (section 2.15) with lysine residues shown in stick representation in green. C) Intact MS profile of ABCB8 after treatment with ABC and formaldehyde with recorded mass in Da.

Methylation of lysines with dimethylaminoborane and formaldehyde

Methylation of lysine was first used by Rayment [1997] for crystallisation of the S1 head of myosin. ABCB8$^{Ala111-Ala714}$ has 15 lysines, which are mainly positioned on the surface (Fig. 3.12A and B). Modification of these lysines introduces a higher degree of hydrophobicity to the surface, which might not be favourable for membrane proteins. However, the change to a neutral side chain could allow for formation of new crystal contacts, that would otherwise be prevented by repulsion of two positive charges. Reductive methylation of lysines was performed using a dimethylamine borane (ABC) solution in a 1:1 mixture with formaldehyde, that triggers a two step reaction process that turns the primary amine group into an uncharged tertiary amine. The N-terminal amine can be methylated with this procedure as well, if it is accessible. Intact mass spectrometry revealed that the treatment gave species with 13 and 14 methylated lysines (Fig. 3.12C). Some of the lysines are potentially too buried to be accessible by the methylation reagents. Robust ATPase activity was detected for the unmodified ABCB8 with a V_{max} of 1345±67 nmol P_i/min/mg protein and a K_M of 0.41±0.07 mM. However, no ATPase activity was observed after reductive lysine methylation (Fig. 3.13). This is not an unexpected result, as the Walker A motif in ABCB8's NBDs has the sequence GQSGGGKT, which includes Lys513- a residue that is crucial for ATP hydrolysis. Consequently, modification of this lysine is likely to impair ATPase activity.

Methylation of lysine residues resulted in almost full prevention of protein precipitation during the concentration step before SEC and gave a sharp SEC peak with reduction of the void peak (Fig. 3.16A/B). However, crystallisation attempts with lysine modified protein did not result in crystals in sparse matrix screens with various nucleotides and crystallisation conditions tested.



	K_M (mM)	Vmax (nmol Pi/min/mg protein)
unmodified	0.41±0.07	1345±67
+methylated lysines	ND	ND

Figure 3.13 – ATPase activity of ABCB8$^{Ala111-Ala714}$ in OGNG/CHS before (black) and after reductive methylation of lysines (green) measured with the Chifflet assay as accumulation of phosphate per minute and mg of protein over a concentration range of 0-5 mM ATP. ATPase activities were plotted against ATP concentrations and a Michaelis-Menten fit was obtained using the Prism 7 GraphPad software. The table below gives V_{max} and K_M values for unmodified protein obtained from the Michaelis-Menten plot in the graph. Error bars for data points in the graph represent S.D. from three individual measurements. Kinetic parameters are given ±S.E.

Cysteine modification using iodoacetamide

We also attempted modification of the cysteine residues in ABCB8$^{Ala111-Ala714}$. As described previously (3.2.4) ABCB8 has a large number of cysteines (13 cysteines in construct c016) (Fig. 3.14A) of which 10 are predicted to be on the protein surface (Fig. 3.14B). Modifying protein with iodoacetamide is a frequently used method for stabilisation, as used in the successful crystallisation of the β2-adrenergic G protein-coupled receptor [Cherezov *et al.*, 2007]. Time and temperature were optimised on a small-scale test modification with ABCB8$^{Ala111-Ala714}$ prior to applying iodoacetamide modification in a large-scale purification. The modification time was 30 minutes at room temperature before unreacted iodoacetamide was removed with a desalting step on a PD-10 column. Longer modification led to precipitation during the concentration step prior to SEC. Intact mass spectrometry analysis of iodoacetamide treated ABCB8 (Δ57 kDa mass difference per alkylation) suggested that one major modification species was formed with ten cysteines alkylated (Fig.

3.14C). A small amount of protein had either nine or eleven modified cysteines.

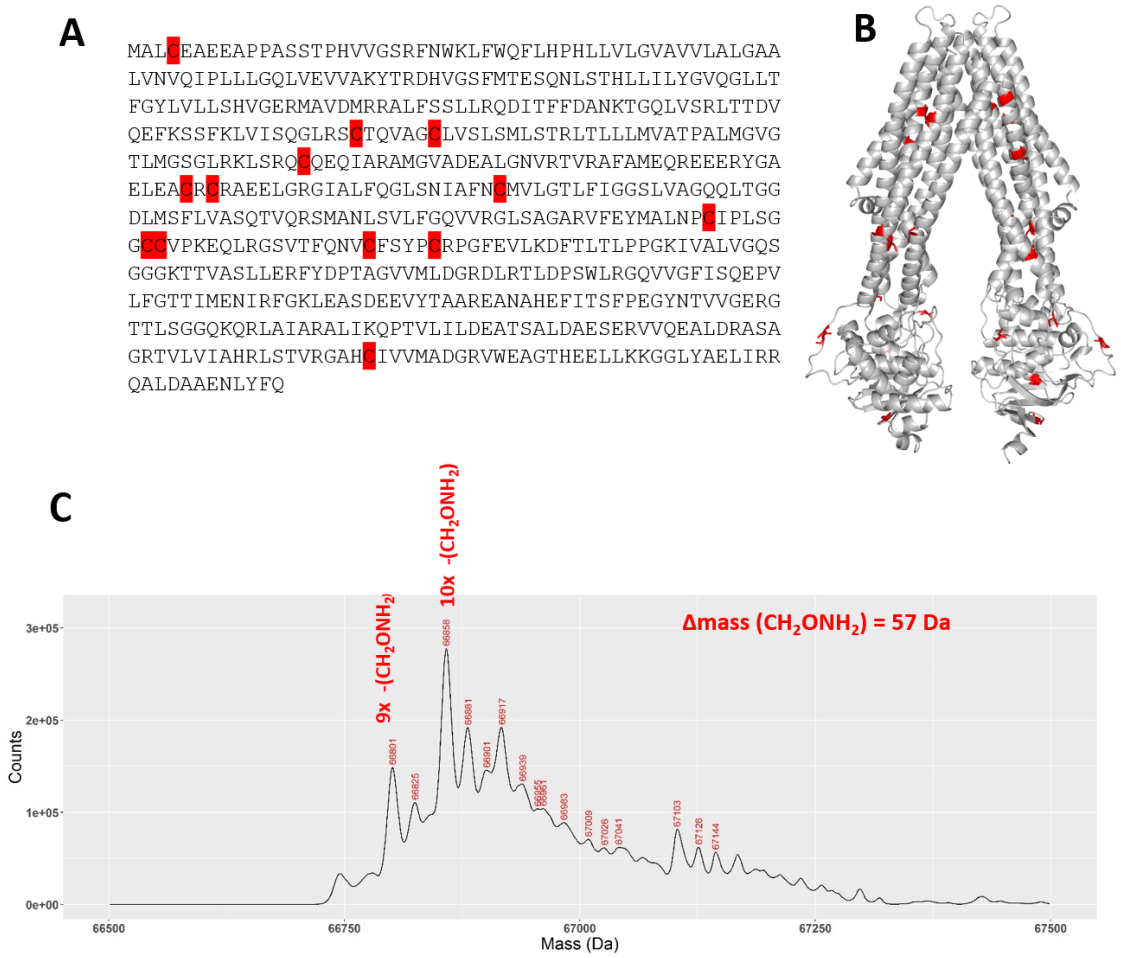
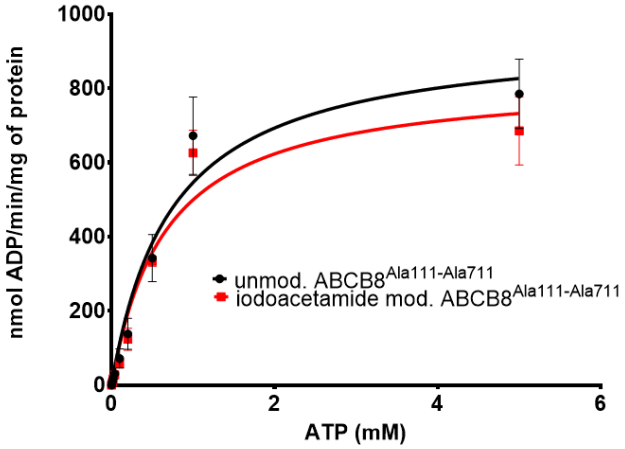


Figure 3.14 – Sequence of ABCB8$^{Ala111-Ala714}$ with cysteines highlighted in red. B)Homology model of ABCB8 with cysteines in stick representation in red. C) Intact MS spectrum of ABCB8$^{Ala111-Ala714}$ after a 30 minute treatment with iodoacetamide.

Modification increased the yield after SEC by decreasing precipitation during the concentration step prior to SEC (Fig. 3.16A). Alkylation of the cysteine residues did not impair the monodispersity of the protein, as evident from a single narrow gel filtration peak (Fig. 3.16B). These observations suggests a similar role for modification of the cysteines and reducing effect of TCEP on the sulfhydryl groups, as both can avoid formation of intermolecular disulphide bonds. The ATPase activity measured before and after iodoacetamide treatment measured for three biological repeats revealed that modification of the sulfhydryl groups in ABCB8 did not affect basal ATPase activity (Fig. 3.15). The iodoacetamide treated ABCB8

is further functionally characterised in chapter 4.

Modification of the cysteine residues was the crucial for obtaining crystals in a new crystal form (crystal form 2, Table 3.2), that gave sufficient diffraction to 4 Å, allowing the structure of ABCB8 to be determined (section 3.21).



	$K_{M,app}$ (mM)	$V_{max,app}$ (nmol Pi/min/mg)
unmodified ABCB8	0.74±0.13	949±59
iodoacetamide modified ABCB8	0.66±0.11	829±51

Figure 3.15 – ATPase activity of ABCB8$^{Ala111-Ala714}$ in OGNG/CHS before (black) and after (red) alkylation of cysteines measured with the ADP-glo assay as accumulation of ADP per minute and mg of protein over a ATP concentration range of 0-5 mM. ATPase activities were plotted against ATP concentrations and a Michaelis-Menten fit was obtained using the Prism 7 GraphPad software. The table below gives the V_{max} and K_M values for unmodified and iodoacetamide treated protein obtained from the Michaelis-Menten plot in the graph. Error bars for data points in the graph represent S.D. from three biological repeats. Kinetic parameters are given ±S.E.

Encouraged by the result that modification of cysteines lead to an improvement in crystal packing, variations of the modification reagents and modification times were evaluated. A decrease of the modification time to 20 or 10 minutes still prevented precipitation during purification. In contrast, 5 minute modification resulted in a lower yield, comparable to unmodified protein. Intact mass spectrometry confirmed the lower extent of modification for 20 and 10 minutes, the main species having 7-9 modified cysteines, whereas with a 5 minute modification, only 5-7 cysteines were

modified (Fig. 8.7). Crystallisation of protein with fewer modified cysteines (7-9) was facilitated by seeding and resulted diffraction to 3.8 Å diffraction. However 5-7 modified cysteines were not sufficient for crystals to grow. Full modification resulted in unstable protein, so it seemed that there is an optimal number of modified cysteines in ABCB8 that improved stability and facilitated crystal growth. Potentially only one modification species with a set amount of modified cysteines is used in the crystal packing and depending on its concentration in the crystallisation sample, yields well-diffracting crystals. Identifying the particular cysteines that were modified was attempted with MS/MS. However, since a full sequence coverage was not achieved with trypsin or chymotrypsin digestion, it was not possible to determine which were the crucial residues requiring modification in order for crystals to be formed (Fig. 8.6).

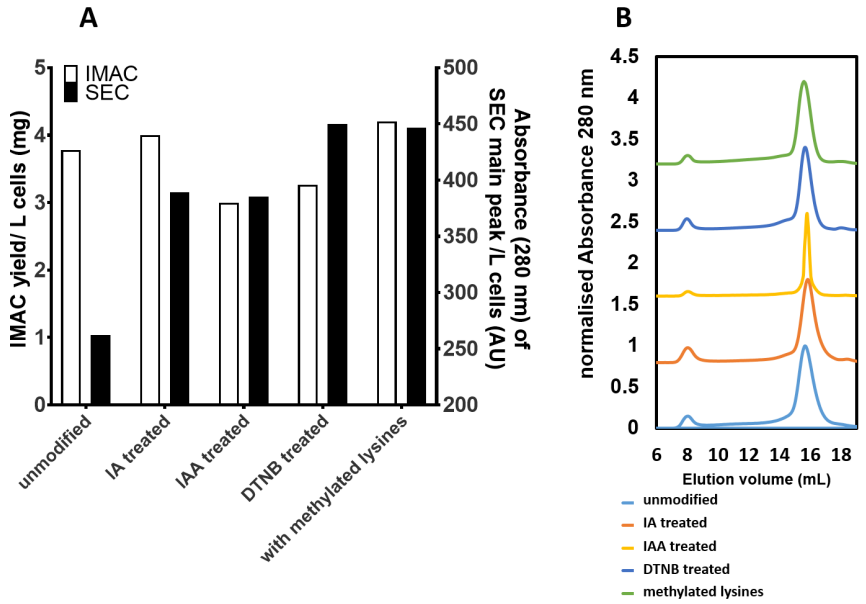


Figure 3.16 – Scale-up purification of ABCB8$^{Ala111-Ala714}$ with modification of lysine with formaldehyde and ABC and cysteine residues with iodoacetamide (IA), iodoacetic acid (IAA) and 5,5-dithio-bis-2-nitrobenzoic acid (DTNB). A) Bar chart representing yield after IMAC and absorbance of SEC main peak, both normalised for L culture volumes used for purification B) SEC profiles of chemically modified protein in SEC buffer containing 0.12 % OGNG and 0.012 %CHS.

Cysteine modification using iodoacetic acid and DTNB

Iodoacetic acid and 5,5-dithio-bis-2-nitrobenzoic acid (DTNB) were also tested as alternative cysteine modification reagents. Iodoacetic acid modifies cysteines with the same mechanism as described for iodacetamide, whereas DTNB forms a mixed disulphide with the cysteine residues. Both resulted in higher yields after SEC compared to unmodified protein and narrow peaks on SEC (Fig. 3.16A and B), but these modifications did not appear to enable crystallisation of ABCB8. Intact mass spectrometry was used to measure the extent of the modification (Fig. 8.8) and it showed that modification with iodoacetic acid gave 3-6 modified cysteines. DTNB was also very inefficient at modifying ABCB8, resulting in only 4 modified cysteines. Unsurprisingly, the ability to crystallise was potentially impaired due to the low extent of modification for DTNB and iodoacetic acid. However, steric hindrance of the aromatic residues added after DTNB modification or repulsion of charges due to the modification with iodoacetic acid could also have interfered with crystallisation.

Further purification optimisation of iodoacetamide treated ABCB8

Iodoacetamide treatment of ABCB8 changed the physiochemical properties of the protein surface affecting purification yields due to decrease in precipitation probability and its crystallisation ability as described in section 3.2.6. Thus, it can be assumed that cysteine modification could improve the stability of ABCB8 in detergents, which in previous experiments failed to give a monodisperse peak. Therefore, a selection of detergents was re-screened by first extracting and purifying ABCB8 in OGNG/CHS. Subsequently, ABCB8 was modified after reverse IMAC and exchanged into standard SEC buffer containing the different detergents selected for a monodispersity screen. Resulting size exclusion chromatograms for this screen (Fig. 3.17) revealed that iodoacetamide treated ABCB8 remains monodisperse when exchanged into DM/CHS. A scale-up purification of ABCB8$^{Ala111-Ala714}$ with

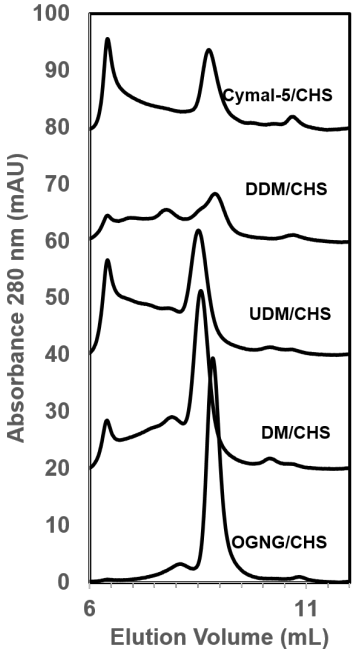


Figure 3.17 – Monodispersity screen of iodoacetamide treated ABCB8$^{Ala111-Ala714}$, which was exchanged into different detergents after purification in OGNG/CHS. SEC profiles were obtained using the Dionex HPLC system in combination with Sepax SRT SEC-300 column in HEPES pH 7, 200 mM NaCl, 2 mM TCEP and 0.5 mM $MgCl_2$.

iodoacetamide treatment and subsequent exchange into DM/CHS was performed for crystallisation trials. This resulted in a narrow peak for monodisperse protein, although a $\sim$ 60 % decrease in yield was observed, compared to the OGNG/CHS sample. Unfortunately, no crystals could be obtained in DM/CHS.

Both, constructs and addition of POPG and CDL, that had previously been screened without chemical modification, were re-tested in crystallisation screens with the altered purification protocol. Although crystals of iodoacetamide treated ABCB8 were obtained in the presence of CDL, diffraction was significantly reduced compared to crystals grown in OGNG/CHS only.

Table 3.2 – Space group and example unit cell dimensions for two crystal forms obtained for ABCB8.

Crystal form	Space group	Lattice	a (Å)	b(Å)	c (Å)	α (°)	β (°)	γ (°)	nucleotide	Max. resolution (Å)
1	$C222_1$	Orthorhombic	276	329	260	90.0	90.0	90.0	ATPγS,AMPPCP, AMPPNP	7
2	$P12_11$	Monoclinic	179	100	213	90.0	90.2	90.0	ATPγS/ADP, ADP	3.8
2*	$P12_11$	Monoclinic	186	109	209	90	90.2	90.0	none	4.4

3.2.7 Crystallisation

Crystallisation screens and first crystal hits

For vapour diffusion crystallisation trials, 96-well sparse matrix screens were used to screen key conditions (pH, salts, precipitant type and concentrations) particularly successful for alpha-helical membrane proteins [Iwata, 2003]. ABCB8 was mixed with precipitant in ratios of 2:1, 1:1 and 1:2 to give an initial drop volume of 150 nL in a sitting drop over a 20 μL well, which contained crystallisation buffers from the sparse-matrix screens in 3-position 96-well plates (SwissCI). As sparse-matrix screens the MemGold2 screen from Molecular Dimensions and in-house adaptations of the MemGold screen [Newstead *et al.,* 2008] and of the MemStart/MemSys screens [Iwata, 2003] were used. Initial crystal hits were obtained with ABCB8$^{Ala111-Ala714}$ (8 mg/ml) in optimised buffer conditions (see section 3.2.4) incubated with 5 mM ATPγS/$MgCl_2$ at 2:1 and 1:1 protein to reservoir solution ratios. The reservoir solution for these initial crystal contained 12% PEG4K, 0.1M sodium chloride, 0.1M acetate pH 4.5 and 0.1M lithium sulfate.

These crystals diffracted to 7.5 Å (Fig. 3.18). Indexing of test images and analysis of one dataset collected revealed that the crystals were in the $C222_1$ space group with the following unit cell parameters a=276, b=329, c=260 Å and α=β=γ=90°(crystal form 1, Table 3.2). Unfortunately, phasing with molecular replacement failed due to lack of higher resolution data. In order to improve the resolution, further crystallisation conditions were screened in addition to the previously mentioned alterations of the construct length and protein purification protocol. The screening involved

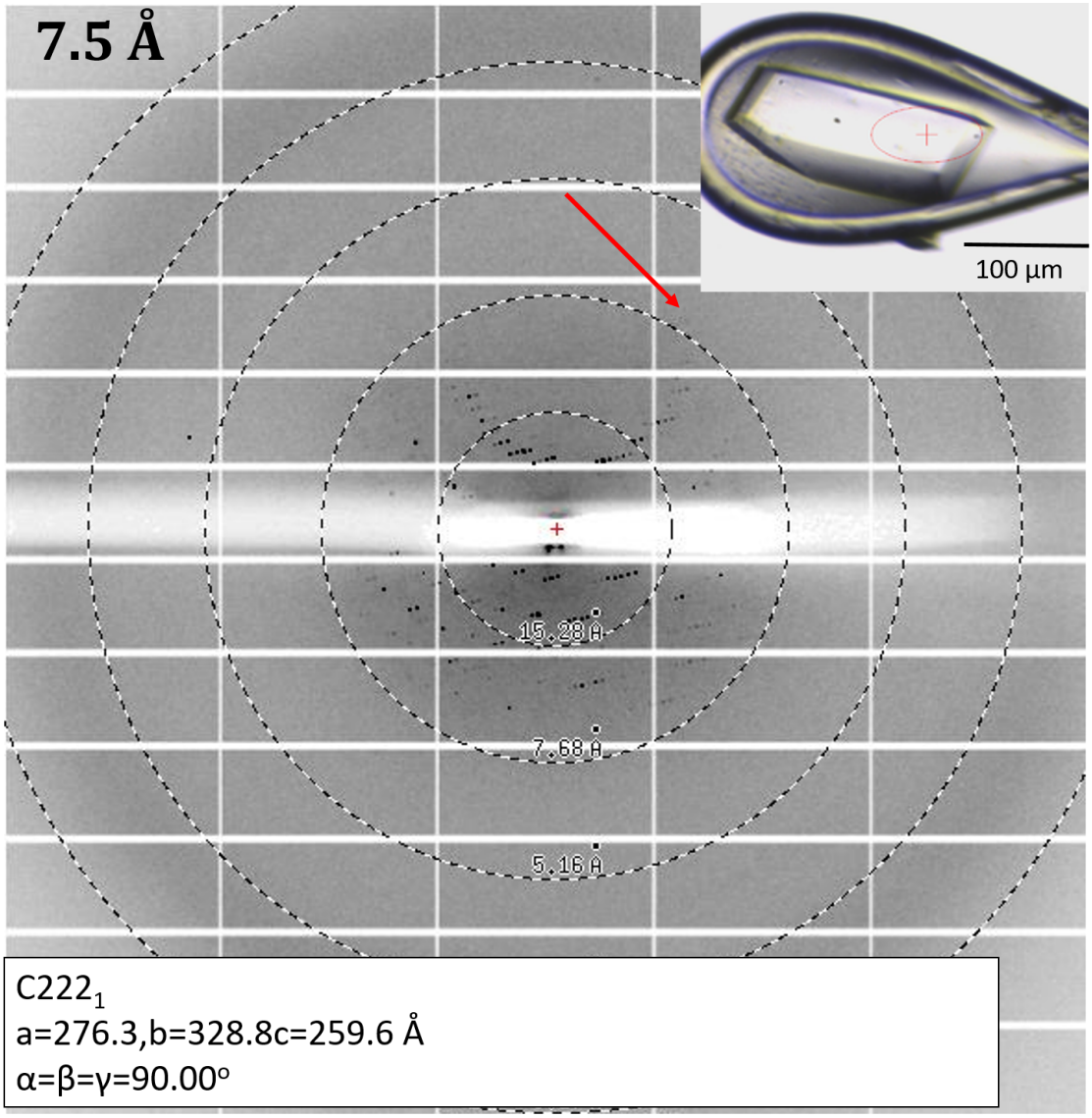


Figure 3.18 – Diffraction image of first crystal hit of ABCB8$^{Ala111-Ala714}$ obtained (mounted crystal in right corner with red cross indicating spot, where crystal was hit) from ABCB8 in SEC buffer (50 mM HEPES, pH 7; 200 mM NaCl, 2 mM TCEP and 0.5 mM $MgCl_2$, 0.12% OGNG and 0.012% CHS) and 5 mM ATPγS/$MgCl_2$ mixed with well solution containing 12% PEG4K, 0.1 M sodium chloride, 0.1 M acetate pH 4.5 and 0.1 M lithium sulphate. Indexing revealed an orthorhombic crystal form (parameters in box; crystal form 1). The arrow indicates highest resolution spots. The crystal and diffraction image were both taken at Diamond Light Source beamline I04.

different PEG types, addition of cyclodextrin for detergent removal and additive screens, in which the initial crystallisation conditions were supplemented with various types of salts, detergents and volatiles. None of these attempts at optimising the crystals resulted in better diffraction.

Optimisation of crystallisation of iodoacetamide modified protein

Iodoacetamide treatment during the purification of ABCB8 and re-screening of crystallisation conditions in sparse-matrix screens, combined with co-crystallisation with a variety of ATP-analogues, gave a new crystal form (crystal form 2; Table 3.2, Fig. 3.19). For that, iodoacetamide treated ABCB8$^{Ala111-Ala714}$ in SEC buffer (50 mM HEPES, pH 7; 200 mM NaCl, 2 mM TCEP and 0.5 mM $MgCl_2$, 0.12 % OGNG, 0.012% CHS) was incubated with 5 ATPγS/$MgCl_2$ prior to crystallisation and set up with crystallisation buffer containing 0.1 M bicine pH 8.5 and 34 % PEG2K in 150 nL vapour diffusion sitting drops as described previously for the non-modified protein. The obtained crystals had a monoclinic $P12_11$ space group with unit cell dimensions of a=181, b=98, c=213 Å and α=γ=90°, β=90.5°, that was likely to be facilitated by the cysteine modification in ABCB8, as discussed in chapter 5.This crystal form showed better diffraction, but a high degree of anisotropy diffracting to 4.0 Å in the best direction and 5.6x6.5 Å in the other two directions.

The resolution was improved to an overall value of 4 Å (4.1x5.7x3.8 Å with CC1/2=0.5 defining the resolution cut-off) by varying addition of 5% PEG400 to the crystallisation buffer, which allowed for better cryo-protection prior to freezing of the crystals (Fig. 3.20). Unfortunately, higher concentrations of PEG400 during the crystallisation itself prevented crystal growth, even in the presence of seeds.

A further increase in resolution to 4.2x5.4x3.5 Å was achieved by reducing the extent of modification due to a decrease of the incubation time with iodoacetamide to 10 minutes (section 3.2.6) (Fig. 3.21)

Attempts to reduce the degree of anisotropy further were undertaken by using

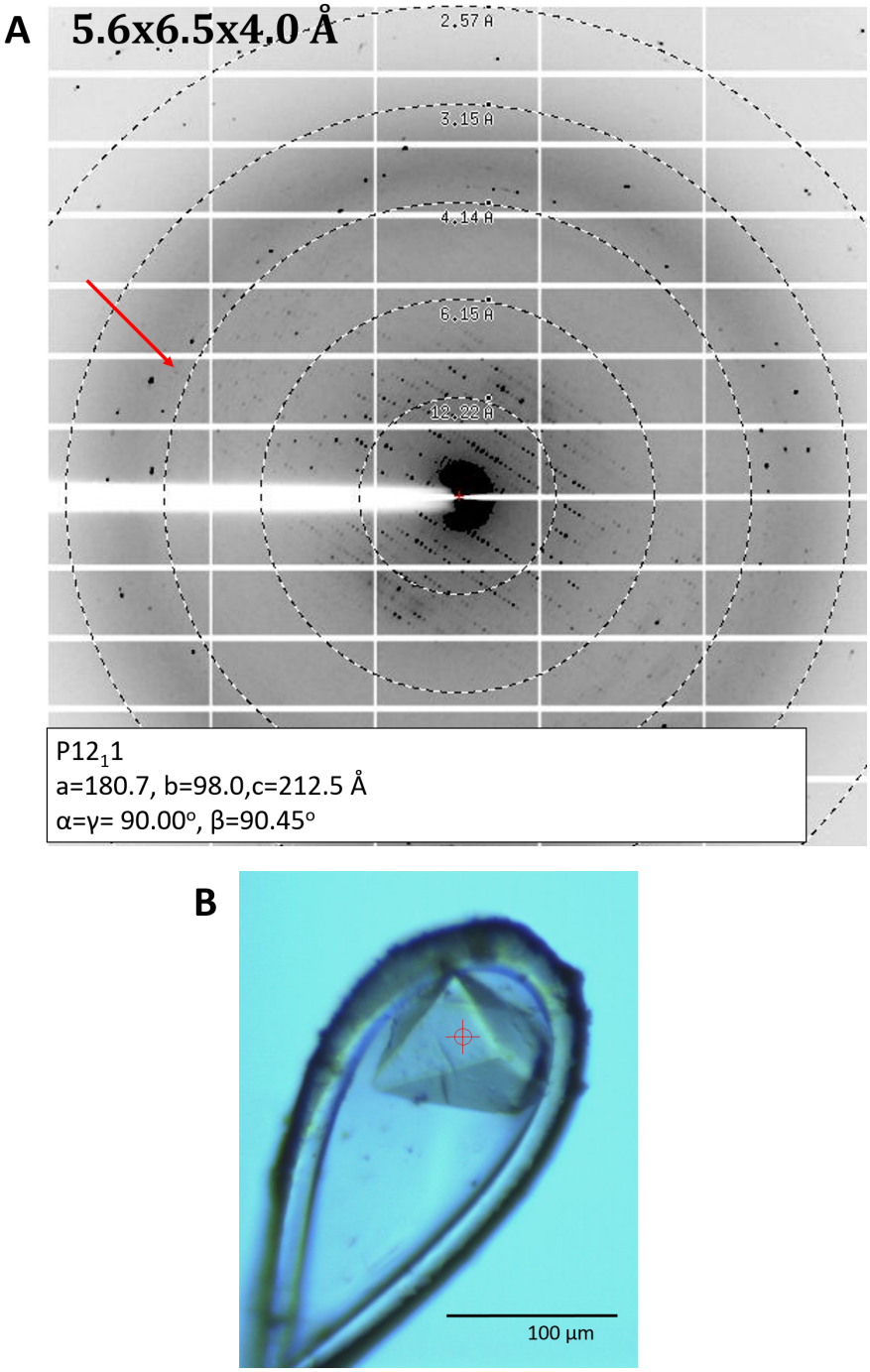


Figure 3.19 – A) Diffraction image for a crystal obtained with iodoacetamide treated ABCB8$^{Ala111-Ala714}$ in SEC buffer (50 mM HEPES, pH 7; 200 mM NaCl, 2 mM TCEP and 0.5 mM $MgCl_2$, 0.12% OGNG and 0.012% CHS) and iodoacetamide treatment in the presence of 5 mM ATPγS and 5 mM $MgCl_2$ with well solution containing 0.1 M bicine pH 8.5 and 34 % PEG2K. Indexing revealed a monoclinic crystal form (crystal form 2; parameters in box). The arrow indicates highest resolution spots. B) Image of mounted crystal with red cross indicating position, where screening image was collected. The crystal and diffraction image were both taken at Diamond Light Source beamline I24.

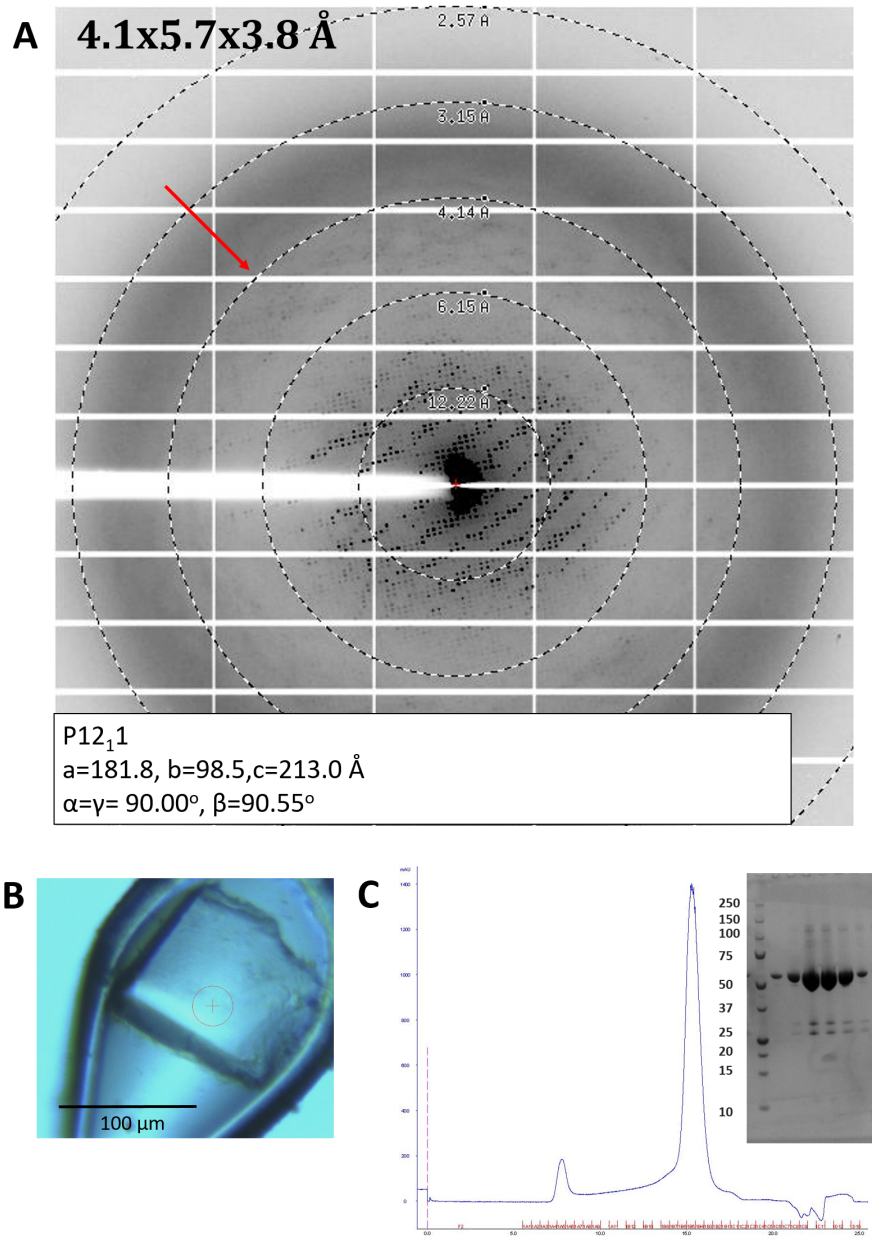


Figure 3.20 – A) Diffraction image for a crystal obtained with iodoacetamide treated ABCB8$^{Ala111-Ala714}$ in SEC buffer (50 mM HEPES, pH 7; 200 mM NaCl, 2 mM TCEP and 0.5 mM $MgCl_2$, 0.12% OGNG and 0.012% CHS) and iodoacetamide treatment in the presence of 5 mM ATPγS and 5 mM $MgCl_2$ with well solution containing 0.1M bicine pH 8.5, 18% PEG4K and 5% PEG400. Indexing revealed a monoclinic crystal form (crystal form 2; parameters in box). The arrow indicates highest resolution spots. B) Image of mounted crystal with red cross indicating position, where screening image was collected. The crystal and diffraction image were both taken at Diamond Light Source beamline I24. C) SEC profile and Coomassie-stained SDS-gel for SEC peak fractions of purification leading to the presented crystal.

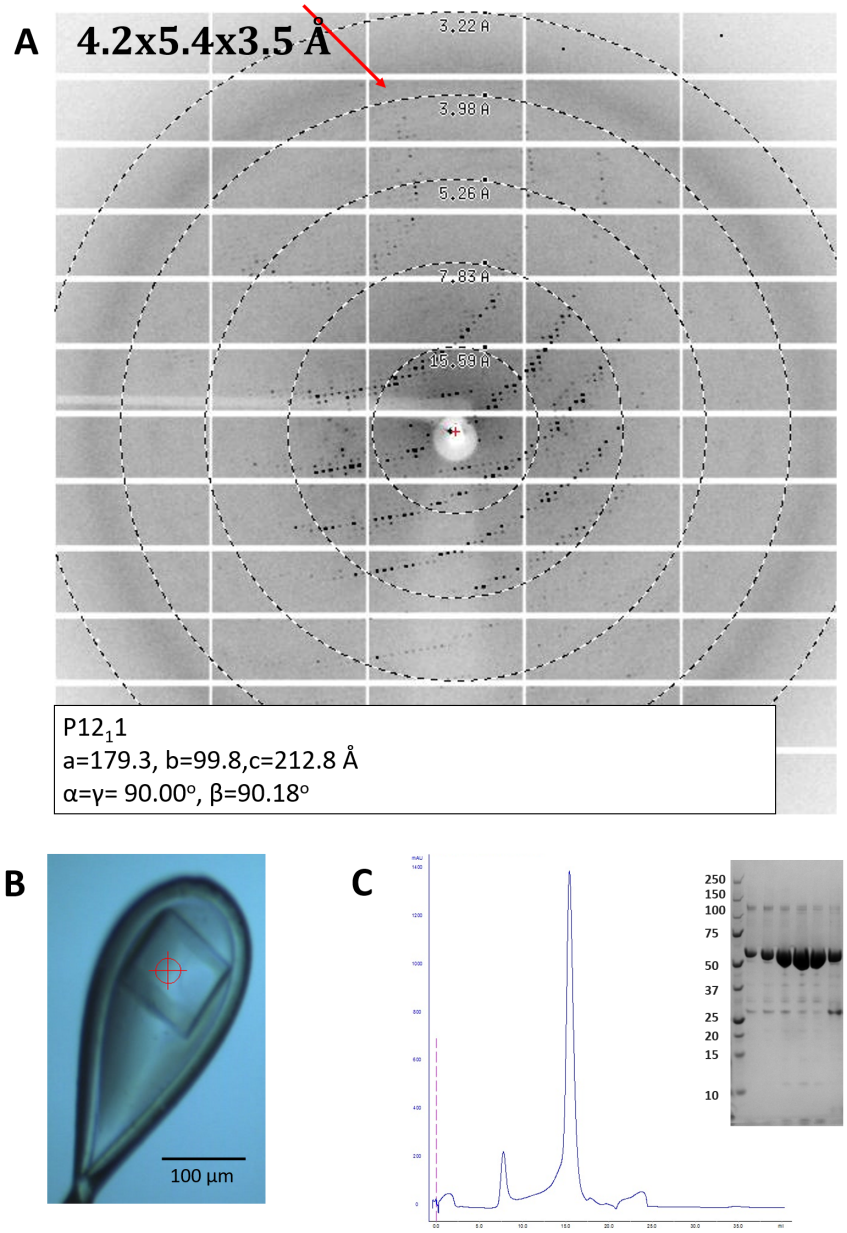


Figure 3.21 – A) Diffraction image for a crystal obtained with iodoacetamide treated ABCB8$^{Ala111-Ala714}$ in SEC buffer (50 mM HEPES, pH 7; 200 mM NaCl, 2 mM TCEP and 0.5 mM $MgCl_2$, 0.12% OGNG and 0.012% CHS) and iodoacetamide treatment in the presence of 5 mM ATPγS and 5 mM $MgCl_2$ with well solution containing 0.1 M HEPES pH 7.5 and 18% PEG3350. Indexing revealed a monoclinic crystal form (crystal form 2; parameters in box). The arrow indicates highest resolution spots. B) Image of mounted crystal with red cross indicating position, where screening image was collected. The crystal and diffraction image were both taken at Diamond Light Source beamline I24. C) SEC profile and Coomassie-stained SDS-gel for SEC peak fractions of purification leading to the presented crystal.

follow-up screens varying PEG types, additive screens, as well as further purification screens with cysteine modified ABCB8 including different constructs, different detergents and lipid addition. A detailed overview of the optimisation attempts is given in Table 3.3.

Table 3.3 – Overview of crystallisation optimisation attempts used for ABCB8 with number of plates set up per method.

	crystals	**number of plates**
Detergents		
OGNG/CHS	3.8 Å	250
DMNG/CHS	no crystals	15
DM/CHS	no crystals	9
C12E8/OGNG	no crystals	5
Crystallisation methods attempted		
Sitting-drop vapour diffusion		255
Bicelles in vapour diffusion	no crystals	12
HiLiDe (with iodoacetamide treated protein)	7 Å	9
LCP	no crystals	3
Modification of ABCB8 in OGNG/CHS		
no modification	7 Å	247
cysteine modification	3.8 Å	189
lysine modification	no crystals	17
Optimisation ABCB8 in OGNG/CHS		
follow-up screening	7 Å	83
PEG screen	7 Å	3
additive screen	7 Å	20
seeding	7 Å	4
addition of cyclodextrin	no crystals	4
addition of CDL or POPG	no crystals	36
variation of constructs	10 Å	28
Optimisation with iodoacetamide treated ABCB8 in OGNG/CHS		
PEG screen	3.8 Å	4
additive screen	4 Å	4
manganese or cadmium	5-6 Å	7
different constructs	4-5 Å	17
surface entropy mutants	5 Å	21
variation of modification type/time	no crystals/3.8Å	34
addition of proteases	no crystals	3
seeding	4 Å	13
addition of CDL	5 Å	8
dead mutant	4-5Å	7
selenomethionine labelled protein	6-7Å	10

Co-crystallisation of ABCB8 with nucleotides

Changing the conformation of the ABC transporter can alter the way the molecules pack in the crystal, which may lead to higher resolution diffraction. Co-crystallisation with nucleotides (ATP and ADP), as well as nucleotide analogues (ATPγS, AMP-PCP, AMPPNP) have been shown to change conformation of ABC transporters by triggering dimerisation of the NBDs. In addition, ATP in the presence of ortho-vanadate (VO_4^{3-}), beryllium fluoride (BeF_3^+) or aluminium fluoride (AlF_4^+) are predicted to capture ATP-transition state conformations [Shimizu & Johnson, 1983; Oldham & Chen, 2011] and were used in co-crystallisation trials with ABCB8. In order to improve resolution and/or obtain different conformations of ABCB8, these nucleotides and nucleotide analogues were tested in sparse-matrix screens and follow-up screens for unmodified and iodoacetamide treated protein. Crystal form 1 was obtained with ATPγS, AMPPCP or AMPPNP with low pH (pH 4.5-6) and high molecular weight PEGs, whereas crystal form 2 was obtained with iodoacetamide treated protein in the presence of ATPγS and ADP at medium pH and high molecular weight PEGs (section 3.2.7) (Fig. 3.22).

Crystals grown in the absence of nucleotides gave a crystal form with a slight expansion of the unit cell in the first and second direction (crystal form 2*: a=185.8, b=109.4, c=209.4 Å and α=γ=90.0 °, β=90.16) and lower diffraction to 4.53x6.7x4.2 Å (Fig. 3.23). No crystals could be obtained with ATP-transition state analogues, such as ATP+V_i, beryllium fluoride (BeF_3^+) or aluminium fluoride (AlF_4^+).

Crystallisation of ABCB8 in lipid environments

Although the majority of crystallisation trials involved the use of the standard sitting-drop vapour diffusion method with protein in detergent, crystallisation was also attempted in LCP using monoolein, MAG7.7 and MAG7.9, as well vapour diffusion with reconstitution of protein in bicelles containing DMPC/cholesterol or DMPC/CDL. In addition, a HiLiDe approach [Gourdon *et al.,* 2011] was tried,

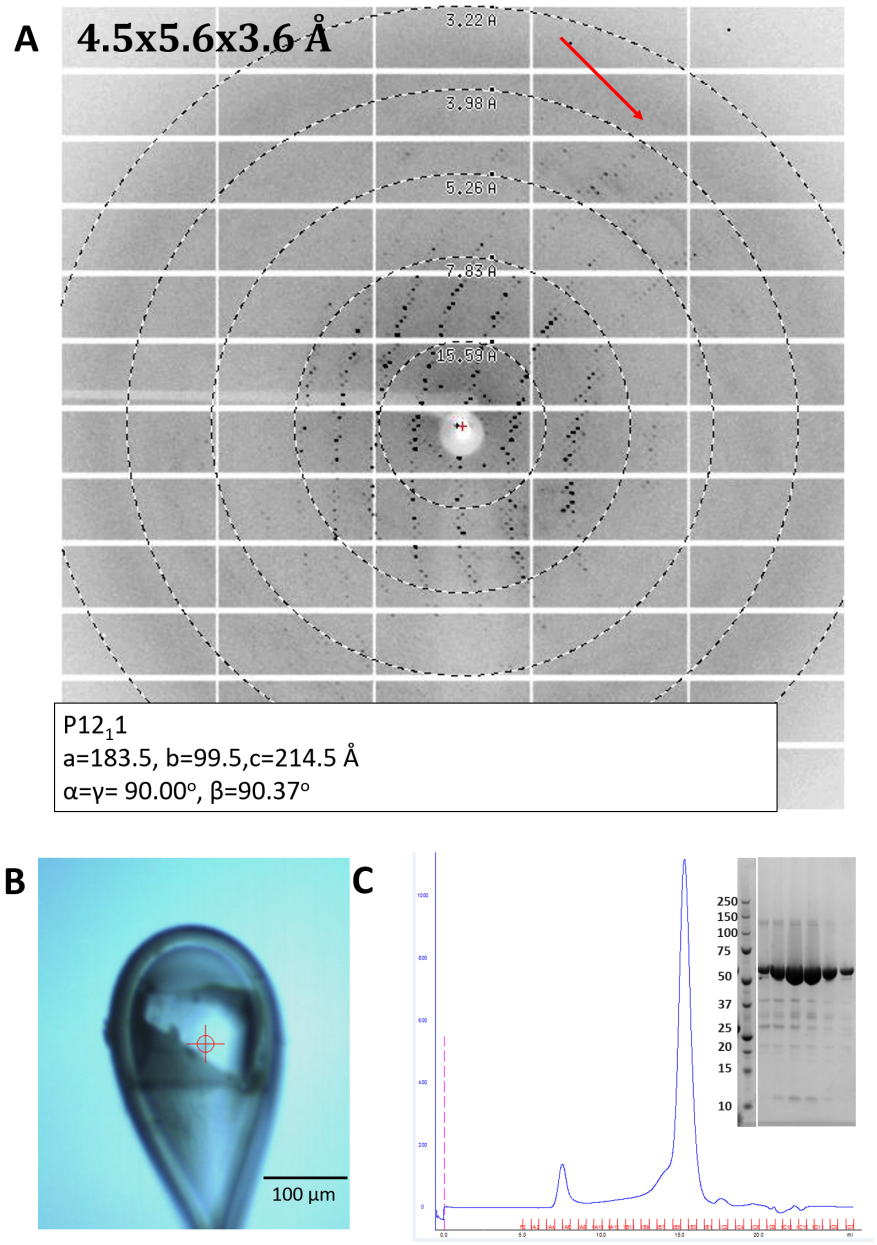


Figure 3.22 – A) Diffraction image for a crystal obtained with iodoacetamide treated ABCB8$^{Ala111-Ala714}$ in SEC buffer (50 mM HEPES, pH 7; 200 mM NaCl, 2 mM TCEP and 0.5 mM $MgCl_2$, 0.12% OGNG and 0.012% CHS) and iodoacetamide treatment in the presence of 1.5 mM ADP and 5 mM $MgCl_2$ with well solution containing 12% PEG4K, 0.1 M sodium chloride, 0.1 M HEPES pH 7.5 and 0.1 M magnesium chloride. Indexing revealed a monoclinic crystal form (crystal form 2; parameters in box). The arrow indicates highest resolution spots. B) Image of mounted crystal with red cross indicating position, where screening image was collected. The crystal and diffraction image were both taken at Diamond Light Source beamline I24. C) SEC profile and Coomassie-stained SDS-gel for SEC peak fractions of purification leading to the presented crystal.

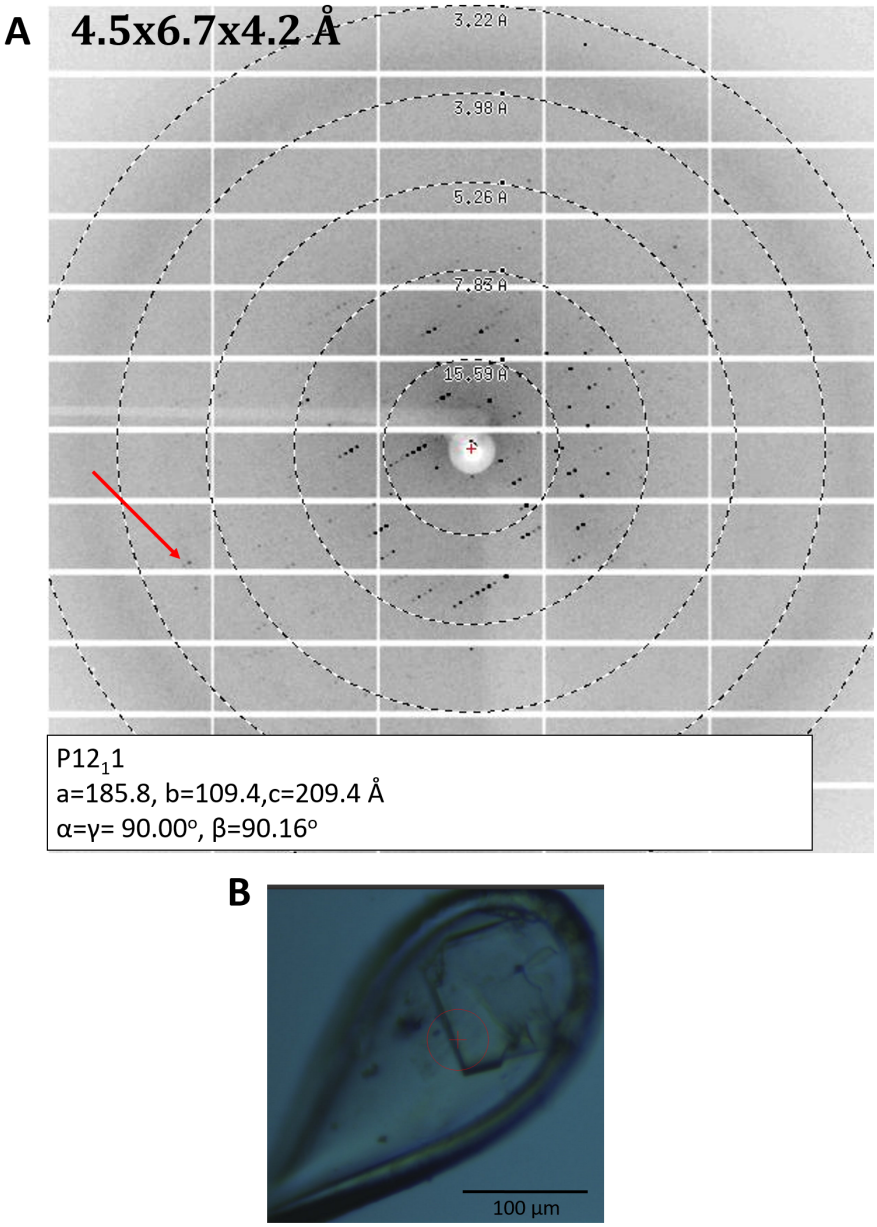


Figure 3.23 – A) Diffraction image for a crystal obtained with iodoacetamide treated ABCB8$^{Ala111-Ala714}$ in SEC buffer (50 mM HEPES, pH 7; 200 mM NaCl, 2 mM TCEP and 0.5 mM $MgCl_2$, 0.12% OGNG and 0.012% CHS) and iodoacetamide treatment in the presence of 1.5 mM ADP and 5 mM $MgCl_2$ with well solution containing 12% PEG4K, 0.1 M sodium chloride, 0.1 M citrate pH 5.5. Indexing revealed a monoclinic crystal form (crystal form 2*; parameters in box). The arrow indicates highest resolution spots. B) Image of mounted crystal with red cross indicating position, where screening image was collected. The crystal and diffraction image were both taken at Diamond Light Source beamline I24. Protein used in this crystallisation is the same as in Fig. 3.21.

in which ABCB8 was incubated over a lipid film (DOPC/CDL (3:1)) with a high amount of detergent (1-2% OGNG/CHS) for relipidation, and subsequently set up in 96-well sitting drop vapour diffusion plates with follow-up screen conditions. Using the latter approach, crystals could were obtained with iodoacetamide treated ABCB8$^{Ala111-Ala714}$ in the presence of 5 mM ATPγS in crystal form 2, but these crystals failed to diffract beyond 7 Å(section 2.8.1).

3.3 Conclusion

This chapter described the establishment and optimisation of a purification protocol for human ABCB8 that yielded pure and stable protein creating the foundation for functional studies described in chapter 4. Particularly introducing chemical modifications of cysteines lead to crystals of ABCB8 with diffraction to 3.8 Å with ATPγS/ADP and ADP, as well as in an apo state to 4.4 Å sufficient for structure determination (chapter 5).

CHAPTER 4

Functional studies on ABCB8

4.1 Introduction

The first part of this chapter (4.2) reports the optimisation of a reconstitution protocol for ABCB8 in order to create the foundation for future work including transport assays required to deorphanise ABCB8's function. In addition, the effects of specific lipids on ATPase activity of ABCB8 was probed.

The second part of this chapter (4.4) describes the effects of ADP, non-hydrolysable ATP analogues and ATP transition states on the conformation and ATPase activity of ABCB8 using thermal stability and ATPase assays. Furthermore, binding affinities for the nucleotides were derived using T-jump measurements in a MST instrument and it was found that there were significant differences between the effects of the commonly used ATP analogues and transition state analogues hinting at differences in the conformational changes they trigger. These measurements complement the structural studies on ABCB8 described in chapter 5. Since a crys-

tal structure of ABCB8 was only obtained after iodoacetamide treatment, it was necessary to test, whether cysteine alkylation had an effect on the function of the protein and ATP analogue and ADP binding in particular. Consequently, thermal stability and nucleotide binding to untreated and iodoacetamide modified protein were compared.

4.2 Results Part I

4.2.1 Optimisation of reconstitution of ABCB8 into proteoliposomes

A reconstitution protocol had been optimised for construct ABCB8$^{Ala111-Ala714}$ on the basis of the method suggested in Geertsma *et al.* [2008], which was further optimised to give a high recovery rate for ABCB8 and ATPase activity. Crucial elements were the lipid mixture, reconstitution detergent, as well as the method and rate of detergent removal. The lipid mixtures initially used were POPC and POPC/*E. coli* polar lipids (EPL) of a 1:2 (w:w) ratio, as well as POPC/POPG and POPC/CDL of a 3:1 (w:w) ratio (Fig. 4.1). Detergents, such as non-ionic OG, Triton-X100 and ionic cholate were tested for solubilising liposomes. However, ABCB8 only showed good recovery in cholate, as OG and especially Triton X-100 caused the protein to precipitate. Liposomes were incubated in a sonication bath with the detergent for 10 minutes in order to break up multilamellar lipid vesicles and make the membranes more accessible for the detergent. The high CMC of cholate (9 mM) compared to its low solubilisation concentration ($\sim$ 20 mM) [Rigaud *et al.,* 1988] is an advantage, as dilution to below the CMC value allows for quick formation of proteoliposomes prior to further slower detergent removal by Bio-Beads over-night. When cholate was not diluted but only slowly removed with Bio-Beads, protein precipitation was observed over-night.

After detergent removal, proteoliposomes were separated from the supernatant by

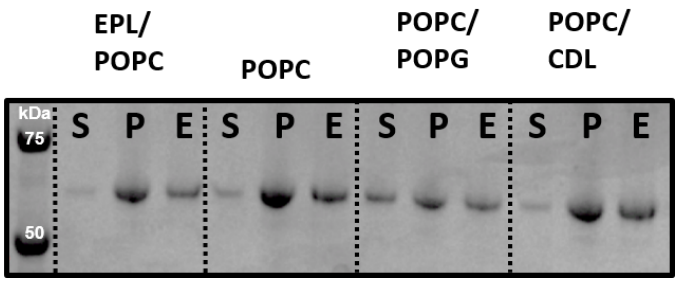


Figure 4.1 – SDS-PAGE gel of ABCB8 reconstituted in different lipid mixtures as indicated on gel. Supernatant (S) after ultracentrifugation step, re-suspended pellet (P) and elution from G-25 column (E) were loaded on gel.

ultracentrifugation. For the POPC/POPG lipid mixture, ABCB8 was still found in the supernatant, suggesting imperfect removal of detergent and formation of soluble aggregates due to failed incorporation into the lipid bilayer. In order to separate insoluble protein aggregate from proteoliposomes after ultracentrifugation, samples were run over a desalting column, which retains large protein precipitate, but not the proteoliposomes. Therefore, a difference in amounts of protein in the pellet sample compared to the sample run over a desalting column suggests loss of protein due to precipitation, as observed for the POPC only and *E. coli*/POPC sample. POPC/CDL showed the best recovery of reconstituted protein.

A number of parameters affect the orientation of the protein in the proteoliposome, including extension of soluble domains, lipid composition and detergent type, as well as rate of detergent removal [Rigaud *et al.,* 1988; Eytan, 1982]. In order to measure ATP hydrolysis of reconstituted ABC transporters, NBDs have to face the external buffer solution that contains ATP. The orientation of ABCB8 in proteoliposomes was tested by using ABCB8 with the uncleaved C-terminal purification tag (Δ2.5 kDa), that contains a TEV protease cleavage site. After reconstitution with the previously described protocol, the proteoliposomes were treated with TEV protease for 1 hour at room temperature. Only TEV protease cleavage sites on the C-terminus facing out of the proteoliposomes are accessible for the protease. The TEV protease treatment of the proteoliposomes gave rise to a downwards shift of the whole ABCB8 band on the SDS-PAGE gel compared to the non-treated sample (Fig. 4.2), suggesting unidirectional incorporation of ABCB8 into the lipid bilayer.

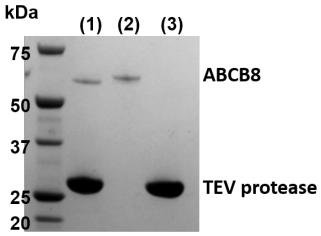


Figure 4.2 – SDS-PAGE gel showing samples from incubation of reconstituted ABCB8 after incubation with TEV protease for 1 hour at room temperature (1) and without TEV protease digest (2). TEV protease only was loaded as a control (3).

Although ABCB8 was likely reconstituted into proteoliposomes with the NBDs facing outside and therefore accessible to ATP, no ATPase activity was detected for ABCB8 initially in the lipid mixtures described earlier. Only reconstitution of iodoacetamide treated protein restored ATPase activity in POPC/CDL of a 3:1 (w:w) ratio and POPC/CDL/POPE of a 2:1:1 (w:w:w) ratio (Fig. 4.3). ATPase activity for ABCB8 was measured here using the ADP-Glo kinase assay that detects ATP hydrolysis rates in amounts of released ADP (see section 2.9.2). Although K_M values for protein in detergent were comparable to ATPase activity measured with the "Chifflet's assay" (section 3.2.6), V_{max} values were about 4-5 times higher with the ADP-Glo assay probably due to its higher sensitivity. Therefore, only values obtained from one methods are compared with each other in this thesis.

Table 4.1 – ATPase activity measured with ADP-Glo Kinase assay for unmodified and iodoacetamide treated ABCB8 in OGNG/CHS and reconstituted into POPC/CDL (3:1; w:w) and POPC/CDL/POPE (2:1:1; w:w:w). K_M and V_{max} values were obtained from a Michaelis-Menten plot (Fig. 4.3). Kinetic parameters are given with with ±S.E for two biological repeats measured in triplicate.

lipid mixture	iodoacetamide treatment	K_M (mM)	V_{max} (nmol P_i/min/mg)
OGNG/CHS	no	0.31±0.06	2771±203
POPC/CDL	no	ND	ND
POPC/CDL/POPE	no	ND	ND
OGNG/CHS	yes	0.35±0.07	2898±240
POPC/CDL	yes	0.46±0.07	1978±127
POPC/CDL/POPE	yes	0.51±0.12	1875±203

K_M values of iodoacetamide treated protein reconstituted into POPC/CDL and

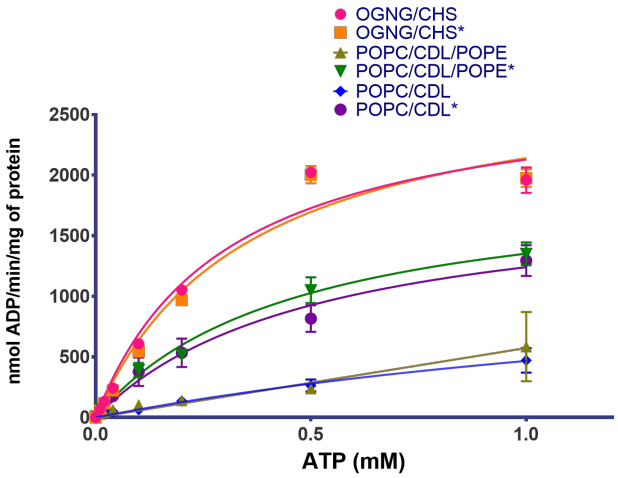


Figure 4.3 – ATPase activity of ABCB8 in proteoliposomes is dependent on iodoacetamide modification of ABCB8. ATPase activity of ABCB8$^{Ala111-Ala714}$ (unmodified and iodoacetamide treated (*)) in OGNG/CHS (0.12%/0.012%), in POPC/CDL (3:1 (w:w)) and POPC/CDL/POPE (2:1:1 (w:w:w)). Nmol ADP/min/mg of protein were measured in a ADP-Glo Kinase assay. ATPase assay data were normalised with protein concentrations from densitometry of SDS-PAGE gel bands. Data points are the mean ±S.D. of two independent biological repeats measured in triplicate. Data were fitted using the Michaelis-Menten equation using GraphPad Prism7.

POPC/CDL/POPE proteoliposomes were 0.51±0.12 mM and 0.45±0.07 mM, respectively (Table 4.1), which is comparable to a K_M value of 0.35±0.07 mM for iodoacetamide treated ABCB8 in OGNG/CHS. This suggests, that there was no major change in affinity for the ATP transition state. However, V_{max} values were decreased by $\sim$ 30 % for reconstituted ABCB8 in comparison to ABCB8 in OGNG/CHS. Reconstitution might have interfered with the protein function, leaving some of the ABC transporters inactive due to partial unfolding. It also has to be considered that measurements for determining the protein amounts in particular for proteoliposomes is error-prone, which might have artificially caused the difference in V_{max}.

4.2.2 The ATPase activity of ABCB8 in proteoliposomes is dependent on CDL

To test the effects of different lipids on the ATPase activity, iodoacetamide treated ABCB8 was reconstitutes into liposomes containing POPC with either CDL, POPG,

POPS, POPE or PI in a 3:1 (w:w) ratio. In addition, ABCB8 was reconstituted into POPC:CDL liposomes with POPG, POPS or POPE in a 2:1:1 (w:w:w) ratio. The ATPase activity of the reconstituted samples were measured at 1 mM ATP using the ADP-Glo Kinase assay (Fig. 4.4A). The ATP hydrolysis rates obtained were normalised against the protein amounts as calculated by densitometry from SDS-PAGE gel bands (Fig. 4.4B) compared to an ABCB8 concentration standard. Cardiolipin had a stimulating effect on the ATPase activity, increasing the ATP turnover by two-fold compared to the POPC only sample. However, no further increase was observed for POPC/CDL mixtures upon addition of POPG, POPE or POPS.

Table 4.2 – ATPase activity measured with the ADP-Glo Kinase assay for iodoacetamide treated ABCB8 reconstituted into lipid mixtures of 2:1 (w:w) and 2:1:1 (w:w:w) ratios. The rate of ATPase activity was measured at 1 mM ATP. Data points ±S.D. were obtained from two biological repeats measured in triplicate.

Lipid mixture	ATPase rate at 1 mM ATP (nmol ADP/min/mg protein)
POPC	580±200
POPC/CDL	1300±130
POPC/POPG	680±80
POPC/POPS	320±30
POPC/POPE	520±250
POPC/PI	330±70
POPC/CDL/POPE	1350±90
POPC/CDL/POPG	1270±370
POPC/CDL/POPS	920±240

Having identified CDL as a significant factor in maximising the basal ATPase activity, an attempt to optimise the POPC/CDL ratio was performed. POPC only and POPC/POPG (2:1; w:w) samples were included as controls. For that, ATPase activity was measured with the "Chifflet's assay" and therefore no comparisons of absolute values can be drawn to the previous measurement. V_{max} values were obtained from a Michaelis-Menten fit of the ATPase activity measured in P_i/min/mg of ABCB8 over an ATP concentration range of 0-1 mM ATP (Fig. 4.5A). POPC/CDL in 2:1, 3:1 and 4:1 (w/w) ratios gave similar V_{max} values, perhaps because they provide CDL amounts over a certain threshold required for stimulation of ATPase activity. However, a 5:1 (w:w) POPC/CDL ratio, which is

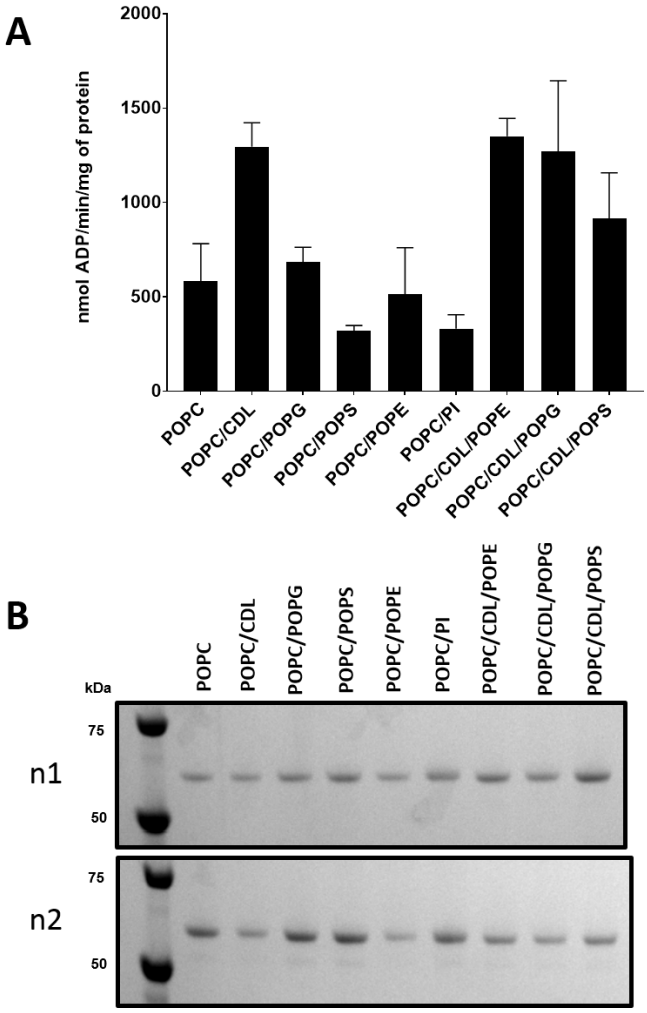


Figure 4.4 – ATPase activity of ABCB8 reconstituted into different lipid mixtures of 3:1 (w/w) and 2:1:1 (w/w/w) ratios. A) ATPase activity rates for reconstituted ABCB8 measured at 1 mM ATP using the ADP-Glo Kinase assay. ATPase assay data were normalised with protein concentrations by densitometry of SDS-PAGE gel bands in Figure B. Data points ±S.D. were obtained from two biological repeats measured in triplicate. B) Coomassie-stained SDS-PAGE gel bands for reconstituted ABCB8 samples.

equivalent to a 10:1 molar ratio, decreased the ATPase activity by two-fold compared to the 3:1 ratio. The ATPase activity for POPC:POPG in a 3:1 (w:w) ratio was four-fold decreased, whereas ATPase activity for the POPC only reconstitution was too low to be detected in the "Chifflet's assay".

The "Chifflet's assay" is lower in sensitivity compared to the ADP-Glo Kinase assay. This explains, why lower overall V_{max} values were detected in the "Chifflet's assay". Furthermore, no ATPase activity at all was measured for ABCB8 reconstituted into POPC only in the "Chifflet's assay", whereas low activity in the ADP-Glo assay could be measured.

The ATPase activity was normalised to protein concentrations as detected on a SDS-PAGE gel using densitometry of band E (section 2.9) (Fig. 4.5B). Comparing band intensities from samples taken after ultracentrifugation (P) and after elution from a desalting column to separate aggregated protein, it is evident that, absence of CDL reduces amounts of reconstituted protein.

Table 4.3 – ATPase activity measured of ABCB8 reconstituted into lipid mixtures containing different ratios of POPC to CDL (w:w ratios). POPC only and a POPC/POPG (3:1; w:w) mixture were included as controls. V_{max} values were obtained from a Michaelis-Menten fit of ATPase activity, measured over an ATP concentration gradient, (0-1 mM) using the "Chifflet's assay". V_{max} values ±S.E. were obtained from one biological repeat in triplicate.

Lipid composition	V_{max} (nmol P_i/min/mg protein)
POPC	ND
POPC:CDL (2:1)	400±20
POPC:CDL (3:1)	430±20
POPC:CDL (4:1)	500±30
POPC:CDL (5:1)	200±20
POPC:POPG (3:1)	100±10

4.3 Conclusion Part I

A protocol for reconstitution of ABCB8 into proteoliposomes could be established and the effects of different lipid compositions of these proteoliposomes on basal ATPase activity were tested. It could be shown that ABCB8's ATPase activity

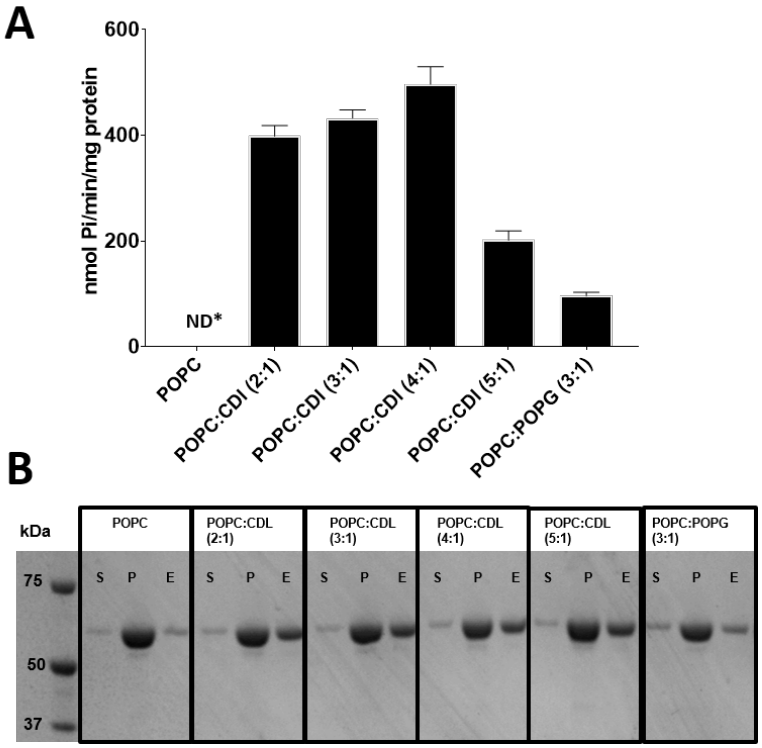


Figure 4.5 – ABCB8 reconstituted into POPC only, POPC/CDL mixtures of different ratios (2:1-5:1 (w:w)) or POPC/POPG. A) V_{max} values were obtained from a Michaelis-Menten fit of ATPase activity, measured over an ATP concentration gradient, (0-1 mM) using the "Chifflet's assay". ATPase activities were normalised with protein concentrations measured by densitometry of Coomassie-stained SDS-PAGE gel bands (bands E in Figure B). V_{max} values ±S.E. were obtained from one biological repeat in triplicate. B) Coomassie-stained SDS-PAGE gel bands for ABCB8 reconstitution with samples taken from supernatant (S) and pellet (P) after the ultracentrifugation step, as well as from subsequent elution (E) of a desalting column.

can be stimulated by cardiolipin. The ratio of POPC to cardiolipin was important for the activating effect on ATPase activity.

4.4 Results Part II

4.4.1 Effects of ATP, ADP and ATP-analogue binding to ABCB8

The purity of the nucleotide analogues (Table 2.4) was evaluated using ESI mass spectrometry. Quantitative analysis of the nucleotide composition is not possible using mass spectrometry, as different chemical and physical properties, such as charge or molecular weight, can influence ionisation of small molecules in ESI-QTOF. However, ADP was detected as an impurity in freshly prepared AMPPNP and ATPγS stocks (Fig. 8.9). Throughout the thesis, it is referred to "ATPγS" and "AMPPNP", although it should be kept in mind that these nucleotides are in fact a mixture of either AMPPNP or ADP and ATPγS and ADP.

Differential scanning fluorimetry of ABCB8 with nucleotides

The melting curves recorded for unmodified ABCB8 in OGNG/CHS after incubation with ADP and ATP analogues were detected observing changes in fluorescence emission at 330 nm (Fig. 4.6). The inflection point, which is referred to as the T_M value, could be determined from the maximum of the first derivative of the melting curve. The fluorescence at 330 nm and to a lesser extend at 350 nm increased for all samples upon unfolding, indicating that an increase in tryptophan quantum yield is observed with change of polarity towards a more hydrophobic environment and/or a decrease of quenching of tryptophans upon release from the folded environment. ABCB8 only has four tryptophans. Trp134 and Trp138, are located at the elbow helix, likely at the interface between the detergent micelle and the protein surface

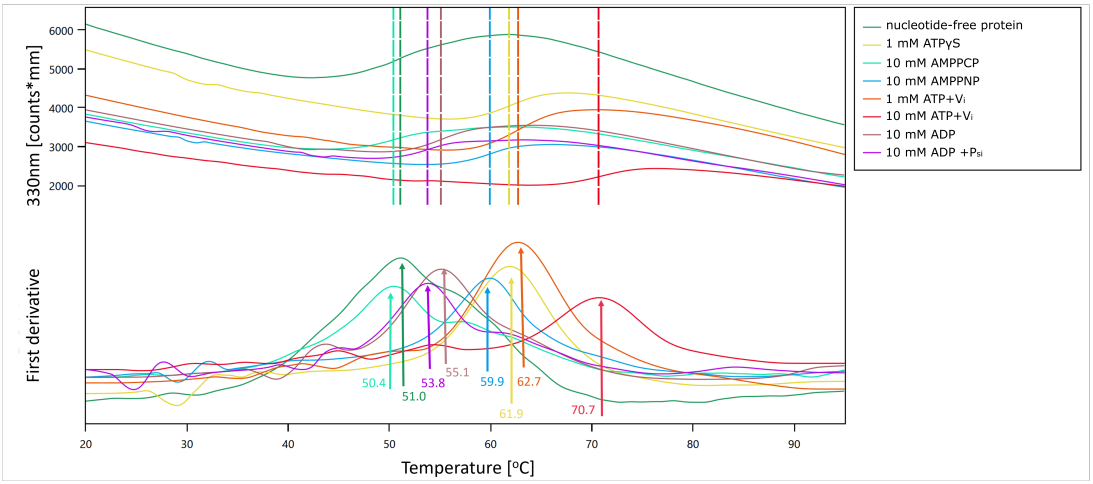


Figure 4.6 – NanoDSF unfolding curves for unmodified ABCB8 in OGNG/CHS incubated with nucleotides prior to measurements. Change of tryptophan fluorescence at 330 nm (top graph) and first derivative (bottom graph) with lines indicating inflection points that represent T_M values.

and are packed against a series of hydrophobic residues (Phe137, Leu141, His142, Leu145, Met312 and Leu439). The third tryptophan (Trp545) is in the NBD and also part of a hydrophobic cluster, involving several aliphatic side chains. The aromatic ring of Trp545 is packed between the sidechain of Cys462 on one side, and Gln549 and Val550 on the other side. Trp688 is also in the NBD on a beta strand before the final helix. It is exposed to solvent in a relatively hydrophilic environment, so unfolding the protein may actually move this aromatic residue into a more hydrophobic environment.The effects of tyrosines and phenylalanines in ABCB8 can be considered negligible due to different excitation wavelengths (240 nm and 260 nm) and generally lower quantum yields. Nucleotides were not found to interfere with excitation and emission wavelengths used in these experiments.

In order to assess the effect of modification of ABCB8 with iodoacetamide treatment, the melting temperatures of unmodified and modified ABCB8 were compared, as described in section 2.10, with each purification and modification repeated in triplicate. Surprisingly, the thermostability of ABCB8 with and without modification by iodoacetamide were remarkably similar, with T_M values of 50.2±0.7 °C and 49.0±0.5 °C measured for unmodified and iodoacetamide treated protein,

respectively.

Next the effects of nucleotides on ABCB8 stability were tested and, as clear from the shifted maxima in the first derivatives of the example melting curves, nucleotides increase the melting temperature of ABCB8 to considerable extents, with increases in temperature ranging from 1.4 °C to 20 °C (Fig. 4.6). These effects were consistent when averaged over three purifications (Fig. 4.7, Table 4.4). Addition of 10 mM ADP to unmodified and modified ABCB8 increased the thermal stability by 5.2±0.9 °C and 4.1±0.7 °C, respectively. Surprisingly, no stabilisation of ABCB8 (unmodified or iodoacetamide treated) outside the error range was observed with the non-hydrolysable ATP analogue AMPPCP at 10 mM, whereas 10 mM AMPPNP showed thermal stabilisation of unmodified protein (9.8±0.9 °C), but not of modified protein. A substantial increase of T_M shifts above 10 °C were observed with non-hydrolysable ATP analogue ATPγS (1 mM) and the transition state analogue ATP+V_i (10 mM). 1 mM ATPγS stabilised the unmodified protein by 13.8±3.6 °C and the iodoacetamide treated protein by 14.7±1.3 °C. This effect was not enhanced, when 10 mM ATPγS were used initially. Incubation with ATP and orthovanadate gave an increase in ΔT_M of 20.8±1.0 °C and 12.4±2.5 °C for unmodified and iodacetamide treated protein, respectively.

To summarise, alkylation of the cysteines did not influence basal thermal stability of ABCB8. Alkylation also had little or no effect on thermostabilisation by ADP, ADP+PS_i, ATPγS or ATP+V_i. It did however significantly decrease the ΔT_M caused by binding of AMPPNP. ADP plus thiophosphate (PS_i) was tested, as it resembles ATPγS hydrolysis products. However, thermal stabilisation of ABCB8 with ADP and (PS_i) was 4 to 6-fold lower compared to ATPγS. With melting temperature shifts of 3.5±0.7 °C for unmodified and 2.3±0.6 °C for iodoacetamide treated protein, it resembled the results obtained for ADP (Fig. 4.7, Table 4.4).

Binding of nucleotides to an ABC transporter can restrict flexibility of the side chains and/or backbone of adjacent residues involved in the nucleotide binding

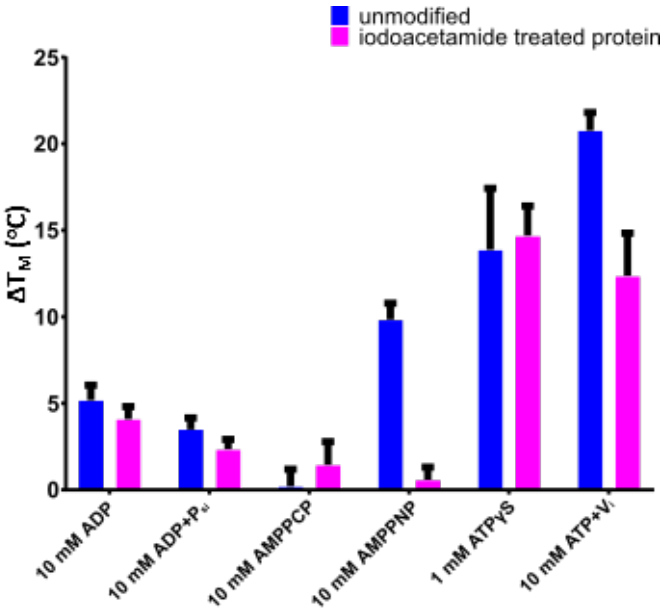


Figure 4.7 – ATP analogues differ in their effect on the stability of ABCB8, when tested by nanoDSF. T_M values were obtained from inflexion points of change in tryptophan fluorescence at 330 nm upon heating the sample with a temperature gradient of 1 °C/min. T_M shifts were calculated from difference between T_M values for samples incubated with and without nucleotide. ΔT_M values are presented in a bar chart for unmodified (blue) and iodoacetamide treated (pink) protein. Data points present the mean ±S.D. of two or three biological repeats measured in triplicate for unmodified or iodoacetamide treated protein, respectively. Nucleotide concentrations were used as indicated on the x-axis.

Table 4.4 – Absolute T_M values for ABCB8 in the absence of nucleotide and ΔT_M shifts after incubation with nucleotides. Temperatures represent the mean ± S.D. for two or three biological repeats measured in triplicate for unmodified or iodoacetamide treated ABCB8, respectively. The nucleotide concentrations were used at 10 mM with the exception of ATPγS where 1 mM was used

	unmodified	**iodoacetamide treated**
	T_M (°C)	**T_M (°C)**
ABCB8	50.2±0.7	49.0±0.5
	ΔT_M (°C)	**ΔT_M(°C)**
ADP	5.2±0.9	4.1±0.7
ADP+P_{si}	3.5±0.7	2.3±0.6
AMPPCP	0.2±1.0	1.4±1.4
AMPPNP	9.8±0.9	0.6±0.7
ATPγS	13.8±3.6 (1mM)	14.7±1.3 (1 mM)
ATP + V_i	20.8±1.0	12.4±2.5

site, as observed for the Walker A motif in ABCB10. In the nucleotide-free structure of ABCB10, residues of the Walker A motif form a helical structure, which unwinds upon AMPPCP and AMPPNP binding, so that the nucleotide can be tightly coordinated [Shintre *et al.,* 2013]. In addition, the NBDs were observed to dimerise upon nucleotide binding [Verhalen *et al.,* 2017; Hellmich *et al.,* 2012; Borbat *et al.,* 2007; Smriti *et al.,* 2009], which would lead to an increase in rigidity of the whole transporter. A larger number of non-covalent interactions, including hydrogen-bonds and vdW contacts, have to be disrupted upon unfolding. This is particularly true, when nucleotide binding triggers conformational changes with a larger dimer interface between the two NBDs and potentially TMDs. Consequently, more energy to unfold the protein is required, which gives rise to higher melting temperatures.

Measuring nucleotide binding using microscale thermophoresis

Microscale thermophoresis (MST) was used to analyse nucleotide analogue binding to ABCB8 in more detail by obtaining thermodynamic parameters as dissociation constants and Hill coefficients.

Apparent K_D values determined with the T-jump method (individual MST traces presented in Fig. 8.10 and Fig. 8.11), showed that ATP analogues have different binding affinities for ABCB8. ATPγS showed a high affinity for ABCB8 with an apparent K_D of 33$\pm$3 μM for unmodified protein and 45$\pm$2 μM for iodoacetamide modified protein (Fig. 4.8). In addition, ATPγS binding suggest a potential positive cooperativity with Hill coefficients being 1.4$\pm$0.1 and 1.7$\pm$0.1 for unmodified and iodoacetamide modified protein, respectively. ABCB8 had a two fold lower apparent affinity for ADP, and this apparent affinity is unaffected by modification of ABCB8. Furthermore, it did not display cooperativity. Unmodified ABCB8 showed a high affinity for AMPPNP comparable to the one for ATPγS. However, the affinity for AMPPNP decreased by an order of magnitude with modification

of the protein. ABCB8 binding to an ATP orthovanadate mixture, which is supposed to form an ATP transition state, exhibited threefold lower affinity and loss of cooperativity with modification of cysteines in the protein. Neither a change in T-jump nor a thermophoresis signal was observed upon titration with AMPPCP.

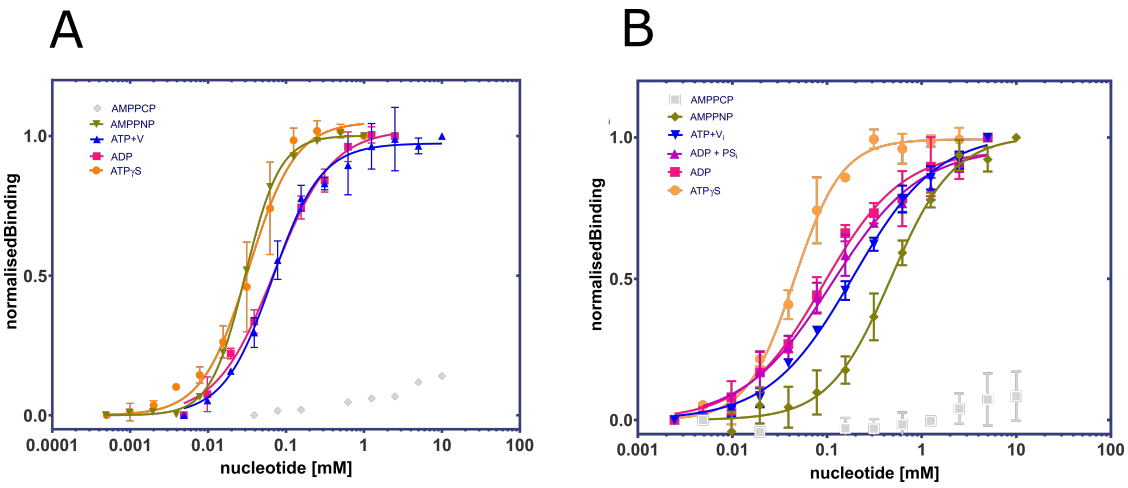


Figure 4.8 – Nucleotide binding to ABCB8. Binding curves derived from change in T-jump signal upon nucleotide titration to unmodified ABCB8 (A) and iodoacetamide treated ABCB8 (B) in OGNG/CHS. ABCB8 was labelled with a P3NTA probe that attaches fluorescein to the C-terminal fusion tag. Data points present the mean ±S.D. of two and three biological repeats for unmodified and iodoacetamide treated protein, respectively (AMPPCP binding to unmodified and iodoacetamide treated ABCB8 was measured in one and two biological repeats, respectively.) $K_{D,app}$ values and Hill coefficients were obtained from fitting the data with a specific binding curve with Hill slope using Prism 7 GraphPad software.

Table 4.5 – $K_{D,app}$ values and Hill coefficients for nucleotide binding to unmodified and iodoacetamide treated ABCB8 wild type (Fig. 4.8) in OGNG/CHS obtained from MST experiments. Parameters ±S.E. were obtained from a saturated binding fit with Hill slope presented in Fig. 4.8

	unmodified		iodoacetamide treated	
	$K_{D,app}$ (µM)	Hill coefficient	$K_{D,app}$ (µM)	Hill coefficient
ADP	70±7	1.2±0.1	90±10	1.0±0.1
ADP+Psi	-	-	110±20	0.9±0.1
AMPPCP	ND	ND	ND	
AMPPNP	30±1	1.9±0.1	480±40	1.3±0.1
ATPγS	33±3	1.4±0.1	45±2	1.7±0.12
ATP + Vi	67±4	1.4±0.1	190±10	1.0±0.1

The T-jump MST results are consistent with the previously described nanoDSF measurements on ABCB8.

The apparent K_D values for unmodified ABCB8 in the presence of either ATPγS or AMPPNP is ~ 30 μM. As is the apparent K_D for iodoacetamide treated protein in the presence of ATPγS. These results are consistent with the significant melting temperature shifts (>10 °C) reported in nanoDSF experiments. Furthermore, the tenfold and threefold reduction in apparent affinity for AMPPNP and ATP+V_i with iodoacetamide modification of the protein, respectively, was also reflected in a drop of ΔT_M values in the nanoDSF experiments. Modified ABCB8 could not be stabilised by AMPPNP at all and a drop in the ΔT_M shift for ATP+V_i from 20 °C to 12 °C was observed for the iodoacetamide treated protein. Neither nanoDSF nor MST showed an effect of AMPPCP interactions with ABCB8.

Inhibition of ATPase activity by nucleotide analogues

Nucleotide analogues such as AMPPNP and AMPPCP are generally regarded as useful mimics of ATP for studies of a range of enzymes, including kinases and ATPases. In the MST experiment described above, certain non-hydrolysable ATP analogues and ADP did bind to iodoacetamide treated ABCB8. However the effects were not entirely consistent, with AMPPNP showing relatively little effect and AMPPCP having no effect in T_M shift and MST. In order to determine if these nucleotide analogues are similar to ATP in their binding properties, their IC_{50} values in ATPase activity were measured. This indicated if they bind ABCB8 with similar affinities to ATP. To answer this question a "Chifflet's assay" (section 2.9.1) was used to measure the apparent ATP hydrolysis rate by colorimetric detection of formation of the product orthophosphate. Another interesting question pursued previously with nanoDSF and MST was, whether ADP binds to ABCB8 with an affinity, that would justify the ADP binding as observed in the outward-facing structure of ABCB8. Inhibition of ATPase activity by the reaction product ADP would further confirm the assumption that ABCB8 has an affinity for ADP. Although ADP-Glo gave better signal-to-noise ratios, this assay could not have been used, as it would not allow determining ADP inhibition of ATP hydrolysis.

For this assay, the protein was incubated with increasing concentrations of ATPγS (0.5 μM to 1 mM), AMPPNP, AMPPCP or ADP (10 μM to 8 mM) at a constant ATP concentration of 1 mM.

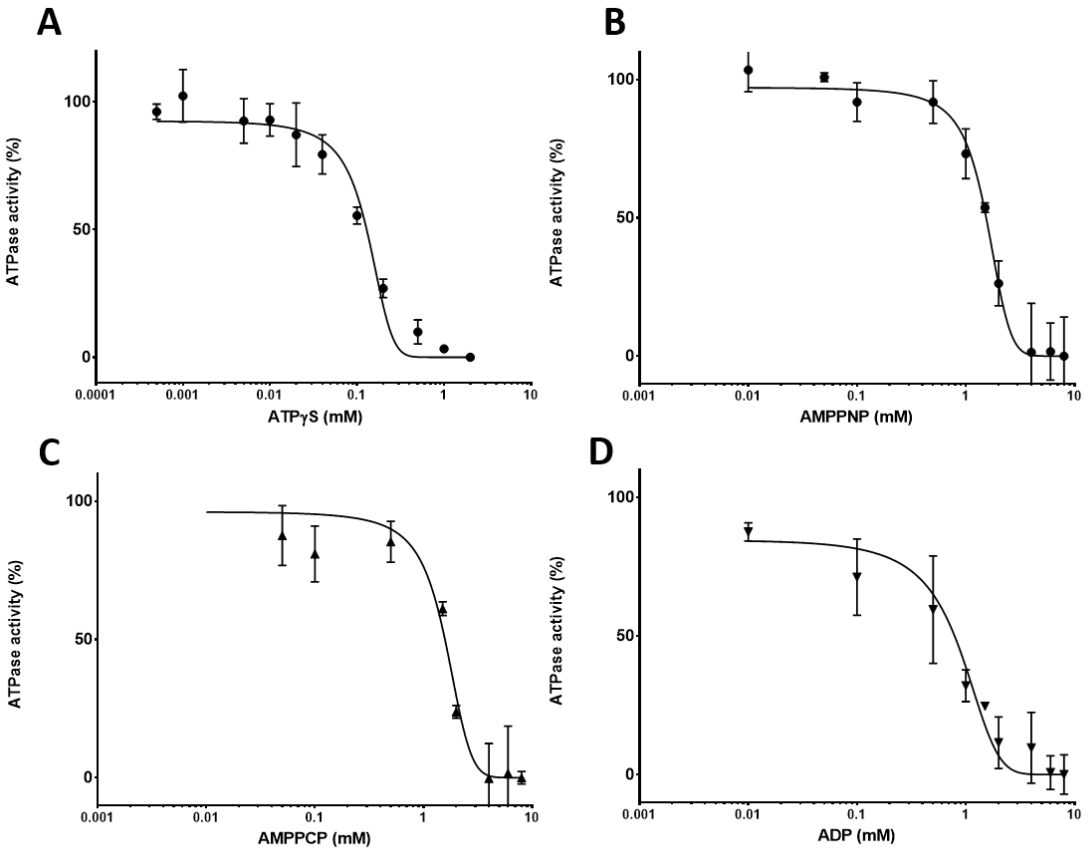


Figure 4.9 – Inhibition of the ATPase activity of iodoacetamide modified ABCB8 by non-hydrolysable ATP analogues ATPγS (A), AMPPNP (B) and AMPPCP (C), as well as ADP (D). Measurements were recorded in triplicate for two biological repeats. IC_{50} values were obtained by fitting the data to an inhibition model for normalised response and variable slope using the Prism 7 GraphPad software.

ATPγ inhibited the ABCB8 ATPase activity (Fig. 4.9A) with an IC_{50} value of 0.13±0.01 mM (Table 4.6). This is in accordance with the previous MST experiments, in which ATPγS exhibited the highest binding affinity of all the ATP analogues tested.

Although neither AMPPCP nor AMPPNP showed an effect on thermal stability in nanoDSF and little or no binding in MST experiments to iodoacetamide treated protein, inhibition of ATPase activity was observed (Fig. 4.9B and C). However,

for both analogues a tenfold higher ATP concentration was required for full inhibition of ATPase activity. This showed that both AMPPNP and AMPPCP have a weak relative binding affinity to modified ABCB8 compared to ATP binding itself. AMPPCP and AMPPNP are weak competitive inhibitors in contrast to ATPγS, which can fully inhibit ATPase activity at concentrations equal to ATP. Since AMPPNP binding was influenced by iodoacetamide treatment of the protein as previously described in the nanoDSF and MST experiments, it would be predicted that AMPPNP might be a potent inhibitor of ATPase activity with unmodified protein. However, further ATPase activity measurements in the presence of AMPPNP are required to verify this.

Interestingly, ADP, which is one of the products of ATP hydrolysis, inhibits the ATPase activity of ABCB8 with a sixfold excess of ADP being required to fully inhibit the ATPase activity (Fig. 4.9D). For example, inhibition of ATPase activity by ADP was shown for CFTR [Randak & Welsh, 2005] An IC_{50} of 770 μM is consistent with ADP concentrations measured in cells **??**. However one has to consider that ATP has a higher affinity and consequently out-competes ADP at higher concentrations. The ability of ADP to bind NBDs and act as a competitive inhibitor at high concentrations is of biological relevance, as high ADP/ATP ratios in the mitochondrial matrix signals energy deficiency in the cell. Thus, product inhibition by ADP would stop the cell from using its remaining ATP resources for ABC transport processes.

Table 4.6 – IC_{50} values for inhibition of ATPase activity of iodoacetamide modified ABCB8 at 1 mM ATP derived from a fitted inhibition model in Fig. 4.9. Data were obtained from two biological repeats measured in triplicate. S.E represent standard errors derived from fit from the Prism 7 GraphPad software

	IC_{50} (mM)
ATPγS	0.13±0.01
AMPPNP	1.57±0.13
AMPPCP	1.54±0.04
ADP	0.77±0.09

Crosslinking of ABCB8 in the presence of nucleotides

As observed in the previously described experiments, ATP analogues have different effects on thermal stability, binding and ability to inhibit ATPase activity. The nature of these experiments suggest that nucleotide binding to ABCB8 causes conformational changes in the NBDs, triggering dimerisation. However, evidence for this change in conformation and whether the transmembrane region also changes conformation into an outward-facing state, as observed in the crystal structure (chapter 5), is missing. Comparing an ABCB8 homology model created by MODELLER [Webb & Sali, 2014] on the basis of an inward-facing state of ABCB10 (PDB code: 4AYX) (Fig. 4.10B) with the outward-facing crystal structure (Fig. 4.10A) suggests that there are lysine residues, that change proximity during the alternating-access cycle. These lysine residues would be suitable for lysine crosslinking, dependent on the conformational state.

The two Lys178, located at the top of TMH1, come as close as ∼11 Å (C_α-C_α distance) in the inward-facing state, whereas their distance is drastically increased to ∼42 Å (C_α-C_α distance) upon transition into the outward-facing state. A less significant change in distances occurs for Lys277 (lower end of TMH3) between both chains from ∼ 16 Å to ∼ 22 Å (C_α-C_α distance) in an opposite transition from the outward-facing into the inward-facing state. The crosslinking between two lysines using DSS would be possible for distances 11-24 Å, if one adds twice the distance of 6.3 Å for the distance from the C_α to the nitrogen on the C_ε in the lysines to the 11 Å spacer of DSS (section 2.12). This distance range would include the distance for Lys178 in the inward-facing state, as well distances of Lys277 in both the inward and outward-facing state. However, sidechain rotamer conformations of the lysines, as well as accessibility of these lysines for the crosslinker are crucial for a successful crosslinking reaction.

Prior to testing the effects of the nucleotides on crosslinking, different protein and DSS crosslinker concentrations were screened to find conditions that cause inter-

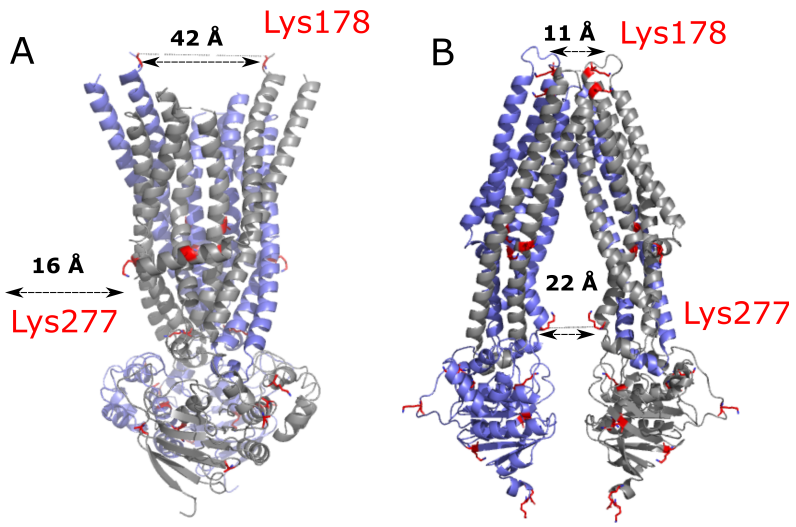


Figure 4.10 – Potential lysine crosslinking sites for DSS in ABCB8 in different conformations. Cartoon representation of the ABCB8 X-ray structure in an outward-facing state (A) and an ABCB8 homology model in an inward-facing state (B). Lysines are presented as red sticks. Distances between potential intermolecular crosslinking sites between the two halves of the homodimer presented in red with crosslinking sites labelled in red.

molecular crosslinks between the two chains of the homodimer, but avoid unspecific crosslinks between different dimers. Subsequently, samples were run on an SDS-PAGE gel for analysis and preliminary results showed successful crosslinking of dimer in the absence of nucleotide.

Following, 0.125 mg/ml of unmodified and iodoacetamide treated ABCB8 wild type was incubated with 1 mM nucleotide for 30 min at room temperature prior to addition of 1 mM DSS to start the crosslinking reaction. Intermolecular crosslinking of the dimer (132 kDa) is identified by a higher band running between the 100 and 150 kDa marker on the SDS-PAGE gel, whereas the lower monomer band is found at 66 kDa (both indicated with arrows in Fig. 4.11A). Quantification of crosslinked dimer amounts was performed using densitometry measurements (Fig. 4.11B). For unmodified protein in the absence of nucleotide, as well as for incubation with ADP and AMPPCP, the majority of protein was crosslinked so that it forms a covalently linked dimer (79%, 70% and 67% dimer fraction, respectively), which cannot be separated during denaturation with SDS. cAMP, which has no interaction with ABCB8, was used as a negative control and gave a similar result with 83% of protein

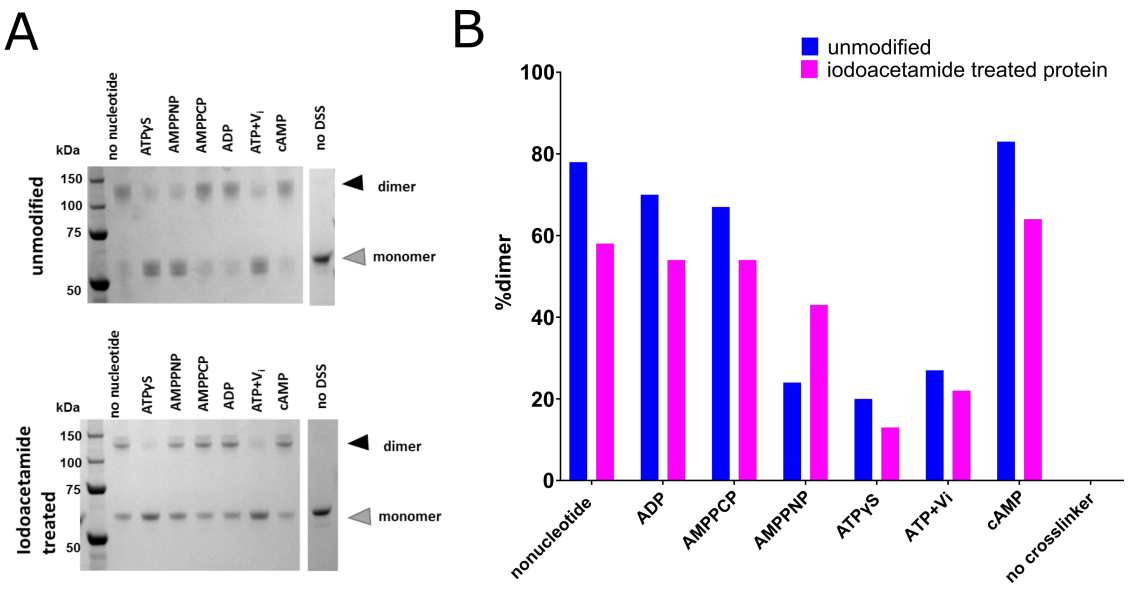


Figure 4.11 – Lysine crosslinking of unmodified and iodoacetamide treated ABCB8 wild type with DSS in the presence and absence of nucleotides. A) SDS-PAGE gel bands showing dimer (132 kDa) and monomer (66 kDa) ABCB8 as indicated with arrows. B) Bar chart presenting amount of dimerised unmodified (blue) and iodoacetamide treated (pink) ABCB8 as derived from densitometry. Measurements were performed in triplicate measurements of one biological repeat using the "Quantity Tool" function of the Image Lab software.

crosslinked. In contrast, AMPPNP, ATPγS and ATP+V_i showed considerable reduction of crosslinking with only 24%, 20% and 27% of crosslinked dimer present, respectively.

Interestingly, iodoacetamide treatment of the cysteines of ABCB8 reduced the amount of crosslinked ABCB8 to 58% and in the cAMP control to 64%. Whereas for ATPγS and ATP+V_i the crosslinked amounts were even more decreased to 13% and 22%, AMPPCP and ADP had little effect on crosslinking of modified protein (54% crosslinked dimer). As observed previously by nanoDSF and MST, the cysteine modifications alter the protein's binding properties for AMPPNP. In accordance with this result, the amount of crosslinked protein was not significantly reduced in the presence of AMPPNP. Crosslinking of unmodified ABCB8 with EGS (spacer arm of 16 Å) resulted in similar distributions for crosslinked dimer and monomer (Fig. 8.13)

By testing lysine crosslinking of the homodimer it could be established that ATPγS

and ATP+V_i cause a conformational change that markedly reduces intermolecular crosslinking of ABCB8. Crosslinking is observed at much higher levels in the absence of nucleotide or with ADP and AMPPCP. Surprisingly, the iodoacetamide treated ABCB8 showed reduced crosslinking, suggesting that the reductive alkylation of specific cysteines in the structure could cause this conformational change.

According to the analysis of the outward-facing structure and inward-facing homology model (Fig. 4.10) crosslinking the Lys178 residues in each chain of the homodimer with DSS or EGS is possible in the inward-facing, but not in an outward-facing state. This is consistent with the observation for nucleotide-free MsbA found predominantly in an inward-facing state with ion mobility mass spectrometry [Marcoux *et al.,* 2013], as well as with low resolution single-particle data obtained for MsbA and P-glycoprotein [Moeller *et al.,* 2015]. Notably, the distance between the top of TMH1 in AMPPNP-bound McjD (4PL0) comes close as $\sim$ 6 Å in the occluded state, which potentially could be too close for crosslinking with DSS or EGS. Consequently, only the inward-facing state would lead to intramolecular crosslinking of the two chains in the dimer, that give a higher molecular weight band on the gel.

If the crosslink dimer corresponds to an inward-facing state (crosslinking of Lys178), then this would suggest, that ATPγS and ATP+V_i binding (and potential hydrolysis) triggers conformational change from the inward-facing state into an occluded or outward-facing state, whereas with no nucleotide or in the presence of ADP and AMPPCP, the TMDs remain in an inward-facing. However, as it is not clear that Lys178 is the only site where crosslinking can occur and as yet there is no occluded state available for ABCB8, it is difficult to be sure which state(s) are represented by the dimerised protein. Since analysis of the crosslinking with SDS-PAGE is ambiguous, further LC-MS/MS experiments have to be undertaken in order to identify the positions of the intermolecular crosslinks. This work is in progress, but unfortunately at time of printing the thesis, the results were not available.

For nucleotide-free unmodified protein, it was observed that ∼ 79% are covalently crosslinked, which suggests that there is a mixture of states even in the nucleotide-free sample. This is not surprising, as ABC transporters have been found predominantly in inward-facing states, but as a mixture of states, as previously reported for MsbA using ion mobility mass spectrometry [Marcoux *et al.,* 2013].

Effects of ATP and ATP analogues on an ATP hydrolysis deficient mutant

Mutating Glu637 to glutamine in the Walker B motif impaired ATP hydrolysis in ABCB8 (termed "dead" mutant) (Fig. 4.12 and Table 4.7). However, since Glu637 is part of the catalytic dyad but it is not thought to be required for nucleotide binding, effects of ATP binding to the transporter are still to be expected.

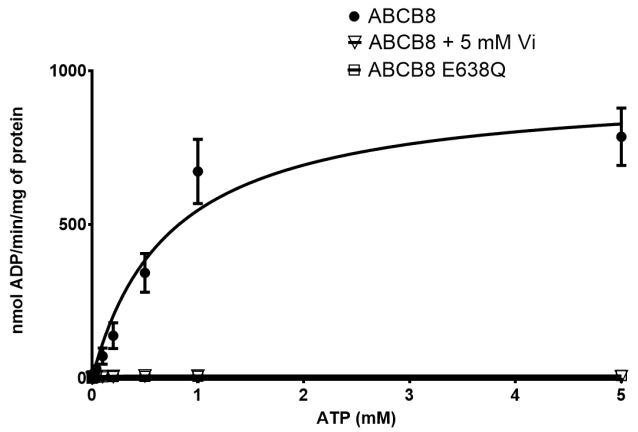


Figure 4.12 – A) ATPase activity of unmodified ABCB8 WT and ABCB8 E637Q in OGNG/CHS, as well as ABCB8 WT in the presence of 5 mM V_i as a control. ATPase activity was obtained using the ADP-Glo assay method measured with increasing ATP concentrations (0-2mM). Data points represent the mean ±S.D. of three biological repeat measured in triplicate for WT ABCB8 and the dead mutant. Data were fitted to obtain $K_{M,app}$ and $V_{max,app}$ values using Michaelis Menten analysis with the Prism 7 GraphPad software.

The dead mutant had similar thermal stability compared to the WT (50.3±0.1 °C for unmodified protein and 49.1±0.0 °C for iodoacetamide modified ABCB8). However, ATPγS and ATP+V_i showed stronger T_M shifts particularly for unmodified protein with ∼30 °C stabilisation in the presence of 1 mM ATPγS or 10 mM ATP+V_i, which suggests stronger binding of these nucleotides to the dead mutant

Table 4.7 – Kinetic parameters for ABCB8 E637Q and ABCB8 wild type in the presence and absence of 5 mM V_i. $K_{M,app}$ and $V_{max,app}$ values as obtained from Michaelis-Menten plot presented in Fig. 4.12 with ±S.E. resulting from fit

	$K_{M,app}$ (mM)	$V_{max,app}$ (nmol ADP/min/mg protein)
ABCB8	0.74±0.13	949±59
ABCB8 + 5 mM V_i	ND	5.9±0.3
ABCB8 E637Q	ND	7.2±0.4

(Table 4.8). A hydrolysis deficient mutant has the advantage that it is possible to measure interactions with ATP without the subsequent catalytic effect. In presence of 10 mM ATP, thermostability was increased by 28.9±0.3 °C and 22.8±0.1 °C for unmodified and iodoacetamide mutant, respectively. Even with 1 mM ATP, a stabilisation of 20.2±0.1 °C was observed for the unmodified protein and 16.2±0.1 °C for the iodoacetamide treated protein (Fig. 4.13, Table 4.8). These values correspond well with T_M shifts obtained for ABCB8 E637Q after incubation with ATPγS and ATP+V_i. Although yielding lower stabilisation than the other nucleotides tested, ADP incubation of the unmodified E637Q mutant also showed a 2-fold increase in ΔT_M compared to the unmodified WT protein (Fig. 4.7B, Table 4.8).

Table 4.8 – Absolute T_M values for unmodified and iodoacetamide treated ABCB8 E637Q and Δ T_M shifts after incubation with nucleotides.Temperatures represent the mean ±S.D. of three measurements performed on one biological repeat. Nucleotide concentrations are indicated in brackets

	unmodified	**iodoacetamide treated**
	T_M (°C)	**T_M (°C)**
ABCB8	50.3±0.1	49.1±0.0
	ΔT_M (°C)	**ΔT_M(°C)**
ADP	10.8±0.1 (10 mM)	5.7±0.1 (10 mM)
ATP	20.2±0.1 (1 mM); 28.9±0.3 (10mM)	16.2±0.1 (1 mM); 22.8±0.1 (10 mM)
ATPγS	31.8±4.2 (1mM)	25±0.1 (1mM)
ATP + V_i	20.0±0.1 (1mM) ; 27.1±0.2 (10 mM)	13.1±0.1 (1mM); 21.3±0.1 (10 mM)

In addition to the T_M shift data, the MST method to assess nucleotide binding to the dead ABCB8 protein was attempted. Surprisingly, ATP and ATP + V_i

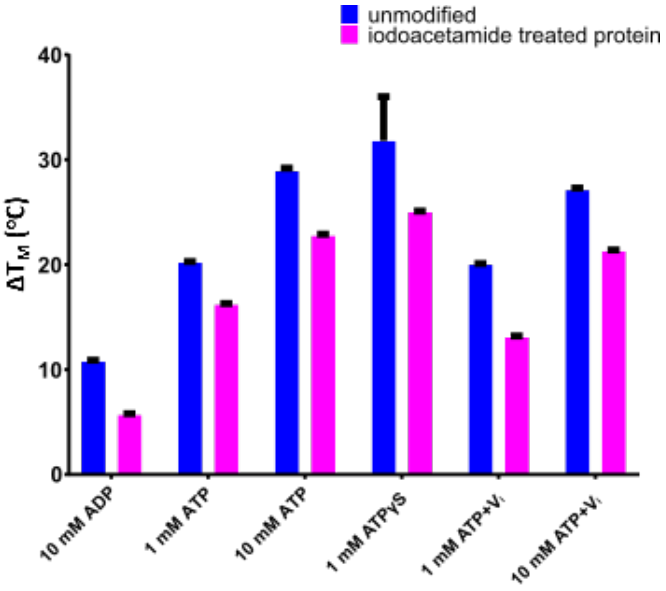


Figure 4.13 – ATP analogues differ in their effect on the stability of ABCB8 E637Q as analysed by nanoDSF. T_M values were obtained from the inflexion points of the change in tryptophan fluorescence at 330 nm upon heating of the sample at a rate of 1 °C/min. T_M shifts were calculated from difference of T_M values for samples incubated with and without nucleotide analogues and ADP. ΔT_M shift values are presented in a bar chart for unmodified (blue) and iodoacetamide treated (pink) protein. Data points present the mean ±S.D. of three individual measurement performed on one biological repeat. Nucleotide concentrations were used in incubation as indicated on the x-axis.

binding to the dead mutant showed a low response unit amplitude (fluorescent signal between bound and unbound states) of 9.3 and 11.2 (Fig. 8.12), compared to 18-23 and 20-25 for ATPγS and ATP+V_i binding to the WT ABCB8, respectively. Binding curves for ATP and ATP + V_i (Fig. 4.14 could only be obtained by combining thermophoresis and T-jump analysis and this data has to be treated with caution, as the response amplitudes are very low. Also at present this data has only been obtained from one biological repeat. Due to the poor data quality and difference in analysis method (T-jump and thermophoresis combined compared to T-jump only) of the data, K_D values could not be obtained. No binding at all was detectable for ATPγS or ADP (Fig. 8.12).

A low signal-to-noise ratio for ATP and ATP+V_i binding to ABCB8 E637Q and the inability to detect binding of ADP or ATPγS at all, although strong thermal shifts were observed with the previous described nanoDSF experiments in the presence of these nucleotides, raises the question whether the overall flexibility in

the structure is changed due to the mutation preventing an observable change in the fluorophore environment as observed for the wild type protein. Indeed mutation E631Q in the catalytical dyad in the nucleotide binding site of HylB-NBDs caused loss of coordination with His662 and increase of flexibility [Zaitseva *et al.,* 2006]. Furthermore, mutation of the aspartate in the D-loop decreased rigidity in TAP1/2-NBDs [Grossmann *et al.,* 2014]. Therefore nucleotide binding detection by MST might have been impaired, as the fluorophore environment was not as tightly coupled to conformational changes in the NBDs any longer.

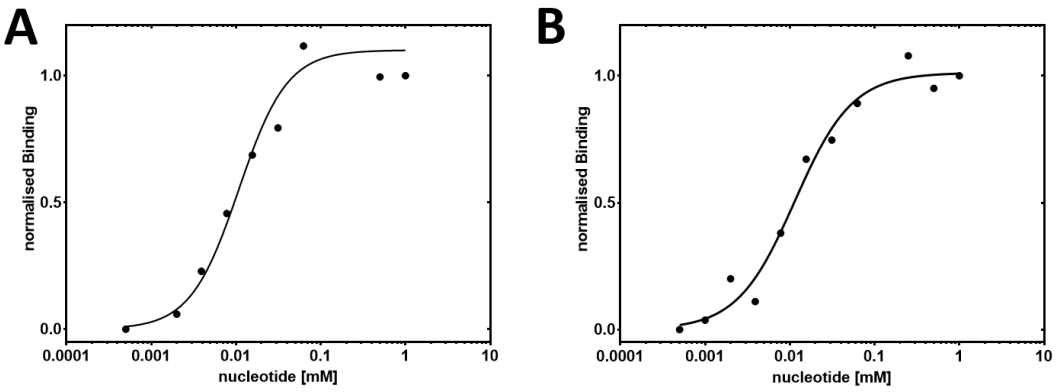


Figure 4.14 – ABCB8 E637Q mutant binding of ATP and ATP+V_i. Binding curves derived from change in T-jump and thermophoresis upon ATP (A) and ATP+V_i (B) titration to constant amounts of ABCB8 E637Q in OGNG/CHS. ABCB8 has a C-terminal fusion tag that interacts with a P3NTA probe for labelling with fluorescein. Data points present the mean ±S.E. of one biological repeat for unmodified protein.

Crosslinking of the ABCB8 E637Q mutant was attempted with DSS to assess the interactions between the chains in different conformations induced by ATP. The mutant did not show any significant difference to the WT protein in the ratio of dimer to monomer seen on SDS-PAGE. 78% of the protein of crosslinked in the absence of nucleotide. The amount of crosslinked protein was reduced drastically to 17% for ATPγS and 19% for ATP (Fig. 4.15).

The ABCB8 dead mutant, that has diminished ATPase activity, was shown to be thermostabilised by ATP binding in the thermal shift assay. ATP, ATP+V_i and ATPγS could stabilise the dead mutant by over 20 °C and reduce crosslinking with

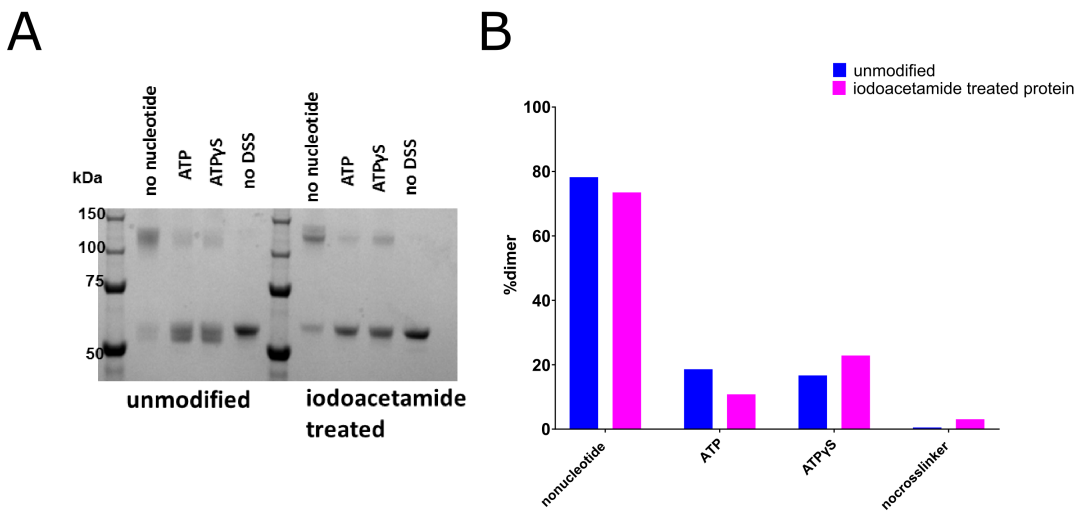


Figure 4.15 – Lysine crosslinking of unmodified ABCB8 E637Q with DSS in the presence and absence of ATP and ATPγS at 1 mM. A) SDS-PAGE gel bands showing dimer (132 kDa) and monomer (66 kDa) ABCB8 as indicated with arrows. B) Bar chart presenting amount of dimerised ABCB8 E637Q mutant as derived from densitometry. Measurements were performed in triplicate of one biological repeat using the "Quantity Tool" function of the Image Lab software.

DSS, as observed for the ATP analogues with ABCB8 WT. However, binding of any of the tested nucleotides was not observed for the dead mutant with MST in contrast to ABCB8 WT. These experiments have to be repeated with more biological repeats to confirm these observations.

4.5 Conclusion Part II

In this chapter the effects of ATP and ATP transition state analogues on ABCB8 were tested in order to understand, which conformational states of ABCB8 could be trapped with these nucleotides. The experiments were performed for the unmodified and iodoacetamide treated protein, that was used in crystallisation. Apparent K_D values for nucleotide binding to ABCB8 using the T-jump method of the MST instrument were obtained, the effects on ABCB8's thermal stability with nanoDSF were probed and the ability of these nucleotides to inhibit basal ATPase activity in competition with ATP was tested. All three methods gave consistent results and it could be established that the ATP analogue ATPγS and the ATP transition state analogue ADP+V_i have strong binding properties for ABCB8 in comparison to AMPPCP, which was not to found to give a signal in the MST experiments with ABCB8 or affect its thermal stability at all. These experiments suggest that not all ATP analogues mimic ATP equally well. Furthermore, thermal stability measurements, as well as lysine crosslinking studies with these analogues and ADP hinted at conformational changes that were triggered by binding of ATPγS or ADP+V_i, but not in the presence of ADP or AMPPCP.

CHAPTER 5

Outward-facing conformations of ABCB8 and the alternating-access mechanism

5.1 Introduction

Although several structures of eukaryotic ABC transporters have recently been solved using X-ray crystallography and cryo-EM, all structures adopt an inward-facing state. This thesis reports the first structure of a human ABC transporter in an outward-facing conformation at sub-4 Å resolution, allowing a crucial insight into the alternating-access mechanism of B-family ABC transporters. This chapter summarises how the structure was obtained, compares to other available structures and how this structure fits in the alternating-access model. Both co-crystallisation with a mixture of ATPγS and ADP, and also crystallisation with ADP on its own, yielded an ADP-bound structure. In addition, a nucleotide-free form at 4.4 Å resolution was solved with a similar TMD arrangement, but with the NBDs separated. ADP binding and subsequent rearrangements of the NBDs and coupling

helices are discussed in detail and compared to the outward-facing structures of Sav1866 and McjD. Furthermore, potential substrate binding sites are discussed on the basis of a conserved residues analysis and binding pockets found in the structure.

5.2 Results

5.2.1 Solving the structure of human ABCB8

Extensive optimisation of the purification and crystallisation conditions, as described in chapter 3, gave crystals that diffracted to beyond 4 Å. Collecting data on these crystals allowed us to solve the first structure of human ABCB8.

ABCB8 crystallised in two crystal forms; a centred orthorhombic space group ($C222_1$; crystal form 1), which diffracted to ∼7 Å, and a primitive monoclinic space group ($P12_11$; crystal from 2), which diffracted to <4 Å. Space group, unit cell dimensions and data quality parameters for the datasets described in this thesis are summarised in Table 8.2. As described in section 2.8.4, data sets were processed using XDS [Kabsch, 2010] and merged using AIMLESS [Evans & Murshudov, 2013]. Subsequently, phases were obtained by molecular replacement (MR) using Phaser-MR [McCoy *et al.,* 2007].

Despite the low resolution diffraction of crystal form 1, attempts to solve the structure with MR were undertaken, as it could have given information on crystal packing and overall conformation, that could have been used to improve the crystals. Since the molecular weight of the protein is known, the Matthews coefficient was used to estimate the number of molecules in the asymmetric unit. Membrane protein crystals, due to the less tight packing of membrane protein molecules surrounded by micelles, have a high solvent content of about 65-80% [Iwata, 2003; Schulz, 2011]. A prediction using the Matthews-coefficient gave an estimate of 12

polypeptide chains per asymmetric unit with a solvent content of 67% or 10 chains with a solvent content of 72%. Since ABCB8 is predicted to form a homodimer, only even numbers of chains are considered. Since ABCB10 has a high degree of homology to ABCB8 (identity=35.0% and similarity=51.1%), ABCB10 structures (4AYW, 4AYT, 4AYX and 3ZDQ) both as monomers and dimers were used as search models for MR. In addition, a structure of ABCB10 in an occluded state (unpublished data Dr Chitra Shintre and Dr Ashley Pike) was tried as a search model. Further attempts involved using "structural monomers" of the ABCB10 inward-facing structures, which were created by combining TMH1-3, TMH6 and NBDs of one chain with TMH4-5 of the adjacent chain (Fig. 8.3). This allowed more flexibility for potential conformations of ABCB8 in these crystals. In addition, MR solutions from standard monomers (from one polypeptide chain) are likely to be rejected, as they can cause clashes of the molecules, if not correctly placed in the unit cell due to their intertwined nature. However, all these attempts at MR were unsuccessful and no structure could be obtained from these data. This is not surprising when considering the high number of molecules in the asymmetric unit (10-12 molecules) and the low resolution (7 Å).

Modification of the protein with iodoacetamide (section 3.2.6) enabled crystallisation of the protein incubated with an ATPγS/ADP mixture in crystal form 2 (Table 3.2) and collection of data (data set d003) that diffracted to better than 4 Å (Table 8.2). Initial phases were obtained for these data using PHASER-MR [Winn *et al.,* 2011; McCoy *et al.,* 2007; McCoy *et al.,* 2007] with a "structural monomer" derived from the nucleotide-free, inward-facing state of ABCB10 (3ZDQ) as a starting model (section 2.8.4). The structure solution revealed, that eight chains forming four dimers were arranged in the asymmetric unit of the monoclinic space group (Fig. 5.1A). Building and refinement strategies are described in detail in the Material and Methods section 2.8.5. Briefly, MR solutions obtained from the structural monomer and a model with half of the TMDs omitted were generated with PHASER-MR [McCoy *et al.,* 2007] and used for model building in COOT [Emsley

et al., 2010]. MR ROSETTA aided model building by automatic model optimisation [Terwilliger *et al.,* 2012]. In addition, the diffraction of this crystal form was improved by slight changes in the purification and crystallisation protocol (see section 3.2.7), leading to collection of a higher resolution dataset (d014), that further improved maps and was used to complete a model after several rounds of building and refinement with BUSTER [Bricogne *et al.,* 2015]. Data processing and refinement statistics are summarised in Table 5.1. The final model contained amino acids Phe132 to Leu718 for the majority of the chains, which equals 80.3% sequence coverage for isoform 1. The quality of the electron density maps is demonstrated for the TMHs of chain A in Fig. 8.15.

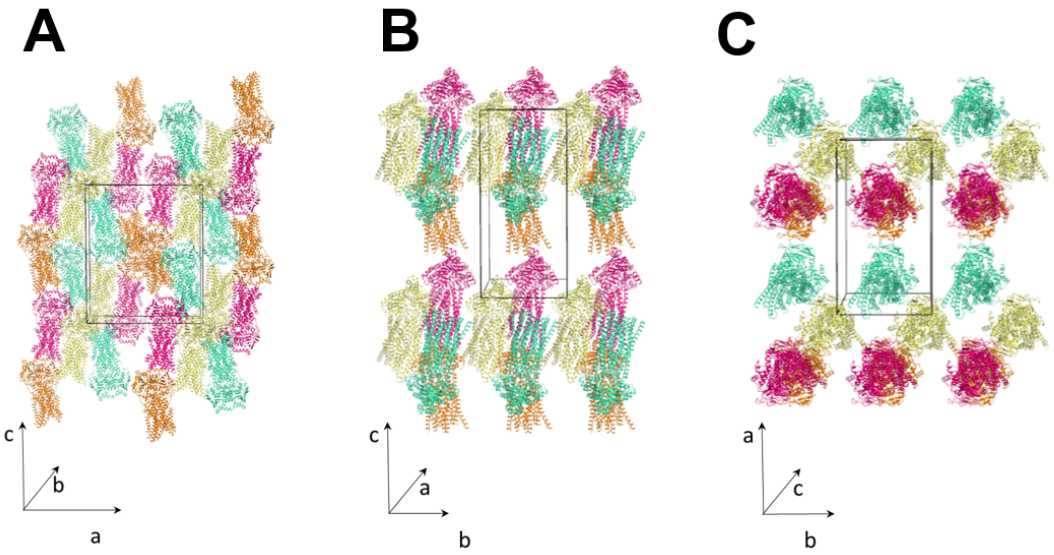


Figure 5.1 – Arrangement of eight chains in the asymmetric unit of the $P12_11$ space group. Packing of four homodimers with chain A and B in yellow, C and D in pink, E and F in cyan and G and H in orange in the unit cell (black) with face-on views of plane a/b in panel A, a/c in panel B an c/b in panel C.

Packing of ABCB8 in the monoclinic crystal system is facilitated by stacking of the dimers due to interactions between the C-termini and extracellular loops ECL1 and ECL2, as well as lateral contacts formed between the NBDs and the NBD-TMD linker regions (Fig. 5.1, Table 5.2).

It is likely that chemical modification of cysteines in ABCB8 enabled packing in

Table 5.1 – Data processing and refinement statistics for dataset d014. * indicates statistical evaluation after STARANISO processing of the data

Dataset number	**d014**	**d014***
Dataset type	native	
Nucleotide	ATPγS/ADP	
Data collection:		
Space group	$P12_11$	
Cell dimensions		
a, b, c (Å)	179.3, 99.8, 212.8	
α, β, γ (^{o})	90.00, 90.18, 90.00	
Resolution (Å)	72.62-3.80 (4.16 x 5.44 x 3.46)	72.61-3.65
Rmerge	0.220 (7.300)	0.122(1.264)
Rmeas	0.238 (7.896)	0.132(1.377)
I/σ	7.0 (0.3)	11.0(1.7)
CC(1/2)	0.998 (0.078)	0.999(0.549)
Wilson B-factor	137.29	
Completeness	99.9	62.1(16.6)
Multiplicity	6.9	6.7
Refinement:	d014	
Resolution	3.8 (72.61-3.43)	
No. of reflections	64839	
Rwork/free (%)	23.10/25.10	
No. of atoms	30741	
Data-to-parameter ratio	2.1	
Mean B-factor (Å^2)	130.92	
Protein	138±22	
TMD	136±12	
NBDs	142±38	
Rmsd		
Bond lengths (Å)	0.008	
Bond angles (^{o})	0.93	

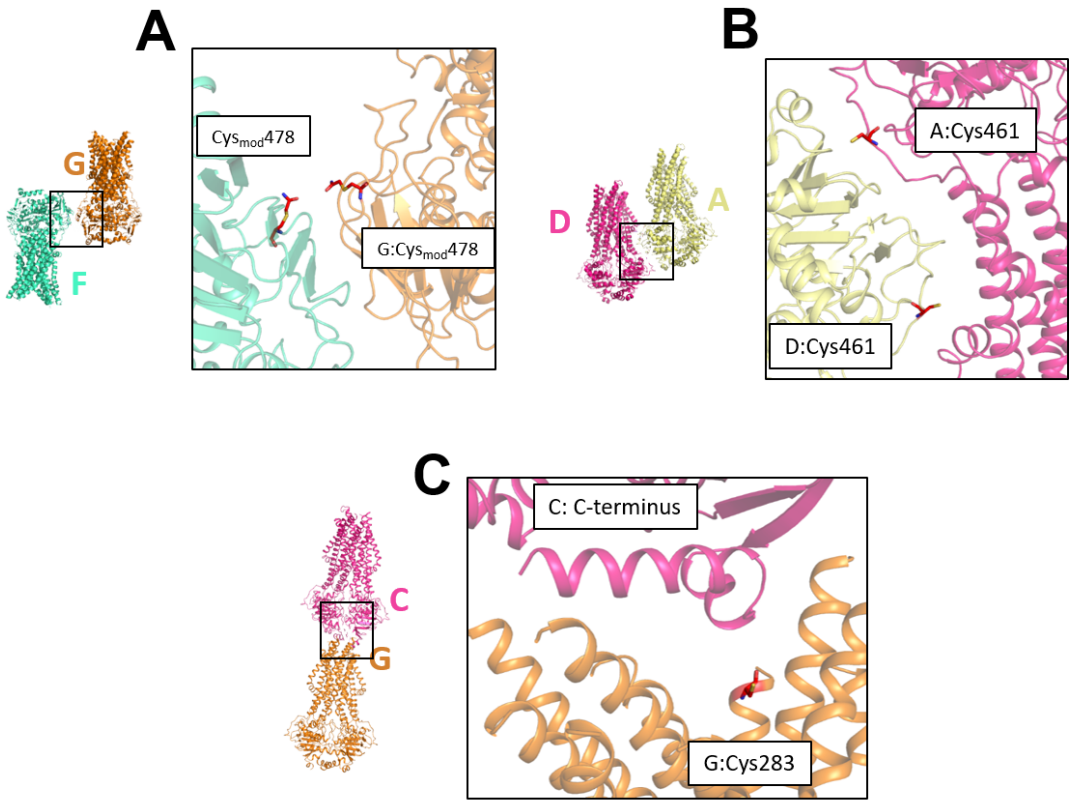


Figure 5.2 – Close-up of the crystal contacts involving cysteine residues (sticks coloured in C=red, N=blue, S=yellow). Chains in cartoon representation are coloured according to Fig. 5.1. Crystal contacts shown for A) chain F/G , B) chain A/D and C) chain C/G.

Table 5.2 – Table listing crystal contacts between chains in crystal form 2 with structural elements involved in crystal contacts (ECL1 (loop TMH1-TMH2) and ECL2 (loop TMH3-TMH4), ELB (elbow helix), TMHs (1-6) and NBDs) and surface area buried.

Chains in crystal contact	Regions involved in crystal contact		Surface area buried (Å²)
F/G	**F**	**G**	541.6
	NBD (linker region)	NBD (linker region)	
	NBD	NBD	
A/D	**A**	**D**	304.6
	NBD (linker region)	ELB1	
	NBD	TMH2	
		NBD	
D/H	**D**	**H**	163.1
	TMH6	NBD	
C/G	**C**	**G**	159.0
	NBD	ECL2	
A/C	**A**	**C**	126.4
	NBD	TMH5	
D/G	**D**	**G**	125.5
	ECL1	NBD	
C/H	**C**	**H**	91.1
	NBD	TMH6	
G/C	**C**	**G**	42.7
	TMH6	NBD	
B/F	**B**	**F**	39.4
	NBD (linker region)	TMH2/ECL1	
A/F	**A**	**F**	34.5
	TMH5	TMH2/ECL1	

this particular crystal form, as cysteines are involved in three of the four major crystal contacts. Densities were observed for modification of Cys483 in chains A-G, whereas Cys461 could only be built in chains B, F and G and Cys366 only in E. Modified cysteines on the surface not trapped the crystal contacts might have been too flexible to be resolved. A crystal contact formed between NBDs and TMD-NBD linker regions of chain F and G buries the biggest surface area (541.6 Å^2). Cys478 in chain F and G, which was identified as modified by MS/MS (Fig. 8.6), is involved in this crystal contact (Fig. 5.2A). Cys461 found on the surface of the NBDs, facilitates the A/D crystal contact from both chains (Fig. 5.2B). Another

cysteine in ECL2 is part of the crystal contact between chain C/G that is formed by the C-terminus of chain C interacting with ECL2 of chain G (Fig. 5.2C; Table 8.4).

In general, the top halves of the transmembrane helices, as well as the α-helical subdomains in the NBDs are the most flexible parts of ABCB8 in this crystal packing (Fig. 5.3A). The packing influences the rigidity of the chains depending on their position in the crystal and the crystal contacts, as evident from the difference in average B-factors (Table 5.3). In particular, packing of dimer AB between dimer CD and dimer GH reduces flexibility of this dimer compared to the other chains, which is reflected in lower average B-factors of 119.38 Å^2 and 113.42 Å^2 for chain A and B, respectively. This explains why dimer AB has a better resolved electron density, particularly in the top halves of the TMDs. Similarly, this is true for the C-termini of dimer GH, as they were packed against the top of dimer AB.

Although all chains were found to have very similar conformations, slight differences caused by individual flexibility of the molecules in the crystal packing gave raise to non-crystallographic symmetry (NCS) (Fig. 5.3B). The root-mean-square deviations (RMSDs) for the C_αs between the chains varied from 0.2 to 1.6 Å^2. Differences between the chains were predominantly observed in TMH4 due to a flexible unwound region, which will be described in detail in section 5.2.6 of this chapter.

Table 5.3 – Average, minimal and maximal B-factors listed for each chain in the asymmetric unit.

Chain	Nr. of atoms	$B_{average}$ (Å^2)	B_{sdv} (Å^2)	B_{min} (Å^2)	B_{max} (Å^2)
A	3968	119.38	37.94	51.22	253.29
B	4114	113.42	44.31	34.96	259.21
C	3569	168.49	36.32	83.89	256.88
D	3991	130.49	41.05	48.83	251.69
E	4003	153.38	39.94	72.4	249.44
F	4110	119.51	34.51	52.02	221.71
G	3861	133.49	36.63	67.1	252.77
H	3662	166.89	41.01	81.14	276.59

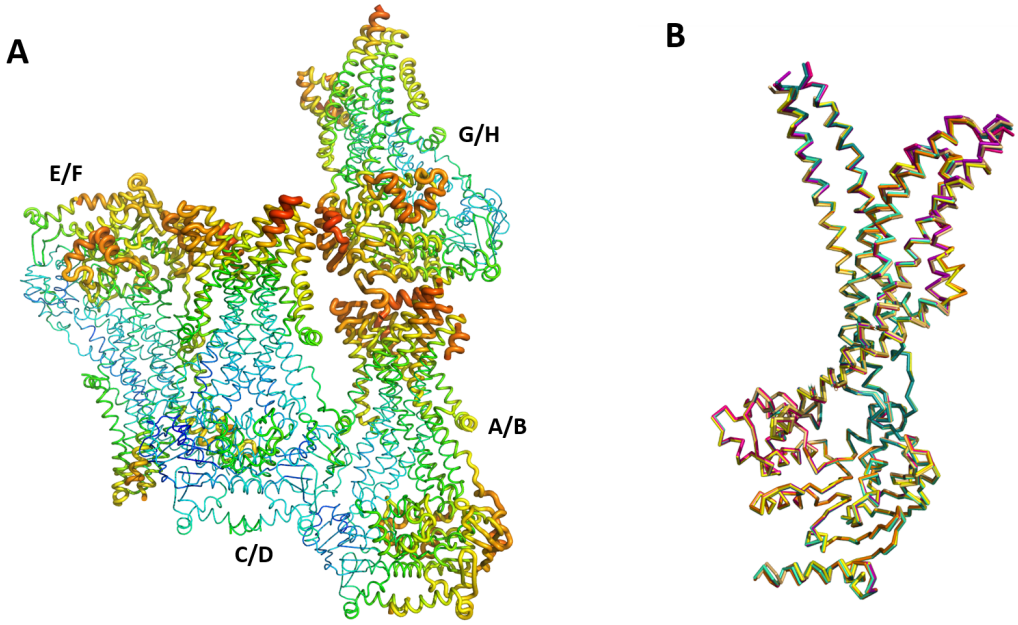


Figure 5.3 – The crystal packing influences rigidity of the ABCB8 dimers A) Four ABCB8 dimers arranged in the asymmetric unit with cartoon representation with chain width and colouring weighted by B-factors (where blue=34 Å^2 and red=277 Å^2) B) Superposition of all eight chains in the asymmetric unit in ribbon representation.

At 3.8 Å resolution only larger side chains were identifiable and thus additional information on positions of other side chains is desired to confirm the sequence assignment. Hence, in addition to the native datasets it was attempted to obtain anomalous scattering data from crystals grown from either selenomethionine containing protein or sodium ethylmercurithiosalicylate (EMTS) soaked crystals to identify methionine and cysteine residue positions. Unfortunately, EMTS modification of free cysteines was hampered by the iodoacetamide treatment essential for crystallisation in this crystal form. Both approaches decreased crystal quality severely and neither selenium or bound Hg^{2+} was identified. Nevertheless, the slightly better resolution of dataset d014 and averaging of the data based on NCS in the eight monomers in the asymmetric unit allowed a good estimate of the register in the ABCB8 structure.

5.2.2 Overall structural features of ABCB8

Chains A and B were chosen as a representative dimer out of the four in the asymmetric unit due to their most complete chain trace. ABCB8 adopts the common ABC exporter topology first revealed for Sav1866 from *S. aureus* [Dawson & Locher, 2006]. The elbow helix sits parallel just below the membrane interacting with the lipid head groups (Fig. 5.4). The top of the TMDs are embedded $\sim$ 30 Å in the membrane protruding further $\sim$ 27 Å into the matrix space followed by the NBDs. The top halves of ABCB8's TMDs are separated by $\sim$ 64 Å (TMH2; Thr172A-Thr172B) at the widest point (Fig. 5.5), defining this structure as an outward-facing state of ABCB8.

The hydrophobic patch on the surface of ABCB8 is lined on both sides with polar and charged residues interacting with the head groups of the membrane (Fig. 5.6A/B), as predicted using the PPM web server (Fig. 8.16) [Lomize *et al.,* 2012]. Conservation analysis using the CONSURF web server [Celniker *et al.,* 2013] with 50 manually chosen ABCB8 homologues (Table 8.5) does not identify a conserved patch on the surface of the protein 5.6D/E), that would suggest a conserved interface for interactions with a binding partner protein. A characteristic feature that was found in this ABCB8 structure is a groove formed above the elbow helix that has several conserved residues and is buried in the membrane bilayer (Fig. 5.7A). In addition, this groove has a patch of highly conserved residues (Fig. 5.6E). Interestingly, a prominent unoccupied density in the $2F_o$-F_c map and F_o-F_c appears, which was modelled as CHS, as described in more detail in section 5.2.7.

In the ABCB8 structure the TMDs are packed against each other in a domain swap arrangement with TMH1-2 of one chain and TMH3-6 of the adjacent chain forming one wing on the top half of the transporter. However, in contrast to the inward-facing structure of ABCB10 with the domain swapped arrangement (between TMH4-5 and TMH1-3/TMH6 of adjacent chains) forming the only dimer interaction, the transporter halves also interact with each other occluding a total

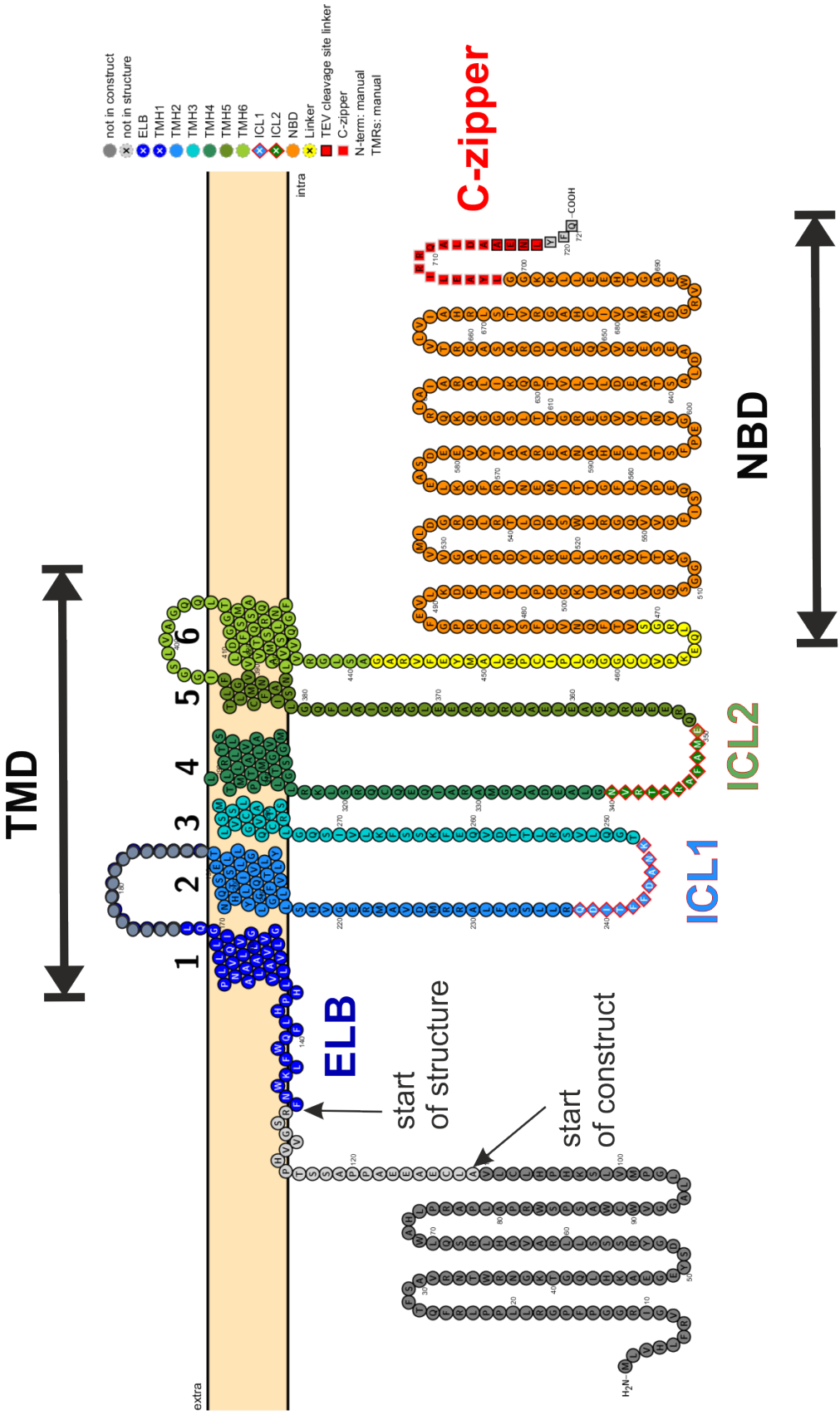


Figure 5.4 – Topology model of ABCB8 isoform 1 on the basis of the crystal structure with residues absent from structure shown in grey. Structural features are colour coded as indicated in the legend on the right.

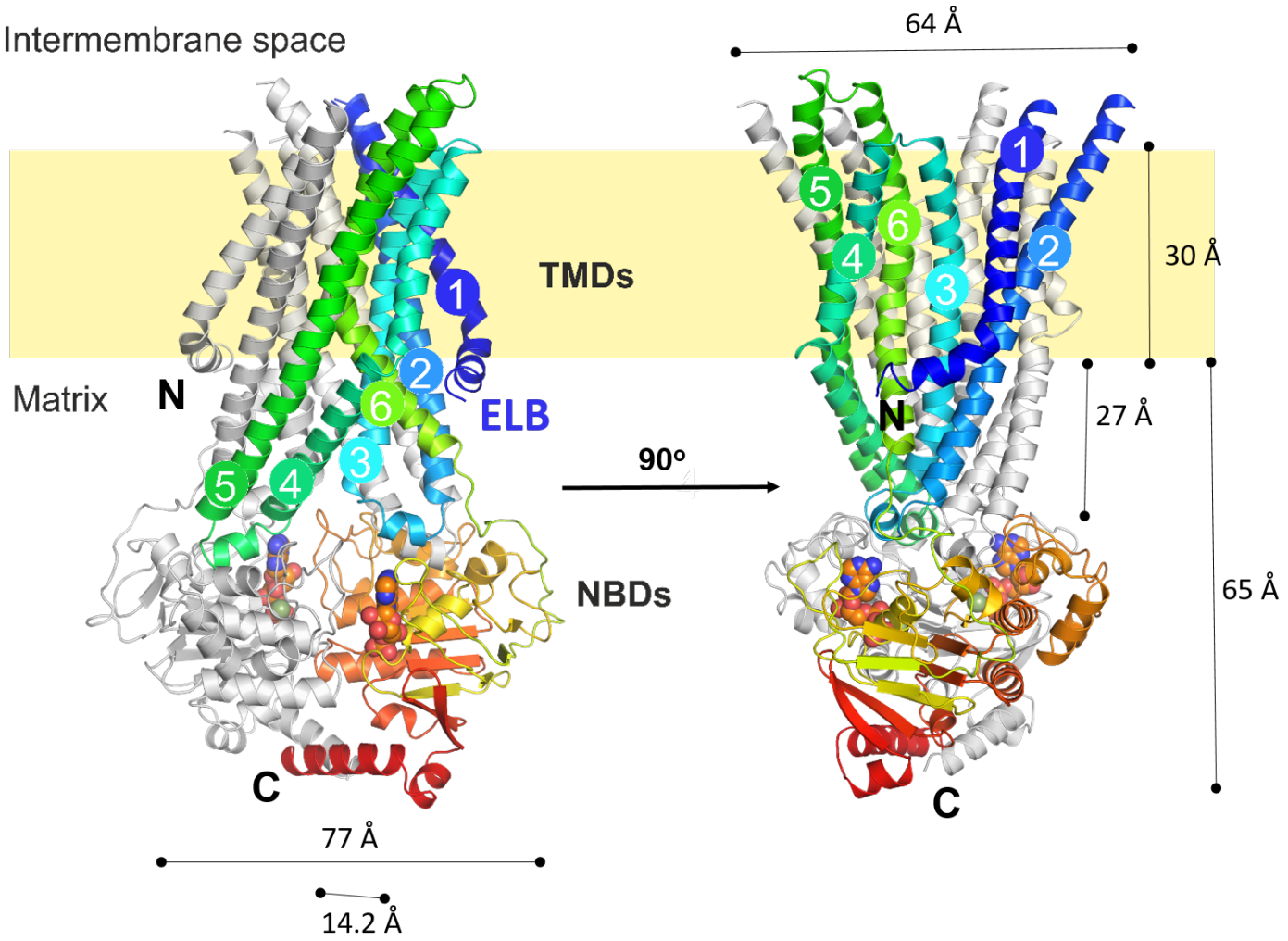


Figure 5.5 – Outward-facing structure of ABCB8 in cartoon presentation with ABCB8 shown perpendicular to the two-fold symmetry axis embedded in the membrane (yellow box) as front view and rotated 90^o around its symmetry axis. ADP (coloured according to elements: C/P=orange, N=blue, O=red) is shown as spheres. Chain A is shown in grey and chain B in rainbow colours (blue=N-terminus to red=C-terminus) according to primary sequence with transmembrane helices labelled from 1-6. Membrane boundaries were predicted using the PPM web server [Lomize *et al.*, 2012].

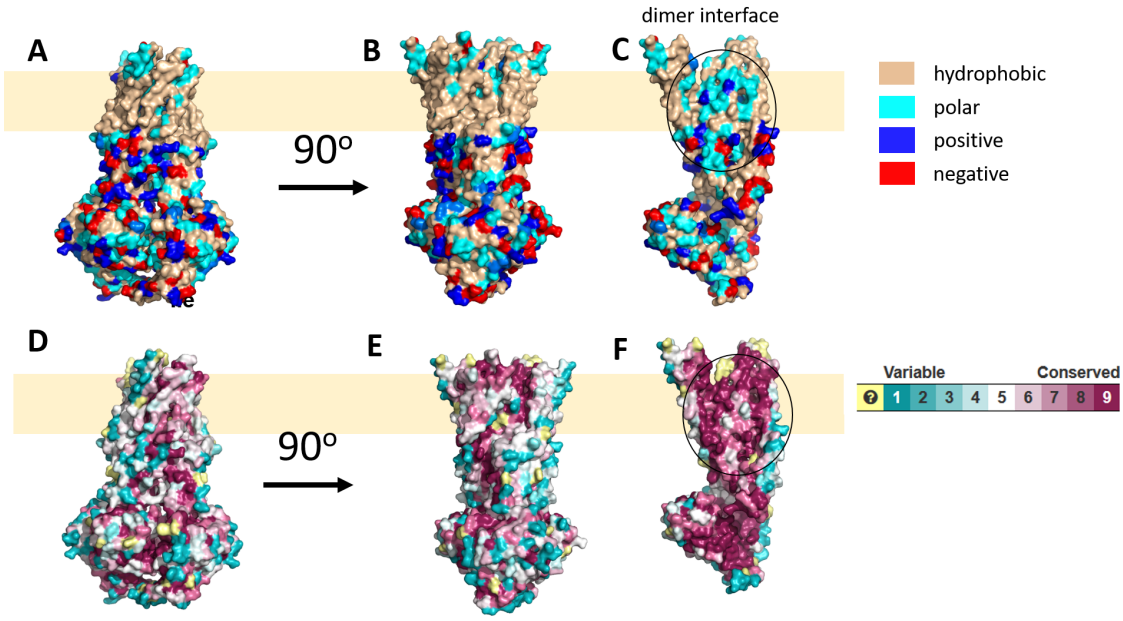


Figure 5.6 – Surface of ABCB8 structure represented perpendicular to the membrane plane with the face-on view of the dimer (left) and in a 90^o turn around the dimer axis (right), as well as the dimer interface. Molecular surfaces are shown and coloured according to A-C) Residue types divided into hydrophobic (sand), polar (turquoise), positive (blue) and negative (red) amino acids. D-F) Conserved residues on the surface highlighted based on CONSURF analysis [Celniker *et al.*, 2013] with 50 homologues of ABCB8. The scale gives the colour coding for degree of conservation. Membrane boundaries were predicted using PPM analysis [Lomize *et al.*, 2012].

dimer interface of $\sim$ 5800 Å^2 (19% of total protein surface) in ABCB8. Upon closure of the transporter the two transporter halves engage with each other by inter-winding by 90^o (Fig. 5.7B). The dimer interface is mainly formed by residues of TMH2-3 and TMH5-6, whereas only the very top halves of TMH1 and the lower halves of TMH4 contribute residues to the dimer interface.

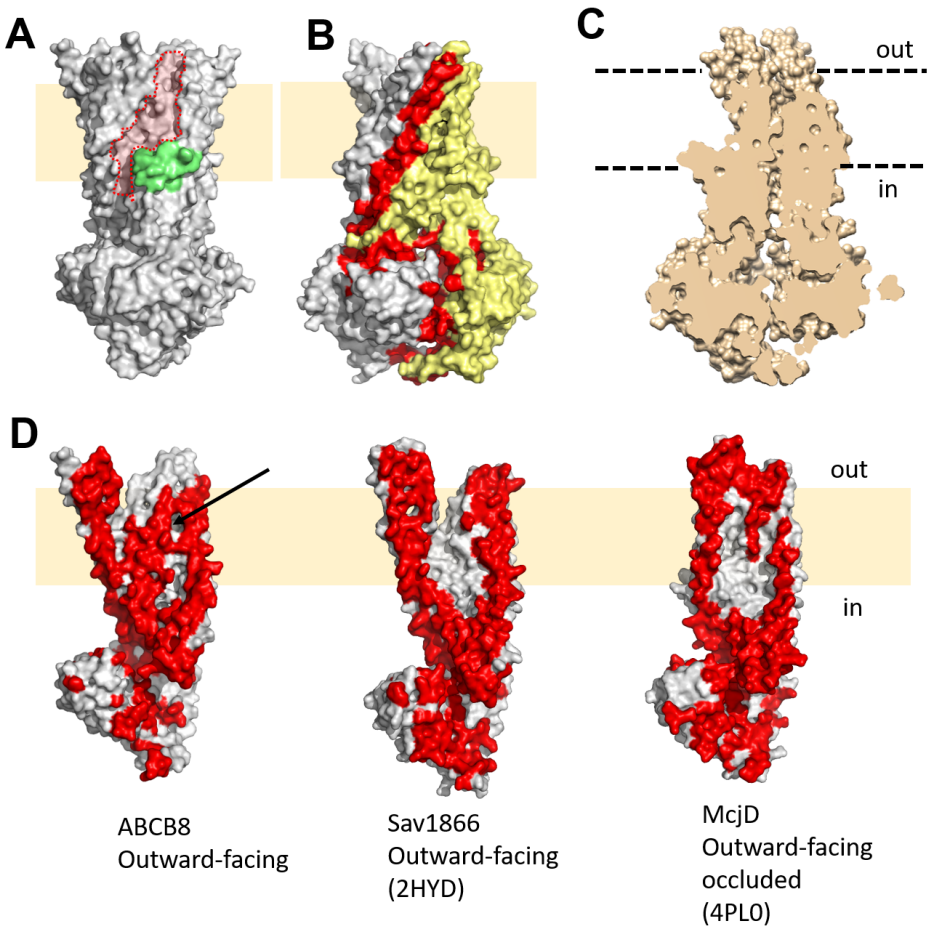


Figure 5.7 – Outward-facing state of ABCB8 in surface representation with membrane boundaries represented as yellow bars and dotted lines, respectively. A) Protein surface with elbow helix in green and groove formed on surface marked in red. B) Surface presentation showing intertwining of chain A (grey) and chain B (pale yellow) with the dimer interface (red) C) Clipped surface presentation of transporter core. D) Comparison of dimer interface (red) in ABCB8, Sav1866 (2HYD) and McjD (4PL0) (grey). The arrow indicates a fenestration leading from the dimer interface to the surface of ABCB8.

The core of the TMDs is almost fully occluded. A small tunnel is formed at the middle, that is occluded from both sides. (Fig. 5.7C). There is a stark contrast to the large surface area in ABCB8 involved in the dimer interface and the dimer interface area of Sav1866 and McjD. In both cases of the open or occluded outward-facing states of Sav1866 and McjD, a large cavity is formed in the transporter that is not part of the dimer interface (Fig. 5.7D). A fenestration connecting to the groove on the outside of ABCB8 is visible from the TMD dimer interface (arrow for ABCB8 monomer Fig. 5.7D). The NBDs, which are covalently connected to the TMDs via a linker region following TMH6, are sandwiched against each other with a distance of $\sim$ 14 Å between the Walker A motif (C_α of Gly511) of chain A and the ABC signature motif (C_α of Gly614) of chain B. Nucleotide bound in the interface participates in the formation of the dimer (see section 5.2.4). However, the NBDs are more separated than in the Sav1866 and McjD structure, where a distance of $\sim$ 11 Å is observed. Moreover, the dimer interface between the NBDs and TMDs is discontinuous, as there is a $\sim$ 17 Å gap beneath the TMDs due to the absence of interactions between the X-loops of the two chains and the ICLs (subsection 5.2.5). This explains the greater overall area covered in the dimer interface in the Sav1866 and McjD structure (both 23% of total dimer surface) compared to the ABCB8 outward-facing conformation (19%). Dimerisation of the NBDs is additionally stabilised by the C-terminal helices interacting in a zipper-like arrangement.

5.2.3 Conservation of residues in the dimer interface

Residues between the TMDs in the dimers interface have been shown to be involved in substrate binding in ABC transporters, such as in Atm1, TAP and MsbA [Srinivasan *et al.,* 2014; Oldham *et al.,* 2016; Mi *et al.,* 2017]. Due to the almost complete occlusion of the TMD core, substrate binding between the TMDs would not be possible in the conformation observed here, unless the substrate is a very

small molecule or an ion. Unsurprisingly, no peak for an unoccupied electron density was observed for ABCB8 in the dimer interface or the opened top half of the transporter that could be attributed to an unknown molecule. However, residues in this surface can potentially be involved in forming a cavity in a different conformation from that observed here, that allows binding of the substrate. Substrate specificity is assumed not to diverge for close homologues of a particular ABC transporter. Consequently, residues in the dimer interface, which are conserved among ABCB8 homologues but not other ABC subfamily B members could play a role in substrate binding. The dimer interface, colour coded according to conservation within 50 ABCB8 homologues (as analysed with CONSURF [Celniker *et al.,* 2013], Table 8.5), points towards distinct patches of conserved residues (Fig. 5.6F). As expected, CONSURF analysis using an alignment of all human members of the B-family does not show any conservation in the interface of the TMDs, suggesting that these residues have a specific function in ABCB8 rather than in all B family ABC transporters (Fig. 8.17B). Patches of high conservation on the TMD interface in ABCB8 coincide with the distribution of mainly polar or positively charges residues (circled area in Fig. 5.6C). This is not surprising, as these residues are likely to be found on a water accessible cavity in an inward-facing state.

5.2.4 The nucleotide binding domains

The outward-facing structure for ABCB8 was obtained by co-crystallisation with nucleotide. A clear unoccupied peak in the electron density was visible in the F_o-F_c and $2F_o$-F_c maps adjacent to the Walker A motif in all eight monomers of the asymmetric unit, indicating symmetrical nucleotide binding. Since the highest resolution data were obtained from co-crystallisation with ATPγS/Mg^{2+}, ATPγS was modelled into the electron density in the binding site. However, it was not possible to obtain a reasonable fit for the γ thiophosphate group of ATPγS while maintaining correct stereo-chemistry and avoiding clashes with the surrounding

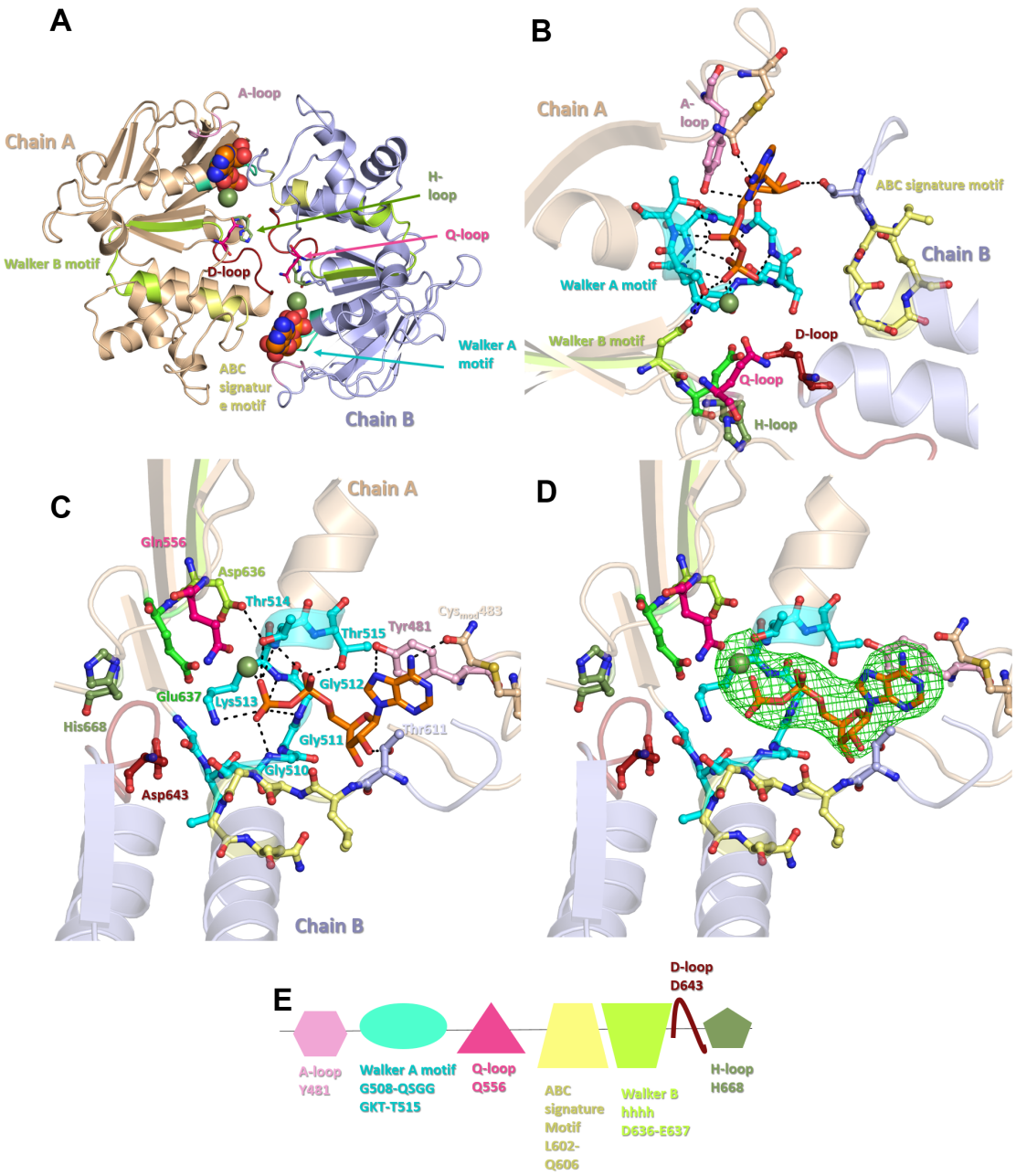


Figure 5.8 – The nucleotide-binding site in ABCB8 with bound ADP and Mg^{2+}. A) View from the membrane plane of dimerised NBDs with ADP and Mg^{2+} (both shown as spheres). B) ADP binding in ABCB8 presented in same orientation as for Sav1866, McjD and ABCB10 in Fig. 1.3. C) The ADP-bound state with residues involved in the binding site in stick representation. D) F_o-F_c omit map around ADP and Mg^{2+} at contour level 3σ presented as mesh. Conserved residues (C=coloured by motif) in the nucleotide binding site and ADP (C=orange) are presented as sticks (N=blue, O=red, S=yellow) with Mg^{2+} (dark green) as sphere.

atoms (Fig. 8.18). Instead ADP coordinating a Mg^{2+} ion fits well in the density of the F_o-F_c map (5.8D). Addition of ADP and Mg^{2+} to all eight NBDs of the asymmetric unit reduced the R_{free} factor from 0.271 to 0.268.

In fact, ATPγS purchased from Sigma is only to $\sim$ 75% pure. MS analyses indicated that the ATPγS sample used in co-crystallisation trials contained ADP besides ATPγS. ADP was been favoured in this crystal packing over ATPγS binding or ATPγS was already completely hydrolysed by the time of crystal formation. Indeed, it has been shown that, ATPγS can hydrolyse by itself and/or can be enzymatically degraded by ATPases as shown for other RecA-like proteins [Peck & Herschlag, 2003; Resetar & Chalovich, 1995].

The interactions between the ADP and chain A of the ABCB8 dimer are similar to those seen in other nucleotide-bound structures, except in the triphosphate binding region. The ADP molecule interacts mainly with the A-loop and the Walker A motif on chain A (Fig. 5.8A). The ADP adenine ring is coordinated by the A-loop in ABCB8 through π-π stacking with the sidechain of its Tyr481. However, Cys483, which is modified by the iodoacetamide treatment, forms an additional hydrogen bond through the amide group oxygen to the primary amine on the adenine ring (Fig. 5.8B/C). The ADP phosphates are coordinated by residues of the Walker A motif. The α phosphate group oxygens interact with the backbone amides of Thr514 and Thr515, as well as the latter's sidechain. The β phosphate group is held in place by hydrogen bonds between its oxygens and the backbone backbone of Gly510 and Gly511, and backbone and the sidechain hydroxyl of Thr514 of the Walker A motif. Thr514 is stabilised by Asp636 of the Walker B motif in the same chain, as also observed for McjD and Sav1866. These interactions are similar to those seen in many ABC transport/ATP analogue complexes. Differences in the interactions with chain A arise at the phosphate end of the nucleotide, where the third phosphate is lost.

In the ABCB8 ADP/Mg^{2+} bound state the Mg^{2+} ion interacts with the sidechain

carbonyl of Thr514 and one of the oxygens on the β phosphate group (Fig. 5.8B/C). The Mg^{2+} ion will be hydrated, although at this resolution the water oxygens are not resolved. These water molecules could provide interactions with Gln556 of the Q loop, Glu637 of the Walker B motif and Asp617 of the Walker B motif, all of which are too far away (>3.8 Å) to interact directly with the Mg^{2+} ion. In this structure the sidechain of His651 of the H-loop points away from the nucleotide. In contrast, in a triphosphate bound structure such as McjD (4PL0), the Mg^{2+} bridges oxygens on the β and γ phosphates and interacts directly with the glutamine from the Q-loop besides the interaction with the serine (equivalent of Thr514 in ABCB8) in the Walker A motif. In McjD the γ phosphate group oxygens interact with the glutamine of the Q loop, the glutamate of the Walker B motif and a serine from the Walker A motif, all on chain A.

The major change in the NBDs and their interactions with ADP compared to AMPPNP arises from a 5 Å movement of the ABC signature motif sequence strand on chain B across the surface of the nucleotide in chain A of ABCB8. This movement effectively disrupts all the interactions between the nucleotide on chain A and NBD of chain B (with similar changes occurring for the ADP bound to chain B in the second nucleotide binding site). The signature motif moves away from the ribose ring, losing all the stacking interactions and leaving only one potential interaction (3.4 Å long) between the backbone carbonyl of Thr617 and the one of the ribose carbonyls (Fig. 5.8B/C). This interaction is the only one still supporting dimerisation of the NBDs in a distance of 14 Å between the Walker A motif and ABC signature motif instead of 11 Å as observed for Sav1866 and McjD. There are no interactions between the phosphates or the Mg^{2+} ion that span the gap between the two NBDs in ABCB8. This contrasts markedly with the interactions formed by the γ phosphate group and Mg^{2+} of the trinucleotide bound state, where an extensive network of interactions stabilizes the inter-NBD interface. This includes i) a hydrogen bond between a γ phosphate group oxygen and the backbone amine of the glycine on the signature motif;, ii) an interaction between the sidechain of the

glutamine from the Q-loop and the carbonyl of a glycine from the signature motif;, iii) the side chain of the Walker A motif serine residue and the glycine backbone of the signature motif on the B chain and iv) the backbone of the Walker A motif serine in chain A with the aspartate of the D-loop of chain B. All these interactions are absent in ABCB8. In the absence of these interactions, the signature motif sequence is not tethered to the nucleotide, so it moves away from the nucleotide. This results in a substantial movement of the whole of the second NBD relative to the first NBD in ABCB8. In particular, the α-helical subdomain, of which the ABC signature motive is a part of, moves away from the RecA-like subdomain of the adjacent chain. These movements might relate to the movements into the outward-facing conformation of the TMDs, as described in the next section.

In this context it is worth comparing the ADP-bound outward-facing states of ABCB8 and Sav1866. In the ADP-bound Sav1866 structure, the interactions between the nucleotide and the protein are similar to those in an ATP analogue bound state, as is confirmed by the fact that it was possible to soak AMPPNP into the ADP-bound crystals. Unlike ABCB8, Sav1866 does not have a Mg^{2+} ion associated with the ADP molecule, despite the fact that Mg^{2+} was added to the crystallisation reservoir solution. In ABCB8 the Mg^{2+} ion is an integral part of the ADP/chain A interactions, forming bonds with several residues, that in the Sav1866 structure could be necessary for the correct formation of the interface with the chain B. In mitochondria at least, Mg^{2+} is present at approximately 2.5 mM, considerably above the concentration of ADP, and ADP is reported to be present mainly as a complex with Mg^{2+} [Gout *et al.,* 2014]. Therefore the complex with ADP/Mg^{2+} is more likely to be relevant to the physiological state, at least in mitochondria.

5.2.5 The coupling helices

The ADP-bound outward-facing structure of ABCB8 gives an insight into how the ATP hydrolysis in the NBDs is coupled to the conformational changes we observe in

the transmembrane domain. Crucial players for communication between the NBDs

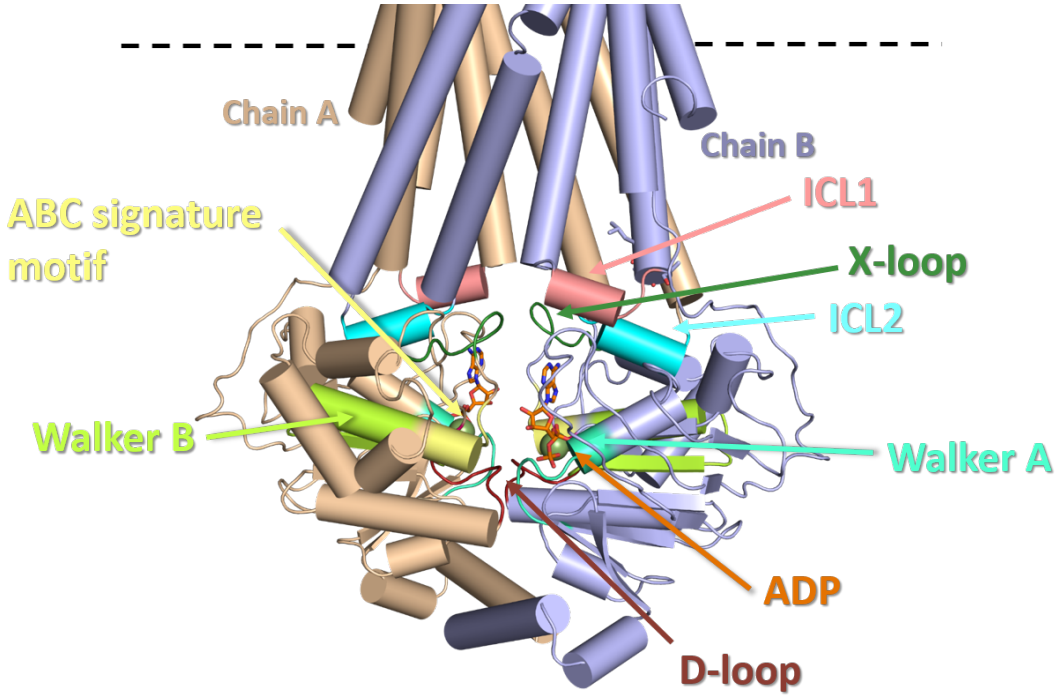


Figure 5.9 – Overview of NBDs and TMD interactions in the outward-facing state of ABCB8 with ICL1 (salmon), ICL2 (cyan), X-loop (dark green) and the conserved nucleotide binding motifs including the Walker A motif (dark cyan), ABC signature motif (yellow), Walker B motif (green) and D-loop (dark red). Chain A and B are coloured in beige and light blue, respectively. ADP presented in stick representation coloured according to element (C/P= orange N=blue and O=red) and Mg^{2+} (dark green) shown as a sphere. Dotted lines represent membrane boundaries.

and TMDs are the X-loops and ICLs. In the Sav1866 structures, the X-loops form short helices, which link the two NBDs with each other and with the TMDs. In contrast, in the ABCB8 structure they are significantly less structured and do not interact with each other, despite the NBDs being dimerised. In ABCB8 the lack of the X-loop interactions with themselves and the opposite transporter half leaves a gap in the core of the NBD-TMD interface (Fig. 5.9).

The coupling helices, ICL1 and ICL2, are an important structural feature in the ABC transporter conformation, providing a communication network between the two monomers and between the NBDs and TMDs. In ABCB8, ICL1 interacts with NBD residues of the same chain and ICL2 of the adjacent chain, whereas ICL2 only links to the NBD residues of the neighbouring chain. ADP binding in

ABCB8 is mainly facilitated by residues of the Walker A motif and the A-loop of one monomer. ADP is also indirectly linked to ICL1 via the modified Cys483, that interacts with both the adenosine ring and Asp244 in ICL1 (Fig. 5.10A).

The cysteine modification introduces an additional interaction in between the A-loop and ICL1. However this modification does not cause any noticeable changes in the positions of the other residues in the vicinity of Cys483, compared to the other nucleotide bound structures. In fact, the relative position of the A-loop and ICL1 seems to be independent of the conformational state, as analysed for the occluded McjD, outward-facing Sav1866 and inward-facing ABCB10 structures. It is therefore highly unlikely that this additional interaction distorts the structure of this conformation. It may however help to stabilize one of the conformations that the transporter adopts during the transport cycle.

It is possible that a similar interaction could be formed via a water network between the cysteine in the A-loop and the aspartate in ICL1 in the absence of the modification. Unfortunately, with the current resolution of the data, it is not possible to see individual water molecules. The cysteine and the aspartate residues are highly conserved in ABCB8 and the cysteine replaced by other polar residues in the B-family, so coordination via a water network is feasible. The significance of Cys483 in coordinating the nucleotide, as well as its role in forming an interaction between nucleotide binding site and ICL1 remains speculative. MD simulation might help to reveal whether the outward-facing state is stable after removal of this modification *in silico*.

ICL1 and ICL2 of adjacent chains are connected by the side chains of Asp244 (ICL1) and Arg342 (ICL2), as well as the backbone of Leu236 and Gln238 (both ICL1) and the side chain of Arg345 (ICL2) (Fig. 5.10A). The latter interaction can be found in ABCB10's inward-facing state, as well as in the outward-facing structures of Sav1866 and McjD, suggesting ICL1 and ICL2 of the two adjacent chains move together as a rigid body.

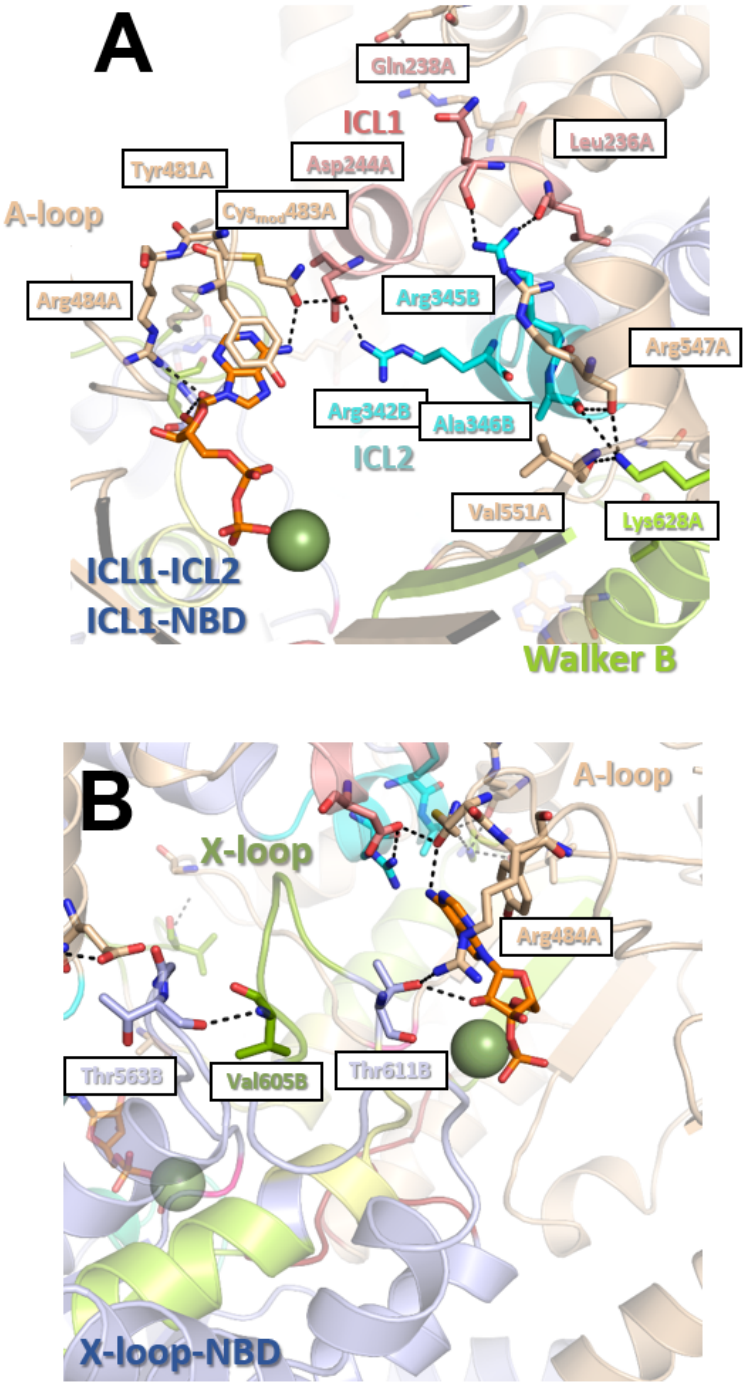


Figure 5.10 – Close-up view of the interactions between A) ICLs and NBDs, and B) the X-loop and the nucleotide binding site. Colouring scheme as used in previous figures (Fig. 5.9) with residues involved in interaction presented as sticks (C=structural feature, N=blue, O=red, S=yellow). ADP and (C/P= orange, N=blue and O=red) and Mg^{2+} (dark green) are shown as sticks and spheres, respectively. Hydrogen bonds are highlighted as black dashes.

The X-loop is highly conserved in mammalian ABC transporters of the B-family, as well as in some prokaryotic ABC transporters. In ABCB8 the X-loops do not form a tight helical structure that interlink the two transporter halves as observed for the outward-facing state in Sav1866 [Dawson & Locher, 2006] and occluded state of McjD [Choudhury *et al.*, 2014]. The higher degree of flexibility is reflected in the higher B-factors of the X-loops in ABCB8 (170 Å^2 for the X-loop motif in comparison to a B-factor of 142 Å^2 for the NBDs) However, the Val605 in the X-loop (TVVGERG) interacts with Thr563 upstream of the Q-loop, that are both located in the same α-helical subdomain. In addition, Thr611, between the X-loop and the ABC signature motif, interacts with Arg484 of the A-loop and the hydroxyl group of ADP's ribose ring, both in the adjacent chain. Consequently, a link between the X-loop and the nucleotide binding site is formed (Fig. 5.10B). These interactions restrain the X-loop movement and prevent the interaction of the X-loops with the ICL1s and the Q-loops of the adjacent chains that is observed in the Sav1866 structure (Fig. 1.7).

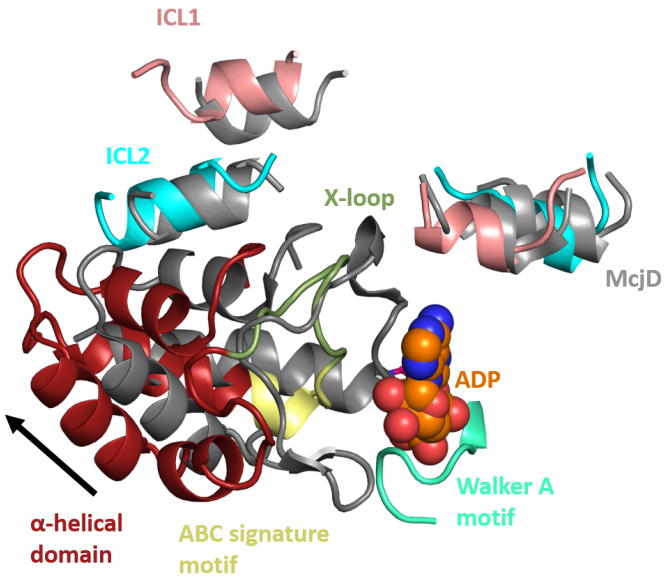


Figure 5.11 – Positions of the α-helical subdomain (red) and ICLs (pink and cyan) for the outward-facing state in ABCB8 in comparison to the outward-facing occluded state of McjD (grey;4PL0) Walker A motif coloured in green cyan, ABC signature motif in yellow and X-loops in dark green. ADP and (C/P= orange N=blue and O=red) and Mg^{2+} (dark green) are shown as sticks and spheres, respectively.

This could suggest that the X-loops could alternate between two conformations; one in which they interlock underneath the TMD and another one that has a less ordered state as in ABCB10's inward-facing structures. Tight interaction of the ABC signature motif with the nucleotide is likely to affect the position of the X-loop, as the they are both located in the α-helical subdomain. Upon nucleotide binding the ABC signature motif and with it the X-loops move into the transporter centre, where they interacts with the Q-loop and ICL1 of the other transporter half. The X-loop's glutamate, forming an interaction with the ICL1 in Sav1866, is conserved in the B-family (with the exception of ABCB11). Following ATP hydrolysis, the ABC signature motif disconnects from the binding site, pulling the X-loops away from the dimer interface. The outward-facing structure of ABCB8 seems to represent this intermediate state, in which the X-loops do not appear to interact with each other and the adjacent transporter half. The α-helical subdomain is shifted significantly away from the dimer interface in comparison to McjD , due to the lack of the interaction between a γ-phosphate and the ABC signature motif in ABCB8 (Fig. 5.11). Not only does that remove the X-loop interaction, but also causes a movement of ICL2 together with ICL1 away from the twofold-symmetry axis of the transporter. Consequently, the displacement of the ICLs with the α-helical subdomain translates into larger changes in the TMDs. (section 5.2.6). However, the X-loops in ABCB8 are still more restrained in their positions compared to ABCB10's inward-facing states, due to their links to the ADP of the adjacent chain via Thr611.

5.2.6 The transmembrane domains

Comparison of the outward-facing state in ABCB8 to the inward-facing state of ABCB10

In order to analyse potential conformational changes required in the alternating-access cycle of B-family ABC transporters, outward-facing ABCB8 is compared

to the nucleotide-free inward-facing state of ABCB10 (3ZDQ). The conformation of the TMDs is dependent on the position of the coupling helices and their interaction with the NBDs. Superimposing the monomers of ABCB8 and ABCB10 demonstrates that the relative position of ICL1 to the NBDs barely changes during the transition between the two states. Consequently, TMH2 and TMH3, which are connected via ICL1, only show rearrangements in the top half of the transporter. In particular TMH3 is straighter in the outward-facing state compared to the inward-facing conformation (Fig. 5.12A).

ICL2 is anchored to ICL1 of the adjacent chain and its NBD (Fig. 5.10B and C). Consequently, dimerisation of the NBDs translates the ICL2s inwards by about 13 Å towards the dimer axis, causing a displacement of TMH4 and TMH5 together in a swing-like movement (Fig. 5.12B). This movement of TMH4 and TMH5 together with TMH1-3 and TMH6 of the adjacent chain, closes the lower transporter half. In contrast to the conformational changes from the inward to the outward-facing occluded state in PglK [Perez *et al.,* 2015], we see a pronounced kink in TMH4 in addition to the rigid-body movement of TMH4 and TMH5. Furthermore, the top halves of TMH3 and TMH6 bend outwards to accommodate the movement of TMH4 and TMH5 (Fig. 5.12C). The top half of TMH1 is moving away from the transporter core (Fig. 5.12D).

Comparison of the outward-facing state of ABCB8 to the outward-facing state of Sav1866 and the occluded state of McjD

Since we observe an outward-facing state of ABCB8 with occluded transporter core, instead of a fully open outward-facing state as in Sav1866, it might be possible that local rearrangements within the helices take place subsequent to the rigid-body movement of TMH4 and TMH5 to enable occlusion of a substrate binding site. We have no structural evidence that there is a universal alternating-access mechanism for prokaryotic or eukaryotic type I ABC exporters. However, if the three structures

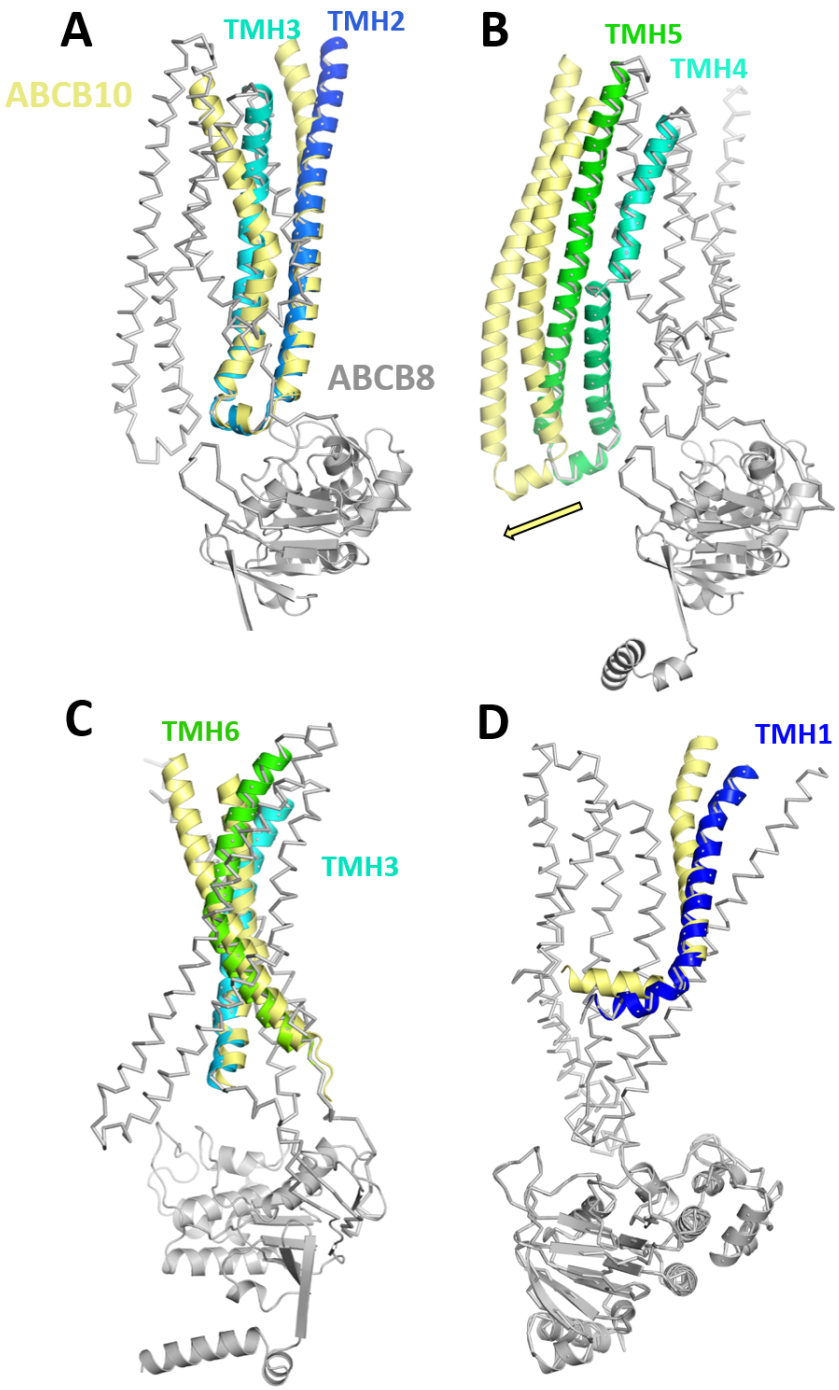


Figure 5.12 – Comparing TMH arrangements in the outward-facing state of ABCB8 with the inward-facing state of ABCB10 (3ZDQ) using aligned NBDs. Single chain of ABCB8 is shown as a ribbon (grey). Highlighted TM helices are presented as cartoon for ABCB8 (rainbow colouring by residue number, see Fig. 5.5) and for ABCB10 (pale yellow). Comparison of A) ICL1, TMH2 and TMH3 B) ICL2, TMH4 and TMH5 C) TMH3 and TMH6 D) ELB and TMH1

of McjD, Sav1866 and ABCB8 are treated as snapshots of different outward-facing states in the alternating-access mechanism, a sequence of conformational changes required to open and close the transporter on the extracellular/intermembrane side can be proposed (Fig. 5.13).

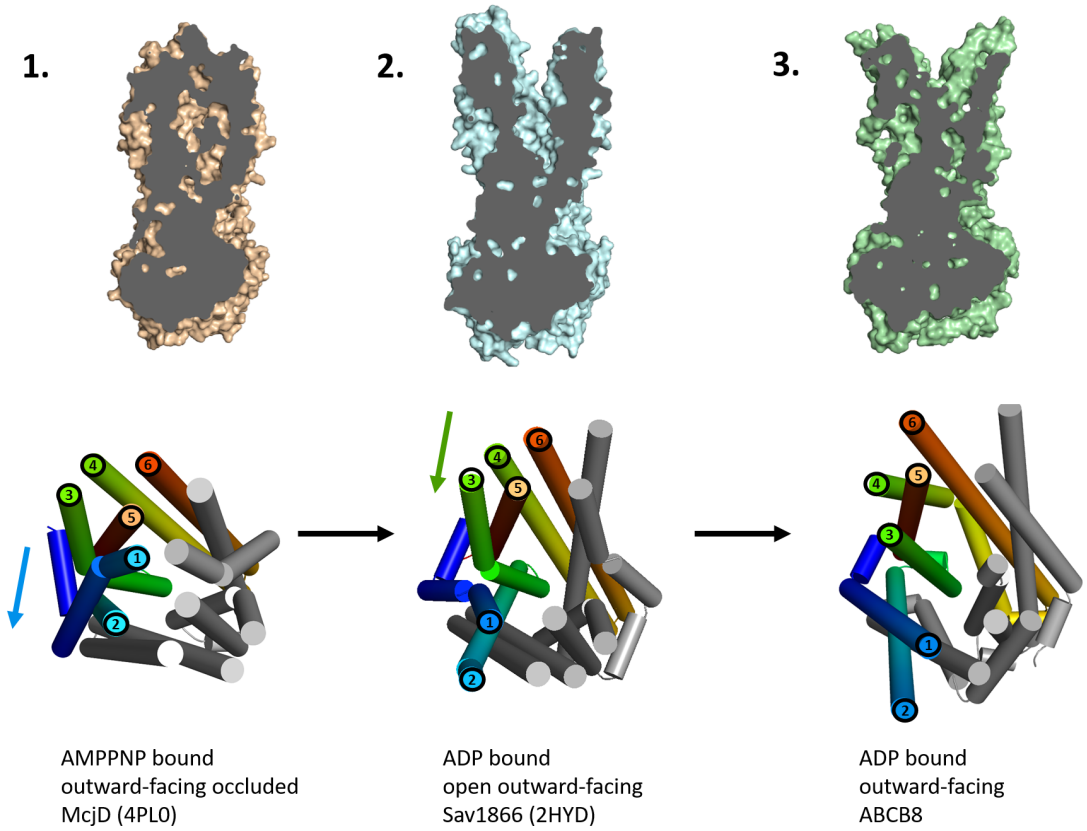


Figure 5.13 – Comparison of ABCB8 with the outward-facing states of Sav1866 and McjD. The top panel shows clipped surfaces of outward-facing states of McjD (4PL0; orange), Sav1866 (2HYD; blue) and ABCB8 (green). Bottom panel shows corresponding TM arrangement (1-3) looking down on the membrane from the extracellular/mitochondrial intermembrane space. Helices are displayed as cylinders with TMH1 and TMH2 in blue, TMH3 and TMH4 in green, TMH5 in orange and TMH6 in red. Blue and green arrows indicate movements of TMH1 and TMH2 away from the transporter centre (blue arrow) and movement of TMH3 and TMH4 towards the centre (green arrow), respectively.

In this mechanism, the outward-facing occluded state of McjD captures a conformation that can accommodate substrate in its binding site due to its large cavity (1). Subsequently, upon full opening of the transporter to the intermembrane space, as observed in the Sav1866 structure, the substrate can be released. In order to grant access to the transporter core, TMH1 and TMH2 have to move away from

the transporter core. In addition, TMH1 moves slightly down (2). Smaller rearrangements are also observed in TMH3 and TMH6, rotating along the outside of the transporter. Subsequently, TMH3 and TMH4 move in the transporter core to produce the occlusion observed in the outward-facing state of ABCB8, whereas this occlusion is mainly triggered by a kink of TMH4 in ABCB8 (3).

The rearrangements in TMH3 and TMH4 compared to the outward-facing state in Sav1866 are likely caused by weaker interactions between the two chains in the nucleotide binding site, as this translates to a movement of the α-helical subdomain and ICLs away from the transporter core.

TMH4 is kinked in the outward-facing state of ABCB8

As mentioned in the previous paragraph, a sharp kink half way through TMH4 with residues Gly313, Ser314 and Gly315 (as is Leu316 in chain A) unwound is observed in this novel outward-facing state (Fig. 5.14A). The question is whether this is specific to ABCB8 and other ABC exporters.

First, both Gly313 and Ser314 show a high degree of conservation among ABCB8 homologues (Fig. 5.14B), indicating this kink to be an important structural feature for operating the alternating-access cycle in ABCB8.

Although Gly313 is conserved in some B-family transporters (ABCB2, ABCB10, ABCB11 (first half)), it cannot be regarded as universal (Fig. 5.14C). However, glycine can be found near this region, creating a predetermined kinking point in TMH4 in these transporters. TMH4 in the inward-facing state of ABCB10, in which Gly313 is conserved, exhibits a slight kink as well. However, in ABCB8's TMH4, the bend is significantly greater, with a 10 ° kink in the outward-facing state (Fig. 5.14D). Interestingly, TMH4 runs straight in the outward-facing states observed in McjD and Sav1866 (Fig. 5.14D). Comparison of ABCB8 with other transporters show that TMH4 kinks 18 ° and 20 ° compared to TMH4 in Sav1866 and McjD, respectively. Sequence alignment with Sav1866, McjD and ABCB8

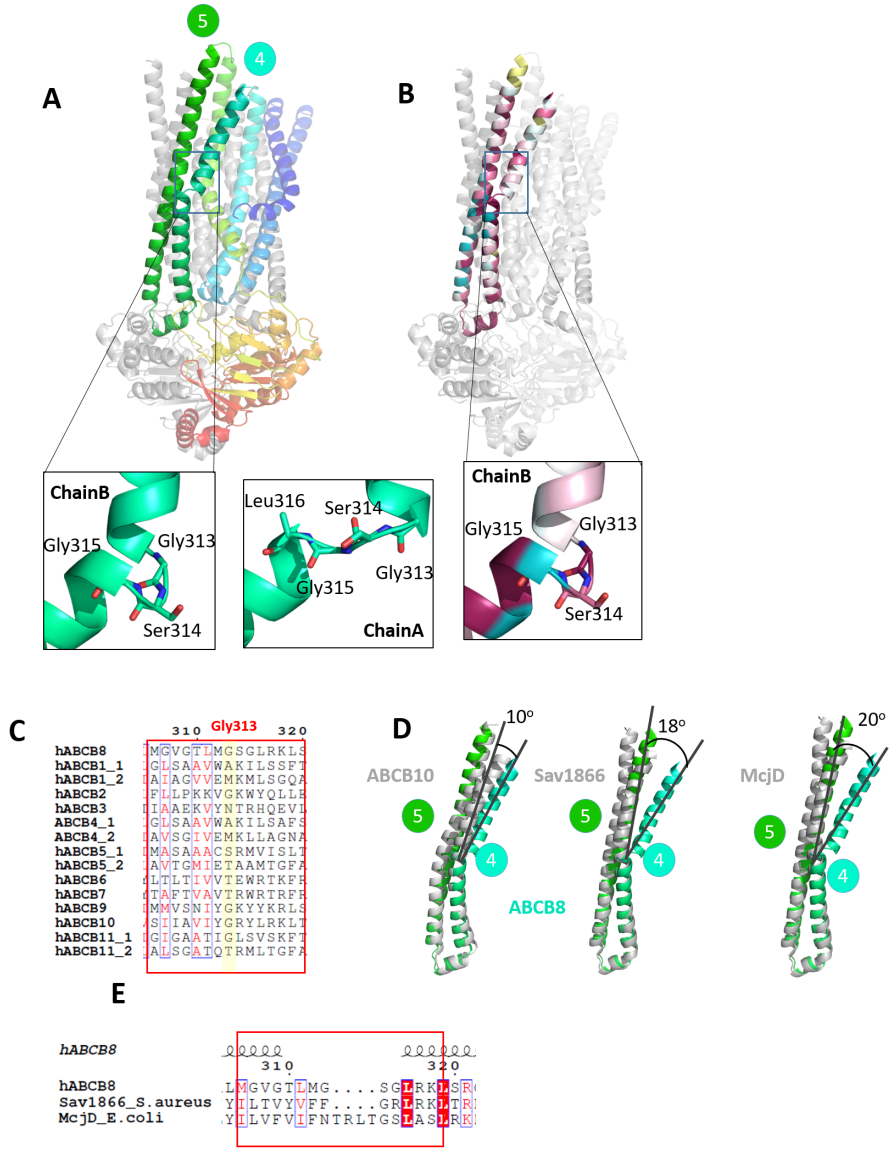


Figure 5.14 – TMH4 forms a kinked helix in ABCB8's outward-facing state. A) Close-up of kinked glycine-rich region in TMH4 for chain A and B with Gly313, Ser314 and Gly315 represented as sticks B) Cartoon representation in grey with TMH4 and TMH5 coloured according to conservation among 50 ABCB8 homologues. C) Sequence alignment of subfamily B with cut-out of sequence around kinked region in TMH4. D)Comparison of TMH4 (cyan) and TMH5 (green) in ABCB8 to ABCB10 (3ZDQ), Sav1866 (2HYD) and McjD (4PL0) (grey). E) Sequence alignment of ABCB8 with Sav1866 and McjD with cut-out of sequence around kinked region in TMH4.

reveal that both bacterial exporters have glycines close to the kinked region in ABCB8, granting potential kinking of the helix too (Fig. 5.14E). Although the exact position for the kink might be variable in the B-family and other type I ABC exporters, it could be a crucial structural feature, that adds extra flexibility to the rigid body movements of TMH4 and TMH5 allowing for local adjustments in the extracellular half of the TMDs during the alternating-access mechanism. Similar kinks have been observed in TMH3 and TMH6 in the inward-facing states of mouse P-glycoprotein (3G5U, 4KSB) [Aller *et al.,* 2009; Ward *et al.,* 2013].

5.2.7 The cholesteryl hemisuccinate binding site

A cleft on the surface above the elbow helix is visible in the outward-facing state of ABCB8, which is completely buried in the lipid bilayer, as predicted by PPM [Lomize *et al.,* 2012]. This cleft is lined by the upper halves of TMH4 and TMH1 and forms a tunnel between the dimer interface and the mitochondrial inter membrane space. After refinement of the main chains, a peak in both the $2F_oFc$ (1σ) and F_oFc (3σ) maps appeared in all eight chains above the elbow helix between TMH5 and TMH6, where a indentation is formed. CHS was modelled into this density, although only in chain B was the density sufficient to model the whole molecule. In the other chains the aromatic ring system was clear, but the hydrophobic tail was less resolved and it was modelled according to the density (Fig. 5.15A).

The binding pocket itself extents all the way through to the dimer interface, where it can be accessed via a small fenestration (Fig. 5.15B). CHS is mainly bound to residues of TMH5 and TMH6, as well as some above the kink in TMH4 and a small patch on TMH3 (Fig. 5.15D). The succinyl group of CHS is coordinated by hydrogen bonds to side chains of Ser382 and Asn383 in TMH5. The hydrophobic rings are packed in vdW interactions between mainly hydrophobic residues in TMH5 and TMH6. The hydrophobic tail is stabilised by vdW interactions provided by

residues of TMH3 and TMH6, as well as a tryptophan pointing upwards from the elbow helix (Fig. 5.15E).

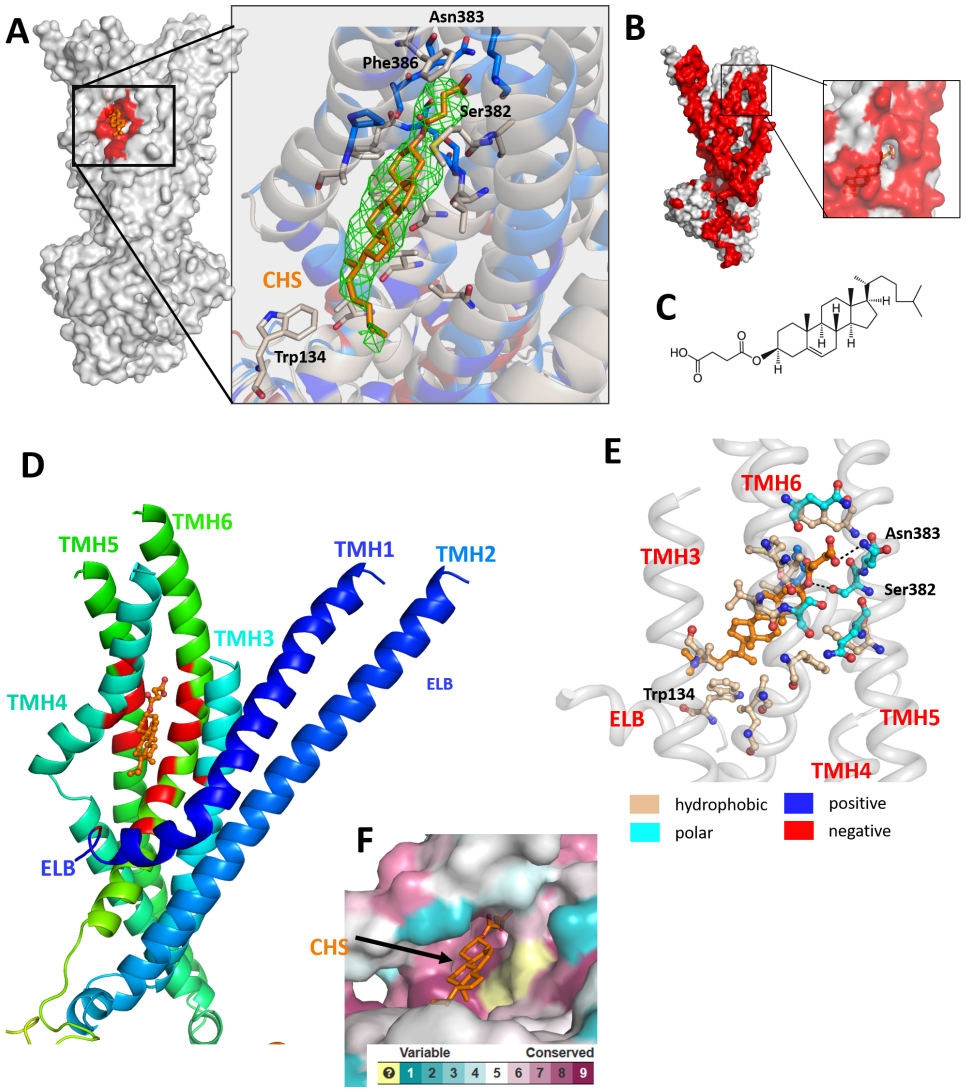


Figure 5.15 – CHS binding to ABCB8. A) Surface representation of ABCB8 dimer (grey) with residues in contact with CHS in red. Close-up of the binding site with F_o-F_c-map in green at a contour level of 3σ. Residues binding CHS are presented in sticks. B) Surface of protomer B with residues involved in the dimer interface in red and close-up of CHS bound in fenestration linked to dimer interface. C) Chemical structure of CHS. D) Cartoon presentation of chain B in rainbow colouring according to residue number with residues involved in the CHS interactions in red. E) Close-up of CHS binding site with CHS in stick presentation and residues involved in CHS binding presented as sticks with colouring according to residue type (see legend). F) Surface of CHS binding site coloured according to conservation among 50 ABCB8 homologues analysed with CONSURF. CHS is presented as sticks coloured according to elements (C=orange, N=blue, O=red).

Residues around the CHS binding site show a high degree of conservation between ABCB8 homologues (Fig. 5.15F), in contrast to a lack of conservation within the

B-family, suggesting a role for this binding site in the function of ABCB8, but not in other ABCB transporters. However, cholesterol amounts are low in the inner mitochondrial membrane (Table 1.2), which suggests that cholesterol itself might not be the substrate for ABCB8. Nevertheless, CHS was crucial for stability of ABCB8 in detergent during the purification procedure even if substituted by other lipids (section 3.2.3, Fig. 3.10). Although protein purified in the presence of CHS showed a high degree of ATPase activity (3.2.6), CHS had an inhibitory effect if present during the reconstitution into a POPC/POPE/CDL lipid mixture. These observations support the hypothesis that CHS plays a role in overall stability of the ABCB8 fold or perhaps even a particular conformation. It is also possible that CHS is binding in the substrate binding pocket for the ABCB8 transport substrate, if some at least of the ABCB8 substrates are lipids, or other hydrophobic molecules, which might reside within the membrane and enter via a fenestration such as the one seen in ABCB8. Interestingly, this binding site is not entirely formed in the inward-facing state, as evident from the ABCB8 homology model (modelled on the basis of ABCB10 (4AYX)). However, part of the binding site exists as a surface that faces the hydrophobic interior of the lipid bilayer in the inward-facing state. Conversion from the inward to the occluded or outward-facing state could capture a lipid or hydrophobic molecule bound on the surface of the binding site, before it gets released onto the other side of the membrane (Fig. 5.16).

Since a physiological role of CHS in this binding site can probably be discounted due to ABCB8's subcellular localisation, it remains unclear what the function of this highly conserved binding site is and whether instead another lipids can bound or even flipped under physiological conditions.

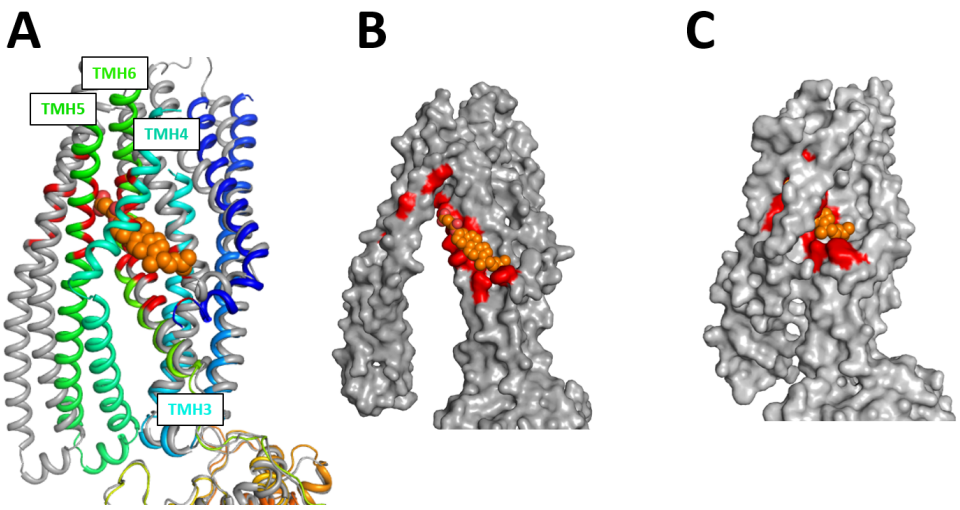


Figure 5.16 – CHS binding to the outward-facing state of ABCB8 in comparison to the homology model of the inward-facing state. A) Aligned transporter halves of the crystal structure (green/blue shades) in the outward-facing state and the homology model in the inward-facing state (grey) both represented as cartoons. B)/C) Surface representation of ABCB8 monomers of the inward-facing homology model (B) and the outward-facing crystal structure (B). Resides involved in CHS coordination are highlighted in red and CHS is shown as orange sticks.

5.2.8 Additional structures of ABCB8 in outward-facing states obtained without nucleotide and with ADP

In addition to co-crystallisation with the ATPγS/ADP/Mg^{2+} mixture, data were collected and molecular replacement solutions were obtained for crystals grown by co-crystallisation with Mg^{2+}/ADP (dataset d015) and in the absence of any added nucleotide (dataset d016). The data obtained from both crystals were highly anisotropic, diffracting to 3.83 Å (3.58x 5.57x 4.35 Å) and 4.35 Å (4.35x6.67x4.53 Å) for the ADP-bound and nucleotide-free form, respectively. Preliminary refinement of these structures was performed in order to compare the overall conformation (Table 5.4). A poly alanine model obtained from dataset d016 was only rigid body refined and further refinement has to be performed to optimise the model.

ADP-co-crystals in the presence of Mg^{2+} grew in the same $P12_11$ space group as the ones obtained with ATPγS/ADP/Mg^{2+} (crystal form 2; unit cell dimensions: a=183.5 Å,b=99.5 Å,c=214.5 Å, α=γ=90.00°, β= 90.37°. Dataset d015 was phased using PHASER-MR [Winn *et al.,* 2011; McCoy *et al.,* 2007; McCoy

Table 5.4 – Data processing and refinement statistics for dataset d015 and d016. * indicates statistical evaluation after STARANISO processing of the data. d016 was refined as a poly-alanine model

Dataset number	**d015**	**d015***	**d016**	**d016***
Dataset type	native		native	
Nucleotide	ADP		none	
Data collection:				
Space group	$P12_11$		$P12_11$	
Cell dimensions				
a, b, c (Å)	183.5, 99.5, 214.5		185.8, 109.4, 209.4	
α, β, γ (^{o})	90.00, 90.37, 90.00		90.00, 90.16, 90.00	
Resolution (Å)	72.94-3.83 (4.45 x 5.57 x 3.58)	72.94-3.70	75.63-4.35 (4.53 x 6.67 x 4.20)	72.94-4.25
Rmerge	0.171 (11.500)	0.089(1.257)	0.191 (3.934)	0.144(1.663)
Rmeas	0.185 (12.640)	0.097(1.365)	0.206 (4.205)	0.156(1.801)
I/σ	6.5 (0.2)	11.6(1.6)	6.3 (0.5)	9.1(1.2)
CC(1/2)	0.999 (0.004)	0.999(0.55)	0.998 (0.291)	0.99(0.551)
Wilson B-factor	140.73		140.61	
Completeness	99.2	55.6	99.9	67.9
Multiplicity	6.8	6.7	6.8	6.6
Refinement:	d015		d016 (rigid body refinement)	
Resolution	3.8 (72.9-3.7)		4.4 (75.4-4.2)	
No. of reflections	56772		39703	
Rwork/free (%)	24.25/26.32		36.61/38.86	
No. of atoms	30741		22016	
Data-to-parameter ratio	1.9		1.8	
Mean B-factor (Å^2)	164.4		161.1	
Rmsd				
Bond lengths (Å)	0.008		0.007	
Bond angles (^{o})	0.93		1	

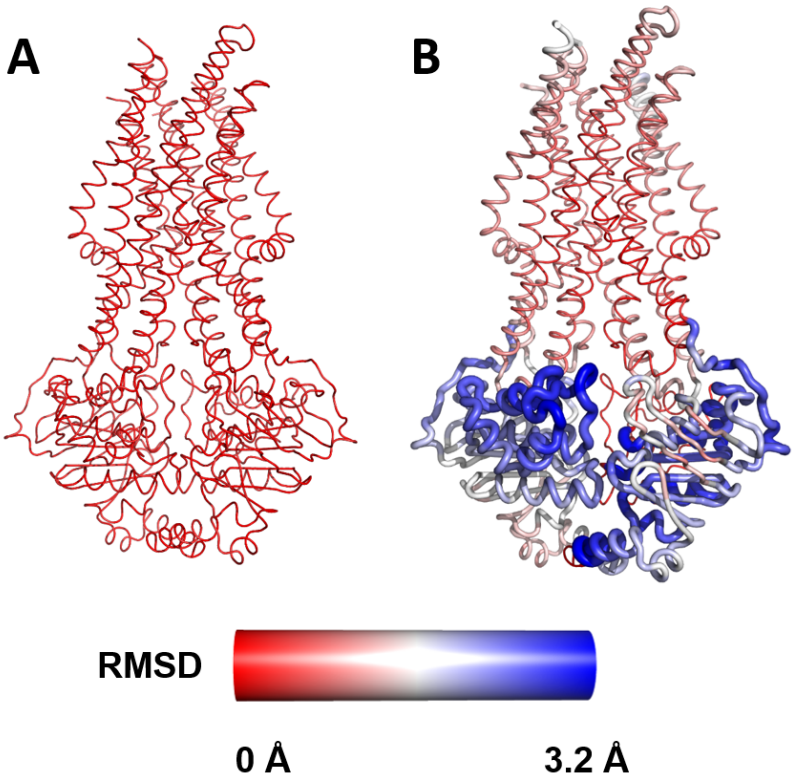


Figure 5.17 – Structure of ABCB8 obtained from co-crystallisation with ATPγS/ADP/Mg^{2+} in comparison with A) an ADP/Mg^{2+} co-crystallised and B) nucleotide-free structure. These structures were aligned by their TMDs excluding the coupling helices using COOT's LSQ algorithm [Emsley *et al.*, 2010]. Structures are presented as cartoons with cartoon width and colouring reflecting RMSD values from C_α alignment. Low RMSD values correlate with thin cartoon traces and red colouring, whereas high RMSD values are presented with thicker cartoon width in blue.

et al., 2007] with a dimer of the previously described outward-facing structure of ABCB8 (obtained from dataset d003 and d014) as a starting model. The resulting model was rigid body refined using REFMAC [Murshudov *et al.,* 2011; Winn *et al.,* 2011; Nicholls *et al.,* 2012], by using TMDs and NBDs as individual rigid bodies. Only first refinement rounds were run using BUSTER [Bricogne *et al.,* 2015] (R_{free}/R_{work}=0.283/0.271) and the building of this model is in process. We obtained a preliminary model that is very similar to the outward-facing structure previously obtained for ABCB8 with a low overall RMSD value for the C_α trace of 0.24 Å (Fig. 5.17A). Peaks in the $2F_o$-F_c map and the omit map in the nucleotide binding site give strong evidence for ADP and Mg^{2+} binding identically to the coordination in the model obtained from ATPγS/ADP/Mg^{2+} co-crystals (Fig. 5.18).

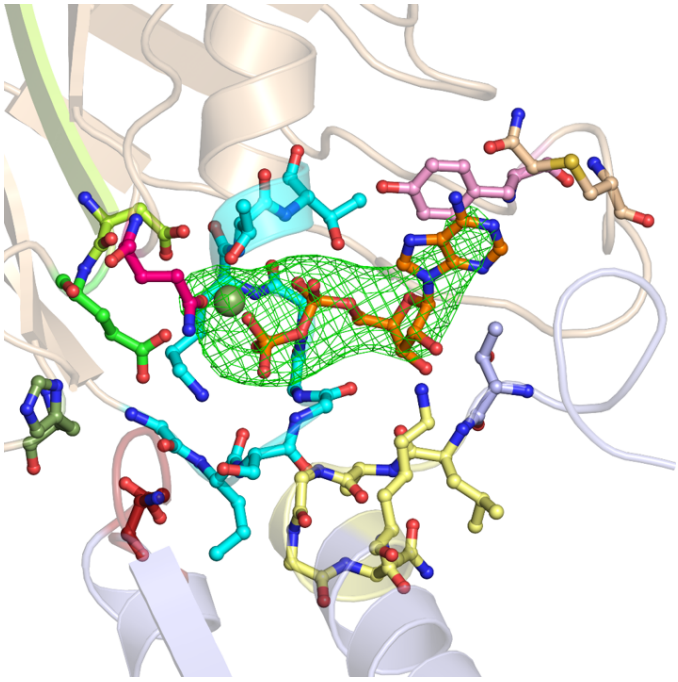


Figure 5.18 – Close up of ADP binding in the ABCB8 structure obtained form co-crystallisation with ADP. Residues of conserved binding motifs (C=motif colour, N=blue, O=red, S=yellow) and ADP (C/P=orange, N=blue, O=red, S=yellow) are presented as stick and Mg^{2+} (dark green) sphere. F_o-F_c map shown in green (map was doubled in Pymol) at contour level 3σ.

The fact that the same crystal form could be obtained by pre-incubation with the ATPγS/ADP/Mg^{2+} mixture and with ADP/Mg^{2+} alone, both resulting in the same conformation, supports the observation of an ADP-bound state, which

is formed despite co-crystallisation with a mixture of ATPγS and ADP. Hence, it is suggested that rather than ATPγS hydrolysis being required to trap this ADP-bound state, it is more likely that the ADP impurity in the ATPγS stock or its non-enzymatic degradation into ADP was sufficient to obtain an ADP-bound outward-facing conformation. Therefore, the ADP-bound state that I observe in both the ADP/Mg^{2+} and ATPγS/ADP/Mg^{2+} grown crystals, does not require a previous state in which a triphosphate nucleotide was bound, it can apparently form simply by binding of ADP/Mg^{2+} to ABCB8. As shown in the previous chapter, crosslinking experiments suggest that when ABCB8 is combined with ADP/Mg^{2+}, it adopts more than one conformation for iodoacetamide treated protein, with approximately a 60:40 ratio of states. It is likely that in solution there are a range of conformations and the ADP-bound state was the one that was able to form crystals, hence the conformation observed in these crystal structures.

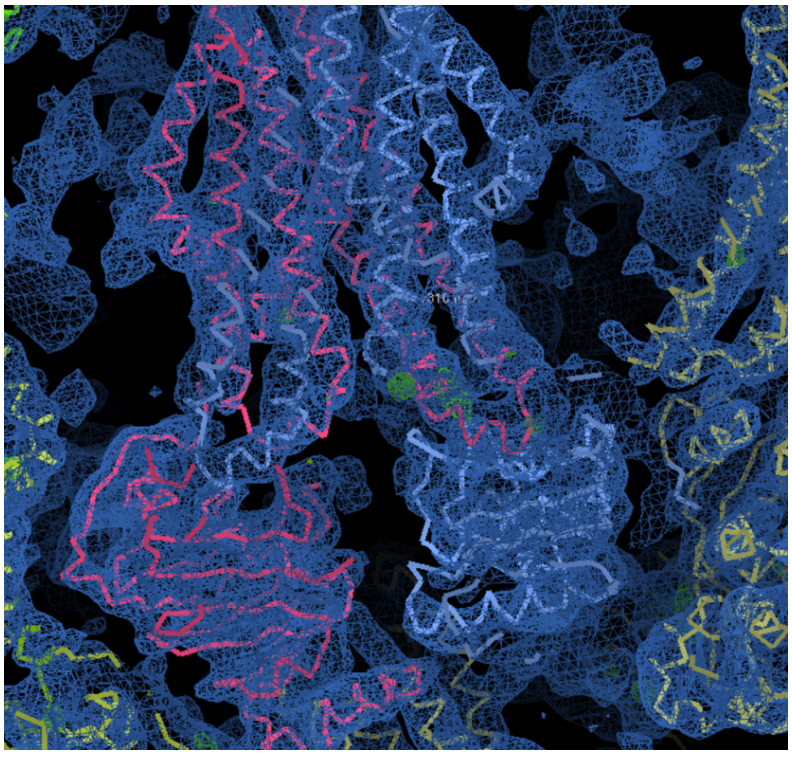


Figure 5.19 – Separation of NBDs in the nucleotide-free outward-facing state of ABCB8. Model as presented as C_α trace with $2F_o$-F_c map (blue) and F_o-F_c map (green) generated from d016 after MR and rigid body refinement using REMAC [Murshudov *et al.,* 2011; Winn *et al.,* 2011; Nicholls *et al.,* 2012].

Crystals obtained in the absence of nucleotide were also found in an $P12_11$ space

group, but in a unit cell (a=185.8 Å,b=109.3 Å,c=209.4 Å, α=γ=90.00°, β= 90.16°; crystal form 2*) that was expanded by $\sim$ 9 % in volume compared to the ATPγS/ADP/Mg^{2+} or ADP/Mg^{2+} co-crystal form, indicating a change in crystal packing (Table 8.2). Dataset d016 could be phased using MR with a full dimer of the outward-facing ABCB8 model, as well as a structural monomer of this model. Interestingly, phasing the data from the nucleotide-free form with the structural monomer gave an output model with the nucleotide binding domains slightly separated. When the MR solution obtained from the full outward-facing dimer (with NBDs dimerised) was refined in rigid body refinement using REFMAC [Murshudov *et al.,* 2011; Winn *et al.,* 2011; Nicholls *et al.,* 2012] with TMDs and NBDs as individual rigid bodies, a separation of the NBDs similar to the structural monomer MR result was observed. In addition, MR was run with just a TMD dimer excluding the coupling helices and NBDs in order to obtain unbiased electron density maps for the position of the NBDs. The resulting electron density map was consistent with a rigid-body refined model containing separated NBDs (Fig. 5.19). In fact, the distance between Gly511 in the Walker A motif of chain A and Gly614 in the ABC signature motif of chain B is $\sim$ 3 Å wider compared to the ADP/Mg^{2+} bound ABCB8 structures (Fig. 5.20).

Despite the 3 Å separation of the NBDs in the nucleotide-free form of ABCB8, the TMDs adopt an outward-facing conformation that is almost identical to the ADP-bound form (Fig. 5.17B). This is also reflected in a considerably higher overall RMSD (of C_αs) for the alignment with the ADP-bound form of 2.97 Å. Since the NBDs have been shown to dimerise over interactions facilitated by the nucleotide, that is sandwiched between the two chains, it is unsurprising that in the nucleotide-free form in the absence of this "glue" the NBDs are separated. However, it is unusual to find the TMDs in an outward-facing conformation in the absence of nucleotide, since their conformation is predicted to only exist in a nucleotide bound form. At an overall resolution of 4.35 Å for the data obtained from the nucleotide-free crystals and with only rigid-body refinement performed so

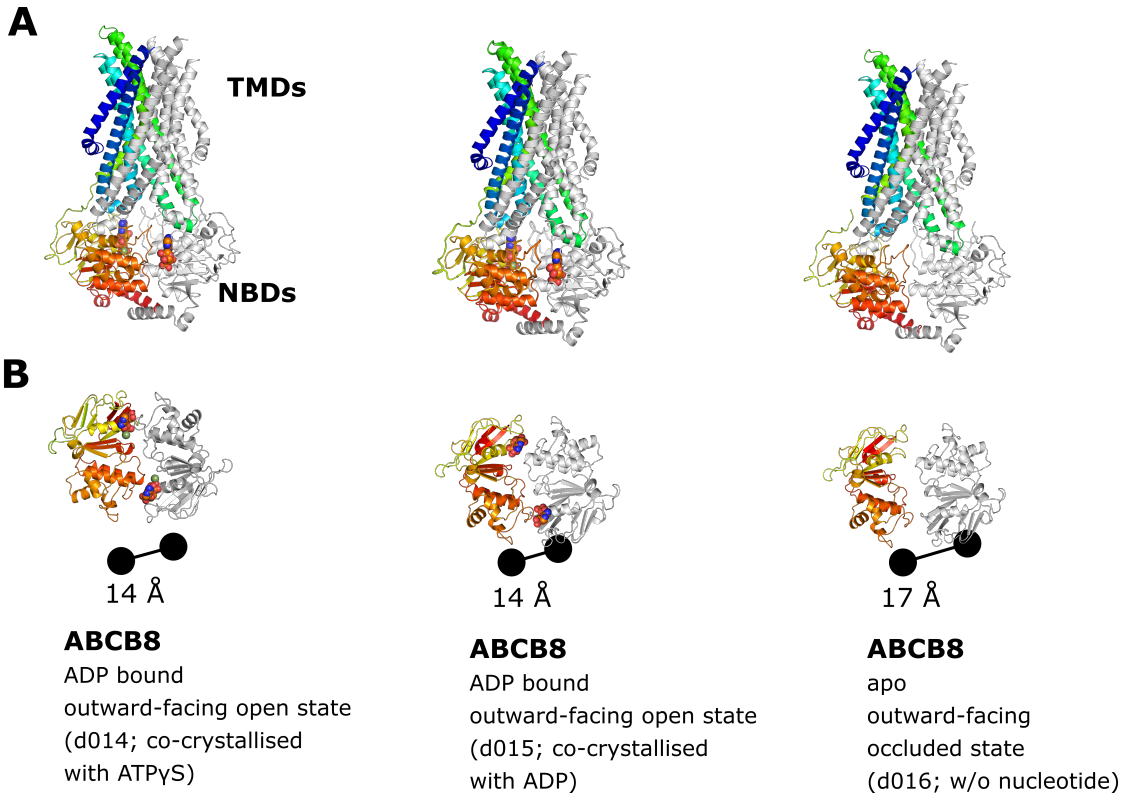


Figure 5.20 – Overview of ABCB8 structures solved in co-crystallisation with ATPγ/ADP/Mg^{2+}, ADP/Mg^{2+} and as a nucleotide-free form. A) Overall structure presented perpendicular to the membrane plane as cartoon with chain A coloured in grey and chain B rainbow coloured according to residue number. B) View of NBDs from the membrane plane. ADP (coloured according to elements: C/P=orange, N=blue, O=red) and Mg^{2+} (dark green) are presented as spheres. Lines and labelled distances describe measured C_α-C_α distance between first glycine (Gly614) of the ABC signature motif in chain A and the last conserved glycine (Gly511) in the Walker A motif of chain B.

far, we cannot say whether slight differences to the ADP/Mg^{2+} bound form exist. It possible that the state, which was trapped in this case is an intermediate form, between the state, in which ADP remained bond after ATP-hydrolysis, and one, in which the TMDs start to separate.

5.3 Conclusion

A 3.8 Å crystal structure of ABCB8 was solved in an outward-facing state, in which the NBDs of ABCB8 are still in contact with an ADP molecule sandwiched between the two chains. However, the NBDs are not as tightly packed as in the outward-facing Sav1866 or occluded McjD structures, suggesting, that in this crystal structure an intermediate state was captured. This ABCB8 structure reflects a state after ATP-hydrolysis, but prior to ADP release and consequently full separation of the NBDs. These changes are also evident in the TMDs, that show an outward-facing state, in which the TMD core is occluded leaving no space for substrate binding in the transporter core. This structure could be obtained in co-crystallisation with ATPγS or ADP at similar resolution. In addition, a nucleotide-free outward-facing state at 4.3 Åresolution was solved. In this structure, the NBDs are fully separated, whereas the TMDs remained in an outward-facing state.

CHAPTER 6

Discussion

6.1 Purification and crystallisation of ABCB8

As described in chapter 3, a purification protocol could be established and optimised for ABCB8 by rigorous screening of buffer conditions, detergents and constructs. Purified ABCB8 was active in detergent as shown by basal ATPase activity. Initial crystals of ABCB8 diffracted to 7 Å. Chemical modification of cysteine residues in ABCB8 increased protein stability during purification and made it possible to obtain protein crystals of sufficient quality so that a structure of human ABCB8 could be solved.

When a homology model of ABCB8 was prepared, it became clear that most of the 13 cysteines in our human ABCB8 construct are exposed on the surface. Modification of the cysteines with iodoacetamide changed the properties of the protein, so that crystals could be grown with diffraction beyond 4 Å, allowing the first structure of human ABCB8 to be solved. This structure was solved from co-crystals

with an ATPγS/ADP mix. Interestingly, decreasing the extent of modification by lowering the modification time improved the resolution further to overall 3.8 Å. Subsequently, datasets were obtained from co-crystallisation with ADP alone and in the absence of nucleotide.

Although modification of these cysteines did not change the overall thermal stability of the protein, it prevented precipitation of ABCB8 when concentrated for crystallisation attempts. In addition, once the structure had been solved, it became clear that three of the cysteines (Cys283, Cys461, Cys478) on the surface were involved in crystal contacts between the ABCB8 dimers. Although only modification for Cys478 and not Cys283 or Cys461 were confirmed with MS/MS, it seems probable, that modification could have facilitated packing of the molecules in this $P12_11$ space group.

6.2 Cardiolipin stimulates the basal ATPase activity of ABCB8 in proteoliposomes

The experiments in chapter 4 suggest that CDL helps to stabilise the protein during reconstitution and stimulates ATPase activity. This observation is not surprising, as ABCB8 is located in the inner mitochondrial membrane, where CDL makes up approximately 18% of all phospholipids [Horvath & Daum, 2013]. POPG, which is structurally related to CDL, has a light stimulating effect on ATPase activity. Stimulation of ATPase activity over basal activity by a transport substrate was shown in several studies e.g. for stimulation of ABCB1 with verapamil, trifluoperazine and cholchizine [Sharom *et al.,* 1995], of ABCB9 with peptide [Chen *et al.,* 2003; Zollmann *et al.,* 2015] and of Atm1 for thiol compounds [Kuhnke *et al.,* 2006]. It therefore raises the question, whether cardiolipin could be a potential substrate of ABCB8, that is transported from one membrane leaflet to the other. Indeed, ABC transporters like ABCA1 have been proven to function as so-called

lipid flippases, as reviewed in Tarling *et al.* [2013]. ABC transporters, such as the bacterial MsbA and PglK [Perez *et al.,* 2015; Mi *et al.,* 2017], as well as the eukaryotic ABCA4 [Weng *et al.,* 1999], have previously been shown to flip lipids between leaflets of the membrane. This process is essential for maintaining the asymmetry of biological membranes and crucial to lipid synthesis pathways distributed over two compartments.

Notably, defects in cardiolipin metabolism result in cardiomyopathy that has some similarity to the effect seen in ABCB8$^{-/-}$ mice [Beranek *et al.,* 2009; Xu *et al.,* 2006]. Not only is the inner mitochondrial membrane distorted, but there are also defects in Fe-S cluster metabolism and accumulation of iron ions within the mitochondria. In the last step of the CDL synthesis, CDL has to be flipped from the inner to the outer leaflet after it is formed, to complete processing of the aliphatic chains [Tamura *et al.,* 2014]. Defects in CDL flipping could potentially affect general mitochondrial function and consequently impair a large number of mitochondrial processes including Fe-S cluster related enzymes and respiration, leading to oxidative stress. We could hypothesise that CDL could be a transport substrate for ABCB8 and that ABCB8 is in fact a CDL flippase. Interestingly, CHS reduces the ATPase activity in the presence of CDL and in the crystal structure it was observed that CHS bound to a conserved pocket on the outer surface of ABCB8. on the basis of that it is tempting to speculate that CDL is flipped by ABCB8.

Alternatively, CDL could stimulate ATPase activity of ABCB8 by stabilising the secondary and tertiary structure and subsequently keeping more protein folded during the reconstitution and assay conditions. Indeed, lipids can play an important role in influencing the structure of a membrane protein by specific binding to the surface, as seen for negatively charged lipids that form an annular belt around the TmrAB structure and also affect ATPase activity [Bechara *et al.,* 2015].

Surprisingly, reconstitution in the presence of an excess of CHS (0.9 mM) reduces

ATPase activity more than three-fold (Fig. 8.14). CHS potentially competes with CDL for specific binding to ABCB8, that has been demonstrated to be required for ATPase activity in proteoliposomes. In detergent cardiolipin binding is not needed for function, so that occupation of the binding site does not inhibit ABCB8's activity. We found a CHS molecule wedged between TMH4, 5 and 6 in the TMDs (section 5.2.7) that supports this hypothesis. Since cholesterol levels are negligible in the inner mitochondrial membrane (total sterol <0.01 mg/mg protein), inhibition of ATPase activity by CHS probably has no physiological relevance.

6.3 Effects of ATP analogue binding on ABCB8

In chapter 4.4.1 the effects of different ATP analogues and ADP on conformational dynamics of ABCB8 were described. One of the main unanswered question in the field is, whether conformational changes for transition into the outward-facing state are triggered by ATP binding itself or require subsequent ATP hydrolysis. Furthermore, the existence of basal ATPase activity in the absence of transport substrate raises the question, if substrate binding to the transporter is necessary for it to undergo the complete transport cycle or whether the binding and hydrolysis of ATP alone is sufficient. One always has to keep in mind with these questions, that ABC exporters might differ in their coupling mechanisms depending on the chemical nature of the substrate, as well as their lipid environment. ABC transporters studied in detergents might not have the same strict coupling mechanism between ATP binding, substrate binding and ATP hydrolysis, as the same transporters in their native environment in a cell.

In general all four methods used to characterise the effect of nucleotide binding, gave consistent trends for the differences observed between the nucleotides and between unmodified and iodoacetamide treated protein. In particular, ATPγS, ATP+V_i

and AMPPNP binding to unmodified WT ABCB8 and ATP binding to ABCB8 E637Q showed the greatest effect, as indicated by shifts in thermal stability of $\geq$ 10 °C, binding constants of <70 μM and decreased intermolecular crosslinking of the homodimer with DSS to less than 30%. It is evident from these experiments that ATP or ATP analogues and transition states trigger conformational changes, that result in a conformation with increased rigidity. The increase in rigidity is likely to be caused by dimerisation of the NBDs that give rise to a positive shift in thermal stability and change of environment of the fluorophore in the MST experiment. Furthermore, lysine crosslinking studies might suggest that dimerisation of the NBDs translates into conformational changes of the TMDs into an outward-facing state, which might allow crosslinking of the top half of the transporter. This particular conformation with dimerised NBDs and TMDs in an outward-facing state was observed in the ABCB8 crystal structure (chapter 5). Whereas ABC transporters have high flexibility in the nucleotide-free state as observed in PELDOR studies on LmrA and MsbA that show broad distance distributions, ATP and ATP analogues binding results in shorter more defined distances that correspond to NBD dimerisation and transition into an outward-facing states [Verhalen *et al.,* 2017; Hellmich *et al.,* 2012; Borbat *et al.,* 2007; Mishra *et al.,* 2014]. Furthermore, crystal structures of the ATPγS bound bacterial polypeptide processing and secreting system PCAT, as well as AMPPNP or ADP+V_i bound antimicrobial ABC transporter McjD adapt an occluded TMD conformation with sandwiched NBDs, suggesting that at least in these cases ATP analogues and ATP transition state analogues can trigger NBD dimerisation followed by conformational changes in the TMDs [Lin *et al.,* 2015; Choudhury *et al.,* 2014; Bountra *et al.,* 2017]. However it is worth noting that the closely related ABCB10 can bind nucleotides without adopting an outward-facing or an occluded state with the NBDs together, so it is not always the case that nucleotide binding automatically induces a state with the NBDs dimerised, at least for protein in detergent [Shintre *et al.,* 2013].

6.4 Interaction of ADP with ABCB8

As described in chapter 4, it was observed that ADP increased thermal stability and bound to ABCB8 with reasonable affinity. However, higher concentrations of ADP were required compared to ATPγS or AMPPNP for unmodified ABCB8. Whether ADP binding also triggers dimerisation of the NBDs, is not deducible from these functional experiments. However, dimerisation of the NBDs in the outward-facing state was observed in the ADP-bound ABCB8 crystal structure, whereas the nucleotide-free form gives evidence of separation of the NBDs. The ability of the hydrolysis product ADP to dimerise the NBDs was also suggested by the ADP-bound outward-facing structure of Sav1866 or the ADP+V_i bound open outward-facing MsbA structure. Moreover, EPR studies on MsbA and LmrA give evidence that the outward-facing state can be formed in the presence of ADP [Dawson & Locher, 2006; Ward *et al.,* 2007b; Hellmich *et al.,* 2012; Borbat *et al.,* 2007; Mishra *et al.,* 2014]. NBD dimerisation upon ADP binding as demonstrated in the ABCB8 crystal structures, but also in the literature seems somehow surprising, as it contradicts the idea that only ATP can cause dimerisation and that following ATP hydrolysis, ADP is released due to its lower affinity for the nucleotide binding site. A process that subsequently separates the NBDs and converts the transporter into an inward-facing state. *In vitro* experiments described here are performed under excess of ADP, whereas under physiological conditions with an ATP/ADP ratio of 2-5 more ATP than ADP, ADP bound to the NBDs after hydrolysis is likely to be replaced by ATP [Tantama *et al.,* 2013; Gout *et al.,* 2014]. If the energy levels of cells are low and ADP concentrations increase, ABC transporters may underlie product inhibition with ADP. ADP binding will trap the transporter in an occluded or outward-facing state, that does not allow further ATP hydrolysis. This explains inhibition of ABCB8's ATPase activity in the presence of ADP, as demonstrated in chapter 4. However, it has to be noted that fivefold more ADP over ATP had to be provided in this experiment to have full inhibition. Another explanation for the

phenomenon of ADP binding to ABC transporters might be given by the adenylase function for bacterial ABC exporters, which was proposed by Kaur *et al.* [2016] for TmrAB, LmrA and MsbA by ^{31}P-MAS NMR. It predicts that two ADP molecules can be converted into one ATP and one AMP molecule. In this mechanism ADP has to remain bound and a second ADP has to bind in an addition binding site in the NBD interface, so that the orthophosphate can be transferred. Although it remains unclear, whether this mechanism is part of eukaryotic ABC exporters and in particular an ABCB8 function, it might give an alternative explanation for why not only ATP but also ADP binds to ABCB8.

ADP binding did not have any cooperativity, reflected in a Hill coefficient of 1.2±0.1 compared to 1.9±0.1 for AMPPNP. The aspartate in the D-loop, which interacts with the Walker A motif of the adjacent chain, and the seven residues downstream located glutamate (Walker B motif), that interacts with the γ phosphate group in a full NBD dimer, were found to mediate allosteric coupling between the two nucleotide binding sites [Jones & George, 2012]. However, in the ADP-bound ABCB8 structure the glutamate cannot interact with ADP due to the lack of a γ phosphate. Consequently, the allosteric communication network is interrupted, explaining the lack of cooperativity for ADP binding.

Lysine crosslinking did not result in a change in the crosslinking pattern in the presence of 1 mM ADP, as observed for other nucleotides. It cannot be ruled out that higher concentrations of ADP were required to see effects in the crosslinking experiment. Whether ADP binding only triggers dimerisation of NBDs in ABCB8 or also couples conformational changes in the TMDs cannot be concluded with the methods applied in this chapter. This is a missing link for the interpretation of the outward-facing state of the ABCB8 structure, that has ADP bound.

6.5 Potential conformational changes induced by nucleotide analogue binding

The nucleotide-free ABCB8, as well as ABCB8 in the presence of AMPPCP, are likely to form open inward-facing states, that are highly flexible. The experiments performed in this chapter do not tell, whether AMPPCP does not bind to the transporter at all or binding does not induce a conformational change and therefore might not be detected. Due to the altered P-C-P angle compared to P-O-P between the β and the γ phosphate, steric hindrance might prevent the formation of a dimer interface. ADP increases the thermal stability of ABCB8 and has been found to bind to it, suggesting that ADP can trigger dimerisation of the NBDs, which leads to a decrease of flexibility of the NBDs. However, dimerisation might be looser compared to ATP or ATP-analogue binding due to the lack of a γ phosphate group, as observed in the ADP-bound structure. In contrast, ATP+V_i, which is likely to form an ADP+V_i complex in the nucleotide binding site ([Oldham & Chen, 2011]), as well as ATPγS and AMPPNP show a significant increase in the thermal stability of ABCB8, which suggests that their binding triggers dimerisation of the NBDs, which is followed by conformational changes into an occluded or outward-facing state. This conformational change is further supported by the lysine cross-linking studies presented here.

6.6 Structures of ABCB8 in outward-facing states

The first structure of ABCB8, reported in chapter 5, was captured in an outward-facing state. This is the first time, this conformation has been determined for an eukaryotic ABC transporter of the subfamily B. Sav1866 [Dawson & Locher, 2006], McjD [Choudhury *et al.,* 2014] and MsbA [Ward *et al.,* 2007b] are the only ABC

transporters solved at high resolution in outward-facing states and they are all from prokaryotes. However, ABCB8 is unique in so far in that we observe occlusion of the core of the TMDs, while the top halves of TMDs adopt an open state.

In addition, I obtained medium resolution data for co-crystallisation of ABCB8 with ADP/Mg^{2+} and in a nucleotide-free state; in both these structures, ABCB8 also adopts an outward-facing state. In the nucleotide-free state the NBDs are more separated. This differs from the ADP/Mg^{2+} and ATPγS/ADP/Mg^{2+} co-crystallised structures, where the NBDs are packed against each other mediated by nucleotide binding.

Although, ABCB8 was co-crystallised with a ATPγS/ADP mixture, it is evident, that a γ phosphate group did not fit into the electron density map without rearranging the backbone of the Walker A motif (Fig. 8.18). Instead ADP in coordination with Mg^{2+} was found to be bound.

ATPγS purchased from Sigma-Aldrich is $\geq 75\%$ pure and mass spectrometry data also suggest that the freshly prepared stock solution for ATPγS contained ADP. Since crystals of ABCB8 in the monoclinic space group only appeared after at least four days, the possibility that ATPγS would be further hydrolysed to ADP and thiophosphate cannot be excluded. The same conformation of ABCB8 was observed after adding ADP to the crystallisation set-up. This result suggests that it is not required for ABCB8 to hydrolyse ATPγS in order to undergo conformational changes into the outward-facing state. ADP binding is either sufficient to convert the transporter into an outward-facing state or the transporter already adopted an outward-facing state that then binds ADP. That would suggest that ABCB8 was trapped in an outward-facing state that exists independent of the presence of nucleotide. The observation of a nucleotide-free ABCB8 structure in an outward-facing state supports this assumption.

This raises the question of what caused this ABC transporter to be trapped in this outward-facing rather than the more frequently observed inward-facing conforma-

tion. Three different explanations could account for this observation; (i) There could be a mixture of conformations in solution, and the crystal packing lattice observed can only form with the particular conformation seen in the crystals. The other forms present in the solution do not have an available lattice, under those crystallisation conditions, and therefore they do not crystallise. (ii) The presence of modified cysteine (Cys483) involved in coordination of both the nucleotide and ICL1 could trap this particular conformation. (iii) The presence of a hydrophobic CHS molecule bound in the hydrophobic cleft on the surface of the transporter could assist the formation of this structure, either acting as a substrate mimetic, or as a conformation stabilising agent.

(i) The asymmetric unit contains 4 dimers, that have different crystal packing environments. Yet, all dimers adopt almost identical outward-facing state, so that crystal packing is unlikely to have forced the protein into a particular conformation.

(ii) The electron density in the structure, and also MS/MS analysis confirmed that Cys483, adjacent to the A-loop in the nucleotide binding site was modified. The additional amide group linked to Cys483 allows for tighter binding of the nucleotide and ICL1 to the nucleotide binding site within the same chain. However, there are no apparent changes in the interactions around the Cys483 modification site relative to other inward- or outward-facing states, suggesting that this region moves as a rigid body. However, the DSS lysine crosslinking experiment revealed, that iodoacetamide treatment of the protein could result in a conformational change itself; the crosslinked dimer to monomer ratio was drastically reduced to 50% potentially indicating a higher percentage of ABCB8 in an outward-facing state. This is surprising, as the melting temperature and ATPase activity (3.2.6) behave very similarly to unmodified protein. Additionally, binding of AMPPNP and to a lesser extent of ATP+V_i was impaired for the iodoacetamide treated protein. The modification of Cys483 enables the residue to form hydrogen bonds to the adenine ring of the nucleotide. This interaction might slightly rearrange binding of AMPPNP and an ATP transition state formed with V_i in the binding site, but does not im-

pact ADP or ATPγS binding. This might suggest, that ADP or ATP analogue binding can be slightly translated in the nucleotide binding site depending on their three dimensional structure adopting slightly different binding modes. On the basis of these result it is difficult to confirm that modification of the cysteines in the structure did not at least facilitate capturing the outward-facing state.

(iii) Clear electron density was observed above the elbow helix between TMH5 and TMH6 that is compatible with CHS. CHS was highly abundant in the crystallisation conditions, as it was used as a purification additive. CHS could have trapped this state by preventing the separation of TMH5 and TMH6, as well as the straightening of TMH4, necessary for recycling the transporter into the inward-facing state.

Structural information can hint towards a potential transport substrate for ABC transporters. In ABCB8 we observe a highly conserved patch in the dimer interface with mainly polar and charged residues. However, no cavity is formed in the transporter core in contrast to McjD or Sav1866 and these residues are occluded unable to provide space for substrate binding. However, a post-ATP-hydrolysis state was captured in this crystal structure, in which the substrate could have been already released and subsequently the substrate binding site already collapsed.

The aforementioned CHS binding site provides another interesting feature that may hint to a substrate binding site. Yet, sterol levels are very low in the inner mitochondrial membrane, so that it seems unlikely that the cholesterol binding is physiological, although this cannot be ruled out completely, as there are low levels of cholesterol in mitochondrial membranes. But it is also possible that CHS sits in the site where another lipid, perhaps even a transport substrate lipid, might bind. Since the substrate transport of ABCB8 remains elusive, it could be speculated that ABCB8 has a lipid flippase activity and the hydrophobic cleft is a substrate binding site for flipped lipids. However, if this conformation represents an outward-facing state, for which low substrate binding affinity is assumed, then perhaps we

would not expect to see a complete substrate binding pocket. The actual lipid substrate might not be formed any longer in this state, but CHS has a smaller polar moiety compared to a big lipid head group and this way remains bound. The conservation of this binding site within ABCB8 homologues in comparison to the conservation in the subfamily B is striking, suggesting a crucial role for ABCB8 function. Lipidomics experiments performed in Prof. Carol Robinson's lab at the Department of Chemistry, University of Oxford (unpublished data Dr Shahid Mehmood) show binding of phosphatidyl ethanolamine and phosphatidyl glycerol, as well as phosphatidyl inositol to detergent purified ABCB8. This binding site, embedded between the hydrophobic lipid tails of the membrane, can also be involved in regulation of ABCB8 activity, whereas binding of a specific lipid in this region could potentially trap this conformation and inhibit transporter activity stabilising the outward-facing conformation.

As the function of ABCB8 remains unclear, we have no proof of ABCB8 being an exporter. However, the presence of an exporter fold and the high conservation of NBDs and coupling helices may suggest that the alternating-access mechanism is comparable to that proposed for P-glycoprotein or ABCB10 [Shintre *et al.,* 2013]. In this mechanism (Fig. 6.1), substrate is shuttled across the membrane by conformational changes in the TMDs triggered by dimerisation of the NBDs. It is unclear whether dimerisation of the NBDs is caused by ATP binding itself or whether subsequent hydrolysis or dissociation of the phosphate is required. In the ABCB8 structure, an outward-facing state is observed that has ADP and Mg^{2+} bound.

In Dawson & Locher [2006] it was claimed that the ADP-bound outward-facing conformation of Sav1866 is an artefact and would present a pre-hydrolysis ATP-bound state rather than the post-hydrolysis state. It is suggested that ATP binding dimerises the NBDs and causes the conformational change of the TMDs to the outward-facing state. Subsequently, hydrolysis takes place and converts the transporter back into the inward-facing state. Alternatively, as described in section 1.2.8, ATP binding can trigger NBD dimerisation and subsequent hydrolysis

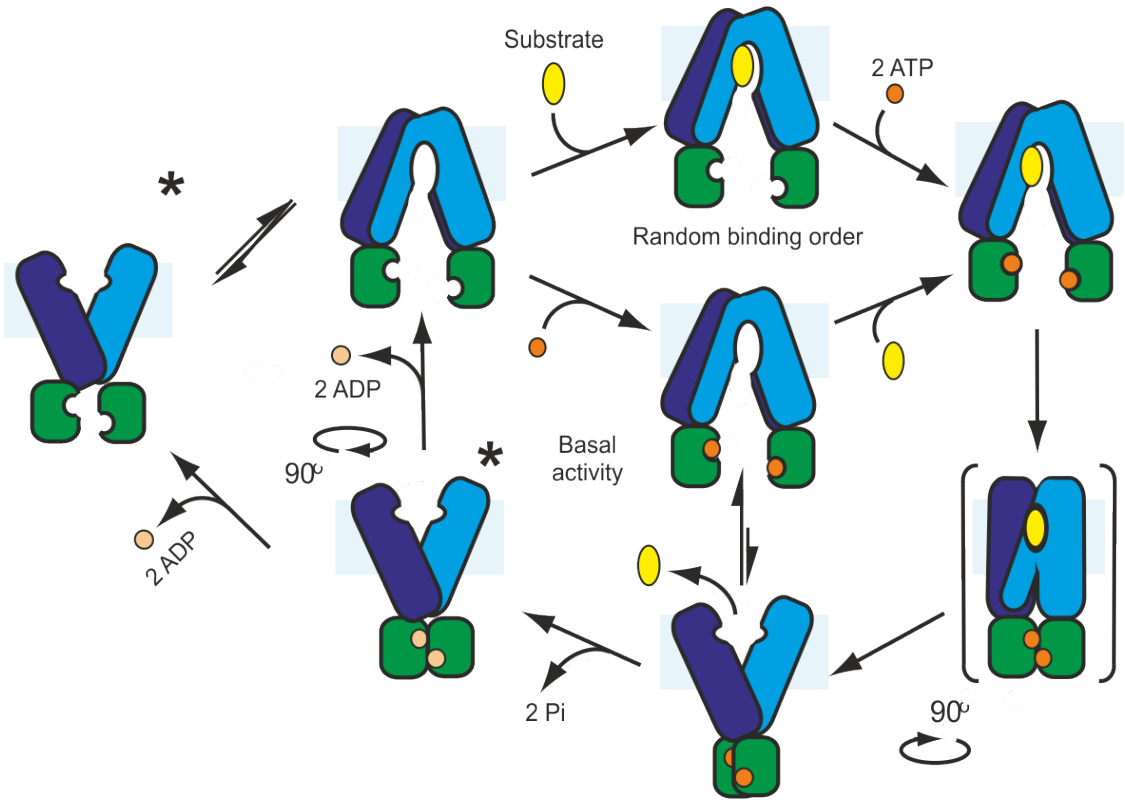


Figure 6.1 – Scheme for alternating-access mechanism in homodimeric ABC transporters of the exporter fold. The two chains are coloured in blue and green for the TMDs and the NBDS. Substrate, ATP and ADP are shown as yellow, orange and beige circle, respectively. Inward-facing states are represented with substrate, nucleotide and both bound, to indicate that the order of substrate binding is not know. Subsequently, a occluded state is formed as an intermediate state (in brackets) followed by ATP hydrolysis either in this occluded state or in an outward-facing state. An outward-facing state, representing the post-ATP-hydrolysis state with two ADP bound, as well as a nucleotide-free outward-facing state were observed in the crystal structures (highlighted with $*$). Hydrolysis leads to recycling of the transporter back into an inward-facing state. (Figure was modified from Shintre *et al.,* 2013).

drives conversion into the outward-facing state. This is consistent with both the ADP-bound outward-facing Sav1866 structure and the ADP/Mg^{2+} bound outward-facing ABCB8 structure. The differences in the extent of occlusion in both structures could be explained by the fact that ABCB8 has additional Mg^{2+} bound. Levels of magnesium are 10-fold higher in the mitochondrial matrix compared to the cytoplasm [Gout *et al.,* 2014], so that ADP/Mg^{2+}binding to ABCB8 under physiological conditions is not unlikely.

The ADP-bound ABCB8 structure could represent a snapshot of a transient state in the alternating-access mechanism, in which after ATP-hydrolysis the γ phosphate group would have been released, but ADP remained bound. A weak interaction only facilitated between the ADP's ribose ring and a Thr611 of the opposite chain, stabilises the NBD dimer in this state. In particular, it is found that the α-helical subdomain in the NBDs shifts significantly compared to the nucleotide-bound structures of McjD and Sav1866 with a tight NBD dimer interface. This shift in the α-helical subdomain translates into loosening of the X-loops and movement of the ICLs interacting with the adjacent domain. As ICL2 in particular is shifted, a movement in TMH4 and TMH5 towards the transporter core is caused, that yields this outward-facing state we find in the ADP-bound ABCB8 structure. Due to the less tight packing of the NBDs, ADP could leave the binding site upon which the transporter reverts to the inward-facing state. An alternative model would be the exchange of ADP with ATP without the requirement of a full alternating-access cycle back into an open inward-facing state, as proposed in Perez *et al.* [2015] and Locher [2016] and potentially consistent with the observation of a nucleotide-free inward-facing state of ABCB8 (section 1.2.8, Fig. 6.1).

The functional role of the nucleotide-free outward-facing conformation with separation of the NBDs is unclear. Interestingly, McjD was recently solved in a nucleotide-free state, in which the TMDs have an occluded conformation, but with the NBDs separated by 7.9 Å [Bountra *et al.,* 2017]. An occluded or outward-facing state that allows exchange of nucleotides during the alternating-access mechanism might

indeed be important for an alternating-access cycle that does not involve an open inward-facing state.

CHAPTER 7

Conclusion and Outlook

7.1 Conclusion

From the Human Genome Project, we obtained the primary sequence of thousands of newly sequenced genes. Yet, knowledge of the protein sequence does not ultimately translate into understanding the role of a protein in the cell. In order to understand how proteins function in cells, it is crucial that we obtain information on their three dimensional structures in a range of conformations. However, particularly for human membrane proteins, structural information is still difficult to accomplish.

Obtaining a three dimensional structure of ABCB8 served as the underlying motivation for this thesis. Furthermore, *in vitro* studies on purified ABCB8 in order to understand its function and interaction with nucleotides were performed.

Obtaining decent amounts of stable and pure protein is one of the main challenges to overcome, when aiming for structural information of membrane proteins. The

work described in chapter 3 demonstrates how strategic optimisation of purification conditions enabled the establishment of a purification protocol for ABCB8. Thus, sufficient yields of stable protein for crystallisation trials were achieved. Besides the standard optimisation procedures involving different protein constructs, buffer conditions and detergent types, alternative methods were tested that have been shown in previous purification protocols to facilitate production of stable membrane proteins, such as addition of lipids, surface entropy mutants and chemical modifications. Purification of stable and active protein allowed the establishment of a successful reconstitution protocol for ABCB8. Consequently, the effects of lipids on the basal ATPase activity could be tested. Notably, it was found that CDL had a stimulating effect on ABCB8 in proteoliposomes.

The data obtained from co-crystals of ABCB8 with an ATPγS/ADP/Mg^{2+} mixture were used to solve a 3.8 Å crystal structure of ABCB8 that was captured in an outward-facing state, as described in chapter 5. All eukaryotic ABC transporters of the subfamily B and related subfamily C (type I ABC exporters) have been solved in inward-facing states. The ABCB8 structure that is described in this thesis, is the first eukaryotic ABC transporter structure observed in an outward-facing state. By comparing this state to the inward-facing states of other subfamily B ABC transporters and outward-facing states of prokaryotic ABC exporters, valuable insights into the alternating-access mechanism were obtained. The outward-facing state of ABCB8 has ADP/Mg^{2+} bound in its nucleotide binding site with two molecules sandwiched between the two NBDs. It is proposed here that this conformation represents a post-ATP-hydrolysis state, in which orthophosphate was released from the binding site, but ADP and Mg^{2+} remained bound. Although dimerisation of the NBDs was still observed, the contacts between the binding sites were less compact than in the outward-facing Sav1866, MsbA or McjD structures. With loss of the γ phosphate group, which bridges residues of the RecA-like subdomain and the α-helical subdomain of two different chains, the dimerisation of the NBDs is significantly weakened. The loosening of the NBD dimer and the subsequent shift of the

α-helical subdomain away from the dimer interface, translates into displacement of the coupling helices away from the two fold-symmetry axis of the transporter. Consequently, the TMDs were rearranged and formed the outward-facing state with a more occluded transporter core in comparison to the outward-facing state of AMPPNP-bound MsbA and ADP-bound Sav1866. This structure provides evidence, that ATP hydrolysis and subsequent phosphate release are the first steps for recycling the transporter back into an state that has the NBDs separated.

ADP is the ATP hydrolysis product and it has been previously suggested that ADP release would instantly follow NBD separation. However, ADP/Mg^{2+} binding to the nucleotide binding site as observed in this outward-facing conformation of ABCB8, was further confirmed in functional studies, as described in chapter 4. The apparent K_D values for ADP binding and melting temperature shifts were less pronounced compared to the ones found for the ATP analogue ATPγS and the ATP transition state analogue ADP+V_i. That is consistent with the observation in the crystal structure of a less tight NBD dimer interface, due to the lack of a γ phosphate group compared to nucleotides with three phosphates moieties.

Furthermore, a nucleotide-free ABCB8 structure at lower resolution was obtained from a crystal showing a variation of the crystal form in the $P12_11$ space group with a slightly enlarged unit cell volume. To our surprise, it was found that the NBDs were separated, although the electron density map indicated that the TMDs were in an outward-facing state. At this point it is not possible to say, whether this is an artefact of the modification or whether this state is part of the alternating-access cycle. Notably, a nucleotide-free occluded state of McjD was recently observed with a similar extent of separation for the NBDs [Bountra *et al.,* 2017]. This state might allow exchange of nucleotide in an "outward-facing only" mechanism for lipid flippases as proposed in Locher [2016].

7.2 Outlook

Stimulation of ATPase activity was observed in proteoliposomes in presence of CDL, which raises the question, whether CDL is transported substrate of ABCB8. However, we are not aware of any publications that investigate the possibility of ABCB8 transporting lipids. Thus, future work on ABCB8 should include testing flippase activity. For that, ABCB8 could be reconstituted into proteoliposomes containing fluorescently labelled CDL. Change in distribution of CDL between the two leaflets of the membrane due to flippase activity can be subsequently observed by application of a quencher, that only quenches the outer membrane leaflet.

In order to investigate potential non-lipid substrates for ABCB8, the development of a transport assay is required. By establishing a reconstitution protocol for ABCB8 into proteoliposomes whilst maintaining its ATPase activity, the prerequisite was fulfilled for future transport studies. In order to allow for a broad variety of physiologically relevant molecules to be tested as potential substrates, a targeted metabolomics based experiment was designed as described in Jansen *et al.* [2015] for ABCC5. This work aims to test accumulation of potential endogenous substrates in ABCB8 proteoliposomes by incubation with various cell and mitochondria lysates. Subsequently, enriched molecules could be identified with mass spectrometry. These hits can be further verified as transporter substrates in an *in vitro* uptake assay with ABCB8 proteoliposomes and pure molecules. This work is ongoing and is outside the scope of this thesis.

Lysine crosslinking studies hinted at conformational changes that were triggered by binding of ATPγS or ADP+V_i, but not in the presence of ADP or AMPPCP. In order to identify these states trapped by the crosslinker, we are in the process of analysing our crosslinked ABCB8 samples with liquid chromatography MS/MS in collaboration with Prof. Matthias Gsteiger at the ETH in Zurich. Preliminary data suggest that ATPγS, AMPPNP and ATP+V_i binding triggers transition into the occluded or outward-facing state. In addition EPR or single molecule FRET studies

would allow us to investigate conformational changes induced by the nucleotide (and potential substrates) binding in more detail in the future.

Further structural studies should be aimed at obtaining different conformations of ABCB8 in an inward and occluded state, so that conformational changes could be traced in one system rather than comparing ABC transporters of different subfamilies and functions. Once the nature of the transport substrate has been determined, co-crystallisation with the substrate will also be of considerable interest. As structures are now emerging for ABC transporters solved by cryo-EM, it will also be of great interest to study ABCB8 by this method. Unfortunately, preliminary attempts to put ABCB8 onto grids suggested that under the conditions used, the protein was denaturing, so considerable further development work will be needed to obtain good quality samples on grids. In the future a combination of X-ray crystallography and cryo-EM would be helpful to get new insights into the alternating-access cycle in ABCB8.

CHAPTER 8

Appendix

8.1 Appendix: Introduction

Table 8.1 – Section 1.2.5: Summary of prokaryotic and eukaryotic ABC transporter structures solved by X-ray crystallography and cryo-EM (∗).

ABC transporter	Organism	Resolution (Å)	Conformation	Nucleotide/ Substrate	Reference and PDB code
Bacterial ABC exporter					
Sav1866	*Staphylococcus aureus*	3.0	outward-facing	ADP	2HYD(Dawson and Locher, 2006)
	Staphylococcus aureus	3.4	outward-facing	AMPPNP	2ONJ(Dawson and Locher, 2007)
MsbA	*Samonella typhimurium*	4.2	outward-facing	ADP+Vi	3B5Z(Ward et al., 2007)
	Samonella typhimurium	4.5/3.7	outward-facing	AMPPNP	3B5Y/ 3B60(Ward et al., 2007)
	Escherichia coli	5.3	inward-facing	apo	3B5W(Ward et al., 2007)
	Vibrio cholera	5.5	inward-facing	apo	3B5X(Ward et al., 2007)
MsbA*	*Escherichia coli*	4.8	occluded	ADP+Vi	5TTP(Mi et al., 2017)
	Escherichia coli	4.2	inward-facing	Lipopoly-saccharide	5TV4(Mi et al., 2017)
TM287/288	*Thermotoga maritima*	2.9	inward-facing	AMPPNP	4Q4A(Hohl et al., 2012)
	Thermotoga maritima	2.5	inward-facing	apo	4Q4H(Hohl et al., 2012)
PglK	*Campylobacter jejuni*	2.9/3.9	inward-facing	apo	5C78/5C76(Perez et al., 2015)
	Campylobacter jejuni	5.9	outward-facing	(AMPPNP)†	5C73(Perez et al., 2015)
	Campylobacter jejuni	3.9	inward-facing	nanobody inhibited	5NBD(Perez et al., 2017)
NaAtm1	*Novosphingobium aromaticivorans*	2.4/2.5/2.97/2.35/2.5	inward-facing	apo	4MRN/4MRP/4MRR/4MRS/4MRV(Lee et al., 2014)
McjD	*Escherichia coli*	2.7	occluded	AMPPNP	4PLO (Choudhury et al., 2014)
	Escherichia coli	3.4	outward-occluded	ADP+V_i	5OFR(Bountra et al., 2017)
	Escherichia coli	4.7	inward-occluded	apo	5OFP(Bountra et al., 2017)
TmrAB	*Thermus thermophilius*	2.7	inward-facing	apo	5MKK(Nöll et al., 2017)
PCAT	*Ruminiclostridium thermocellum*	5.5	occluded	(ATPγS) †	4SDF(Lin et al., 2015)
	Ruminiclostridium thermocellum	3.6	inward-facing	apo	4RY2(Lin et al., 2015)
CmABCB1	*Cyanidioschyzon merolae*	2.8/2.6/2.4	inward-facing	Apo/apo/peptide inhibitor	3WME/3WMF/3WMG(Kodan et al., 2014)
Eukaryotic ABC transporter					
ABCA1*	*Homo sapiens*	4.1	inward-facing	apo	5XJY(Qian et al., 2017)
ABCB10	*Homo sapiens*	2.9	inward-facing	apo	3ZDQ (Shintre et al., 2013)
	Homo sapiens	3.3/2.9	inward-facing	AMPPNP	4AYW/4AYX(Shintre et al., 2013)
	Homo sapiens	2.9	inward-facing	AMPPCP	4AYT(Shintre et al., 2013)
ABCB7(Atm1)	*Saccharomyces cerevisiae*	3.06	inward-facing	apo	4MYC(Srinivasan et al., 2014)
	Saccharomyces cerevisiae	3.38	inward-facing	GSH bound	4MYH(Srinivasan et al., 2014)
ABCB2/3 (TAP1/2)*	*Homo sapiens*	4.0	inward-facing open	apo	5U1D(Oldham et al., 2016)
ABCB1 (P-glycoprotein)	*Mus musculus*	3.8	inward-facing	apo	4M1M(Li et al., 2014)
	Mus musculus	3.4	inward-facing	apo	4Q9H(Szewczyk et al., 2015)
	Mus musculus	3.8/4.4/4.4	inward-facing	ligand	3G5U/3G60/3G61(Aller et al., 2009)
	Mus musculus	3.8/4.0/4.1	inward-facing	apo	4KSB/4KSC/4KSD(Ward et al., 2013)
	Caenorhabditis elegans	3.4	inward-facing	apo	4F4C(Jin et al., 2012)
ABCC1*	*Bos taurus*	3.3/3.5	inward-facing	Apo/leukotriene C4	5UJA/5UJ9 (Johnson et al., 2017)
ABCC8 (SUR1)*	*Rattus norvegicus*	6.3	inward-facing	In complex with Kir6.2, ATP	5TWV(Martin et al., 2017)
	Mus musculus	5.6	inward-facing	In complex with Kir1.6	5WUA(Li et al., 2017)
ABCC7 (CFTR)*	*Danio rerio*	3.7	inward-facing		5UAR(Zhang and Chen, 2016)
		3.4	occluded	ATP (EQ mutation)	5W81(Zhang et al., 2017)
	Homo sapiens	3.9	inward-facing	apo	5UAK(Liu et al., 2017)
ABCG5/8	*Homo sapiens*	3.9	inward-facing	apo	5DO7(Lee et al., 2016)
ABCG2*	*Homo sapiens/Mus musculus*	3.8	inward-facing	Apo, Fab 5D3 antibody	5NJ3(Taylor et al., 2017)

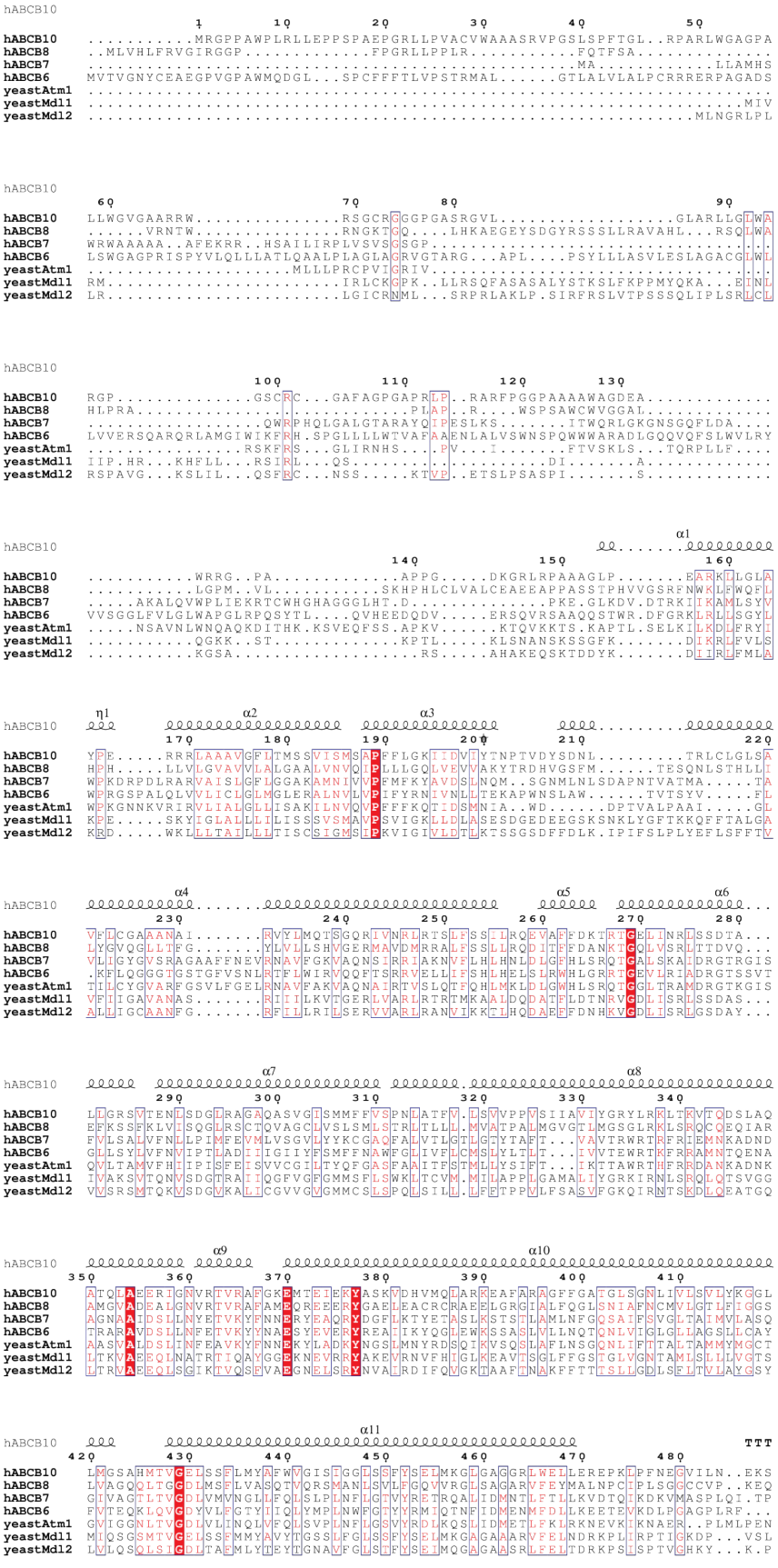


Figure 8.1 – Section 1.3.2: Multi-sequence alignment (Clustal Omega [Sievers *et al.*, 2011]) of putative human mitochondrial ABC transporters ABCB6, ABCB7, ABCB8 and ABCB10 with Atm1, Mdl1 and Mdl2 from *S. cerevisiae*

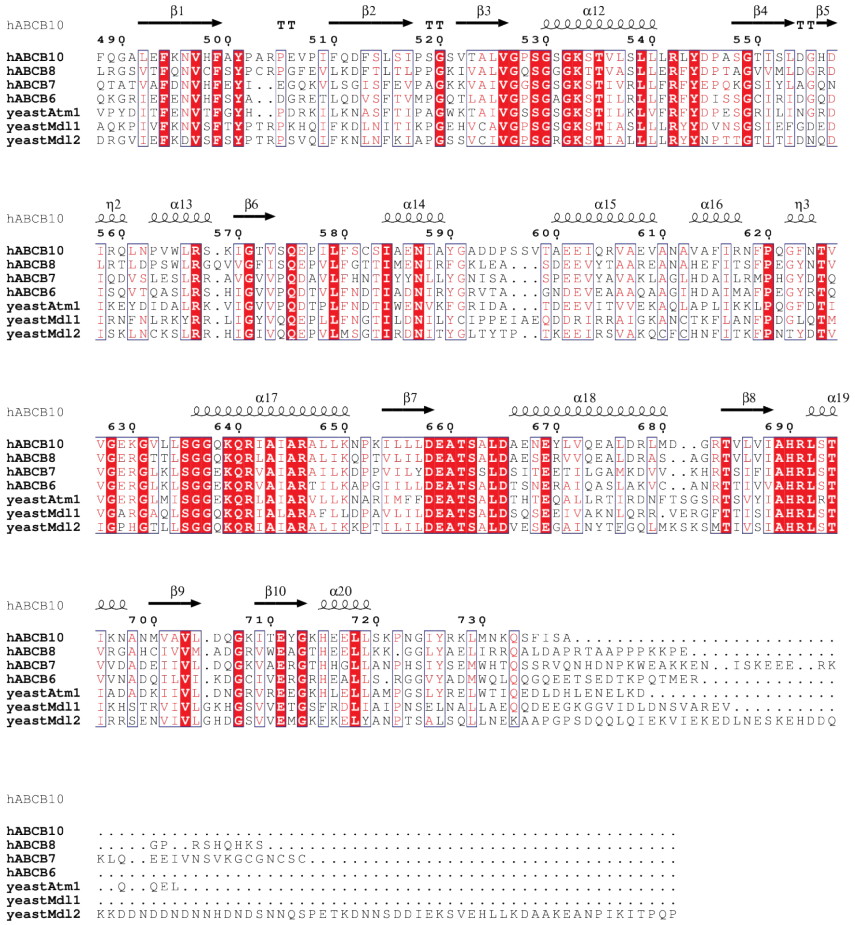


Figure 8.1 – Section 1.3.2: Multi-sequence alignment (Clustal Omega [Sievers *et al.*, 2011]) of human mitochondrial ABC transporters ABCB7, ABCB8 and ABCB10 with Mdl1 and Mdl2 from *S. cerevisiae*.

8.2 Appendix: Material and Methods

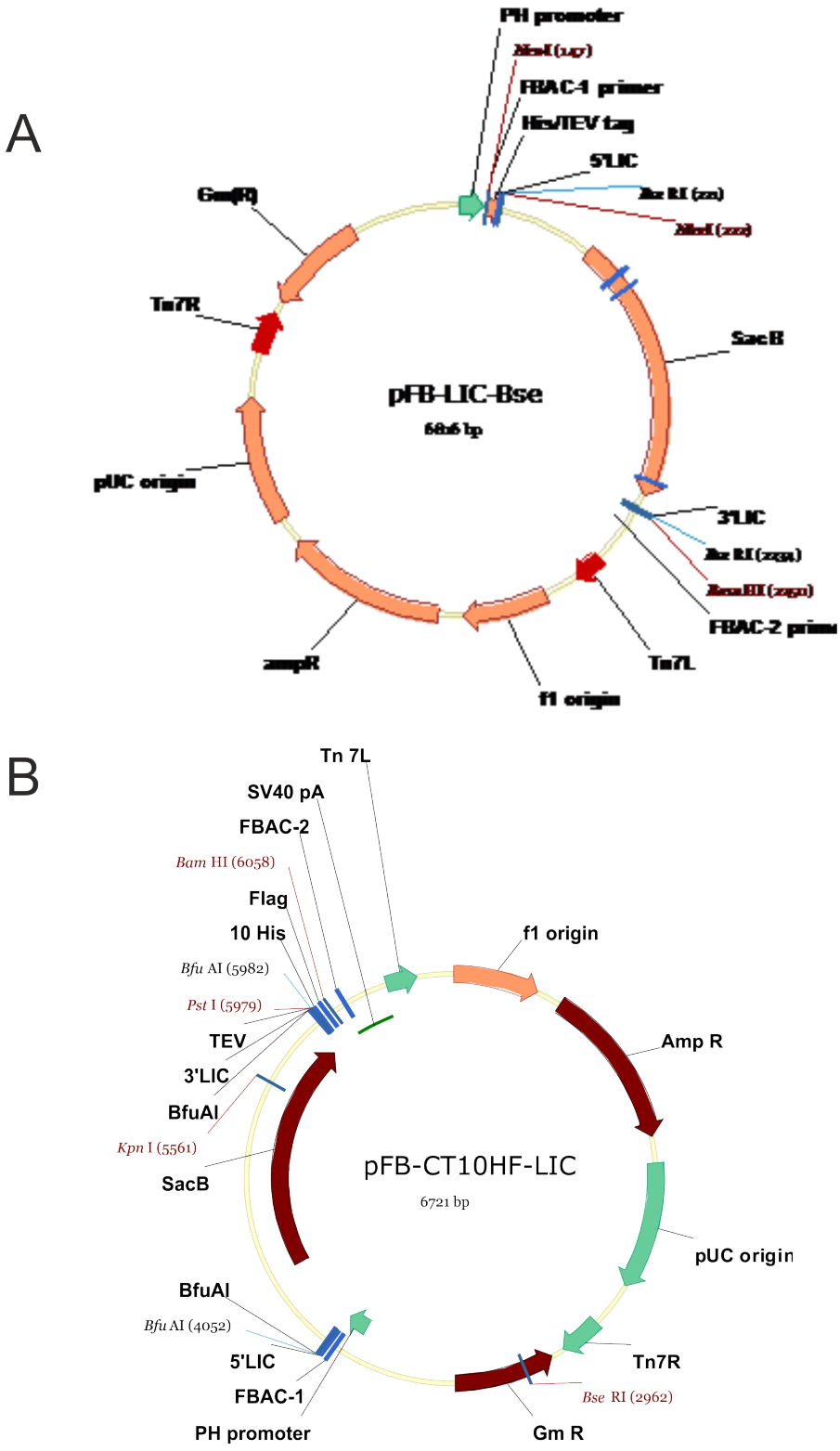


Figure 8.2 – Section 2.2: Vector card of baculovirus transfer vectors A) pFB-LIC-Bse and B) pFB-CT10HF-LIC.

Table 8.2 – Section 2.8.4/5.2.8: Table showing data processing statistics for selected datasets collected on ABCB8 crystals

Dataset number	**d001**	**d003**	**d013**	**d014**	**d014***
Dataset type	native	native	Se-Met	native	
Nucleotide	ATPγS	ATPγS	ATPγS	ATPγS	
Data collection:					
Space group	C222(1)	P12(1)1	P12(1)1	P12(1)1	
Cell dimensions					
a, b, c (Å)	276.33, 328.79, 259.6	181.79,98.48, 213.06	181.79, 98.48, 213.06	179.30,99.80x,212.80	
α,β,γ (°)	90.0, 90.0, 90.0	90.0, 90.55, 90.0	90.0, 90.55, 90.0	90.00, 90.18,90.00	
Resolution	7.05 (7.2 x 7.9 x 6.49)	3.83(4.07x5.68x3.80)	6.50(6.50x7.43x6.50)	3.80 (4.16 x 5.44 x 3.46)	3.65
Rmerge	0.124 (4.457)	0.215(3.155)	0.247(1.614)	0.220 (7.300)	0.122(1.264)
Rmeas	0.146 (5.341)	0.277(3.321)	0.258(1.685)	0.238 (7.896)	0.132(1.377)
I/σ	10.2 (0.5)	7.4(0.8)	8.1 (1.9)	7.0 (0.3)	11.0(1.7)
CC(1/2)	0.99 (0.126)	0.999 (0.487)	0.996(0.504)	0.998 (0.078)	0.999(0.549)
Wilson B-factor			137.29	140.73	
Completeness	99.2(99.0)	99.8 (98.0)	99.9	99.9	62.1(16.6)
Multiplicity	6.7	10.6	12.5	6.9	6.7

Dataset number	**d015**	**d015***	**d016**	**d016***	**d017**
Dataset type	native		native		Hg
Nucleotide	ADP		none		ATPγS
Data collection:					
Space group	P12(1)1		P12(1)1		P12(1)1
Cell dimensions					
a, b, c (Å)	183.53, 99.49, 214.50		185.78,109.37,209.38		181.1, 98.5, 214.9
α,β,γ (°)	90.00, 90.37, 90.00		90.0,90.16,90.0		90.00, 90.10, 90.00
Resolution	3.83(4.35x5.57x3.58)	3.70	4.35(4.53x6.67x4.20)	4.25	6.00(6.80x7.70x6.00)
Rmerge	0.171(11.50)	0.089 (1.257)	0.191(3.934)	0.144(1.663)	0.288(3.338)
Rmeas	0.185(12.64)	0.097 (1.365)	0.206(4.205)	0.156(1.801)	0.313(3.623)
I/σ	6.5(0.2)	11.6 (1.6)	6.3 (0.5)	9.1(1.2)	5.1 (0.6)
CC(1/2)	0.999 (0.04)	0.999 (0.55)	0.998(0.291)	0.999(0.511)	0.998(0.351)
Wilson B-factor	140.73		140.61		
Completeness	99.2	55.6	99.9	67.9	99.9
Multiplicity	6.8	6.7	6.9	6.8	6.6

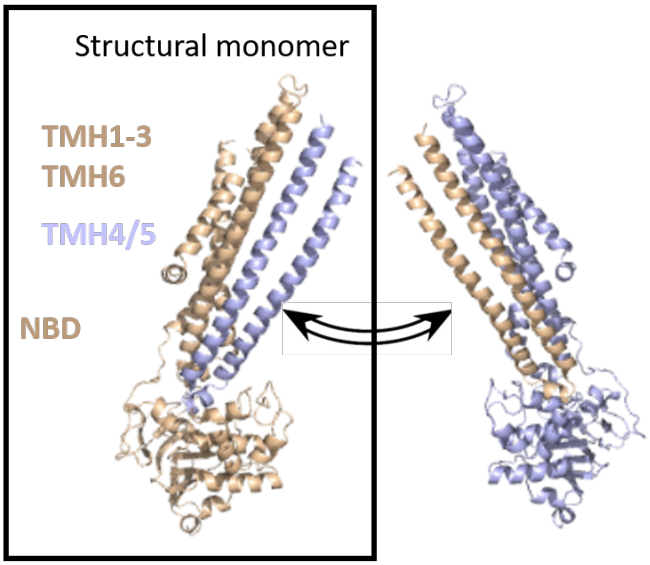


Figure 8.3 – Section 2.8.4: Structural monomers of ABCB10 (3ZDQ) created from TMH1-3, TMH6 of one chain with TMH4-5 of the adjacent chain as used as input model for MR

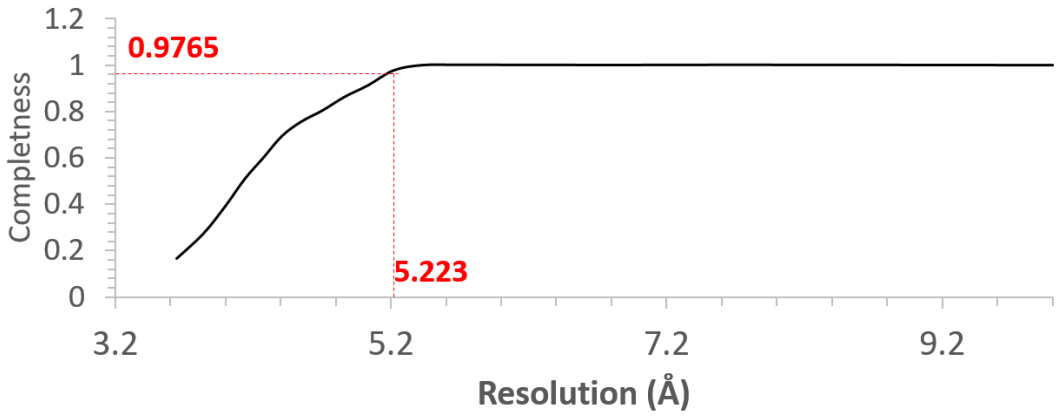


Figure 8.4 – Section 2.8.4: Graph showing the loss of completeness over resolution as analysed by the STARANISO web server [Tickle *et al.*, 2017].

Table 8.3 – Section 2.8.5: In detail listing of refinement steps and statistics. Numbers in table header describe (1) RMSD bonds and angles (Å/^{o}), (2) bad rotamers, (3) Ramachandran outliers and (4) Molprobity clash score.

Nr	Dataset	B-factor	TLS	Res.(Å)	Nr atoms	R-factors	(1)	(2)	(3)	(4)	Comment
1a	d003	None	no	3.94	25912	0.3585/0.3549	0.008/0.94	191	40	1.8	
1b	d003	None	yes	3.94	25912	0.3391/0.3466	0.008/0.99	240	71	2.11	
1a	d014	None	no	3.4	26528	0.3736/0.3754	0.008/0.94	186	48	1.41	Better data d014
1b	d014	None	no	3.4	25456	0.3619/0.3622	0.008/0.94	153	26	1.27	Small fixes in model
1d	d014	None	yes	3.4	25456	0.3251/0.3274	0.008/0.99	189	48	1.97	With TLS alternate
1d*	d014	None	yes	3.4	25456	0.3685/0.3720	0.008/0.99	179	56	1.87	Without STARANISO processing of dataset
2d	d014	None	yes	3.6	27032	0.3289/0.3385	0.008/0.95	174	49	1.93	TMH4 built and loops added
3a	d014	None	yes	3.6	29061	0.2938/0.3051	0.008/0.90	94	12	1.61	C-terminus added and further fixes
3b	d014	None	yes	3.4	29061	0.2916/0.3016	0.008/0.90	101	13	1.47	See 3a but lower resolution
4a	d014	None	yes	3.6	31120	0.2704/0.2891	0.008/0.91	148	9	2.03	
4b	d014	None	yes	3.4	31120	0.2749/0.2941	0.008/0.90	129	9	1.88	
4c	d014	yes	yes	3.6	31120	0.2481/0.2710	0.008/0.93	155	3	2.02	B individual!!!
4d	d014	yes	yes	3.6	31124	0.2485/0.2682		138	8	1.84	8 ADP and Mg2+molecules added
5a	d014	yes	yes	3.6	30677	0.2304/0.2504	0.008/0.93	82	10	2.45	8 CHS molecules added
5b	d014	yes	yes	3.6	30677	0.2321/0.2511	0.008/0.93	91	10	2.56	Same as 5a, without Mg2+
5c	d014	yes	yes	3.4	30677	0.2317/0.2524	0.008/0.94	78	11	2.4	Back to 3.4 resolution
5d	d014	yes	yes	3.4	30677	0.2315/0.2522	0.008/0.94	76	0	2.53	Fixing Ramachandran outliers
5e	d014	yes	yes	3.4	30677	0.2313/0.2522	0.008/0.94	78	0	2.58	Distance and angle restraints for Mg2+
5f	d014	yes	yes	3.4	30677	0.2497/0.2633	0.008/0.94	72	0	2.38	Refinement without STARANISO correction
5g	d014	yes	yes	3.4	30677	0.2302/0.2511	0.008/0.94	65	0	2.4	Modified gelly file to insert restraints for Mg2+
5h	d014	yes	yes	3.4	30801	0.2304/0.2510	0.008/0.94	60	0	2.46	Modification of Cys483 in chain A-G added Cys478 to GH
5i	d014	yes	yes	3.4	30741	0.2300/0.2505	0.008/0.94	58	0	2.38	Further fixes in model
5j	d014	yes	yes	3.4	30741	0.2310/0.2510	0.008/0.93	55	0	2.38	Final model deposited
$5j^2$	d014	yes	yes	3.4	30741!	0.2349/0.2535	0.008/0.93	55	0	2.38	Removed CHS molecules from final model
$5j^1$	d014	yes	yes	3.4	30741!	0.2382/0.2572	0.008/0.93	55	0	2.38	Removed ADP molecules from final model
5k		None	yes	3.4	30741	0.2531/0.2672	0.008/0.91	59	0	2.16	No individual B-factor refinement

8.3 Appendix: Optimisation of purification and crystallisation of ABCB8

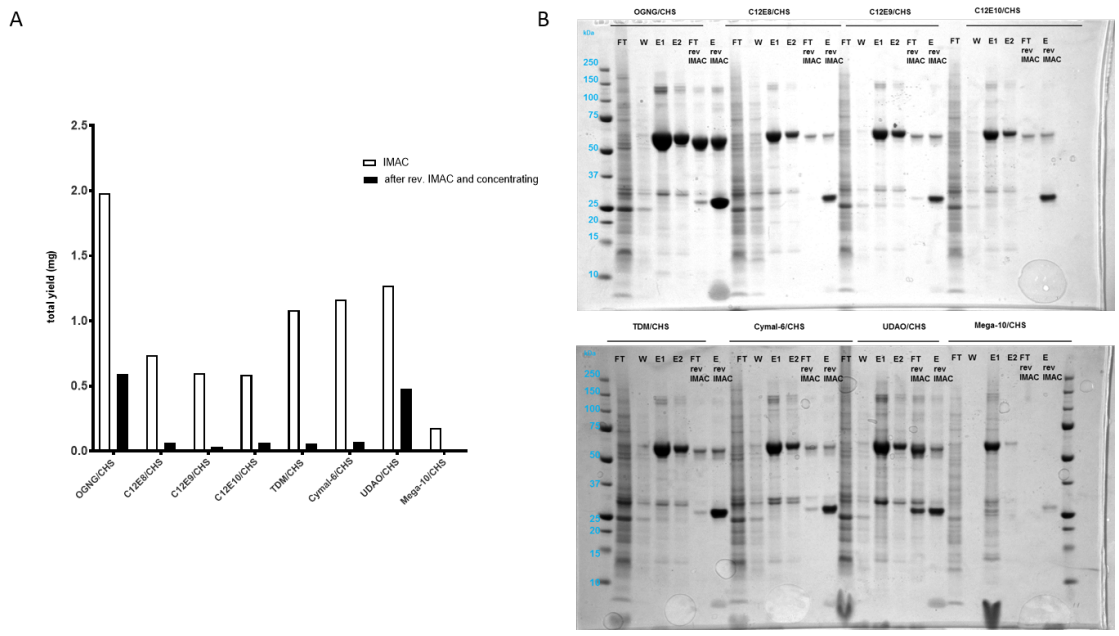


Figure 8.5 – Section 3.2.3: A) Bar chart representing total IMAC yield (white) and yield after the reverse IMAC step (black). B) Coomassie-stained SDS-PAGE gels with samples for IMAC purification and reverse IMAC (FT= flow through fraction, W= wash fraction, E=elution fractions) steps as described in section 2.5.

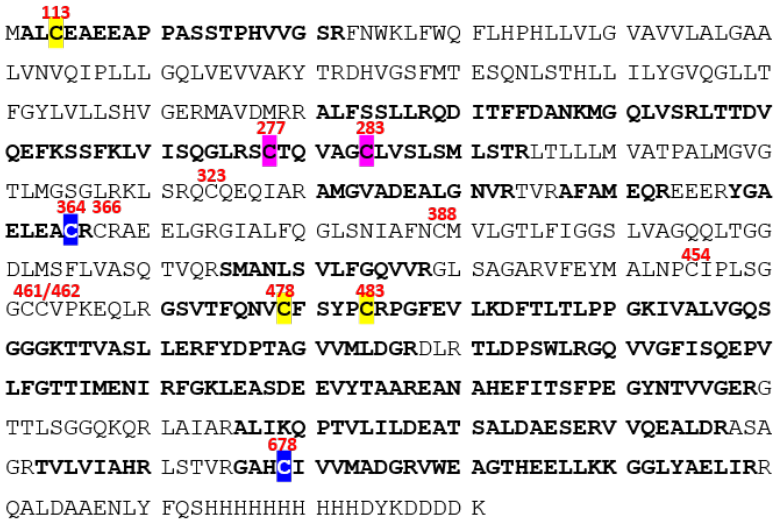


Figure 8.6 – Section 3.2.6: Sequence of ABCB8$^{Ala111-Ala714}$ with cysteines identified by MS/MS as modified with iodoacetamide. MS/MS analysis was performed with in-solution digest using trypsin. Detected peptides are highlighted in bold in the sequence. Residue numbers of cysteines are given above. Cysteines are labelled indicating whether they were unambiguously identifiable (yellow), only one out of two cysteines in the detected peptide were modified (pink) or whether an unmodified and alkylated cysteine species was detected (blue).

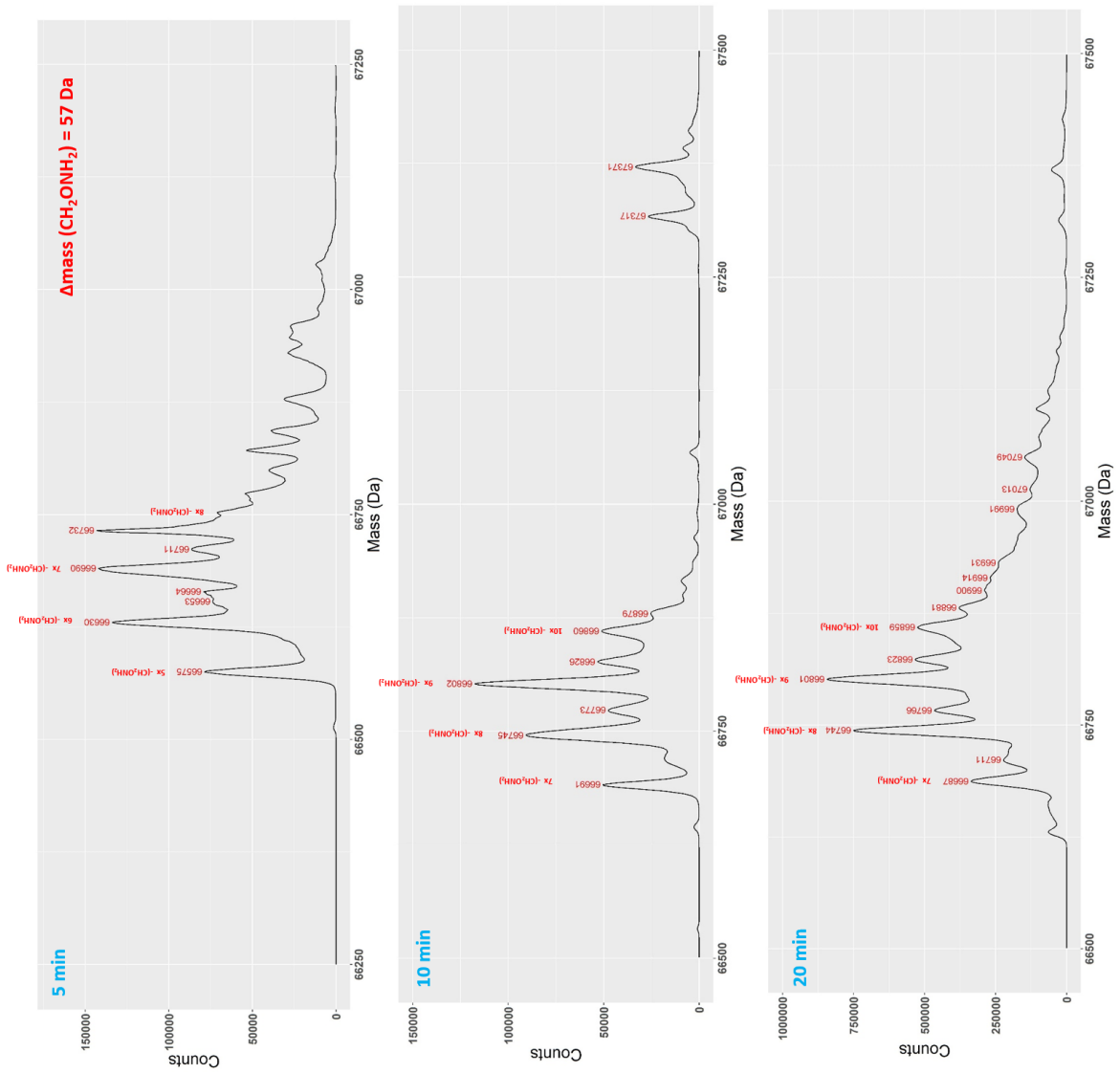


Figure 8.7 – Section 3.2.6: Cut out of deconvoluted intact mass spectrum of ABCB8$^{Ala111-Ala714}$ after iodoacetamide treatment with different modification times as indicated in the graph.

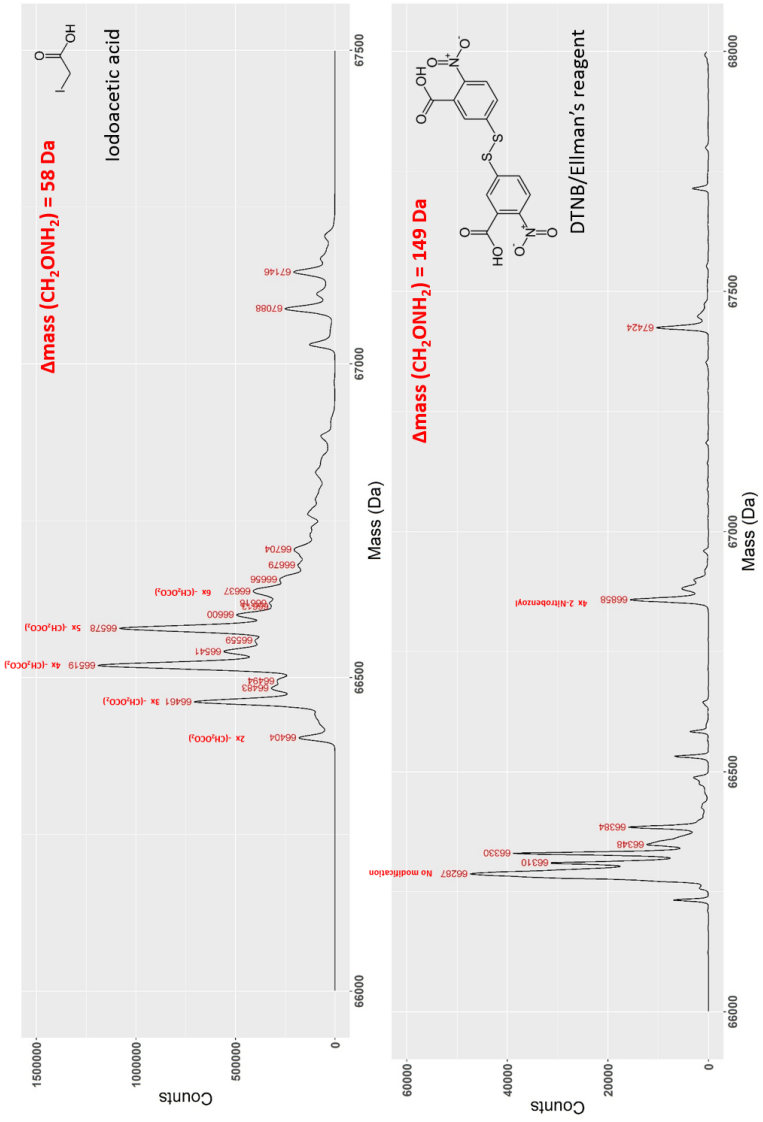


Figure 8.8 – Section 3.2.6: Cut out of deconvoluted intact mass spectrum for ABCB8$^{Ala111-Ala714}$ after treatment with iodoacetic acid or DTNB for 30 minutes.

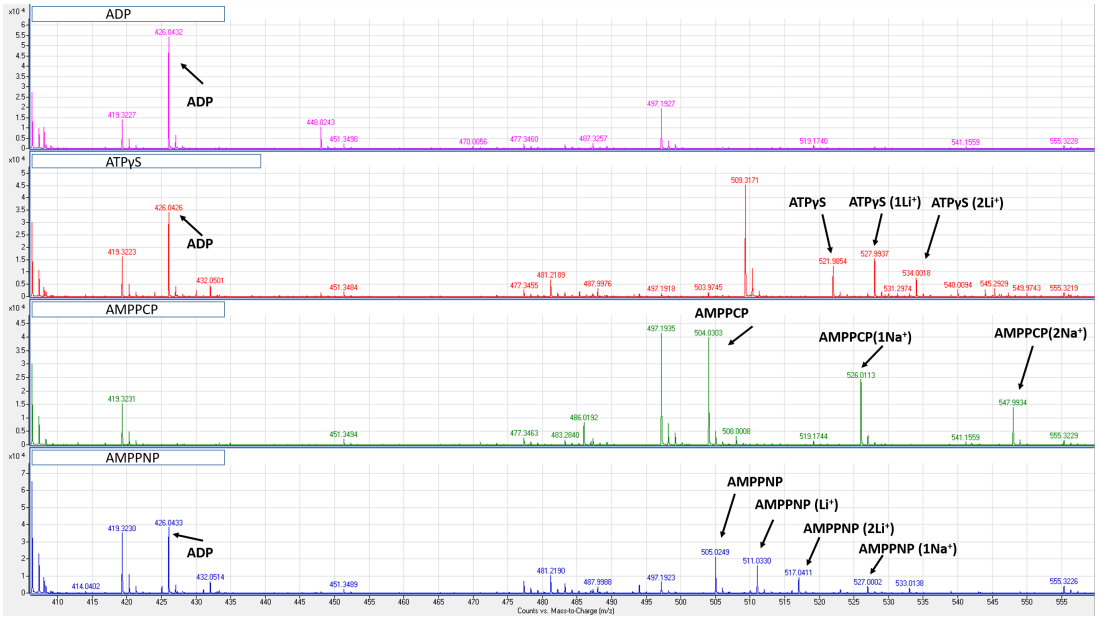


Figure 8.9 – Section 4.4.1: Negative ion ESI-QTOF mass spectrometry of nucleotides. Mass spectrum for m/z range of 400-560 for 5 mM ADP, ATPγS, AMPPCP and AMPPNP freshly prepared and adjusted to pH 7 in 100 mM HEPES.

8.4 Appendix: Exploring effects of nucleotide and putative substrate binding on ABCB8

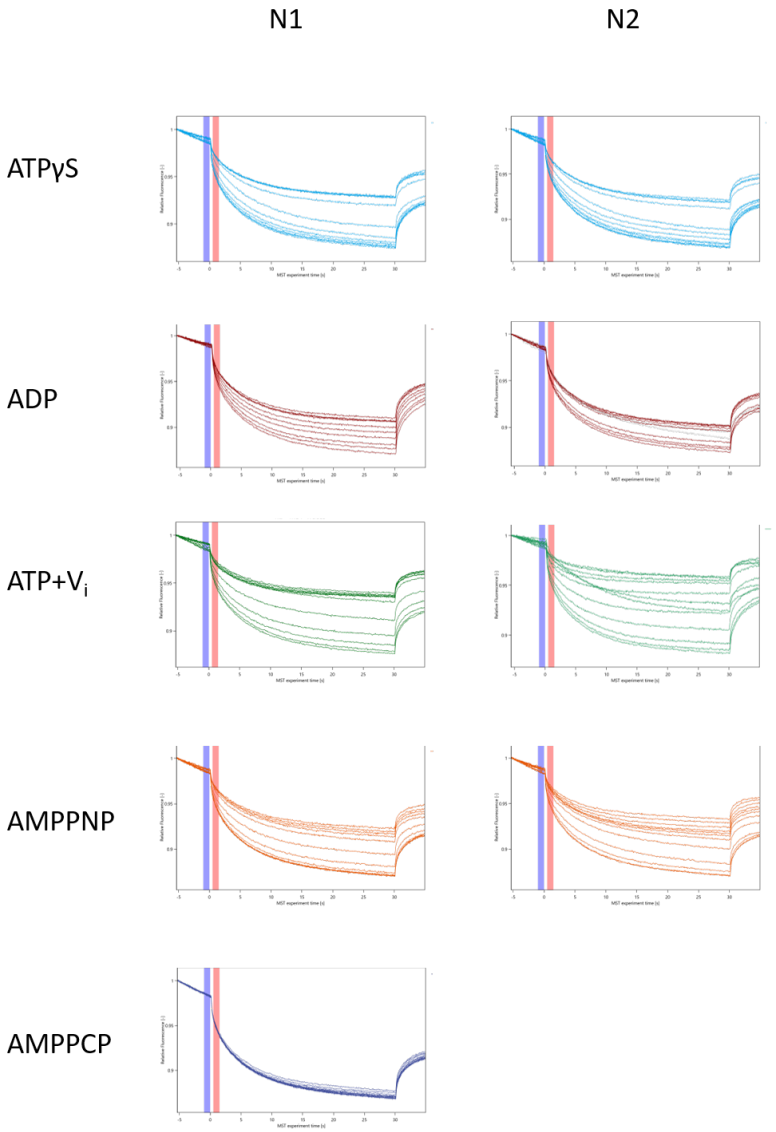


Figure 8.10 – Section 4.4.1: MST raw traces for individual measurement of unmodified ABCB8 with ATPγS, ADP, ATP+V_i, AMPPNP and AMPPCP. Normalised fluorescence is plotted versus time of measurement in seconds. Blue and red bar indicate time points used for deriving data for a binding constant with the T-jump method.

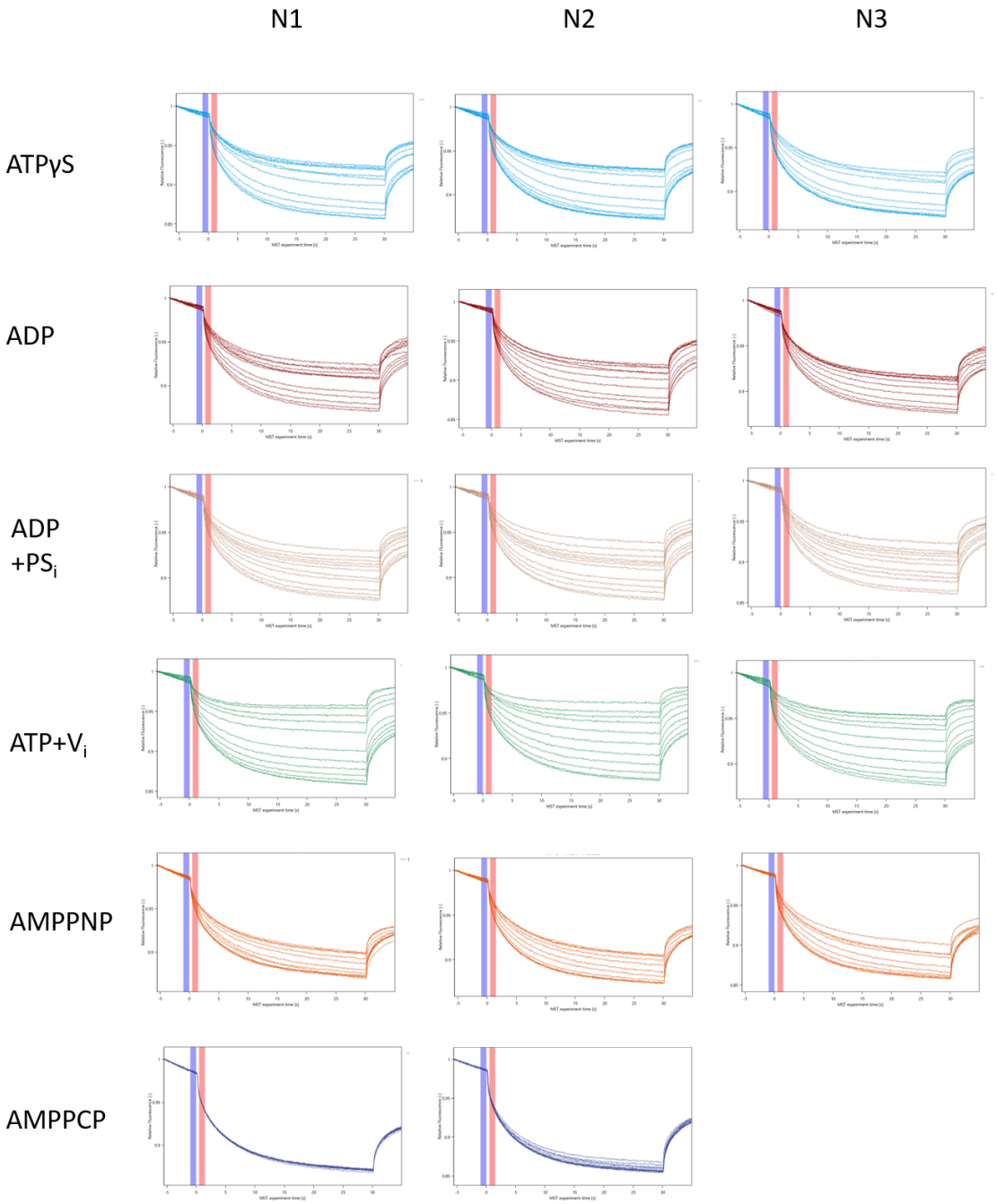


Figure 8.11 – Section 4.4.1: MST raw traces for individual measurement of iodoacetamide treated ABCB8 with ATPγS, ADP, ADP+PS$_i$ ATP+V$_i$, AMPPNP and AMPPCP. Normalised fluorescence is plotted versus time of measurement in seconds. Blue and red bar indicate time points used for deriving data for a binding constant with the T-jump method.

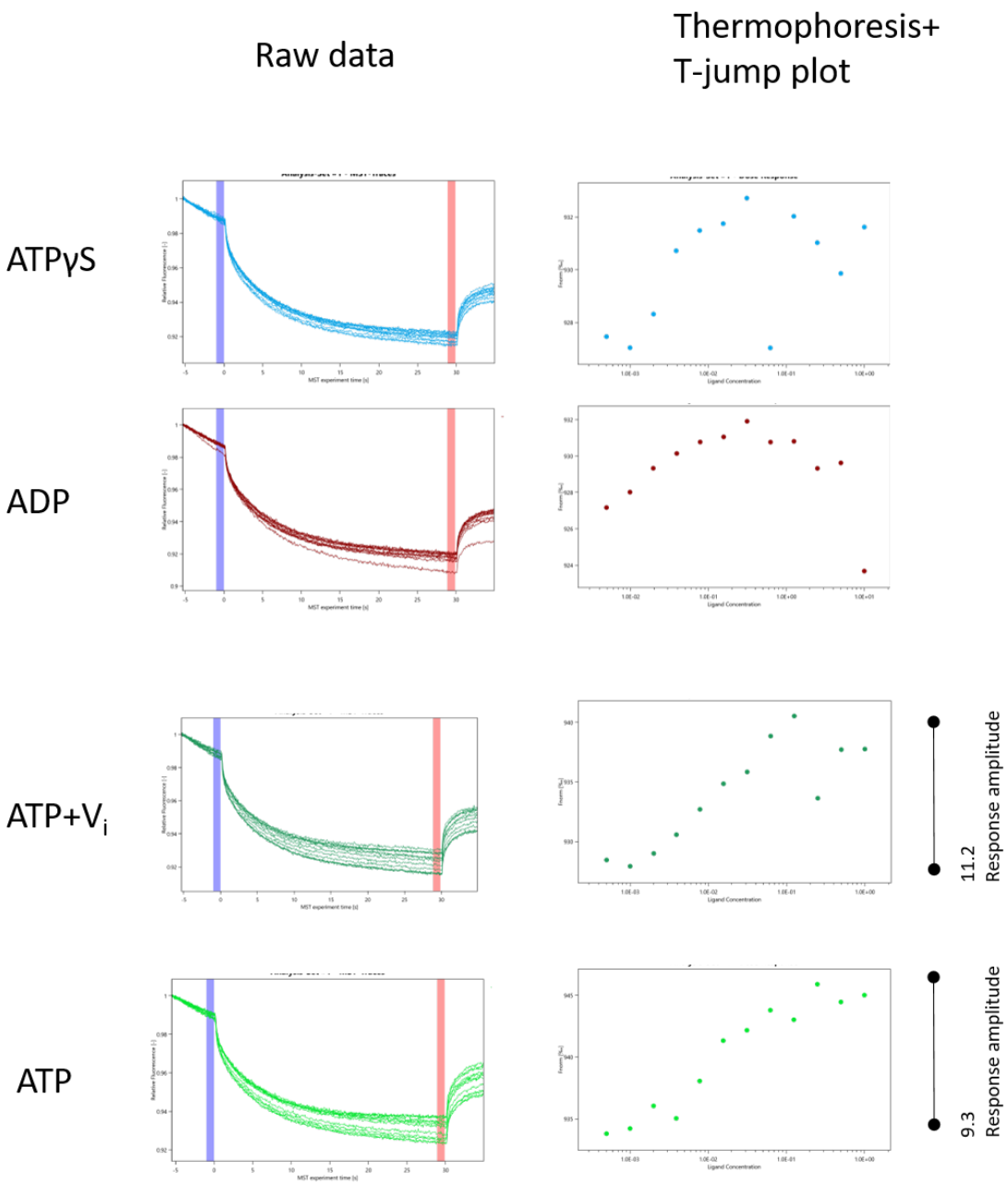


Figure 8.12 – Section 4.4.1: A) MST raw traces for individual measurement of unmodified ABCB8 E637Q with ATPγS, ADP, ATP+V$_i$ and ATP. Normalised fluorescence is plotted versus time of measurement in seconds. Blue and red bar indicate time points used for deriving data for a binding constant with the thermophoresis + T-jump method. B) Data points for binding curve derived from the MST trace using the fluorescence difference for the thermophoresis and T-jump method.

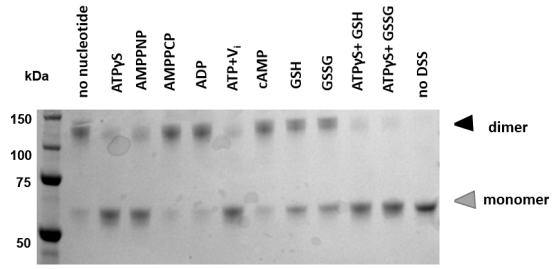


Figure 8.13 – Section 4.4.1: Coomassie-stained SDS-PAGE gel of ABCB8 WT samples after incubated with 1 mM ATP analogues and ADP and subsequent crosslinking using EGS.

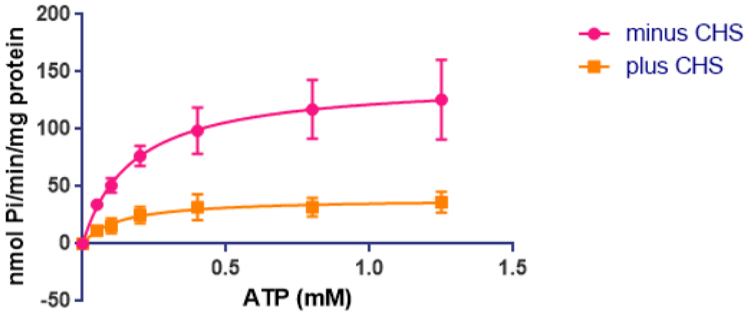


Figure 8.14 – Section 6.2: ATPase activity of reconstituted ABCB8 is reduced by addition of CHS. ATPase activity of reconstituted iodoacetamide treated ABCB8 in POPC/CDL (3:1 (wt/wt)) with and without CHS added during the reconstitution protocol. The amount of phosphate was measured in nmol/min/mg of protein using the Chifflet assay. ATPase assay data were normalised with protein concentrations from densitometry of SDS-PAGE gel bands using the "Quantity Tool" function of the Image Lab software. Data points present the mean ± S.D. of three individual measurements of one biological repeat. Data were fitted using the Michaelis-Menten equation using GraphPad Prism7.

8.5 Appendix: Outward-facing conformations of ABCB8 and the alternating-access mechanism

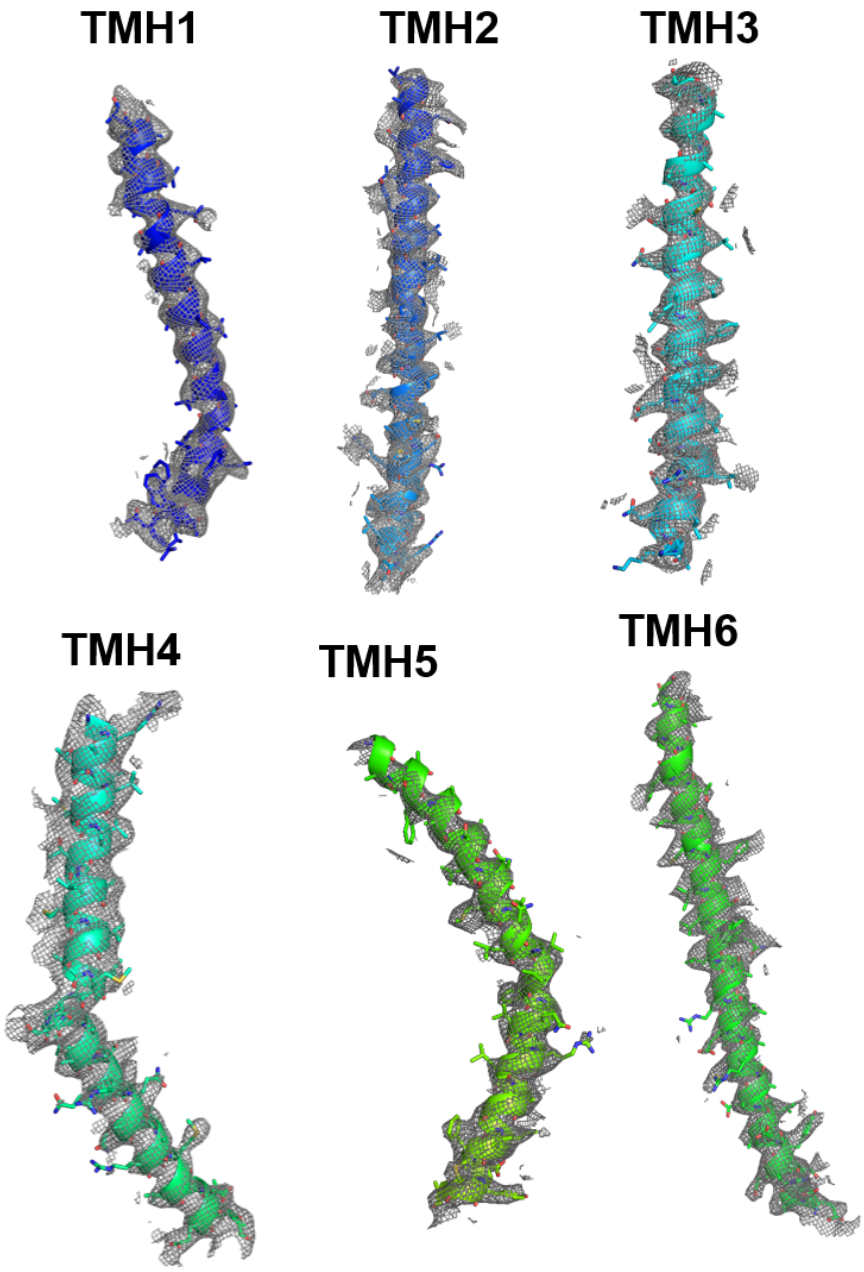


Figure 8.15 – Section 5.2.1: TMHs 1-6 of chain A presented as cartoon and sticks placed in the $2F_o{-}F_c$ map at 1σ contour level. Colouring of TMHs according to presentation in Fig. 5.5A

Table 8.4 – Section 5.2.1: Table listing crystal contacts between chains in crystal form 2 in $P12_11$ space group. Crystal contacts are ranked by surface area buried. Cysteines, involved in crystal contacts are labelled in red. Structural elements are listed ECL1 (loop TMH1-TMH2) and ECL2 (loop TMH3-TMH4), ELB (elbow helix), TMHs (1-6) and NBDS and colour coded.

Chains in crystal contact	Residues		Region	Residues		Region
F/G	F			G		
	Val	463	NBD (linker region)	Cys	478	NBD
	Thr	473	NBD	Val	463	NBD (linker region)
	Cys	478	NBD	Thr	473	NBD
	Thr	527	NBD	Thr	527	NBD
	Asp	534	NBD	Asp	534	NBD
A/D	A			D		
	Ser	458	NBD (linker region)	Gln	139	ELB1
	Val	463	NBD (linker region)	His	142	ELB1
	Pro	499	NBD	Arg	222	TMH2
	Thr	540	NBD	Ser	234	TMH2
	Ala	659	NBD	Gly	460	NBD
	Gly	660	NBD	Cys	461	NBD
				Ser	544	NBD
D/H	D			H		
	Gly	408	TMH6	Val	687	NBD
	Ser	413	TMH6	Glu	695	NBD
				Leu	697	NBD
				Leu	702	NBD
C/G	C			G		
	Val	687	NBD	Cys	283	ECL2
	Glu	689	NBD	Val	285	ECL2
	Lys	698	NBD			
A/C	A			C		
	Ser	471	NBD	Glu	350	TMH5
	Pro	499	NBD	Gln	351	TMH5
	Gly	535	NBD	Glu	354	TMH5
D/G	D			G		
	Val	173	ECL1	Leu	712	NBD
	Glu	174	ECL1	Ala	715	NBD
	Ala	177	ECL1	Glu	716	NBD
C/H	C			H		
	Ala	711	NBD	Gly	408	TMH6
	Leu	712	NBD	Gly	409	TMH6
	Ala	715	NBD	Met	412	TMH6
	Glu	716	NBD			
G/C	C			G		
	Met	412	TMH6	Ala	715	NBD
B/F	B			F		
	Ser	458	NBD (linker region)	Thr	189	TMH2/ECL1
A/F	A			F		
	Gln	351	TMH5	Met	187	TMH2/ECL1

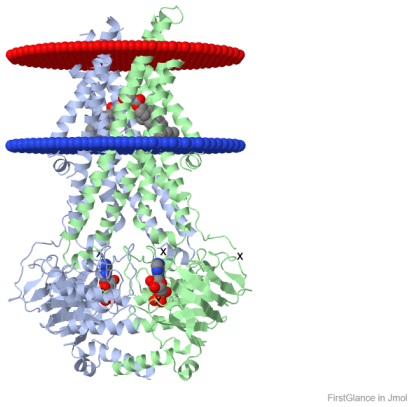


Figure 8.16 – Section 5.2.2: Membrane boundaries as predicted with the PPM server[Lomize *et al.*, 2012].

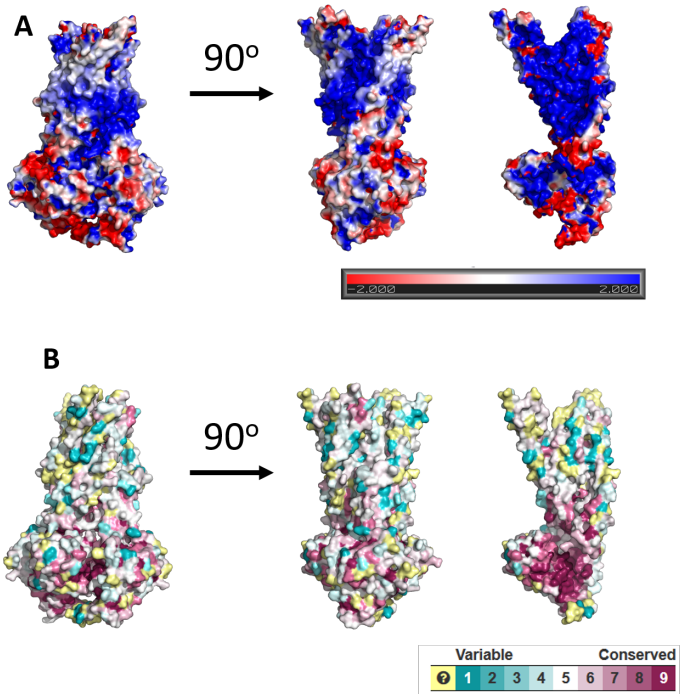


Figure 8.17 – Section 5.2.3: Surface of ABCB8 presented perpendicular to the membrane plane phase-on view on the dimer and in a 90^o turn around the symmetry axis. A) Colouring of surface according electrostatic potential with the APBS (Adaptive Poisson-Boltzmann Solver)-plugin [Baker *et al.*, 2001]. B) Surface colouring according to conserved residues in B-family on the surface obtained from the CONSURF webserver [Celniker *et al.*, 2013] with all human B-family orthologues of human ABCB8. Scale presents colour coding for degree of conservation.

Table 8.5 – Section: 5.2.2: ABCB8 homologues with UniProt entries used for CONSURF analyses

UniProt entry	species
A0A1J4JI66	9EUKA
A0A0X3PQL6	SCHSO
A0A0C9PXR9	9HYME
A0A0A1XEY9	BACCU
A0A0K8TXX5	BACLA
A0A0B2W342	TOXCA
H9G837	ANOCA
V8NC04	OPHHA
F7GIR2	MONDO
A0A1S3AKS9	ERIEU
ABCB8	MOUSE
ABCB8	RAT
G3T2H7	LOXAF
G3MYQ9	BOVIN
W5NWK0	SHEEP
G1PQL4	MYOLU
I3LMV8	PIG
F6Q7W3	HORSE
E2RHJ0	CANLF
G1M5L5	AILME
M3WIE3	FELCA
H0V320	CAVPO
A0A1S3G1M1	DIPOR
I3LXJ6	ICTTR
G1SVN5	RABIT
H0WJB0	OTOGA
A0A1U7UL18	TARSY
U3F3I1	CALJA
A0A096MWC9	PAPAN
F6W6T0	MACMU
H9FPC9	MACMU
G1QVG8	NOMLE
ABCB8	HUMAN
ABCB8	PONAB
H3AJ22	LATCH
A0A0G2ST67	PETMA
A0A1W5AKT8	9TELE
C0HA20	SALSA
H2S548	TAKRU
I3JSU2	ORENI
A0A1A7YYW6	9TELE
A0A1A8FE50	9TELE
A0A1A8UMY7	NOTFU
A0A1A8GPK7	9TELE
ABCB8	DANRE
W5UB71	ICTPU
ABCB8	XENTR
F6YPB6	XENTR
A0A1D5P356	CHICK
A0A151NBG9	ALLMI

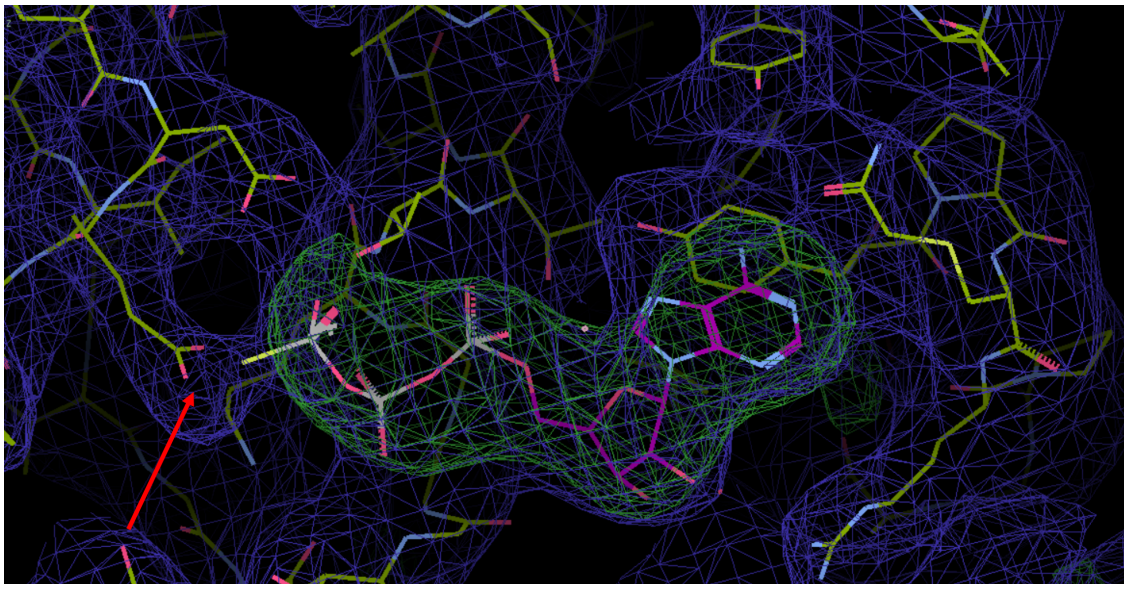


Figure 8.18 – Section 5.2.4: Attempt to model ATPγS into nucleotide binding site of chain A. ATPγS in purple sticks and final ABCB8 model in yellow. $2F_o$-F_c and F_o-F_c electron density maps shown in blue and green, respectively.

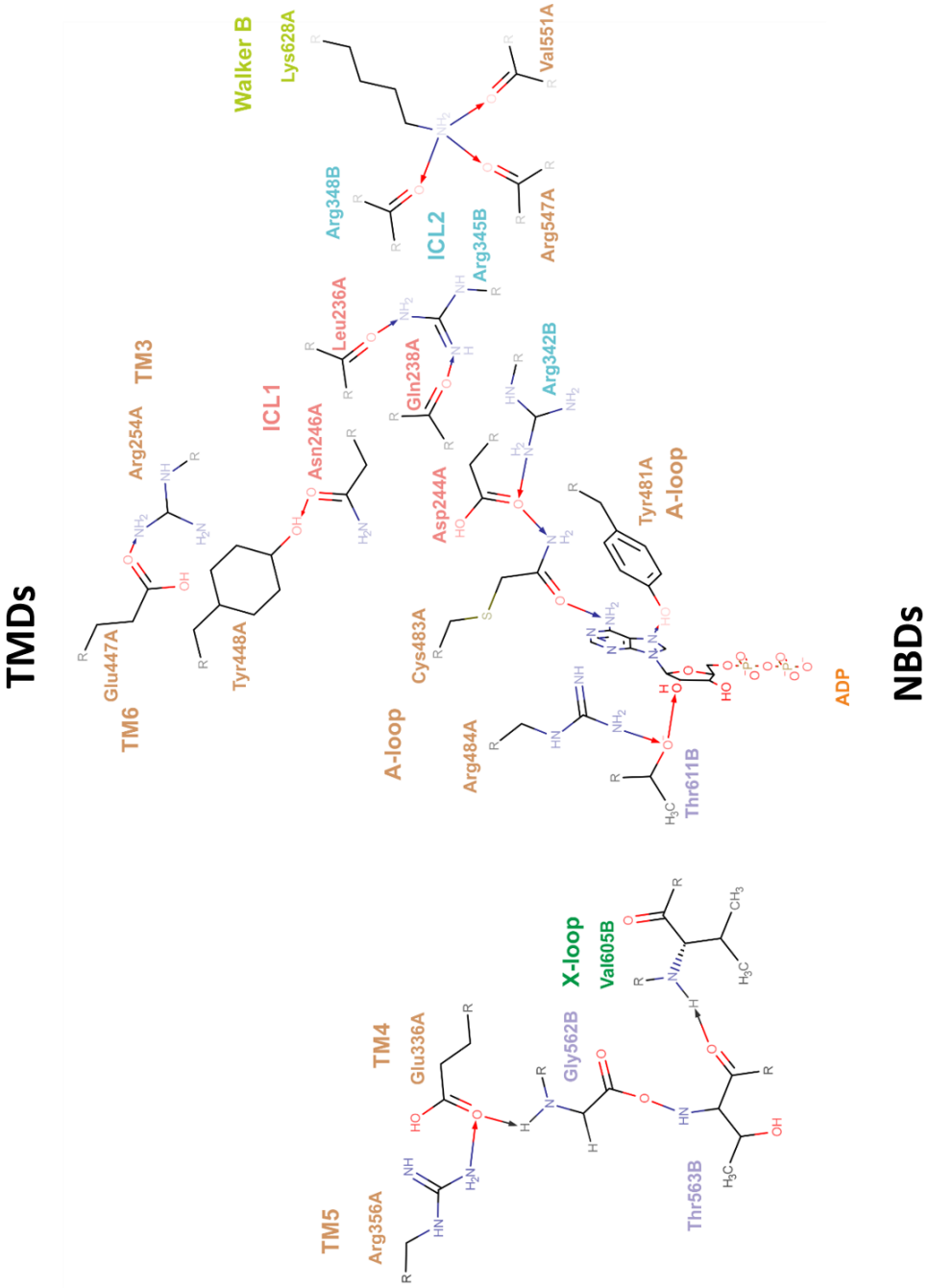


Figure 8.19 – Section 5.2.5: Schematic representation of the interaction network between the ADP binding site, X-loops and coupling helices (ICL1 and ICL2) in ABCB8. Arrows indicate hydrogen bonds.

Bibliography

1. Abele, R. & Tampé, R. The ABCs of Immunology: Structure and Function of TAP, the Transporter Associated with Antigen Processing. *Physiology* **19,** 216–224. ISSN: 1548-9213 (2004).
2. Adam, A. C., Bornhovd, C., *et al.* The Nfs1 interacting protein Isd11 has an essential role in Fe/S cluster biogenesis in mitochondria. eng. *The EMBO journal* **25,** 174–183. ISSN: 0261-4189 (2006).
3. Adams, P. D., Afonine, P. V., *et al.* PHENIX: A comprehensive Python-based system for macromolecular structure solution. *Acta Crystallographica Section D: Biological Crystallography* **66,** 213–221. ISSN: 09074449 (2010).
4. Aittoniemi, J., Fotinou, C., *et al.* SUR1: a unique ATP-binding cassette protein that functions as an ion channel regulator. *Philosophical Transactions of the Royal Society B: Biological Sciences* **364,** 257–267. ISSN: 0962-8436 (2009).
5. Aleksandrov, L., Aleksandrov, A. A., Chang, X. B. & Riordan, J. R. The first nucleotide binding domain of cystic fibrosis transmembrane conductance regulator is a site of stable nucleotide interaction, whereas the second is a site of rapid turnover. *Journal of Biological Chemistry* **277,** 15419–15425. ISSN: 00219258 (2002).
6. Alexandrov, A. I., Mileni, M., *et al.* Microscale Fluorescent Thermal Stability Assay for Membrane Proteins. *Structure* **16,** 351–359. ISSN: 09692126 (2008).
7. Aller, S. G., Yu, J., *et al.* Structure of P-Glycoprotein Reveals a Molecular Basis for Poly-Specific Drug Binding. *Science* **323,** 1718–1722. ISSN: 1095-9203 (2009).
8. Andersson, S. G. E., Zomorodipour, A., *et al.* The genome sequence of Rickettsia prowazekii and the origin of mitochondria. *Nature* **396,** 133–140. ISSN: 00280836 (1998).
9. Ardehali, H., O'Rourke, B. & Marbán, E. Cardioprotective role of the mitochondrial ATP-binding cassette protein 1. *Circulation Research* **97,** 740–742. ISSN: 00097330 (2005).
10. Ardehali, H., Xue, T., Dong, P. & Machamer, C. Targeting of the mitochondrial membrane proteins to the cell surface for functional studies. eng.

Biochemical and biophysical research communications **338,** 1143–1151. ISSN: 0006-291X (2005).

11. Ashcroft, F. M. & Kakei, M. ATP-sensitive K+ channels in rat pancreatic beta-cells: modulation by ATP and Mg2+ ions. *The Journal of physiology* **416,** 349–67. ISSN: 0022-3751 (1989).
12. Backmark, A. E., Olivier, N, *et al.* Fluorescent probe for high-throughput screening of membrane protein expression. *Protein science : a publication of the Protein Society* **22,** 1124–1132. ISSN: 1469-896X (2013).
13. Baker, N. A., Sept, D, *et al.* Electrostatics of nanosystems: application to microtubules and the ribosome. *Proceedings of the National Academy of Sciences of the United States of America* **98,** 10037–41. ISSN: 0027-8424 (2001).
14. Bastidas, A. C., Deal, M. S., *et al.* Phosphoryl transfer by protein kinase A is captured in a crystal lattice. *Journal of the American Chemical Society* **135,** 4788–4798. ISSN: 00027863 (2013).
15. Battye, T. G. G., Kontogiannis, L., *et al.* iMOSFLM: A new graphical interface for diffraction-image processing with MOSFLM. *Acta Crystallographica Section D: Biological Crystallography* **67,** 271–281. ISSN: 09074449 (2011).
16. Bayeva, M., Khechaduri, A., *et al.* ATP-binding cassette B10 regulates early steps of heme synthesis. *Circulation Research* **113,** 279–287. ISSN: 00097330 (2013).
17. Bechara, C., Nöll, A., *et al.* A subset of annular lipids is linked to the flippase activity of an ABC transporter. *Nature Chemistry* **7,** 255–262. ISSN: 1755-4330 (2015).
18. Bennett, B. D., Kimball, E. H., *et al.* Absolute metabolite concentrations and implied enzyme active site occupancy in Escherichia coli. *Nature Chemical Biology* **5,** 593–599. ISSN: 15524469 (2009).
19. Beranek, A., Rechberger, G., *et al.* Identification of a cardiolipin-specific phospholipase encoded by the gene CLD1 (YGR110W) in yeast. *Journal of Biological Chemistry* **284,** 11572–11578. ISSN: 00219258 (2009).
20. Berger, E. A. & Heppel, L. A. Different Mechanisms of Energy Coupling for the Shock-sensitive and Shock-resistant Amino Acid Permeases of Escherichia coli. *J. Biol. Chem.* **249,** 7747–7755. ISSN: 0021-9258 (1974).
21. Bernard, D. G., Netz, D. J., *et al.* Requirements of the cytosolic iron-sulfur cluster assembly pathway in Arabidopsis. *Philos Trans R Soc Lond B Biol Sci* **368,** 20120259. ISSN: 1471-2970 (2013).
22. Bleffert, F., Misetic, V., *et al.* nanoDSF Thermal Unfolding Analysis of a Membrane-bound Esterase in Various Detergents. *Application Note* **NT-PR-012** (2016).
23. Borbat, P. P., Surendhran, K., *et al.* Conformational motion of the ABC transporter MsbA induced by ATP hydrolysis. *PLoS Biology* **5,** 2211–2219. ISSN: 15449173 (2007).
24. Bountra, K., Hagelueken, G., *et al.* Structural basis for antibacterial peptide self-immunity by the bacterial ABC transporter McjD. eng. *The EMBO journal.* ISSN: 1460-2075 (2017).
25. Bricogne, G., Blanc, E., *et al.* BUSTER version 2.10.2. *Cambridge, United Kingdom: Global Phasing Ltd.* (2015).

26. Burnham-Marusich, A. R. & Berninsone, P. M. Multiple proteins with essential mitochondrial functions have glycosylated isoforms. *Mitochondrion* **12,** 423–427. ISSN: 15677249 (2012).
27. Carpenter, E. P., Beis, K., Cameron, A. D. & Iwata, S. Overcoming the challenges of membrane protein crystallography. *Current Opinion in Structural Biology* **18,** 581–586. ISSN: 0959440X (2008).
28. Celniker, G., Nimrod, G., *et al.* ConSurf: Using evolutionary data to raise testable hypotheses about protein function. *Israel Journal of Chemistry* **53,** 199–206. ISSN: 00212148 (2013).
29. Chang, G & Roth, C. B. Structure of MsbA from E. coli: a homolog of the multidrug resistance ATP binding cassette (ABC) transporters. *Science* **293,** 1793–800. ISSN: 0036-8075 (2001).
30. Chang, G, Roth, C. B., *et al.* Retraction. *Science* **314,** 1875. ISSN: 0036-8075 (2006).
31. Chappe, V., Irvine, T., *et al.* Phosphorylation of CFTR by PKA promotes binding of the regulatory domain. *The EMBO Journal* **24,** 2730–2740. ISSN: 0261-4189 (2005).
32. Chen, C. J., Chin, J. E., *et al.* Internal duplication and homology with bacterial transport proteins in the mdr1 (P-glycoprotein) gene from multidrug-resistant human cells. *Cell* **47,** 381–389. ISSN: 00928674 (1986).
33. Chen, M., Abele, R. & Tampé, R. Peptides induce ATP hydrolysis at both subunits of the transporter associated with antigen processing. *Journal of Biological Chemistry* **278,** 29686–29692. ISSN: 00219258 (2003).
34. Chen, V. B., Arendall, W. B., *et al.* MolProbity: All-atom structure validation for macromolecular crystallography. *Acta Crystallographica Section D: Biological Crystallography* **66,** 12–21. ISSN: 09074449 (2010).
35. Chen, W., Dailey, H. A. & Paw, B. H. Ferrochelatase forms an oligomeric complex with mitoferrin-1 and Abcb10 for erythroid heme biosynthesis. *Blood* **116,** 628–630. ISSN: 00064971 (2010).
36. Cherezov, V. *Lipidic cubic phase technologies for membrane protein structural studies* 2011.
37. Cherezov, V., Rosenbaum, D. M., *et al.* High-resolution crystal structure of an engineered human beta2-adrenergic G protein-coupled receptor. *Science* **318,** 1258–65. ISSN: 1095-9203 (2007).
38. Chifflet, S., Torriglia, A., Chiesa, R. & Tolosa, S. A method for the determination of inorganic phosphate in the presence of labile organic phosphate and high concentrations of protein: Application to lens ATPases. *Analytical Biochemistry* **168,** 1–4. ISSN: 10960309 (1988).
39. Chloupková, M., LeBard, L. S. & Koeller, D. M. MDL1 is a high copy suppressor of ATM1: Evidence for a role in resistance to oxidative stress. *Journal of Molecular Biology* **331,** 155–165. ISSN: 00222836 (2003).
40. Choudhury, H. G., Tong, Z., *et al.* Structure of an antibacterial peptide ATP-binding cassette transporter in a novel outward occluded state. *Proceedings of the National Academy of Sciences* **111,** 9145–9150. ISSN: 0027-8424 (2014).
41. Ciccarone, V. C., Polayes, D. a. & Luckow, V. a. Generation of Recombinant Baculovirus DNA in E.coli Using a Baculovirus Shuttle Vector. *Methods in molecular medicine* **13,** 213–35. ISSN: 1543-1894 (1998).

42. Cogliati, S., Frezza, C., *et al.* Mitochondrial cristae shape determines respiratory chain supercomplexes assembly and respiratory efficiency. *Cell* **155,** 160–171. ISSN: 00928674 (2013).
43. Cohn, M. Some properties of the phosphorothioate analogs of adenosine triphosphate as substrates of enzymic reactions. *Accounts of Chemical Research* **15,** 326–332 (1982).
44. Collauto, A., Mishra, S., *et al.* Direct Spectroscopic Detection of ATP Turnover Reveals Mechanistic Divergence of ABC Exporters. *Structure* **25,** 1264–1274.e3. ISSN: 18784186 (2017).
45. Colombini, M. *A candidate for the permeability pathway of the outer mitochondrial membrane [19]* 1979. arXiv: `arXiv:1011.1669v3`.
46. Dauter, Z. Estimation of anomalous signal in diffraction data. *Acta Crystallographica Section D: Biological Crystallography* **62,** 867–876. ISSN: 09074449 (2006).
47. Dawson, R. J. P. & Locher, K. P. Structure of a bacterial multidrug ABC transporter. *Nature* **443,** 180–185. ISSN: 0028-0836 (2006).
48. Dawson, R. J. P. & Locher, K. P. Structure of the multidrug ABC transporter Sav1866 from Staphylococcus aureus in complex with AMP-PNP. *FEBS Letters* **581,** 935–938. ISSN: 00145793 (2007).
49. Dawson, R. J. P. & Locher, K. P. Structure of the multidrug ABC transporter Sav1866 from Staphylococcus aureus in complex with AMP-PNP. *FEBS Letters* **581,** 935–938. ISSN: 00145793 (2007).
50. DeLano, W. L. The PyMOL Molecular Graphics System, Version 1.8. *Schrödinger LLC,* http://www.pymol.org. ISSN: 1348-4214 (2014).
51. Duval, S., Danyal, K., *et al.* Electron transfer precedes ATP hydrolysis during nitrogenase catalysis. *Proceedings of the National Academy of Sciences of the United States of America* **110,** 16414–9. ISSN: 1091-6490 (2013).
52. Eckstein, F. Phosphorothioate Analogues of NucleotidesTools for the Investigation of Biochemical Processes. *Angewandte Chemie International Edition in English* **22,** 423–439. ISSN: 15213773 (1983).
53. Elliott, A. M. & Al-Hajj, M. A. ABCB8 Mediates Doxorubicin Resistance in Melanoma Cells by Protecting the Mitochondrial Genome. *Molecular Cancer Research* **7,** 79–87. ISSN: 1541-7786 (2009).
54. Emsley, P., Lohkamp, B., Scott, W. G. & Cowtan, K. Features and development of Coot. *Acta Crystallographica Section D: Biological Crystallography* **66,** 486–501. ISSN: 09074449 (2010).
55. Eswar, N., Webb, B., *et al.* Comparative protein structure modeling using MODELLER. *Current Protocols in Protein Science* **Chapter 2,** Unit 2.9. ISSN: 1934-3663 (2007).
56. Evans, P. Scaling and assessment of data quality. *Acta Crystallographica Section D: Biological Crystallography* **62,** 72–82. ISSN: 09074449 (2006).
57. Evans, P. R. & Murshudov, G. N. How good are my data and what is the resolution? *Acta Crystallographica Section D: Biological Crystallography* **69,** 1204–1214. ISSN: 09074449 (2013).
58. Eytan, G. D. Use of liposomes for reconstitution of biological functions. *Biochimica et Biophysica Acta (BBA) - Reviews on Biomembranes* **694,** 185–202. ISSN: 03044157 (1982).

59. Faham, S. & Bowie, J. U. Bicelle crystallization: A new method for crystallizing membrane proteins yields a monomeric bacteriorhodopsin structure. *Journal of Molecular Biology* **316,** 1–6. ISSN: 00222836 (2002).
60. French, S. & Wilson, K. On the treatment of negative intensity observations. *Acta Crystallographica Section A* **34,** 517–525. ISSN: 16005724 (1978).
61. Frey, P. & Sammons, R. Bond order and charge localization in nucleoside phosphorothioates. *Science* **228,** 541–545. ISSN: 0036-8075 (1985).
62. Fukasawa, Y., Tsuji, J., *et al.* MitoFates: Improved Prediction of Mitochondrial Targeting Sequences and Their Cleavage Sites. *Molecular & Cellular Proteomics* **14,** 1113–1126. ISSN: 1535-9476 (2015).
63. Gabaldón, T. & Huynen, M. A. Shaping the mitochondrial proteome. *Biochimica et Biophysica Acta - Bioenergetics* **1659,** 212–220. ISSN: 00052728 (2004).
64. Geertsma, E. R., Nik Mahmood, N. a. B., Schuurman-Wolters, G. K. & Poolman, B. Membrane reconstitution of ABC transporters and assays of translocator function. *Nature protocols* **3,** 256–266. ISSN: 1754-2189 (2008).
65. Gerlach, J. H., Endicott, J. A., *et al.* Homology between P-glycoprotein and a bacterial haemolysin transport protein suggests a model for multidrug resistance. *Nature* **324,** 485–9. ISSN: 0028-0836 (1986).
66. Gillet, J.-P., Efferth, T., *et al.* Microarray-based detection of multidrug resistance in human tumor cells by expression profiling of ATP-binding cassette transporter genes. *Cancer research* **64,** 8987–8993. ISSN: 0008-5472 (2004).
67. Gilson, E., Higgins, C. F., *et al.* Extensive homology between membrane-associated components of histidine and maltose transport systems of Salmonella typhimurium and Escherichia coli. *Journal of Biological Chemistry* **257,** 9915–9918. ISSN: 00219258 (1982).
68. Gourdon, P., Andersen, J. L., *et al.* HiLiDe-systematic approach to membrane protein crystallization in lipid and detergent. *Crystal Growth and Design* **11,** 2098–2106. ISSN: 15287483 (2011).
69. Gout, E., Rebeille, F., Douce, R. & Bligny, R. Interplay of Mg2+, ADP, and ATP in the cytosol and mitochondria: unravelling the role of Mg2+ in cell respiration. eng. *Proceedings of the National Academy of Sciences of the United States of America* **111,** E4560–7. ISSN: 1091-6490 (2014).
70. Graf, S. A., Haigh, S. E., Corson, E. D. & Shirihai, O. S. Targeting, import and dimerization of a mammalian mitochondrial ATP binding cassette (ABC) transporter, ABCB10 (ABC-me). *Journal of Biological Chemistry* **279,** 42954–42963. ISSN: 00219258 (2004).
71. Gray, M. W. & Doolittle, W. F. Has the endosymbiont hypothesis been proven? *Microbiological reviews* **46,** 1–42. ISSN: 0146-0749 (1982).
72. Gray, M. W., Cedergren, R, Abel, Y & Sankoff, D. On the evolutionary origin of the plant mitochondrion and its genome. *Proceedings of the National Academy of Sciences of the United States of America* **86,** 2267–71. ISSN: 0027-8424 (1989).
73. Gros, P., Croop, J. & Housman, D. Mammalian multidrug resistance gene: Complete cDNA sequence indicates strong homology to bacterial transport proteins. *Cell* **47,** 371–380. ISSN: 00928674 (1986).
74. Grossmann, N., Vakkasoglu, A. S., *et al.* Mechanistic determinants of the directionality and energetics of active export by a heterodimeric ABC transporter. *Nature Communications* **5,** 5419. ISSN: 2041-1723 (2014).

75. Guenther, B, Onrust, R, *et al.* Crystal structure of the delta' subunit of the clamp-loader complex of E. coli DNA polymerase III. *Cell* **91,** 335–45. ISSN: 0092-8674 (1997).
76. Gulati, S., Jamshad, M., *et al.* Detergent free purification of ABC transporters. *Biochem J* **44,** 1–24. ISSN: 1470-8728 (2014).
77. Gunderson, K. L. & Kopito, R. R. Effects of pyrophosphate and nucleotide analogs suggest a role for ATP hydrolysis in cystic fibrosis transmembrane regulator channel gating. *Journal of Biological Chemistry* **269,** 19349–19353. ISSN: 00219258 (1994).
78. Haffke, M., Rummel, G., *et al.* Thermal Unfolding of GPCRs nanoDSF : Label-free Thermal Unfolding Assay of G Protein- Coupled Receptors for Compound Screening and Buffer Composition Optimization. *Application Note* **NT-PR-008,** 1–8 (2016).
79. Haun, R. S., Serventi, I. M. & Moss, J. Rapid, reliable ligation-independent cloning of PCR products using modified plasmid vectors. *BioTechniques* **13,** 515–518. ISSN: 07366205 (1992).
80. He, Y., Wang, K. & Yan, N. *The recombinant expression systems for structure determination of eukaryotic membrane proteins* 2014.
81. Heimerl, S., Bosserhoff, A. K., *et al.* Mapping ATP-binding cassette transporter gene expression profiles in melanocytes and melanoma cells. *Melanoma research* **17,** 265–273. ISSN: 0960-8931 (2007).
82. Hellmich, U. A., Lyubenova, S., *et al.* Probing the ATP hydrolysis cycle of the abc multidrug transporter LmrA by pulsed EPR spectroscopy. *Journal of the American Chemical Society* **134,** 5857–5862. ISSN: 00027863 (2012).
83. Higgins, C. F., Hiles, I. D., *et al.* A family of related ATP-binding subunits coupled to many distinct biological processes in bacteria. *Nature* **323,** 448–450. ISSN: 0028-0836 (1986).
84. Higgins, C. F., Haag, P. D., *et al.* Complete nucleotide sequence and identification of membrane components of the histidine transport operon of S. typhimurium. *Nature* **298,** 723–7. ISSN: 0028-0836 (1982).
85. Higgins, C. F. & Linton, K. J. The ATP switch model for ABC transporters. *Nature Structural & Molecular Biology* **11,** 918–926. ISSN: 1545-9993 (2004).
86. Hofacker, M., Gompf, S., *et al.* Structural and functional fingerprint of the mitochondrial ATP-binding cassette transporter Mdl1 from Saccharomyces cerevisiae. *Journal of Biological Chemistry* **282,** 3951–3961. ISSN: 00219258 (2007).
87. Hogue, D. L., Liu, L & Ling, V. Identification and characterization of a mammalian mitochondrial ATP-binding cassette membrane protein. *Journal of molecular biology* **285,** 379–89. ISSN: 0022-2836 (1999).
88. Hohl, M., Briand, C., Grütter, M. G. & Seeger, M. a. Crystal structure of a heterodimeric ABC transporter in its inward-facing conformation. *Nature Structural & Molecular Biology* **19,** 395–402. ISSN: 1545-9993 (2012).
89. Hohl, M., Hürlimann, L. M., *et al.* Structural basis for allosteric cross-talk between the asymmetric nucleotide binding sites of a heterodimeric ABC exporter. *Proceedings of the National Academy of Sciences of the United States of America* **111,** 11025–30. ISSN: 1091-6490 (2014).

90. Hollenstein, K., Frei, D. C. & Locher, K. P. Structure of an ABC transporter in complex with its binding protein. *Nature* **446,** 213–216. ISSN: 1476-4687 (2007).
91. Hopfner, K. P., Karcher, A., *et al.* Structural biology of Rad50 ATPase: ATP-driven conformational control in DNA double-strand break repair and the ABC-ATPase superfamily. *Cell* **101,** 789–800. ISSN: 0092-8674 (2000).
92. Horvath, S. E. & Daum, G. Lipids of mitochondria. *Progress in Lipid Research* **52,** 590–614. ISSN: 01637827 (2013).
93. Hung, L. W., Wang, I. X., *et al.* Crystal structure of the ATP-binding subunit of an ABC transporter. eng. *Nature* **396,** 703–707. ISSN: 0028-0836 (1998).
94. Hwang, T. C., Nagel, G, Nairn, A. C. & Gadsby, D. C. Regulation of the gating of cystic fibrosis transmembrane conductance regulator C1 channels by phosphorylation and ATP hydrolysis. *Proceedings of the National Academy of Sciences of the United States of America* **91,** 4698–702. ISSN: 0027-8424 (1994).
95. Hyde, B. B., Liesa, M., *et al.* The mitochondrial transporter ABC-me (ABCB10), a downstream target of GATA-1, is essential for erythropoiesis in vivo. *Cell Death and Differentiation* **19,** 1117–1126. ISSN: 1350-9047 (2012).
96. Hyde, S. C., Emsley, P, *et al.* Structural model of ATP-binding proteins associated with cystic fibrosis, multidrug resistance and bacterial transport. *Nature* **346,** 362–365. ISSN: 0028-0836 (1990).
97. Ichikawa, Y., Bayeva, M., *et al.* Disruption of ATP-binding cassette B8 in mice leads to cardiomyopathy through a decrease in mitochondrial iron export. *Proceedings of the National Academy of Sciences* **109,** 4152–4157. ISSN: 0027-8424 (2012).
98. Ichikawa, Y., Ghanefar, M., *et al.* Cardiotoxicity of doxorubicin is mediated through mitochondrial iron accumulation. *Journal of Clinical Investigation* **124,** 617–630. ISSN: 00219738 (2014).
99. Iwata, S. *Methods and Results in Crystallization of Membrane Proteins* ISBN: 9780963681799 (International University Line, 2003).
100. Jansen, R. S., Mahakena, S., *et al.* ATP-binding cassette subfamily C member 5 (ABCC5) functions as an efflux transporter of glutamate conjugates and analogs. *Journal of Biological Chemistry* **290,** 30429–30440. ISSN: 1083351X (2015).
101. Jardetzky, O. Simple allosteric model for membrane pumps. *Nature* **211,** 969–970. ISSN: 0028-0836 (1966).
102. Jerabek-Willemsen, M., Andre, T., *et al.* MicroScale Thermophoresis: Interaction analysis and beyond. *Journal of Molecular Structure* **1077,** 101–113. ISSN: 00222860 (2014).
103. Jerabek-Willemsen, M., Wienken, C. J., *et al.* Molecular Interaction Studies Using Microscale Thermophoresis. *ASSAY and Drug Development Technologies* **9,** 342–353. ISSN: 1540-658X (2011).
104. Jin, M. S., Oldham, M. L., Zhang, Q. & Chen, J. Crystal structure of the multidrug transporter P-glycoprotein from Caenorhabditis elegans. *Nature* **490,** 566–9. ISSN: 1476-4687 (2012).
105. Johnson, Z. L. & Chen, J. Structural Basis of Substrate Recognition by the Multidrug Resistance Protein MRP1. *Cell* **168,** 1075–1085.e9. ISSN: 10974172 (2017).

106. Jones, P. M. & George, A. M. Role of the D-loops in allosteric control of ATP hydrolysis in an ABC transporter. *Journal of Physical Chemistry A* **116,** 3004–3013. ISSN: 10895639 (2012).
107. Juliano, R. L. & Ling, V. A surface glycoprotein modulating drug permeability in Chinese hamster ovary cell mutants. *BBA - Biomembranes* **455,** 152–162. ISSN: 00052736 (1976).
108. Kabsch, W. XDS. *Acta Crystallographica Section D: Biological Crystallography* **66,** 125–132. ISSN: 09074449 (2010).
109. Kadaba, N. S., Kaiser, J. T., *et al.* The high-affinity E. coli methionine ABC transporter: structure and allosteric regulation. *Science* **321,** 250–3. ISSN: 1095-9203 (2008).
110. Kantardjieff, K. A. & Rupp, B. Matthews coefficient probabilities: Improved estimates for unit cell contents of proteins, DNA, and protein-nucleic acid complex crystals. *Protein Science* **12,** 1865–1871. ISSN: 09618368 (2003).
111. Kartner, N, Riordan, J. R. & Ling, V. Cell surface P-glycoprotein associated with multidrug resistance in mammalian cell lines. *Science* **221,** 1285–8. ISSN: 0036-8075 (1983).
112. Kaur, H., Lakatos-Karoly, A., *et al.* Coupled ATPase-adenylate kinase activity in ABC transporters. *Nature communications* **7,** 13864. ISSN: 2041-1723 (2016).
113. Kessler, D. Enzymatic activation of sulfur for incorporation into biomolecules in prokaryotes. *FEMS Microbiology Reviews* **30,** 825–840. ISSN: 01686445 (2006).
114. Kispal, G., Csere, P., Guiard, B. & Lill, R. The ABC transport Atm1p is required for mitochondrial iron homeostasis. *FEBS Letters* **418,** 346–350. ISSN: 00145793 (1997).
115. Kispal, G., Csere, P., Prohl, C. & Lill, R. The mitochondrial proteins Atm1p and Nfs1p are essential for biogenesis of cytosolic Fe/S proteins. *EMBO Journal* **18,** 3981–3989. ISSN: 02614189 (1999).
116. Krishnamurthy, P. C., Du, G., *et al.* Identification of a mammalian mitochondrial porphyrin transporter. *Nature.* ISSN: 0028-0836 (2006).
117. Krissinel, E. & Henrick, K. Inference of Macromolecular Assemblies from Crystalline State. *Journal of Molecular Biology* **372,** 774–797. ISSN: 00222836 (2007).
118. Kuhnke, G., Neumann, K., Mühlenhoff, U. & Lill, R. Stimulation of the ATPase activity of the yeast mitochondrial ABC transporter Atm1p by thiol compounds. *Molecular Membrane Biology* **23,** 173–184. ISSN: 0968-7688 (2006).
119. Laganowsky, A., Reading, E., *et al.* Membrane proteins bind lipids selectively to modulate their structure and function. *Nature* **510,** 172–5. ISSN: 1476-4687 (2014).
120. Landau, E. M. & Rosenbusch, J. P. Lipidic cubic phases: A novel concept for the crystallization of membrane proteins. *Proceedings of the National Academy of Sciences* **93,** 14532–14535. ISSN: 0027-8424 (1996).
121. Lane, N. & Martin, W. The energetics of genome complexity. *Nature* **467,** 929–34. ISSN: 1476-4687 (2010).

122. Lecher, J., Schwarz, C. K. W., *et al.* An RTX transporter tethers its unfolded substrate during secretion via a unique N-terminal domain. *Structure* **20,** 1778–1787. ISSN: 09692126 (2012).
123. Lee, J. Y., Yang, J. G., *et al.* Structural basis for heavy metal detoxification by an Atm1-type ABC exporter. *Science* **343,** 1133–6. ISSN: 0036-8075 (2014).
124. Lee, J.-Y., Kinch, L. N., *et al.* Crystal structure of the human sterol transporter ABCG5/ABCG8. *Nature* **533,** 561–564. ISSN: 0028-0836 (2016).
125. Lee, M., Choi, Y., *et al.* The ABC transporter AtABCB14 is a malate importer and modulates stomatal response to CO2. *Nature Cell Biology* **10,** 1217–1223. ISSN: 1465-7392 (2008).
126. Lévy, D., Bluzat, A., Seigneuret, M. & Rigaud, J. L. A systematic study of liposome and proteoliposome reconstitution involving Bio-Bead-mediated Triton X-100 removal. *BBA - Biomembranes* **1025,** 179–190. ISSN: 00052736 (1990).
127. Li, J. & Cowan, J. A. Glutathione-coordinated [2Fe-2S] cluster: a viable physiological substrate for mitochondrial ABCB7 transport. *Chemical communications (Cambridge, England)* **51,** 2253–2255. ISSN: 1364-548X (2015).
128. Li, N., Wu, J. X., *et al.* Structure of a Pancreatic ATP-Sensitive Potassium Channel. *Cell* **168,** 101–110.e10. ISSN: 10974172 (2017).
129. Liesa, M., Qiu, W. & Shirihai, O. S. Mitochondrial ABC transporters function: The role of ABCB10 (ABC-me) as a novel player in cellular handling of reactive oxygen species. *Biochimica et Biophysica Acta - Molecular Cell Research* **1823,** 1945–1957. ISSN: 01674889 (2012).
130. Liesa, M., Luptak, I., *et al.* Mitochondrial transporter ATP binding cassette mitochondrial erythroid is a novel gene required for cardiac recovery after ischemia/reperfusion. *Circulation* **124,** 806–813. ISSN: 00097322 (2011).
131. Lill, R. Function and biogenesis of iron-sulphur proteins. *Nature* **460,** 831–8. ISSN: 1476-4687 (2009).
132. Lill, R. & Kispal, G. Mitochondrial ABC transporters. *Research in Microbiology* **152,** 331–340. ISSN: 09232508 (2001).
133. Lim, S., Smith, K. R., *et al.* Regulation of mitochondrial functions by protein phosphorylation and dephosphorylation. *Cell & bioscience* **6,** 25. ISSN: 2045-3701 (2016).
134. Lin, D. Y.-w., Huang, S. & Chen, J. Crystal structures of a polypeptide processing and secretion transporter. *Nature* **523,** 425–430. ISSN: 0028-0836 (2015).
135. Liu, F., Zhang, Z., *et al.* Molecular Structure of the Human CFTR Ion Channel. *Cell* **169,** 85–92. ISSN: 10974172 (2017).
136. Locher, K. P. Mechanistic diversity in ATP-binding cassette (ABC) transporters. *Nature structural & molecular biology* **23,** 487–93. ISSN: 1545-9985 (2016).
137. Locher, K. P., Lee, A. T., *et al.* The E. coli BtuCD structure: a framework for ABC transporter architecture and mechanism. *Science (New York, N.Y.)* **296,** 1091–8. ISSN: 1095-9203 (2002).
138. Lomize, M. A., Pogozheva, I. D., *et al.* OPM database and PPM web server: Resources for positioning of proteins in membranes. *Nucleic Acids Research* **40.** ISSN: 03051048 (2012).

139. Mancia, F. & Love, J. High-throughput expression and purification of membrane proteins. *Journal of Structural Biology* **172,** 85–93. ISSN: 10478477 (2010).
140. Marcoux, J., Wang, S. C., *et al.* Mass spectrometry reveals synergistic effects of nucleotides, lipids, and drugs binding to a multidrug resistance efflux pump. *Proceedings of the National Academy of Sciences* **110,** 9704–9709. ISSN: 0027-8424 (2013).
141. Martin, C., Berridge, G., *et al.* Drug binding sites on P-glycoprotein are altered by ATP binding prior to nucleotide hydrolysis. *Biochemistry* **39,** 11901–11906. ISSN: 00062960 (2000).
142. Martin, C., Higgins, C. F. & Callaghan, R. The vinblastine binding site adopts high- and low-affinity conformations during a transport cycle of P-glycoprotein. *Biochemistry* **40,** 15733–15742. ISSN: 00062960 (2001).
143. Martin, G. M., Yoshioka, C., *et al.* Cryo-EM structure of the ATP-sensitive potassium channel illuminates mechanisms of assembly and gating. *eLife* **6.** ISSN: 2050084X (2017).
144. Matthews, B. Solvent content of protein crystals. *Journal of Molecular Biology* **33,** 491–497. ISSN: 00222836 (1968).
145. McCoy, A. J., Grosse-Kunstleve, R. W., *et al.* Phaser crystallographic software. *Journal of Applied Crystallography* **40,** 658–674. ISSN: 00218898 (2007).
146. McGuffin, L. J., Bryson, K. & Jones, D. T. The PSIPRED protein structure prediction server. *Bioinformatics (Oxford, England)* **16,** 404–405. ISSN: 1367-4803 (2000).
147. McPherson, A, Nguyen, C, Cudney, R & Larson, S. The role of small molecule additives and chemical modification in protein crystallization. *Crystal Growth & Design* **11,** 1469–1474 (2011).
148. McWilliam, H., Li, W., *et al.* Analysis Tool Web Services from the EMBL-EBI. *Nucleic acids research* **41.** ISSN: 13624962 (2013).
149. Mi, W., Li, Y., *et al.* Structural basis of MsbA-mediated lipopolysaccharide transport. *Nature* **549,** 233–237. ISSN: 1476-4687 (2017).
150. Milić, D. & Veprintsev, D. B. Large-scale production and protein engineering of G protein-coupled receptors for structural studies. *Frontiers in Pharmacology* **6,** 66. ISSN: 1663-9812 (2015).
151. Mishra, S., Verhalen, B., *et al.* Conformational dynamics of the nucleotide binding domains and the power stroke of a heterodimeric ABC transporter. *eLife* **3,** e02740. ISSN: 2050084X (2014).
152. Mitsuhashi, N., Miki, T., *et al.* MTABC3, a novel mitochondrial ATP-binding cassette protein involved in iron homeostasis. *Journal of Biological Chemistry* **275,** 17536–17540. ISSN: 00219258 (2000).
153. Moeller, A., Lee, S. C., *et al.* Distinct Conformational Spectrum of Homologous Multidrug ABC Transporters. *Structure* **23,** 450–460. ISSN: 18784186 (2015).
154. Moos, C, Alpert, N. R. & Myers, T. C. Effects of a phosphonic acid analog of adenosine triphosphate on actomyosin systems. eng. *Archives of biochemistry and biophysics* **88,** 183–192. ISSN: 0003-9861 (1960).
155. Murshudov, G. N., Skubák, P., *et al.* REFMAC5 for the refinement of macromolecular crystal structures. *Acta Crystallographica Section D: Biological Crystallography* **67,** 355–367. ISSN: 09074449 (2011).

156. Neupert, W. & Herrmann, J. M. Translocation of Proteins into Mitochondria. *Annual Review of Biochemistry* **76,** 723–49. ISSN: 0066-4154 (2007).
157. Newstead, S., Ferrandon, S. & Iwata, S. Rationalizing alpha-helical membrane protein crystallization. *Protein science : a publication of the Protein Society* **17,** 466–72. ISSN: 0961-8368 (2008).
158. Nicholls, R. A., Long, F. & Murshudov, G. N. Low-resolution refinement tools in REFMAC5. *Acta Crystallographica Section D: Biological Crystallography* **68,** 404–417. ISSN: 09074449 (2012).
159. Nicolson, G. L. The Fluid-Mosaic Model of Membrane Structure: Still relevant to understanding the structure, function and dynamics of biological membranes after more than 40 years. *Biochimica et Biophysica Acta (BBA) - Biomembranes* **1838,** 1451–1466. ISSN: 18792642 (2014).
160. Niesen, F. H., Berglund, H. & Vedadi, M. The use of differential scanning fluorimetry to detect ligand interactions that promote protein stability. *Nature Protocols* **2,** 2212–2221. ISSN: 1754-2189 (2007).
161. Oldham, M. L. & Chen, J. Snapshots of the maltose transporter during ATP hydrolysis. *Proceedings of the National Academy of Sciences of the United States of America* **108,** 15152–15156. ISSN: 0027-8424 (2011).
162. Oldham, M. L., Khare, D., *et al.* Crystal structure of a catalytic intermediate of the maltose transporter. *Nature* **450,** 515–521. ISSN: 1476-4687 (2007).
163. Oldham, M. L., Grigorieff, N. & Chen, J. Structure of the transporter associated with antigen processing trapped by herpes simplex virus. *eLife* **5.** ISSN: 2050084X (2016).
164. Omasits, U., Ahrens, C. H., Müller, S. & Wollscheid, B. Protter: Interactive protein feature visualization and integration with experimental proteomic data. *Bioinformatics* **30,** 884–886. ISSN: 13674803 (2014).
165. Paradkar, P. N., Zumbrennen, K. B., *et al.* Regulation of mitochondrial iron import through differential turnover of mitoferrin 1 and mitoferrin 2. *Molecular and cellular biology* **29,** 1007–1016. ISSN: 0270-7306 (2009).
166. Paterson, J. K., Shukla, S., *et al.* Human ABCB6 localizes to both the outer mitochondrial membrane and the plasma membrane. *Biochemistry* **46,** 9443–9452. ISSN: 00062960 (2007).
167. Patrick, M. H. Crystallography made crystal clear: A guide for users of macromolecular models (3rd Ed.) *Biochemistry and Molecular Biology Education* **35,** 387–388. ISSN: 14708175 (2007).
168. Paytubi, S., Wang, X., *et al.* ABC50 promotes translation initiation in mammalian cells. *Journal of Biological Chemistry* **284,** 24061–24073. ISSN: 00219258 (2009).
169. Peck, M. L. & Herschlag, D. Adenosine 5'-O-(3-thio)triphosphate (ATPgammaS) is a substrate for the nucleotide hydrolysis and RNA unwinding activities of eukaryotic translation initiation factor eIF4A. *RNA (New York, N.Y.)* **9,** 1180–7. ISSN: 1355-8382 (2003).
170. Perez, C., Gerber, S., *et al.* Structure and mechanism of an active lipid-linked oligosaccharide flippase. *Nature* **524,** 433–438. ISSN: 0028-0836 (2015).
171. Pettersen, E. F., Goddard, T. D., *et al.* UCSF ChimeraA Visualization System for Exploratory Research and Analysis. *J Comput Chem* **25,** 1605–1612. ISSN: 15426270 (2004).

172. Pisarev, A. V., Skabkin, M. A., *et al.* The Role of ABCE1 in Eukaryotic Posttermination Ribosomal Recycling. *Molecular Cell* **37,** 196–210. ISSN: 10972765 (2010).
173. Pondarré, C., Campagna, D. R., *et al.* Abcb7, the gene responsible for X-linked sideroblastic anemia with ataxia, is essential for hematopoiesis. *Blood* **109,** 3567–3569. ISSN: 00064971 (2007).
174. Pondarré, C., Antiochos, B. B., *et al.* The mitochondrial ATP-binding cassette transporter Abcb7 is essential in mice and participates in cytosolic iron-sulfur cluster biogenesis. *Human Molecular Genetics* **15,** 953–964. ISSN: 09646906 (2006).
175. Privé, G. G. Detergents for the stabilization and crystallization of membrane proteins. *Methods* **41,** 388–397. ISSN: 10462023 (2007).
176. Putnam, C. D., Clancy, S. B., *et al.* Structure and mechanism of the RuvB holliday junction branch migration motor. *Journal of Molecular Biology* **311,** 297–310. ISSN: 00222836 (2001).
177. Qi, W., Li, J. & Cowan, J. A. A structural model for glutathione-complexed ironsulfur cluster as a substrate for ABCB7-type transporters. *Chemical Communications* **50,** 3795. ISSN: 1359-7345 (2014).
178. Qian, H., Zhao, X., *et al.* Structure of the Human Lipid Exporter ABCA1. *Cell* **169,** 1228–1239.e10. ISSN: 10974172 (2017).
179. Quazi, F., Lenevich, S. & Molday, R. S. ABCA4 is an N-retinylidene phosphatidylethanolamine and phosphatidylethanolamine importer. *Nature communications* **3,** 925. ISSN: 2041-1723 (2012).
180. Ramakrishnan, C., Dani, V. & Ramasarma, T. A conformational analysis of Walker motif A [GXXXXGKT (S)] in nucleotide-binding and other proteins. *Protein Engineering Design and Selection* **15,** 783–798. ISSN: 1741-0126 (2002).
181. Randak, C. O. & Welsh, M. J. ADP inhibits function of the ABC transporter cystic fibrosis transmembrane conductance regulator via its adenylate kinase activity. *Proceedings of the National Academy of Sciences of the United States of America* **102,** 2216–2220. ISSN: 0027-8424 (2005).
182. Rayment, I. Reductive alkylation of lysine residues to alter crystallization properties of proteins. *Methods in Enzymology* **276,** 171–179. ISSN: 00766879 (1997).
183. Read, R. J. & Schierbeek, A. J. A phased translation function. *Journal of Applied Crystallography* **21,** 490–495. ISSN: 0021-8898 (1988).
184. Rees, D. C., Johnson, E. & Lewinson, O. ABC transporters: the power to change. *Nature reviews. Molecular cell biology* **10,** 218–27. ISSN: 1471-0080 (2009).
185. Resetar, A. M. & Chalovich, J. M. Adenosine 5'-(gamma-thiotriphosphate): an ATP analog that should be used with caution in muscle contraction studies. eng. *Biochemistry* **34,** 16039–16045. ISSN: 0006-2960 (1995).
186. Rigaud, J. L., Paternostre, M. T. & Bluzat, A. Mechanisms of membrane protein insertion into liposomes during reconstitution procedures involving the use of detergents. 2. Incorporation of the light-driven proton pump bacteriorhodopsin. *Biochemistry* **27,** 2677–2688. ISSN: 0006-2960 (1988).
187. Rigaud, J. L. & Lévy, D. Reconstitution of Membrane Proteins into Liposomes. *Methods in Enzymology* **372,** 65–86. ISSN: 00766879 (2003).

188. Robert, X. & Gouet, P. Deciphering key features in protein structures with the new ENDscript server. *Nucleic Acids Research* **42.** ISSN: 13624962 (2014).
189. Rodionov, D. A., Hebbeln, P., *et al.* A novel class of modular transporters for vitamins in prokaryotes. *Journal of Bacteriology* **91,** 42–51. ISSN: 00219193 (2009).
190. Saier, M. H., Tran, C. V. & Barabote, R. D. TCDB: the Transporter Classification Database for membrane transport protein analyses and information. *Nucleic acids research* **34,** D181–6. ISSN: 1362-4962 (2006).
191. Saier, M. H., Reddy, V. S., *et al.* The Transporter Classification Database (TCDB): Recent advances. *Nucleic Acids Research* **44,** D372–D379. ISSN: 13624962 (2016).
192. Sainsbury, S., Ren, J., *et al.* The structure of a reduced form of OxyR from Neisseria meningitidis. *BMC structural biology* **10,** 10. ISSN: 1472-6807 (2010).
193. Sali, A. MODELLER A Program for Protein Structure Modeling Release 9v4, r6262. *Structure,* 779–815 (2008).
194. Savitsky, P., Bray, J., *et al.* High-throughput production of human proteins for crystallization: The SGC experience. *Journal of Structural Biology* **172,** 3–13. ISSN: 10478477 (2010).
195. Schaedler, T. A., Faust, B., *et al.* Structures and functions of mitochondrial ABC transporters. *Biochem Soc Trans* **43,** 943–951. ISSN: 0300-5127 (2015).
196. Schaedler, T. A., Thornton, J. D., *et al.* A conserved mitochondrial ATP-binding cassette transporter exports glutathione polysulfide for cytosolic metal cofactor assembly. *Journal of Biological Chemistry* **289,** 23264–23274. ISSN: 1083351X (2014).
197. Schmidt, O., Pfanner, N. & Meisinger, C. Mitochondrial protein import: from proteomics to functional mechanisms. *Nature reviews. Molecular cell biology* **11,** 655–667. ISSN: 1471-0072 (2010).
198. Schulz, G. E. Validation of the detergent micelle classification for membrane protein crystals and explanation of the Matthews Graph for soluble proteins. *Protein Science* **20,** 1765–1770. ISSN: 09618368 (2011).
199. Schulz, H, Fabianek, R. A., *et al.* Heme transfer to the heme chaperone CcmE during cytochrome c maturation requires the CcmC protein, which may function independently of the ABC-transporter CcmAB. *Proceedings of the National Academy of Sciences of the United States of America* **96,** 6462–7. ISSN: 0027-8424 (1999).
200. Seddon, A. M., Curnow, P. & Booth, P. J. Membrane proteins, lipids and detergents: Not just a soap opera. *Biochimica et Biophysica Acta - Biomembranes* **1666,** 105–117. ISSN: 00052736 (2004).
201. Senior, A. E., Al-Shawi, M. K. & Urbatsch, I. L. The catalytic cycle of P-glycoprotein. *FEBS Letters* **377,** 285–289. ISSN: 00145793 (1995).
202. Sharom, F. J., Yu, X, Chu, J. W. & Doige, C. A. Characterization of the ATPase activity of P-glycoprotein from multidrug-resistant Chinese hamster ovary cells. *The Biochemical journal* **308,** 381–90. ISSN: 0264-6021 (1995).
203. Shaw, G. C., Cope, J. J., *et al.* Mitoferrin is essential for erythroid iron assimilation. *Nature* **440,** 96–100. ISSN: 0028-0836 (2006).

204. Shimizu, T. & Johnson, K. A. Presteady state kinetic analysis of vanadate-induced inhibition of the dynein ATPase. *Journal of Biological Chemistry* **258,** 13833–13840. ISSN: 00219258 (1983).
205. Shintre, C. A., Pike, A. C. W., *et al.* Structures of ABCB10, a human ATP-binding cassette transporter in apo- and nucleotide-bound states. *Proc Natl Acad Sci USA* **110,** 9710–9715. ISSN: 1091-6490 (2013).
206. Shoemaker, C. J. & Green, R. Kinetic analysis reveals the ordered coupling of translation termination and ribosome recycling in yeast. *Proceedings of the National Academy of Sciences of the United States of America* **108,** E1392–E1398. ISSN: 0027-8424 (2011).
207. Sickmann, A., Reinders, J., *et al.* The proteome of Saccharomyces cerevisiae mitochondria. *Proceedings of the National Academy of Sciences of the United States of America* **100,** 13207–12. ISSN: 0027-8424 (2003).
208. Sievers, F., Wilm, A., *et al.* Fast, scalable generation of high-quality protein multiple sequence alignments using Clustal Omega. *Molecular systems biology* **7,** 539. ISSN: 1744-4292 (2011).
209. Singer, S. J. J & Nicolson, G. L. L. The fluid mosaic model of the structure of cell membranes. *Science* **175,** 720–731. ISSN: 0036-8075 (1972).
210. Smith, A. C. & Robinson, A. J. A metabolic model of the mitochondrion and its use in modelling diseases of the tricarboxylic acid cycle. *BMC systems biology* **5,** 102. ISSN: 1752-0509 (2011).
211. Smith, P. C., Karpowich, N., *et al.* ATP binding to the motor domain from an ABC transporter drives formation of a nucleotide sandwich dimer. *Molecular Cell* **10,** 139–149. ISSN: 10972765 (2002).
212. Smriti, Zou, P. & Mchaourab, H. S. Mapping daunorubicin-binding sites in the ATP-binding cassette transporter MsbA using site-specific quenching by spin labels. *Journal of Biological Chemistry* **284,** 13904–13913. ISSN: 00219258 (2009).
213. Srinivasan, V., Pierik, A. J. & Lill, R. Crystal Structures of Nucleotide-Free and Glutathione-Bound Mitochondrial ABC Transporter Atm1. *Science* **343,** 1137–1140. ISSN: 0036-8075 (2014).
214. Stein, N. CHAINSAW: A program for mutating pdb files used as templates in molecular replacement. *Journal of Applied Crystallography* **41,** 641–643. ISSN: 00218898 (2008).
215. Story, R. M. & Steitz, T. A. Structure of the recA protein-ADP complex. *Nature* **355,** 374–6. ISSN: 0028-0836 (1992).
216. Suzuki, Y., Shimizu, T., Morii, H. & Tanokura, M. Hydrolysis of AMPPNP by the motor domain of nod, a kinesin-related protein. *FEBS Letters* **409,** 29–32. ISSN: 00145793 (1997).
217. Tamura, Y., Sesaki, H. & Endo, T. Phospholipid transport via mitochondria. *Traffic* **15,** 933–945. ISSN: 16000854 (2014).
218. Tantama, M, Martinez-Francois, J. R., Mongeon, R & Yellen, G. Imaging energy status in live cells with a fluorescent biosensor of the intracellular ATP-to-ADP ratio. *Nat Commun* **4,** 2550. ISSN: 2041-1723 (2013).
219. Tarling, E. J., de Aguiar Vallim, T. Q. & Edwards, P. A. Role of ABC transporters in lipid transport and human disease. *Trends in endocrinology and metabolism: TEM* **24,** 342–50. ISSN: 1879-3061 (2013).

220. Taylor, a. M., Storm, J, *et al.* Detailed characterization of cysteine-less P-glycoprotein reveals subtle pharmacological differences in function from wild-type protein. *British journal of pharmacology* **134,** 1609–18. ISSN: 0007-1188 (2001).
221. Taylor, N. M. I., Manolaridis, I., *et al.* Structure of the human multidrug transporter ABCG2. *Nature.* ISSN: 0028-0836 (2017).
222. Terwilliger, T. C., Di Maio, F., *et al.* Phenix.mr-rosetta: Molecular replacement and model rebuilding with Phenix and Rosetta. *Journal of Structural and Functional Genomics* **13,** 81–90. ISSN: 1345711X (2012).
223. Theodoulou, F. & Kerr, I. ABC transporter research: going strong 40 years on. *Biochemical Society transactions* **43,** 1033–40. ISSN: 1470-8752 (2015).
224. Thomas, J. A. & Tate, C. G. Quality Control in Eukaryotic Membrane Protein Overproduction. *Journal of Molecular Biology.* ISSN: 10898638 (2014).
225. Tickle, J. I., Flensburg, C., Keller, P. & Paciorek, W. *STARANISO United Ltd., Kingdom: Global Phasing* Cambridge, UK, 2017.
226. Timachi, M. H., Hutter, C. A., *et al.* Exploring conformational equilibria of a heterodimeric ABC transporter. *eLife* **6.** ISSN: 2050-084X (2017).
227. Tsuchida, M., Emi, Y., Kida, Y. & Sakaguchi, M. Human ABC transporter isoform B6 (ABCB6) localizes primarily in the Golgi apparatus. *Biochemical and Biophysical Research Communications* **369,** 369–375. ISSN: 0006291X (2008).
228. Tsui, L.-C. & Dorfman, R. The cystic fibrosis gene: a molecular genetic perspective. *Cold Spring Harbor perspectives in medicine* **3,** a009472. ISSN: 2157-1422 (2013).
229. Vanaken, T., Foxall-Vanaken, S., Castleman, S. & Ferguson-Miller, S. Alkyl Glycoside Detergents: Synthesis and Applications to the Study of Membrane Proteins. *Methods in Enzymology* **125,** 27–35. ISSN: 15577988 (1986).
230. Vedovato, N., Ashcroft, F. M. & Puljung, M. C. *The Nucleotide-Binding Sites of SUR1: A Mechanistic Model* 2015.
231. Verhalen, B., Koteiche, H. A., *et al.* Energy transduction and alternating access of the mammalian ABC transporter P-glycoprotein. *Nature* **543,** 738–741. ISSN: 0028-0836 (2017).
232. Viklund, H. & Elofsson, A. OCTOPUS: Improving topology prediction by two-track ANN-based preference scores and an extended topological grammar. *Bioinformatics* **24,** 1662–1668. ISSN: 13674803 (2008).
233. Von Heijne, G. Mitochondrial targeting sequences may form amphiphilic helices. *The EMBO journal* **5,** 1335–1342. ISSN: 0261-4189 (1986).
234. Wackerhage, H, Hoffmann, U, *et al.* Recovery of free ADP, Pi, and free energy of ATP hydrolysis in human skeletal muscle. *Journal of applied physiology (Bethesda, Md. : 1985)* **85,** 2140–2145. ISSN: 8750-7587 (1998).
235. Walker, J. E., Saraste, M., Runswick, M. & Gay, N. J. Distantly related sequences in the alpha- and beta-subunits of ATP synthase, myosin, kinases and other ATP-requiring enzymes and a common nucleotide binding fold. *The EMBO Journal* **1,** 945–951. ISSN: 0261-4189 (1982).
236. Ward, A., Reyes, C. L., *et al.* Flexibility in the ABC transporter MsbA: Alternating access with a twist. *Proceedings of the National Academy of Sciences* **104,** 19005–19010. ISSN: 0027-8424 (2007).

237. Ward, A. B., Szewczyk, P., *et al.* Structures of P-glycoprotein reveal its conformational flexibility and an epitope on the nucleotide-binding domain. *Proceedings of the National Academy of Sciences* **110,** 13386–13391. ISSN: 0027-8424 (2013).
238. Ward, A., Reyes, C. L., *et al.* Flexibility in the ABC transporter MsbA: Alternating access with a twist. *Proceedings of the National Academy of Sciences of the United States of America* **104,** 19005–10. ISSN: 1091-6490 (2007).
239. Webb, B. & Sali, A. Comparative Protein Structure Modeling Using MODELLER. *Current Protocols in Bioinformatics* **47,** 5.6.1–5.6.32. ISSN: 1934-340X (2014).
240. Weng, J., Mata, N. L., *et al.* Insights into the function of rim protein in photoreceptors and etiology of Stargardt's disease from the phenotype in abcr knockout mice. *Cell* **98,** 13–23. ISSN: 00928674 (1999).
241. Wiedemann, N., Urzica, E., *et al.* Essential role of Isd11 in mitochondrial iron-sulfur cluster synthesis on Isu scaffold proteins. *The EMBO journal* **25,** 184–95. ISSN: 0261-4189 (2006).
242. Willis, J. A. & Schleich, T. Oxidative-stress induced protein glutathione mixed-disulfide formation in the ocular lens. *Biochimica et Biophysica Acta - Molecular Cell Research* **1313,** 20–28. ISSN: 01674889 (1996).
243. Wingert, R. a., Galloway, J. L., *et al.* Deficiency of glutaredoxin 5 reveals Fe-S clusters are required for vertebrate haem synthesis. *Nature* **436,** 1035–1039. ISSN: 0028-0836 (2005).
244. Winn, M. D., Ballard, C. C., *et al.* Overview of the CCP4 suite and current developments. *Acta Crystallographica Section D: Biological Crystallography* **67,** 235–242. ISSN: 09074449 (2011).
245. Xiong, J., Feng, J., *et al.* Tracing the structural evolution of eukaryotic ATP binding cassette transporter superfamily. *Scientific Reports* **5,** 16724. ISSN: 2045-2322 (2015).
246. Xu, K., Zhang, M., *et al.* Crystal structure of a folate energy-coupling factor transporter from Lactobacillus brevis. *Nature* **497,** 268–71. ISSN: 1476-4687 (2013).
247. Xu, W., Barrientos, T. & Andrews, N. C. Iron and copper in mitochondrial diseases. *Cell Metabolism* **17,** 319–328. ISSN: 15504131 (2013).
248. Xu, Y., Malhotra, A., Ren, M. & Schlame, M. The enzymatic function of tafazzin. *Journal of Biological Chemistry* **281,** 39217–39224. ISSN: 00219258 (2006).
249. Yamamoto, M., Arimura, H., *et al.* Abcb10 role in heme biosynthesis in vivo: Abcb10 knockout in mice causes anemia with protoporphyrin IX and iron accumulation. *Molecular and Cellular Biology* **34,** 1077–84. ISSN: 1098-5549 (2014).
250. Young, L, Leonhard, K, *et al.* Role of the ABC transporter Mdl1 in peptide export from mitochondria. *Science* **291,** 2135–2138. ISSN: 00368075 (2001).
251. Yount, R. G., Babcock, D., Ballantyne, W. & Ojala, D. Adenylyl Imidodiphosphate, an Adenosine Triphosphate Analog Containing a P-N-P Linkage. *Biochemistry* **10,** 2484–2489. ISSN: 15204995 (1971).

252. Zaitseva, J, Jenewein, S, *et al.* A molecular understanding of the catalytic cycle of the nucleotide-binding domain of the ABC transporter HlyB. *Biochemical Society transactions* **33,** 990–995. ISSN: 03005127 (2005).
253. Zaitseva, J., Oswald, C., *et al.* A structural analysis of asymmetry required for catalytic activity of an ABC-ATPase domain dimer. *The EMBO Journal* **25,** 3432–3443. ISSN: 0261-4189 (2006).
254. Zegzouti, H., Zdanovskaia, M., Hsiao, K. & Goueli, S. A. ADP-Glo: A Bioluminescent and Homogeneous ADP Monitoring Assay for Kinases. *ASSAY and Drug Development Technologies* **7,** 560–572. ISSN: 1540-658X (2009).
255. Zhang, Z. & Chen, J. Atomic Structure of the Cystic Fibrosis Transmembrane Conductance Regulator. *Cell* **167,** 1586–1597.e9. ISSN: 10974172 (2016).
256. Zhang, Z., Liu, F. & Chen, J. Conformational Changes of CFTR upon Phosphorylation and ATP Binding. *Cell* **170,** 483–491.e8. ISSN: 10974172 (2017).
257. Zollmann, T., Moiset, G., *et al.* Single liposome analysis of peptide translocation by the ABC transporter TAPL. *Proceedings of the National Academy of Sciences of the United States of America* **112,** 2046–2051. ISSN: 0027-8424 (2015).
258. Zolnerciks, J. K., Akkaya, B. G., *et al.* The Q loops of the human multidrug resistance transporter ABCB1 are necessary to couple drug binding to the ATP catalytic cycle. *FASEB Journal* **28,** 4335–4346. ISSN: 15306860 (2014).
259. Zutz, A., Hoffmann, J., *et al.* Asymmetric ATP hydrolysis cycle of the heterodimeric multidrug ABC transport complex TmrAB from Thermus thermophilus. *Journal of Biological Chemistry* **286,** 7104–7115. ISSN: 00219258 (2011).